ON THE MECHANICS OF NON-WOVEN FABRICS

BY

DEWITT ROSS PETTERSON

S.B. Roanoke College,
(1948)

S.M. Institute of Textile Technology
(1950)

Submitted in Partial Fulfillment of the
Requirements for the Degree of

Doctor of Science

at the

MASSACHUSETTS INSTITUTE OF TECHNOLOGY

August, 1958

Signature of Author _____

Certified By _____
Thesis Supervisor

Accepted By _____
Chairman, Departmental Committee on Graduate Students

TABLE OF CONTENTS

TABLE OF FIGURES

TABLES

FORWARD

I wish to express my sincere appreciation to Professor Backer for his council, guidance, and encouragement in this investigation, and during my entire graduate career.

I further wish to express my gratitude to the Union Carbide Chemical Corporation, Charleston, West Virginia, for the financial assistance which made this investigation possible; and in particular, to Mr. A. T. Walters and Dr. G. M. Bryant, of the Fibers Research Group, for their valuable suggestions and constructive criticisms.

I am indebted to Professor E. R. Schwarz of the Textile Technology Division of the Mechanical Engineering Department, Professor A. G. H. Dietz of the Building and Engineering Construction Division of the Civil Engineering Department, and Professor F. A. McClintock of the Mechanical Engineering Department for the interest they showed by serving on my doctoral committee, and for their guidance during the course of this investigation.

I would also like to thank C. H. Dexter and Sons, Inc., Windsor Locks, Connecticut and in particular, Mr. F. H. Osborne, Vice President and Technical Director, and Mr. J. Kurgan, Research Manager, for their cooperation in supplying the materials used in this investigation, and in the preparation of special materials.

I wish to express my appreciation to Miss Barbara Langell for her many trying hours in the preparation and typing of this thesis.

Lastly, I take this opportunity to recognize the patience and sacrifices of my wife and family, whose encouragement and devotion have made my entire graduate program possible.

SYMBOLS

FABRIC, EXPERIMENTAL

σ_y, Specific Stress in y direction, grams/denier (gpd)

e_y, Strain in y direction, %

E_y, Specific Initial Modulus, gpd

σ_p, Specific Proportional Limit Stress, gpd (0.25% Strain Offset)

σ_m, Specific Rupture Stress, gpd

ν_{yx}, Poisson's Ratio relative to y and x axes

G_{yx}, Specific Modulus of Rigidity relative to y and x axes (gpd)

D, Average Area Density (grams/sq. inch or denier)

FIBER

σ_f, Specific Fiber Stress, gpd

e_f, Fiber Strain, %

E_f, Specific Initial Modulus, gpd

P, Intercept of Specific Plastic Modulus and Stress Axis, gpd

q, Specific Plastic Modulus, gpd

e_p, Fiber Proportional Limit Strain, %

$\bar{e}_m$, Average Rupture Strain of Fiber, %

S_{e_m}, Standard Deviation of Rupture Strain

$(e_m)_{min}$, Minimum Fiber Rupture Strain $= \bar{e}_m - 3S_{e_m}$

UNIT CELL

σ_c, Specific Stress, gpd

e_c, Unit Cell or Average Fabric Strain, %

$\bar{\sigma}_{cm}$, Specific Rupture Stress of Average Unit Cell, gpd.

S_σ, Standard Deviation of Rupture Stress of Unit Cell of Average Area Density

d, Area Density of Unit Cell

S_d, Standard Deviation of Area Density of Unit Cell

F_o, Rupture Force/unit width of Average Unit Cell = $D\bar{\sigma}_{cm}$

F_c, Rupture Force/unit width of Any Unit Cell = $d\,\sigma_{cm}$

$S_{d\sigma}$, Standard Deviation of Rupture Force/unit width of Unit Cell

$C_{d\sigma}$, Coefficient of Variation of Rupture Force or Rupture Stress of Unit Cell.

FABRIC PREDICTED

$\bar{\sigma}_{cm}$, Average Rupture Stress, gpd

σ_{hj}, Predicted Rupture Stress of Fabric Sample of hj Unit Cells

$\bar{E}_y^*$ Specific Modulus, gpd

ν_{yx}^* Poisson's Ratio

Boundary Conditions

$\sigma_x = 0$, $e_{yx} = 0$

ABSTRACT

On the Mechanics of Non-Woven Fabrics; Devitt R. Petterson.

Submitted to the Department of Mechanical Engineering on August 25, 1958, in partial fulfillment of the requirements of the degree of Doctor of Science in Fibrous High Polymers.

This investigation has provided a method for predicting the mechanical properties of certain bonded fibrous structures (usually termed "non-woven" fabrics) without the assumptions of Hookean behavior or product uniformity. The fabric properties are predicted directly from the engineering properties of the fiber, the orientation distribution of fibers within the fabric, and local variations in area density and orientation of fibers. The orthotropic theory previously developed for plywood has been applied to two fabric materials. The measured material constants of the orthotropic axes allow the orthotropic theory to predict the elastic engineering properties at angles intermediate to the orthotropic axes.

A fiber web theory was developed to translate the engineering properties of the fiber and the fiber web geometry into the engineering properties of the fabric. Under the assumptions of straight, non-buckling fibers; all elastic constants are well predicted. The boundary conditions of the typical tensile test are discussed and the fiber web theory solved for uniaxial tension (real,); and for a tensile test where the shear strain is zero (real,). The latter boundary conditions appear to approximate more closely the experimental test conditions.

The fiber web theory allows consideration of the post-yield plastic region of the fiber and the resulting non-elastic region of the fabric. The analysis has been carried out for straight fiber webs, but a discussion of the effect of curved is given. The effects of poor bonding and bunched fibers on the predicted mechanical properties are discussed.

The fabric has been considered as a matrix of analytical model units, or "unit cells", each independent, yet with definite boundary displacements under stress. The assumptions involved are carefully noted and justified, where possible. The variation in rupture stress of the unit cells has been determined, and Peirce's "Weakest Link" theory applied to determine the rupture stress of various sized samples. The predicted rupture stresses are in good agreement with the experimental data. A number of fiber orientation distributions are analyzed theoretically.

The fiber web theory presents a method for designing non-woven fabrics with certain specific characteristics, predicting the properties of such "ideal" fabrics, thus providing a bench-mark against which actual fabrics and processes can be evaluated.

Thesis Supervisor_____

Title: Associate Professor of Mechanical Engineering

BIOGRAPHICAL NOTE

The author was born March 27, 1928 in Roanoke, Virginia, where he attended public grammar and secondary schools. In 1944 he received the academic diploma from Jefferson Senior High School, Roanoke, Virginia, and entered Roanoke College, Salem, Virginia. In 1948 he received the Bachelor of Science degree, with major in physics, with first honors. That fall he received a two year fellowship at the Institute of Textile Technology, Charlottesville, Virginia. The summer of 1949 was spent in a cotton textile mill learning all phases of the manufacturing process. He received the Master of Science degree in Textile Technology in June of 1950 and joined the Research Division, Chicopee Manufacturing Corporation, Chicopee Falls, Massachusetts. Until February, 1953, he conducted investigations on the physics of non-woven fabrics and their bonding materials.

He entered M.I.T. Graduate School in February, 1953 and held an appointment as a research assistant, working on a non-destructive test for adhesives. He entered the United States Army as a private in July 1954, and conducted research on the ballistic impact behavior of textile yarns and fabrics at Body Armor Branch, Biophysics Division, Directorate of Medical Research, Army Chemical Center, Maryland. In September, 1956, he returned to M.I.T. on a Coats and Clark Fellowship in the Textile Division, Mechanical Engineering Department.

He is married and has two daughters.

I. SUMMARY

This investigation was basically concerned with the translation of textile fiber properties to the tensile properties of non-woven bonded fibrous structures without the usual assumptions of Hookean behavior and product uniformity. It was an attempt to provide analytical procedure for use in the design of non-woven fabrics with specific properties. The general purpose was to determine the physical mechanisms governing the translation of fiber properties into the engineering properties of flexible fibrous structures. The immediate goal was to predict the properties of an ideal non-woven structure; one in which all components - fiber, bonding, and geometry - are fully utilized. At the same time, practical considerations of the manufacturing process were to be examined, in order to relate the real non-woven fabric to the ideal fabric. The program was divided into three phases:

1. To predict from the engineering properties in the orthotropic direction (under the assumptions of Hookean behavior), the engineering properties at various test angles to the orthotropic axes.
2. To isolate and study the mechanics of a small element of the fabric, a unit cell, which might serve as a model for analytical predictions, and whose mode of deformation can be reasonably justified.
3. To join these two phases, such that fabric properties can be predicted from the behavior of the unit cell and subsequently the fiber, and the geometric arrangement of fibers in the fabric.

The orthotropic theory for uniaxial tensile stress was applied to

tow non-woven fabrics of essentially straight fibers and bonded with a rigid binder. The mechanical properties with respect to the orthotropic axes were measured, and used to predict the properties in other test directions. The properties in these directions were then measured, and compared to the predicted values. The general agreement was good for the elastic modulus, E, the proportional stress limit, σ_p and the rupture stress, σ_m . The agreement for Poisson's ratio, ν , was fair, depending upon the validity of the assumption of fibers taking compressive stresses without buckling. No experimental data on Modulus of Rigidity, G, were obtained.

The fabric was examined microscopically to determine the simplest element for analysis which might reasonably be used to predict the properties of the fabric. A unit cell was selected, in which a number of fibers were present, and where the hypothetical boundaries of the cell could be expected to displace in a known manner under stress. The unit cell was taken as a square of sufficient size to negate any fiber ends; and within which a sufficient number of bonds per fiber allowed the strain in the fiber to be approximated by the strain induced by parallel displacement of the boundaries as if the fiber were bonded only at the boundaries. The use of this finite sized element as an analytical model allowed measurement of the relative orientation distribution of fibers within the cell, and subsequent determination of the average fiber orientation distribution of the fabric. Then for a hypothetical strain of the unit cell, the fiber strains could be found. These strains are converted to fiber stresses, and the components of the stresses summed to find the stress on the unit cell necessary to cause the given strain. In this manner, a stress-strain curve of the average unit cell (or the uniform fabric) was constructed. This same average unit cell

allowed prediction of Poisson's ratio and Modulus of Rigidity.

A fiber web theory was developed for the behavior of the average unit cell, or fabric, under the assumptions of straight fibers, with rigid bonds between fibers, and without fiber buckling. The boundary conditions of uniaxial tension were changed to meet better the actual test conditions. These were one stress real, σ_y, with $\sigma_x = e_{yx} = 0$. The boundary conditions. for uniaxial orthotropic theory were σ_y real, $\sigma_x = \sigma_{yx} = 0$. Either set of conditions for unit cell behavior could be used, but the former were applied in a general solution of the post-yield region of the fiber. The measured fiber orientation distribution, $\phi(\beta)$, was empirically fitted with a five term cosine power series, and equations develped for E, ν, φ G in the elastic region, dependent only on the fiber modulus, the constants of the $\phi(\beta)$ expression, and the direction of stress relative to the orthotropic axes of the fabric.

The same procedure using thepost-yield properties of the fiber gives, after translation of the secondary modulus intercept, the post-yield region of the fabric. Thus the entire stress-strain curve of the fabric under tensile stress in any direction can be predicted, using the behavior of the fiber and the average unit cell.

The observation that the unit cells were not identical, and that the fiber rupture elongations were variable, lead to an estimate of the distribution of rupture stress of the unit cells. This distribution, together with Peirce's "Weakest Link" theory, was employed to determine the rupture stress of a specific sample size, based upon the calculated rupture stress of the average unit cell, or uniform fabric. The original analysis was based on non-buckling fibers, but an approximation was made for the case where fibers would buckle under compressive stresses.

Rupture depends upon three fabric parameters, and was assumed to occur when the first fiber in the fabric failed. Thus for unit cells under equal force, the rupture stress of a number of unit cells is given by the rupture stress of the cell with 1) the minimum number of fibers and 2) the poorest orientation of fibers for stress in the given direction. The distribution of rupture stress was found from the joint distribution of 1) variation of number of fibers - area density - and 2) variation in rupture stress due to changes in the fiber orientation for cells of average area density. The standard deviation of the rupture stress of the unit cell was used in Peirce's "Weakest Link" theory to predict the rupture stress of a given size of specimen. These predicted data agree quite well with experimental data obtained for various gauge length specimens. Rupture stresses were predicted at various stress orientations to the orthotropic axes and found to agree well with the experimental data on the two fabrics tested.

Several practical aspects were considered, among them the effect of fiber length, fiber curvature, bunching of fibers, and different degrees of bonding of the fabric. A number of theoretical fiber orientations were examined, to illustrate the use of the fiber web theory in the design of non-woven fabrics with certain specified characteristics.

Certain conclusions are warranted, under the limiting assumptions:

1. For straight fibers*, flexible, non-woven fabrics and bonded with a rigid material: the measured properties in the orthotropic directions and at 45° to these axes allow the orthotropic theory for uniaxial tension to predict the elastic properties and rupture stress of the fabric in intermediate directions of stress.

*The restriction of straight fibers, and of rigid bonds, may prove, with further experimental evidence, to be unnecessary.

2. Under the assumptions of straight fibers, rigid bonds, and the concepts of the unit cell model and rupture: the fiber web theory predicts well the elastic and post-yield engineering properties of a bonded fabric from the engineering properties of the fiber and the fiber orientation distribution. From the variability of rupture stress of the unit cells, the rupture stress of various sizes of specimens can be predicted quite well. The boundary conditions of σ_y real, $\sigma_x = e_{yx} = 0$, appear to approximate more closely the given test arrangement. However, the fiber web theory can be adapted to any set of boundary conditions or stress conditions by the use of the complete orthotropic equations and the fiber web theory.

The rupture stress of non-woven fabrics has been shown highly dependent upon the local variations in fiber orientation and area density. In practical terms, this is a most important characteristic of the structure. The fiber web theory provides a bench-mark for the evaluation of new fiber orientations without manufacturing the fabric, and indicates the theoretical maximums for new processes under the specified conditions.

This investigation has provided the beginning of a complete theory of non-woven bonded structures, and a number of other areas of investigation are given in Recommendations, XIII.B.

II. INTRODUCTION

A. The Non-Woven Fibrous Structure: Definitions

The textile and paper industries are based on two of the oldest arts of man. For centuries, they have been thought of as two distinct processes, using different raw materials, and producing entirely different products. Yet in certain segments of both industries, the differences have been more in degree than in kind.

Paper-making was held to be the art of forming a suspension of short, cellulosic fibers in water and subsequently draining off the water to yield a matrix of intermingled fibers held together by the hydrogen bonding associated with finely divided cellulosic elements. The fibers generally employed were short (1-2mm in length) and stiff. Yet the long fibers of the Asiatic palms were used in Japan to make very decorative papers of fibers up to ¼" or more in length. Frequently, natural gums were added to the suspension of fibers to give added holding or bonding of the fibers.

Compare this to the segment of the textile industry making wool felts. Here the long wool fibers (1-4 inches in length) were formed into thick bolts or mats by the plying of many layers. In the absence of natural bonding, the felts were beaten, and mechanically manipulated to intermix thoroughly the wool fibers. The natural scaly surface and migration tendency of the wool fiber combined to increase the density of the fiber mat. The resulting fiber entanglement produced a self-supporting non-woven structure of textile length fibers.

Thus for many years, the practical dividing line between a paper or textile product was established on the basis of the length of fiber used. Natural textile fibers shorter than ½ inch could not be spun into yarn, and papers

employing the longer wood fibers were difficult to manufacture. This natural boundary designation of commercial fiber length was further justified by the properties and usage of the end products. Paper became characterized as opaque, smooth, dense, non-porous, and relatively stiff. Textile materials were more porous, not as dense, very flexible, and offered extremely small resistance to bias tension.

In the last 15 years, these distinctions have become more and more blurred. The development of synthetic resins allowed the paper-maker to use non-cellulosic fibers, for strength could be developed with fiber to fiber bonds not dependent on fibrillation of the cellulosic fiber ends. Creping gave paper more flexibility, and the new resins gave wet strength.

At the same time, these new resins gave the textile manufacturer a chance to by-pass the process of spinning and weaving and to form webs of textile fibers other than wool. Such products had much in common with paper. The two materials began to have more similarities than differences. The trade definition "non-woven" has come to mean a textile product because it has been made on textile fabricating machinery, and the fibers were of typical textile length. The papers made of non-paper type fibers (either longer or non-cellulosic fibers) have been called "specialty papers".

Only two major differences remain. The paper process uses water as the method of controlling and depositing textile fibers - fibers which are seldom longer than 3/8". The textile process employs solid mechanical devices or air as a deposition system, and generally uses fibers over 1" in length. All other differences are a result of the pre-determined process or subsequent treatment of the material.

For the purpose of this study, the term "non-woven structure" will refer to the product of either process. Thus a "non-woven" fabric is an essentially two-dimensional assemblage of textile-type fibers held together with some additive bonding material, resulting in a self-supporting web-like structure. Examples of a textile fabricated and paper-machine manufactured non-woven are shown as Exhibits I and II.

B. Purpose of the Study

The "non-woven" structure is becoming an important material for both consumer and industrial use. In 1956, 90 million pounds of non-woven materials were manufactured by the textile industry alone, representing 1.5% of the total fiber poundage produced in this year. (12)* Much has been claimed for the future of the non-woven, and no limits can be set as to its adaptability and applicability for certain uses. The literature contains many articles about market potential and possible developments, but very little has been published on the design criteria for the non-woven. It would appear that certain of the analytical techniques developed for other stress-carrying materials could be applied to the non-woven; and that a fundamental study might provide analytical tools to utilize the adaptability of the non-woven process to the utmost. The immediate questions are those of fiber properties, fiber arrangement, and the characteristics of the bonding system. The first two of these have been the subject of much investigation as applied to woven fabrics. The problems of translating fiber properties to yarn properties, and yarn properties to woven fabric properties, have received much study. The translation of fiber properties to yarn properties is generally predictable provided the yarn is maintained straight. The translation of yarn to fabric properties has met with less success. One of the major stumbling blocks has been the three dimensional nature of a woven fabric.

*Numbers underlined and in parentheses refer to the bibliography

The "non-woven" structure, on the other hand, is essentially two dimensional, and thus lends itself to two-dimensional stress analysis. With this immediate advantage, this investigation was undertaken with the following purpose:

TO DETERMINE THE PHYSICAL MECHANISMS GOVERNING THE TRANSLATION OF FIBER PROPERTIES INTO THE ENGINEERING PROPERTIES OF FLEXIBLE NON-FIBROUS STRUCTURES

The complete goal, of which this study is a part, is to provide a method of predicting, from the properties of the fiber and bonding agent, and their geometric arrangement in the structure, the general mechanical properties of the final non-woven material. In order to accomplish this, the major variables in the formation of a non-woven must be established, and some estimates made as to their relative importance.

The immediate objective is to gain a clearer understanding of the properties of an ideal non-woven structure; one in which all components fiber, bonding, and geometry - are fully utilized. Thus it is not the type of bonding, nor the particular bonding agent which is of interest; but whether or not the necessary idealizations are met. For the same reasons, the particular fiber used is unimportant. What is desired is a non-woven fabric in which the fibers are utilized to their utmost, and in terms of strength, this implies fiber failure rather than bond failure.

C. The Program

In order to study the non-woven fabric, the research program can be broken down into three main problems, as follows:

1. To predict theoretically, and measure experimentally, the gross engineering properties of orthotropic non-woven bonded fabrics.

In the majority of engineering applications, the stress-bearing material is considered isotropic; i.e., the engineering properties are the same in all directions. Any material which does not have this characteristic is called anisotropic; i.e., where the engineering constants, such as modulus of elasticity and modulus of rigidity, are not the same in all directions. Many materials are anisotropic, such as cold-rolled steel sheet, paper, and wood. One particular type of anisotropy occurs when the essentially two-dimensional material possesses two definite axes of symmetry at right angles to each other. Such a material is called orthotropic, and usually the engineering properties are specified for both axes of symmetry. Paper, wood, and woven textile fabrics are orthotropic. An analytical theory has been developed for wood and plywood (5-9) to predict the behavior of orthotropic materials when the principal stresses are not along the axes of symmetry. This theory is given in detail in III-A, and will be used to attempt prediction of the engineering properties of non-woven fabrics in the initial Hookean region. The analysis will take into account the effect of free fiber lengths between bonded areas, characteristic of flexible, or low binder content, non-wovens.

2. To isolate and study the basic building block or "unit cell" of the fabric. The "unit cell" can be considered as the simplest structural element in the fabric whose boundaries can be defined with some degree of confidence, justifying the necessary assumptions for an analytical approach. In the stress analysis of metals, the

differential element is chosen to be infinitely small, and all differential elements assumed uniform and homogeneous. This is done even if minute voids or cracks are known to be present, simply by changing the physical properties assigned to the differential elements. However, in a non-woven fabric containing fibers, bonds, and voids; homogeneity and uniformity are invalid assumptions on any differential element. The fabric will be studied microscopically to arrive at the geometrical form and size of the unit cell, and various analytical techniques will be used to establish the behavior of the unit cell in terms of the fibers and their geometry.

3. To join these two phases, such that the fabric deformations can be transformed into unit cell and subsequently fiber deformations; fabric stresses into fiber stresses; ultimately leading to the prediction of fabric properties from fiber properties. In this attempt, the restriction of Hookean behavior and perfect uniformity will be removed, in order to establish the importance of the actual fiber properties and of some of the manufacturing process variables on the properties of the fabric.

D. The Literature

As mentioned previously, almost all of the published literature on non-woven fabrics or papers has been concerned with applications. Very little has been published concerning the mechanical performance of these materials. This is understandable, although regretable, in view of the present state of the manufacturing art. In all phases of the industry, the techniques of manufacture are closely guarded secrets.

The only analytical approach to this subject was that of Cox (2) in 1951 with reference to paper. Cox analyzed the effect of fiber orientation on the stiffness and strength of paper and other fibrous materials. He hypothesized that the effects could be represented completely by the first three Fourier coefficients of the distribution function for a planar (two-dimensional) material, and that all possible types of elastic behavior could be represented by the composition of four sets of parallel fibers in appropriate ratios.

Further comment will be made upon his approach later, but it will suffice to note here certain of his restricting assumptions. Cox proposed the concept of an ideal matrix of fibers, perfectly homogeneous, with each fiber assumed to extend in one straight line throughout the body of the material and to be loaded only at its ends. Furthermore, he assumed that if compression loads exist, the fibers are so supported as to carry compression, or that the whole mat is subject to biaxial tension sufficient to annul any compressive component afterwards applied.

These assumptions severely limit the analysis of flexible non-woven fabrics composed of non-Hookean or plastic fibers, and thus a more general approach will be developed.

E. Experimental and Theoretical Limits on the Investigation

Some restrictions and assumptions must be made, in order to make any analysis possible. Certain of these limitations will be discussed later, notably the ones concerning fiber straightness and fabric uniformity. However, the following serve to define initially the scope of the investigation.

1. All non-woven fabrics will be considered as one material, or one ply, even if possessing two or more primary fiber orientations, in order that the analysis be confined to two dimensions. Thus all fibers are considered as lying in the plane of the fabric, and relatively light weight fabrics will be used in the experiments.
2. Flexible non-woven fabrics will be defined as structures which, although stiff, contain considerably less bonding agent than fiber, and, in which lengths of free fiber separate the bonded areas. Such flexible fabrics might be lightly impregnated, sprayed with binder, or the bonding agent applied or activated at separate discrete points (such as in fused Acetate fiber webs where the bonds are only at intersections of fibers, or in the MASSLINN* type printing).
3. Fabric bonding will be considered of such type and with suitable materials to produce the maximum amount of fiber failure. General problems of bonding (bond size and shape, adhesion of bonding agent to fiber, etc.) will not be considered within the scope of this investigation. The properties of the binder will be assumed to be proper to cause all of the extension of the fibers (and thus the fabric) to take place in the free lengths of the fibers between bonds. The size of the bonds will be negligibly small compared to the length of the fibers between bonds, so that the bond points can be considered <u>rigid points</u>.

* MASSLINN, Trade mark of Chicopee Mills, Inc., a non-woven with discrete, preselected bond areas.

4. A fabric was desired which most closely approximated a theoretical structure in which the unit cell could be easily visualized and analyzed. For this purpose, a "completely" oriented non-woven, with the fibers lying parallel, might appear most promising. However, it was desired to eliminate, as much as possible, the influence of resin binder properties and placement from the investigation. Obviously, the properties in the direction perpendicular to the fibers of such a highly oriented fabric depend almost entirely on the characteristics of the binder and its positioning in the non-woven.

   Since the properties of the resin-fiber bond are very difficult to determine, fabrics of somewhat less than perfect orientation were selected in order to make the transverse properties of the non-woven more dependent on the fiber properties, and less influenced by the binder and its placement in the fabric. A binder system was selected in which the elongation of the binder would be very small.

5. The initial limitation that fibers should be relatively straight and the fabric reasonably dense and uniform pointed toward a non-woven of short fibers manufactured by a wet process. One source of such fabrics is C. H. Dexter and Sons, Windsor Locks, Conn. whose Dexstar* papers are shown as Exhibits I and III. The present textile fabricated non-woven fabrics are structures with curled or crimped fibers, presenting many difficulties in the analytical approach.

* Dexstar, trademark of C. H. Dexter and Sons, Inc.

6. Experimental investigation is limited to the case of uniaxial tension even though it might be desirable to conduct experiments under biaxial stress conditions. The absence of literature on ideal fabric properties as a function of fiber orientation and the author's own experience in the field of non-wovens indicated that experimental information under uniaxial tensile loads was greatly needed. Only the treatment by Cox has taken into account the effect of fiber orientation on the non-woven fabric properties, and his work was not substantiated by experimental results. Both analytical and experimental investigations were deemed necessary to establish the simplest of theories for mechanical properties and rupture conditions. An applicable theory for tensile behavior will provide a bench mark for future investigators in the area of the mechanics of non-woven structures.

III. THE GROSS MECHANICAL BEHAVIOR OF ORTHOTROPIC MATERIALS

A. Theory

1. Transformation Equations For Stress and Strain

Consider a thin (essentially two-dimensional) sheet of material subjected to uniformly distributed loads applied at its edges and acting in the plane of the sheet.* This is a case of plane stress where the material is free to contract or expand in thickness. The stresses and strains in the sheet are referred to the orthogonal axes y and x, or to the orthogonal axes 1 and 2. The y axis makes an angle θ with the 1 axis, measured positively counterclockwise from the 1 axis to the y axis (Figure 3.1). The stresses are f_y, f_x, f_{yx} related to the y, x axes, and f_1, f_2, f_{12} related to the 1, 2 axes. Those stresses with a single subscript are direct stresses acting in the direction of the axis indicated by the subscript, a positive value indicating tension. Those with two subscripts are shear stresses associated with the axes indicated by the subscripts. Similarly, the strains are e_y, e_x, e_{yx}, e_1, e_2, and e_{12}. The two sets of stresses are related to each other by the equations

$$\begin{aligned} f_1 &= f_y \cos^2\theta + f_x \sin^2\theta + 2 f_{yx} \sin\theta \cos\theta \\ f_2 &= f_y \sin^2\theta + f_x \cos^2\theta - 2 f_{yx} \sin\theta \cos\theta \\ f_{12} &= -f_y \sin\theta \cos\theta + f_x \sin\theta \cos\theta + f_{yx} (\cos^2\theta - \sin^2\theta) \end{aligned} \qquad (3.1)$$

or

$$\begin{aligned} f_y &= f_1 \cos^2\theta + f_2 \sin^2\theta - 2 f_{12} \sin\theta \cos\theta \\ f_x &= f_1 \sin^2\theta + f_2 \cos^2\theta + 2 f_{12} \sin\theta \cos\theta \\ f_{yx} &= f_1 \sin\theta \cos\theta - f_2 \sin\theta \cos\theta + f_{12} (\cos^2\theta - \sin^2\theta) \end{aligned} \qquad (3.2)$$

*This analysis will follow closely that given by Erickson and Norris (9) following the treatment by Love (11) and is given in detail in order to consider carefully the assumptions involved.

FIGURE 3.1

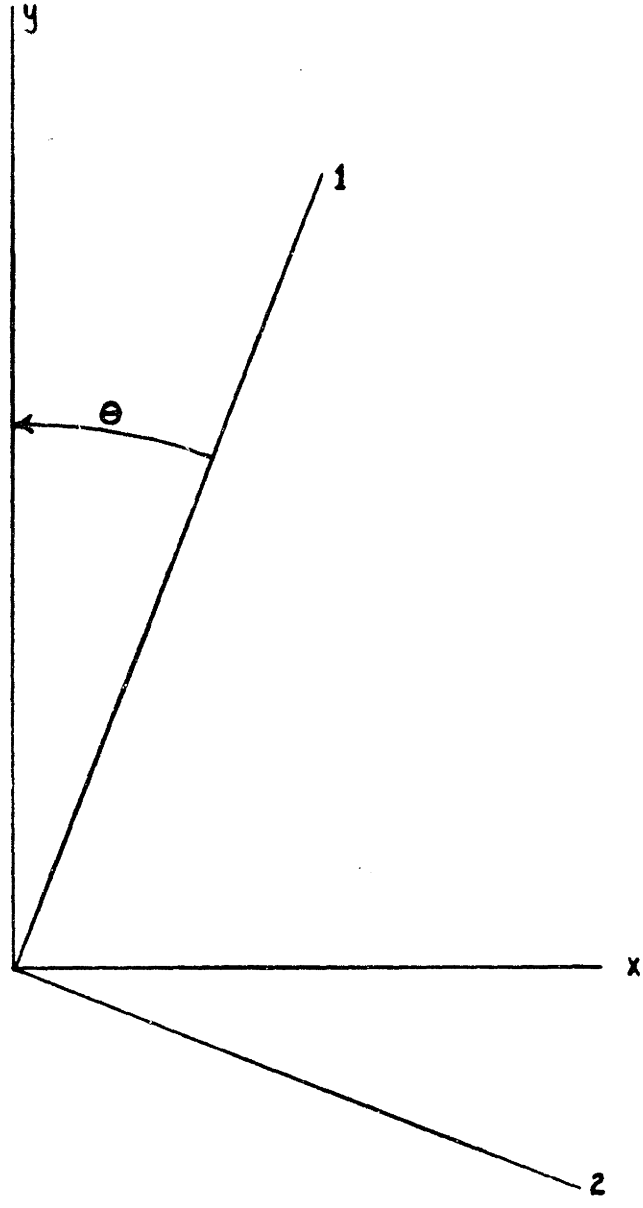

CHOICE OF AXES FOR MATHEMATICAL ANALYSIS

OF ELASTIC PROPERTIES

The two sets of strains are related to each other by the equations

$$\begin{aligned} e_1 &= e_y \cos^2\theta + e_x \sin^2\theta + e_{yx} \sin\theta\cos\theta \\ e_2 &= e_y \sin^2\theta + e_x \cos^2\theta - e_{yx} \sin\theta\cos\theta \\ e_{12} &= -2e_y \sin\theta\cos\theta + 2e_x \sin\theta\cos\theta + e_{yx}(\cos^2\theta - \sin^2\theta) \end{aligned} \tag{3.3}$$

or

$$\begin{aligned} e_y &= e_1 \cos^2\theta + e_2 \sin^2\theta - e_{12} \sin\theta\cos\theta \\ e_x &= e_1 \sin^2\theta + e_2 \cos^2\theta + e_{12} \sin\theta\cos\theta \\ e_{yx} &= 2e_1 \sin\theta\cos\theta - 2e_2 \sin\theta\cos\theta + e_{12}(\cos^2\theta - \sin^2\theta) \end{aligned} \tag{3.4}$$

The sets of equations 3.1 - 3.4 are obtained from purely geometrical considerations and equilibrium of forces, and therefore, are completely independent of the properties of the material to which they are applied. Their derivations may be found in any standard text on the theory of elasticity.

2. The Relations Between Stress and Strain

According to the generalized Hooke's Law, each strain is linearly related to the three stresses, resulting in 9 elastic constants for the material. These nine properties are not independent of each other because of the existence of a strain-energy function (See Appendix A). Furthermore, any additional axes of symmetry will further reduce the number of independent properties. The most general relations between strain and stress, in two dimensions, are given by

$$e_1 = a_{11} f_1 + a_{12} f_2 + a_{13} f_3$$

$$e_2 = a_{21} f_1 + a_{22} f_2 + a_{23} f_3 \qquad (3.5)$$

$$e_{12} = a_{31} f_1 + a_{32} f_2 + a_{33} f_3$$

The meanings of some of the coefficients in equations 3.5 are made evident by allowing two of the stresses to be zero. Thus;

$$a_{11} = \frac{1}{E_1} \qquad a_{22} = \frac{1}{E_2} \qquad a_{33} = \frac{1}{G_{12}} \qquad (3.5A)$$

where E_1 and E_2 are the moduli of elasticity in the 1 and 2 directions, and G_{12} is the modulus of rigidity associated with the 1 and 2 axes. Also by the Maxwell reciprocity relations (see Appendix A):

$$a_{12} = -\frac{\nu_{12}}{E_1} = a_{21} = -\frac{\nu_{21}}{E_2} \qquad (3.5B)$$

where ν_{21} and ν_{12} are Poisson's ratios of a contraction in the direction of the second subscript to an elongation in the direction of the first subscript, due to a tensile stress in the direction of the first subscript.

The values of a_{13} and a_{23} are applicable in the case of direct strains caused by shear stresses, and vice versa; and will be defined later.

3. Transformation Of The Stress-Strain Equations

Equations 3.5 may be transformed to refer to the x, y axes by use of equations 3.1 and 3.4. Let the stresses associated with the x, y axes be zero except one. Substitute this one stress in equations 3.1

to obtain values of $\underline{f}_1$, $\underline{f}_2$, and $\underline{f}_{12}$. These values substituted into equations 3.5 give the $\underline{1}$, $\underline{2}$ direction strains. These strains (e_1, e_2, e_{12}) are then substituted into equations 3.4 (one equation at a time) so that the ratios of the strains to the stresses associated with the $\underline{x}$, $\underline{y}$ axes are obtained. The transformed equations are:

$$
\begin{aligned}
e_y &= b_{11} f_y + b_{12} f_x + b_{13} f_{yx} \\
e_x &= b_{21} f_y + b_{22} f_x + b_{23} f_{yx} \qquad (3.6) \\
e_{yx} &= b_{31} f_y + b_{32} f_x + b_{33} f_{yx}
\end{aligned}
$$

where

$$
\begin{aligned}
b_{11} &= a_{11}\cos^4\theta + 2a_{13}\cos^3\theta\sin\theta + (2a_{12}+a_{33})\cos^2\theta\sin^2\theta \\
&\quad + 2a_{23}\cos\theta\sin^3\theta + a_{22}\sin^4\theta \\
b_{12} &= a_{12}\cos^4\theta + (a_{23}-a_{13})\cos^3\theta\sin\theta + (a_{11}+a_{22}-a_{33})\cos^2\theta\sin^2\theta \\
&\quad + (a_{13}-a_{23})\cos\theta\sin^3\theta + a_{12}\sin^4\theta \\
b_{13} &= a_{13}\cos^4\theta + (2a_{12}+a_{33}-2a_{11})\cos^3\theta\sin\theta + 3(a_{23}-a_{13})\cos^2\theta\sin^2\theta \\
&\quad + (2a_{12}+a_{33}-2a_{22})\cos\theta\sin^3\theta - a_{23}\sin^4\theta \qquad (3.7) \\
b_{22} &= a_{22}\cos^4\theta - 2a_{23}\cos^3\theta\sin\theta + (2a_{12}+a_{33})\cos^2\theta\sin^2\theta \\
&\quad - 2a_{13}\cos\theta\sin^3\theta + a_{11}\sin^4\theta \\
b_{23} &= a_{23}\cos^4\theta + (2a_{22}-a_{33}-2a_{12})\cos^3\theta\sin\theta + 3(a_{13}-a_{23})\cos^2\theta\sin^2\theta \\
&\quad - (2a_{11}-2a_{12}-a_{33})\cos\theta\sin^3\theta - a_{13}\sin^4\theta
\end{aligned}
$$

$$b_{33} = a_{33}\cos^4\theta + 4(a_{23}-a_{13})\cos^3\theta\sin\theta + 2(2a_{22}+2a_{11}-4a_{12}-a_{33})\cos^2\theta\sin^2\theta + 4(a_{13}-a_{23})\cos\theta\sin^3\theta + a_{33}\sin^4\theta$$

All of the equations given up to this point are perfectly general, and apply to all materials provided:

(a) That Hooke's Law is valid for the stress levels imposed.

(b) That the material does not creep with time.

(c) That no hysteresis effect is present in loading and unloading the specimen.

(d) That only small strains are considered.

It is the purpose of this study to examine the applicability of this theory to flexible non-woven fiber structures. Thus, experimental procedures will be established that tend to minimize the latter three assumptions, in order to test the first.

4. Orthotropic Materials

The equations developed above apply to the most general material, i.e., one which has only radial symmetry. If various additional symmetries are imposed, the coefficients in equations 3.5 assume particular values. If the material has one axis of symmetry (L), it also has another axis of symmetry (T), at right angles to it, because of the radial symmetry, and such a material is called orthotropic. It can be shown that

if equations 3.5 for such a material are written for the L and T axes, rather than the 1 and 2 axes, the values of a_{13} , a_{31} , a_{23} and a_{32} are zero. (Appendix A). Thus, equations 3.5 become

$$e_L = \frac{1}{E_L} f_L - \frac{\nu_{LT}}{E_L} f_T$$

$$e_T = -\frac{\nu_{TL}}{E_T} f_L + \frac{1}{E_T} f_T \qquad (3.8)$$

$$e_{LT} = \frac{1}{G_{LT}} f_{LT}$$

These equations (8) may be transformed to the axes x and y, by simply making the L axis the 1 axis, the T axis the 2 axis, with θ again measured positively counter clockwise from the L axis to the y axis. Thus, by the use of equations 3.6, the strains relative to the x, y axes are:

$$e_y = C_{11} f_y + C_{12} f_x + C_{13} f_{yx}$$

$$e_x = C_{21} f_y + C_{22} f_x + C_{23} f_{yx} \qquad (3.9)$$

$$e_{yx} = C_{31} f_y + C_{32} f_x + C_{33} f_{yx}$$

Relations 3.7 become:

$$C_{11} = \frac{\cos^4\theta}{E_L} + \frac{\sin^4\theta}{E_T} + \left[\frac{1}{G_{LT}} - \frac{2\nu_{LT}}{E_L}\right] \sin^2\theta \cos^2\theta$$

(3.10)
$$C_{12} = \left[\frac{1}{E_L} + \frac{1}{E_T} - \frac{1}{G_{LT}}\right] \sin^2\theta \cos^2\theta - \frac{\nu_{LT}}{E_L}\left[\sin^4\theta + \cos^4\theta\right]$$

$$C_{13} = \left[\frac{1}{G_{LT}} - \frac{2\nu_{LT}}{E_L} - \frac{2}{E_L}\right] \sin\theta \cos^3\theta - \left[\frac{1}{G_{LT}} - \frac{2\nu_{LT}}{E_L} - \frac{2}{E_T}\right] \sin^3\theta \cos\theta$$

$$C_{22} = \frac{\sin^4\theta}{E_L} + \frac{\cos^4\theta}{E_T} + \left[\frac{1}{G_{LT}} - \frac{2\nu_{LT}}{E_L}\right]\sin^2\theta\cos^2\theta$$

(3.10) cont.

$$C_{23} = \left[\frac{1}{G_{LT}} - \frac{2\nu_{LT}}{E_L} - \frac{2}{E_L}\right]\sin^3\theta\cos\theta - \left[\frac{1}{G_{LT}} - \frac{2\nu_{LT}}{E_L} - \frac{2}{E_T}\right]\sin\theta\cos^3\theta$$

$$C_{33} = 4\left[\frac{1}{E_L} + \frac{1}{E_T} + \frac{2\nu_{LT}}{E_L}\right]\sin^2\theta\cos^2\theta + \frac{1}{G_{LT}}\left[\cos^2\theta - \sin^2\theta\right]^2$$

In the event that only one stress acts, (f_y) as, for example, in a uniaxial tensile test (f_x , $f_{yx} = 0$); then the equations 3.9 and 3.10 reduce to the following:

$$e_y = C_{11} f_y$$

$$e_x = C_{12} f_y \qquad (3.11)$$

$$e_{yx} = C_{13} f_y$$

Equations 3.10 with certain manipulation, reduce to:

$$C_{11} = \frac{e_y}{f_y} = \frac{1}{E_y} = \frac{\cos^4\theta}{E_L} + \frac{\sin^4\theta}{E_T} + \left[\frac{1}{G_{LT}} - \frac{2\nu_{LT}}{E_L}\right]\sin^2\theta\cos^2\theta \qquad (3.12)a$$

$$C_{12} = \frac{e_x}{f_y} = -\frac{\nu_{yx}}{E_y} = -\frac{\nu_{LT}}{E_L} + \left[\frac{1}{E_L} + \frac{1}{E_T} + \frac{2\nu_{LT}}{E_L} - \frac{1}{G_{LT}}\right]\cos^2\theta\sin^2\theta \qquad b$$

$$C_{13} = \frac{e_{yx}}{f_y} = \left[\frac{1}{G_{LT}} - \frac{2\nu_{LT}}{E_L} - \frac{2}{E_L}\right]\sin\theta\cos^3\theta - \left[\frac{1}{G_{LT}} - \frac{2\nu_{LT}}{E_L} - \frac{2}{E_T}\right]\sin^3\theta\cos\theta \qquad c$$

$$C_{33} = \frac{e_{yx}}{f_{yx}} = \frac{1}{G_{yx}} = \frac{1}{G_{LT}}\cos^2 2\theta + 4\left[\frac{1}{E_L} + \frac{1}{E_T} + \frac{2\nu_{LT}}{E_L}\right]\sin^2\theta\cos^2\theta \qquad d$$

Knowledge of the material constants E_L , E_T , ν_{LT} , and G_{LT} will allow prediction of the corresponding constants for any arbitrary set of orthogonal axes. The moduli E_L and E_T can be measured directly. Determination of ν_{LT} requires simultaneous measurement of both e_L and e_T. A method for accomplishing this will be given in the following section.

The modulus of rigidity, G_{LT} , is difficult to measure directly. Even on rigid laminates of wood and fiberglass, to which this theory has been applied, no completely successful experimental method of determining G_{LT} has been found. Experience on plywood has shown that a better measure of G_{LT} is obtained by determining Ey when $\theta = 45^\circ$ (i.e. maximizing the term containing G_{LT} in coefficient C_{11}) and calculating G_{LT} from C_{11} . (9).

Since from Equation 3.5B:

$$\frac{\nu_{LT}}{E_L} = \frac{\nu_{TL}}{E_T} \qquad (3.13)$$

all five constants needed are determined. In order to satisfy the requirement of Hookean behavior, only the initial relatively elastic region of the stress-strain curve will be considered by this theory.

B. Experimental Procedure

1. Tensile Testing

All testing was carried out on a commercial electronic type of tensile tester ("Instron")*. The load sensing element consists of SR-4 strain

*"Instron", a trade name of Instron Engineering Corporation, Canton, Mass.

gauges, whose signal is amplified and plotted against time on a 10" strip recorder. A photograph of the tensile tester is shown in Figure 3.2. Provision is made for changes of the crosshead (lower jaw) velocity, and for the velocity of chart motion. The load cell used had a range of 1 to 50 pounds of force. The specimen jaws were self-aligning; jaw faces were 1-3/4" wide of rubber surfaced steel. All tests were performed at constant rates of strain.

2. Strain Measurements

Simplification of the preceding theory depends on a uniaxial tensile stress (f_y). Specimens should be long enough to allow free contraction of the center of the specimen (f_x=0), and to minimize clamping effects. The general rule in such cases (St. Venant's Principle) is that one specimen width away from the clamp, restraint conditions imposed by clamping will have disappeared. Thus for a specimen one inch wide, a length of at least three inches is necessary to provide one square inch in the center of the specimen under uniaxial tension. Preliminary testing indicated a large amount of fabric wrinkling, or corrugating, during application of load. As it was desired to measure transverse strain occurring within the fabric itself, in order to determine Poisson's ratio, some method of eliminating this wrinkling effect was necessary.

Several methods were tried, and two seemed satisfactory; 1) A dumbbell shaped specimen, with the center portion about 1/2 to 3/4 the maximum sample width; or 2) a specimen of uniform width supported at the center with a smooth plate designed to keep the fabric flat. Dumbbell or oddly shaped specimens were undesirable, since a comparison was needed between the strain as determined by the Instron, and strain measured directly between two marks on the specimen. Thus, a relatively long, uniform width

FIGURE 3.2

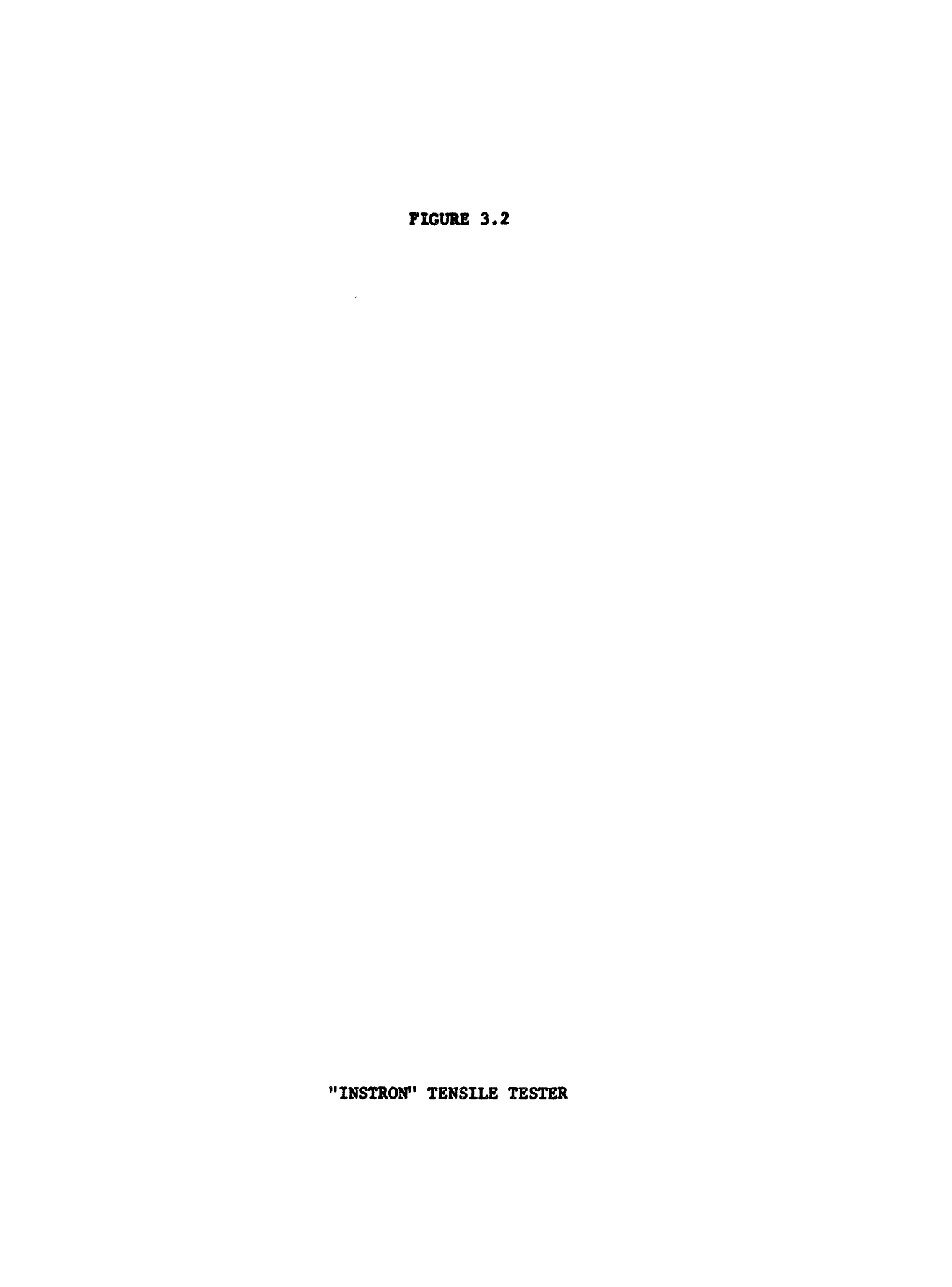

"INSTRON" TENSILE TESTER

specimen was selected; and the center of this specimen supported by a smooth backing plate. This plate was wider than the specimen and slightly longer than the distance between gauge marks, and was placed parallel to and slightly forward of the plane located by the jaw faces. As the selected gauge length for independent measurement of strain in the direction of stress (y)was 1-1/2 inches, the backing plate was made two inches long overall with the upper and lower edges bent away from the sample. This arrangement is shown diagramatically in Figure 3.3 and also, as mounted on the testing machine, in Figure 3.4. The presence of the backing plate altered slightly the condition of uniaxial stress, but experiments with the plate showed no change in the shape of the machine stress-strain curve of the unsupported specimen and less than a 5% lowering of the average rupture stress. The total gauge length of the specimen was selected as eight inches, in order to provide about three inches of unsupported specimen on either side of the backing plate. This permitted contraction without buckling on the backing plate.

Several methods of simultaneously measuring strain in both the y and x direction were considered, and a photographic procedure selected. This method offered ease of operation and more observations within the relatively short time to break, which was desired in order to minimize the effects of fiber creep and bond slippage. It was found that photographs could be taken every three seconds, and the rate of strain was selected as 6.25%-8% strain per minute, giving rupture times from 20 to 40 seconds.

A 35 mm camera with lens of 50 mm focal length was used. In order to enlarge the image on the film, the camera was fitted with a 20 mm extension tube. The arrangement gave an object to image reduction of 2.2: 1, or a

FIGURE 3.3

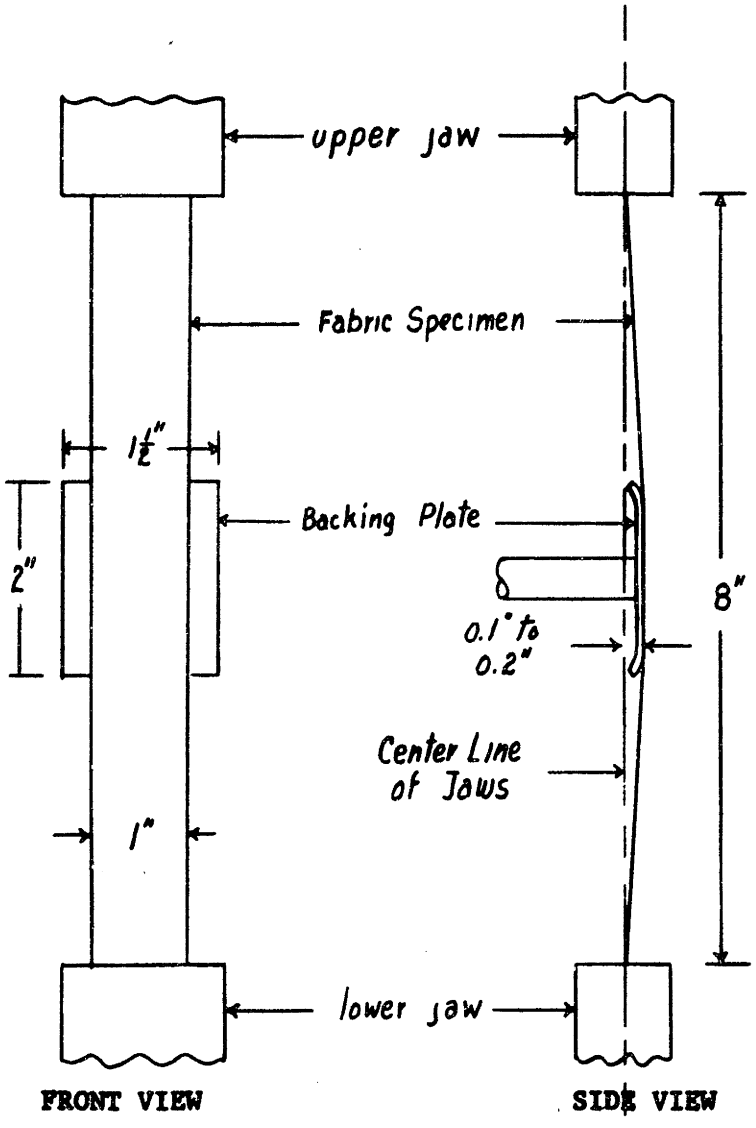

DIAGRAM OF SPECIMEN MOUNTED IN TESTER WITH BACKING PLATE

FIGURE 3.4

PHOTOGRAPHIC ARRANGEMENT FOR RECORDING FABRIC STRAINS

field of view of approximately 2 x 2.8 inches. The lens to object distance was 6.0 inches. In order to avoid vignetting of light at the corners of the film plane and to decrease distortion (and subsequent error); the lens opening was set at f:6.3. This gave no distortion in a 1" x 1½" section in the center of the field of view. Illumination was supplied by a Burton 100 watt Microscope lamp (with heat filter), placed to the left and below the specimen and eight inches away. This gave oblique lighting sufficient to photograph at an exposure of 1/20 of a second on high contrast Kodak Microfile film (Tungsten rating 16).

The gauge marks were placed on the fabric sample with a 2" x 2" rubber stamp, consisting of a grid of one-half inch squares (Figure 3.5). The sample was then mounted such that four horizontal lines (1½" in y direction) were always on the surface of the backing plate during the test.

The camera, light source and backing plate were mounted on a rigid framework surrounding the tester, but separate from it and attached to the table in order to minimize vibration (as shown in Figure 3.2 and 3.4). In operation, the specimen was placed in the jaws at a gauge separation of eight inches. The lower jaw (crosshead) was moved manually until the sample lay flat on the backing plate (a pre-tension of 2% of the rupture load). The camera was focused with the aid of a ground glass placed at the film plane, the film threaded in the camera, and the camera back closed. A photograph was taken to determine the control, or zero strain, gauge. The film was advanced for the next photograph and the recording chart started. Then the crosshead and a stopwatch were started at the same time, and after three seconds had elapsed, the camera shutter was tripped. The film was advanced, the shutter cocked and again tripped when the elapsed time was six

FIGURE 3.5

MARKING STAMP, GROUND-GLASS MAGNIFIER, AND

MARKED & UNMARKED FABRIC SPECIMENS

seconds. Successive photographs were taken in the same manner, the time of these photographs being selected according to the behavior of previous tests of samples at the same angle θ from the symmetry axis (L) to the test direction axis (y). The procedure was to alter the time between photographs such that three strain measurements could be made in the elastic region of the stress-strain curve, and three during the plastic region. Thus photographs were usually taken at 0, 3, 6, 9, 12, 15, 20, 25, etc. seconds until rupture. Since the relationship between the crosshead velocity and chart velocity was known, the displacement on the chart could be interpreted both as elapsed time in seconds, and as strain based on the original jaw separation.

Thus, if J is the original jaw separation in inches, C. H. the velocity of the crosshead in inches/minute, and C the velocity of the chart in inches/minute; the strain rate (S.R.) in %/minute is the ratio of C.H. to J. Similarly the ratio of S.R. to C. is the percent strain in the sample per inch of chart. Also the reciprocal of C multiplied by 60 is the number of seconds per inch of chart. Summarizing:

$$\text{Strain Rate (\%/min)} = \frac{\text{Crosshead Velocity (inches/minute)}}{\text{Original Jaw Separation (inches)}}$$

$$\frac{\text{Percent Strain}}{\text{Inch of Chart}} = \frac{\text{Strain Rate (\%/minute)}}{\text{Chart velocity (inches/minute)}}$$

$$\frac{\text{No. of Seconds}}{\text{Inch of Chart}} = \frac{\text{60 second/minute}}{\text{Chart velocity (inches/minute)}}$$

The Microfile film was tank developed in Kodak D-11 (a high contrast developer) for five minutes at 68° F., fixed and washed. Each frame or exposure is identified by a number already on the film, increasing numbers indicating increasing elapsed time. A reproduction of a typical strip of

film is shown in Figure 3.6. The high contrast is produced at the edges of the sample by painting the backing plate a flat black, such that the fabric edges can be used as gauge marks for the measurement of transverse contraction, e_x. Strain measurements were carried out in two ways. In the first method, the film was placed emulsion side up over an illuminated ground glass. A ten power ground-glass magnifier (Figure 3.5) with a 20 mm. scale divided into tenths of millimeters on its glass face was placed directly on the emulsion. One inch on the fabric corresponds to approximately 11 millimeters on the magnifier scale. Since the magnifier scale can be visually interpolated to one-fifth of each scale division, or .020 millimeters, the observational error is .020/11.0 or approximately 0.20% or 0.20% strain. For measurements of large strains in the fabric this method is quite satisfactory.

The second method was to place the film, emulsion side down, between two glass plates in a standard photographic enlarger, and to project the image onto unlined white paper. The magnification was usually about 11 times. Thus one inch on the fabric was about 5.5 inches when projected. The negative of the control was measured first and light pencil marks placed on the paper at both edges of the sample at two separate places, providing two original lengths for the determination of transverse strain, e_x. Along the direction of the sample, two sets of marks were placed in the center of the gauge marks which were 1½" apart on the sample, providing two original lengths for the determination of longitudinal strain, e_y. Successive photographs were examined, and the displacement of one of the marks noted with the film positioned so as to match the other mark made for the control for that set. The distance between marks was then measured in scale units of 50ths of an inch, estimated to one-fifth of a scale unit,

FIGURE 3.6

PHOTOGRAPHIC RECORD OF SUCCESSIVE STATES OF STRAIN

or 1/250 of an inch. Thus the measurements are accurate to 1/250 x 1/5.5 or about 0.10% or 0.10% strain. This is about the error involved in originally placing the pencil marks and is about the best accuracy with fabric gauge marks of one or one and one-half inches. Increased accuracy requires larger gauges on the fabric.

Measurements of this type result in data as shown in Table 3.1. The table shows length measurements as a function of time, the conversion of lengths to strain, as well as the conversion of time to force in kilograms/inch width, as taken from the Instron chart. The final three lines of Table 3.1 constitute the desired information; i.e., $\underline{e_x}$ and $\underline{e_y}$ for various levels of $\underline{f_x}$, $\underline{f_y}$.

3. Fabric Material

It was desired to obtain a commercial material which most closely satisfied the limitations cited in section II.E. The original concept of translating fiber properties to fabric properties of an orthotropic structure, together with the restrictions of relatively thin fabrics of straight fibers bonded with a rigid material, seriously limited the choice of material.

All non-woven fabrics formed from typical textile fibers (approximately 1½ denier, 1-3 inches long) by processing mechanically or in air have curled or crimped fibers. Those fabrics composed of shorter fibers (less than 0.5") and formed in water have relatively straight fibers. The major source of water-laid textile fiber non-wovens is C. H. Dexter and Sons, Inc. Inquiries of this firm indicated a number

TABLE 3.1

TYPICAL PHOTOGRAPHIC MEASUREMENTS OF STRAINS

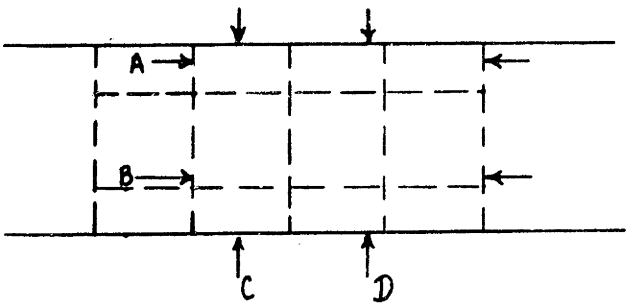

Time, secs.		0	3	6	9	12	15	20	25	35
Lengths	A	437.5	438.5	439.7	441.4	442.0	442.0	444.0	448.0	453.0
in 1/50"	B	437.2	438.5	440.0	441.2	442.2	442.2	444.5	447.0	451.5
	C	279.5	278.0	277.5	276.0	274.5	273.2	269.0	266.0	251.5
	D	280.0	278.8	277.2	276.6	275.5	274.0	271.5	26.50	252.0

Strains,	A	0	.23	.50	.89	1.02	1.02	1.48	2.4	3.55
%	B	0	.30	.64	.92	1.14	1.14	1.66	2.24	3.27
	C	0	- .54	-.71	-1.25	-1.78	-2.25	-3.75	-4.80	-10.00
	D	0	- .41	-.96	-1.16	-1.54	-2.05	-2.90	-5.1	- 9.6

Average	$\bar{e}_y$	0	.27	.57	.91	1.08	1.08	1.57	2.32	3.42
Strain	$\bar{e}_x$	0	- .48	-.84	-1.21	-1.66	-2.15	-3.33	-4.95	- 9.8
Force,	f_y	0	.66	1.23	1.68	1.89	2.07	2.30	2.42	2.60

kilograms
inch width

of materials in the desired weight range, but the highest orientation available with adequate binder at that time was approximately a 5:1 ratio of moduli. This material was selected as Fabric A for the first phase of the program; i.e. to determine if the orthotropic theory will predict the performance of a fibrous structure when the fibers are not embedded in a resin matrix. The specifications follow:

Fabric A. (Dexstar #210) - See Exhibit I

Nominal weight - 10# ream or 10#/380 sq. yards

Actual weight at 65% RH - 16 grams/sq. yard

Fiber - Regular tenacity viscose rayon, 1½ denier ¼" to 3/8" in length.

Binder - Regenerated viscose solution, 1 to 2% on weight of fiber.

Formation - Uniform weight with very few clumps of fibers; and apparently uniform orientation of fibers. Furnished in 24" x 36" sheets.

C. EXPERIMENTAL DATA

1. Conversion of Force/unit Width to Specific Stress

The general orthotropic equations (III.A) have been derived in terms of stresses defined in the usual manner as force/unit area. However, the experimental procedure determines force/unit width for a given fabric weight/unit area. No problem arises as long as comparison is made on fabrics of the same weight/unit area, but it is desirable to establish some uniform system of designating stresses.

Textile fiber strengths and stresses are defined in terms of force/weight/particular length. In the case of synthetic fibers, stresses are usually given in grams/denier, where denier is defined as the weight in

grams of 9000 meters of fiber or yarn. Then the weight of a unit width of non-woven fabric 9000 meters long is its equivalent denier. Dividing the measured force/unit width by this equivalent denier gives specific stress in units of grams/denier.

For example, one square yard of Fabric A weighed 16 grams at 65% R.H. A strip one inch wide and one meter long weighs 16 x 1/36 x 39.4/36 or .486 grams; and 9000 meters one inch wide weighs 9000 x .486 = 4380 grams. Thus the equivalent denier of a one inch wide specimen of Fabric A is 4380 (or 4400) denier, and if the rupture load for a one inch wide specimen were three kilograms, the specific rupture stress for this fabric would be $\frac{3000}{4380}$ = .685 grams/denier (gpd)*.

2. Specific Stress-Strain Curves at Various Angles

The rate of strain was selected as 6.25%/minute, in order to give rupture times of 20-40 seconds, or 2-4% elongation to rupture. The use of relatively short times to break minimizes any time effects, or creep, in the fabric; and the 4% maximum elongation justifies the use of small strain approximation. Since the specimen is ruptured during the initial loading cycles, no hysteresis effect enters. Thus three of the four conditions for orthotropic theory are satisfied (III.A.3) and the analysis can be used to test for Hookean behavior.

As indicated previously, a long specimen of uniform width was selected in order to compare the photographically measured strain in the center of the specimen with the strain obtained from the Instron chart.

* The abbreviation gpd for grams/denier will be used hereafter in both text and figures.

With a gauge length of eight inches, specimens were cut 10" x 1".

One 24" x 36" sheet of Fabric A was divided in half, and the edges of one piece reversed. Specimens were cut from both sheets simultaneously. All of the specimens were tested with the backing plate in position. The plate was set 0.2" forward of the jaw centerline for angles of θ from 0° to 30°, and 0.1" forward for angles of θ from 45° to 90°. Three or four specimens, selected randomly from the total number of specimens at that angle θ were photographed for determination of transverse strain. The remaining specimens were tested to insure that the photographed specimens were a representative sample. At least six specimens were tested at each angle of test θ. The strains as a function of time and stress were measured by one of the two procedures described, as illustrated by Table 3.1 The final three lines of this table give the desired information. This data is summarized for four specimens in Table 3.2, giving the information for the four photographed specimens in the $\theta = 0^{\circ}$ (L) direction. The last two lines of the table give the average stress of the four specimens for given strain levels determined from the original 8" gauge of the specimen (Instron Data). The results of Table 3.2 are plotted in Figure 3.7, as specific stress (gpd) vs. percent strain. The plotted points indicate the close agreement between the average curve as obtained from the Instron chart based on original jaw separation, and the strain measured over 1½" in the center of the specimen. The symbol $\oplus$ indicates the average rupture point (or Specific Rupture Stress) of the photographed

TABLE 3.2

FABRIC A, STRESS - STRAIN DATA, $\theta = 0$ (L)

Specimen										
	Time, sec.	0	3	6	9	12	15	20	25	35
X	σ_y, gpd	0	.15	.28	.38	.43	.47	.52	.55	.59
	e_y	0	.27	.57	.91	1.08	1.08	1.57	2.32	3.42
	e_x	0	.48	.84	1.21	1.66	2.15	3.33	4.95	9.8
	Time	0	3	6	9	12	15	20	25	35
12	σ_y	0	.13	.27	.36	.42	.46	.49	.53	.55
	e_y	0	.28	.53	1.11	1.38	1.70	2.45	2.92	3.30
	e_x	0	.53	1.02	1.02	1.50	2.21	3.35	4.85	7.45
	Time	0	3	8	13	18	24	31		
3	σ_y	0	.14	.34	.44	.48	.52	.53		
	e_y	0	.42	.93	1.41	1.85	2.19	2.82		
	e_x	0	.40	.82	1.34	2.09	3.05	4.5		
	Time	0	4	8	12	16	20	25	30	
10	σ_y	0	.18	.32	.40	.44	.47	.50	.52	
	e_y	0	.36	.70	1.12	1.65	2.18	2.48	3.2	
	e_x	0	.36	.77	1.46	2.16	3.2	4.6	6.8	
Instron	e_y	0	.31	.63	.94	1.25	1.88	2.5	3.13	3.75
Data	$\bar{\sigma}_y$	0	.15	.27	.37	.42	.47	.51	.54	.57

FIGURE 3.7

FABRIC A, STRESS-STRAIN CURVE, $\theta = 0^{\circ}$ (L)

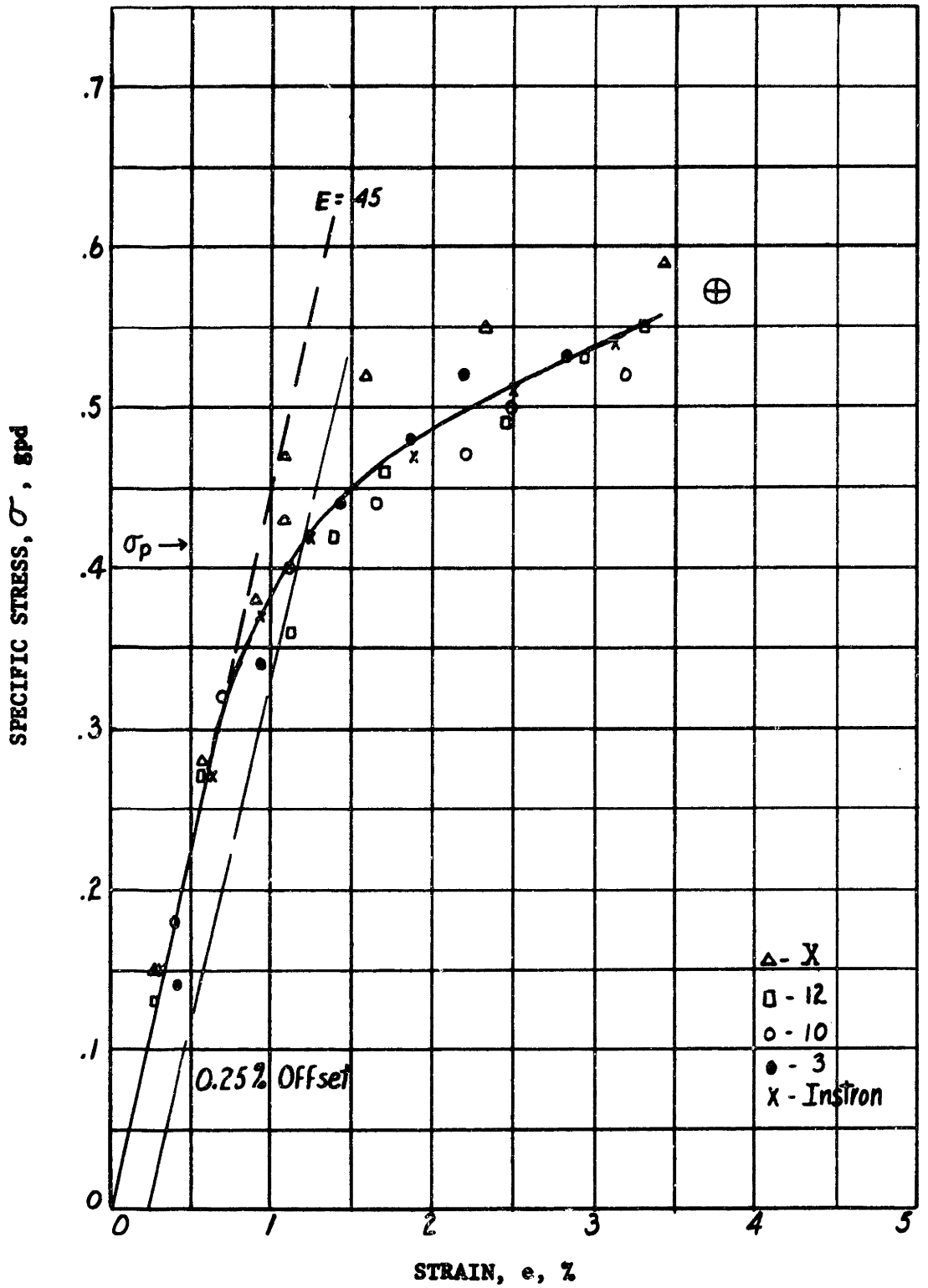

specimens. The dashed line gives the initial specific modulus, E, of the fabric in gpd. The specific proportional limit stress is indicated by σ_p, and was arbitrarily chosen as 0.25% strain offset from the initial modulus line.

Similar curves are given for $\theta = 15^\circ$, 30°, 45°, 60°, 75°, and 90°, as figures 3.8 through 3.13 inclusive. The Instron stress-strain curves agree quite well with the photographic measurements of the center of the specimen, except for $\theta = 60^\circ$ and 75°, where both average Instron and average photographic curves are shown.

When testing specimens at $\theta = 60^\circ$ or 75°, the fiber tensions develop components both parallel and perpendicular to the direction of jaw movement. The unbalanced perpendicular components distort (or shear) the whole specimen into a letter -S- or letter -Z- form. The shear deformation at the center of the specimen and the distortion of the specimen near the jaws combine to give larger normal strains between jaws than those observed photographically at the center of the specimen. This is the result (as is known for orthotropic materials) of shear stresses causing normal strains. Thus the stress-strain curves obtained from recording jaw movement will always lie to the right of those obtained by means of photographic measurement. Both stress-strain curves are given for $\theta = 60^\circ$

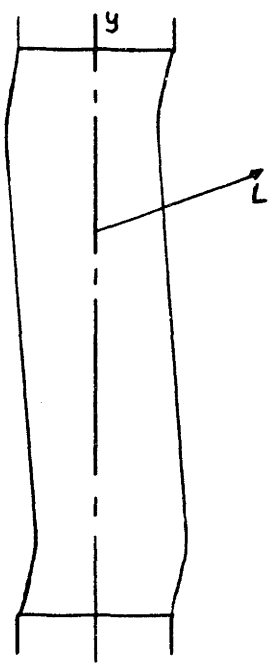

FIGURE 3.8

FABRIC A, STRESS-STRAIN CURVE, $\theta = 15^{\circ}$

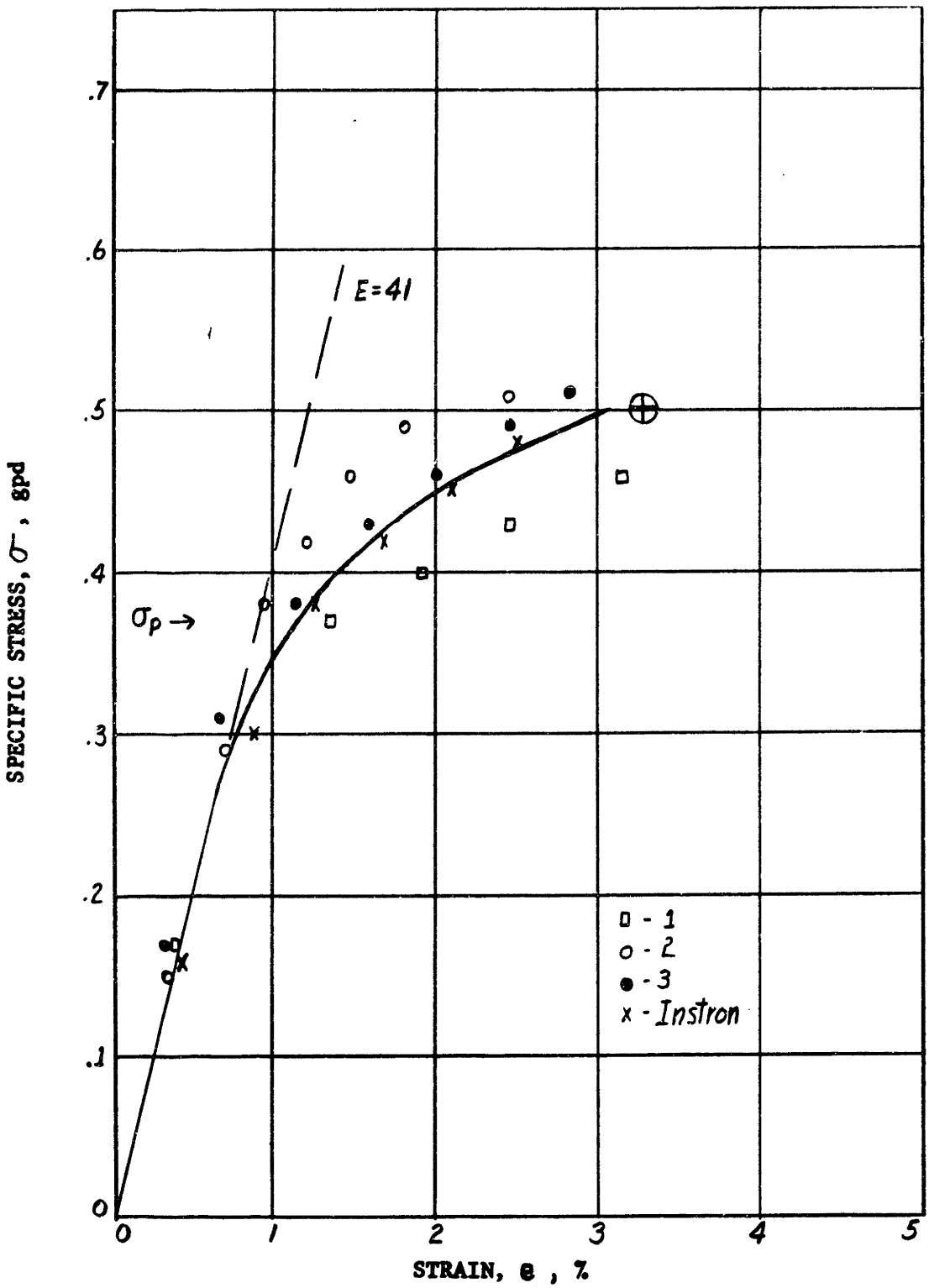

FIGURE 3.9

FABRIC A, STRESS-STRAIN CURVE, $\theta = 30^{\circ}$

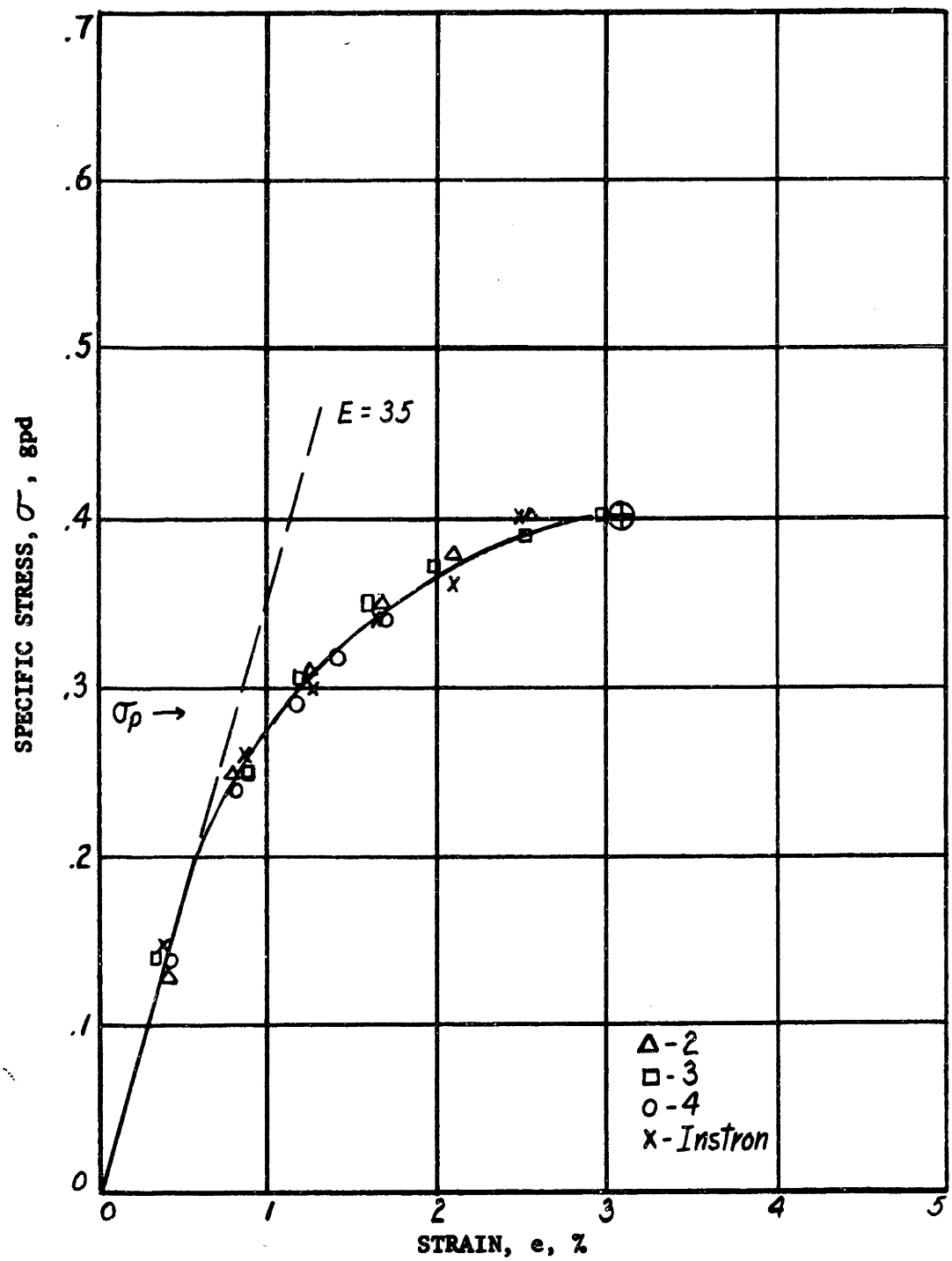

FIGURE 3.10

FABRIC A, STRESS-STRAIN CURVE, $\theta = 45^{\circ}$

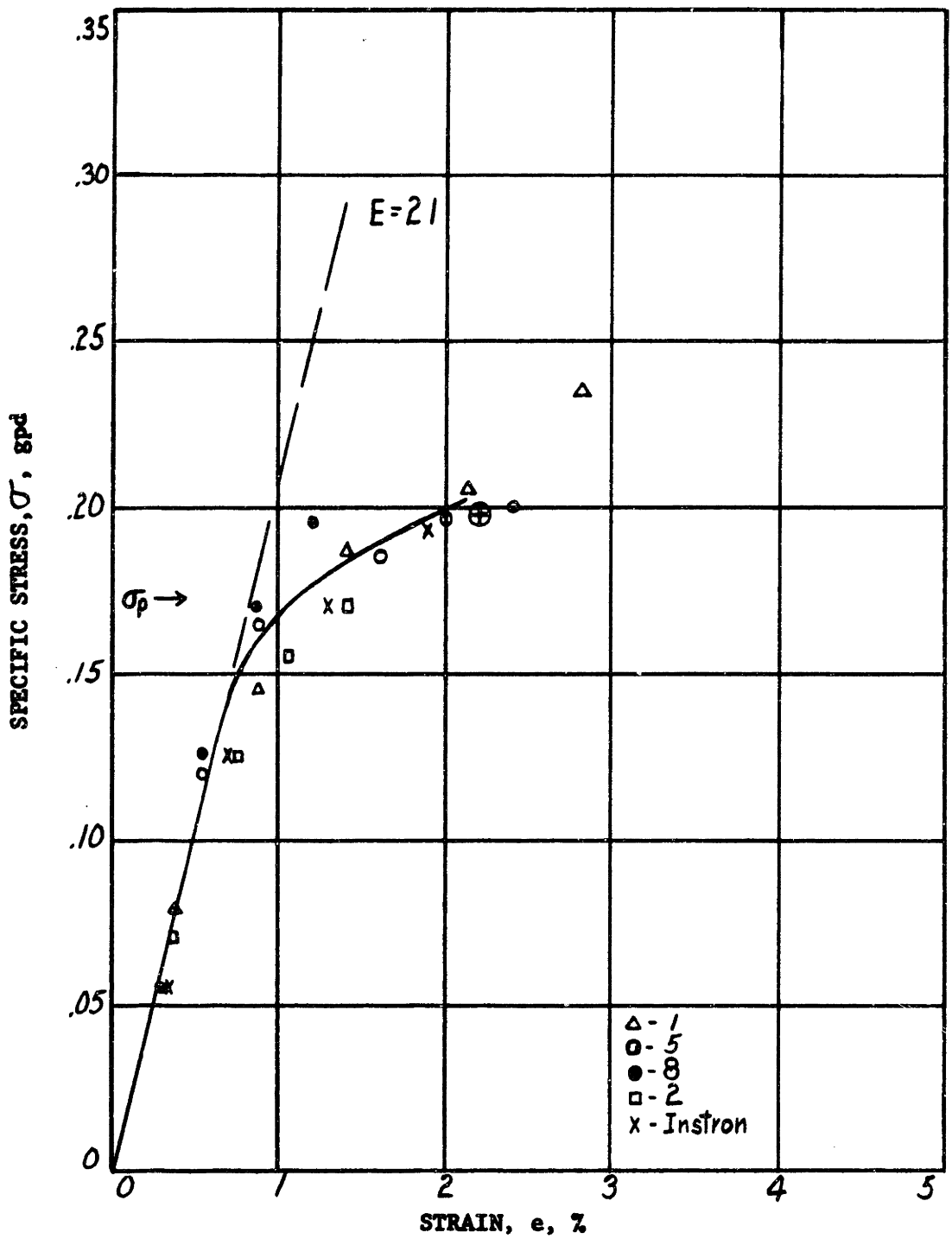

FIGURE 3.11

FABRIC A, STRESS-STRAIN CURVES, $\theta = 60^{o}$

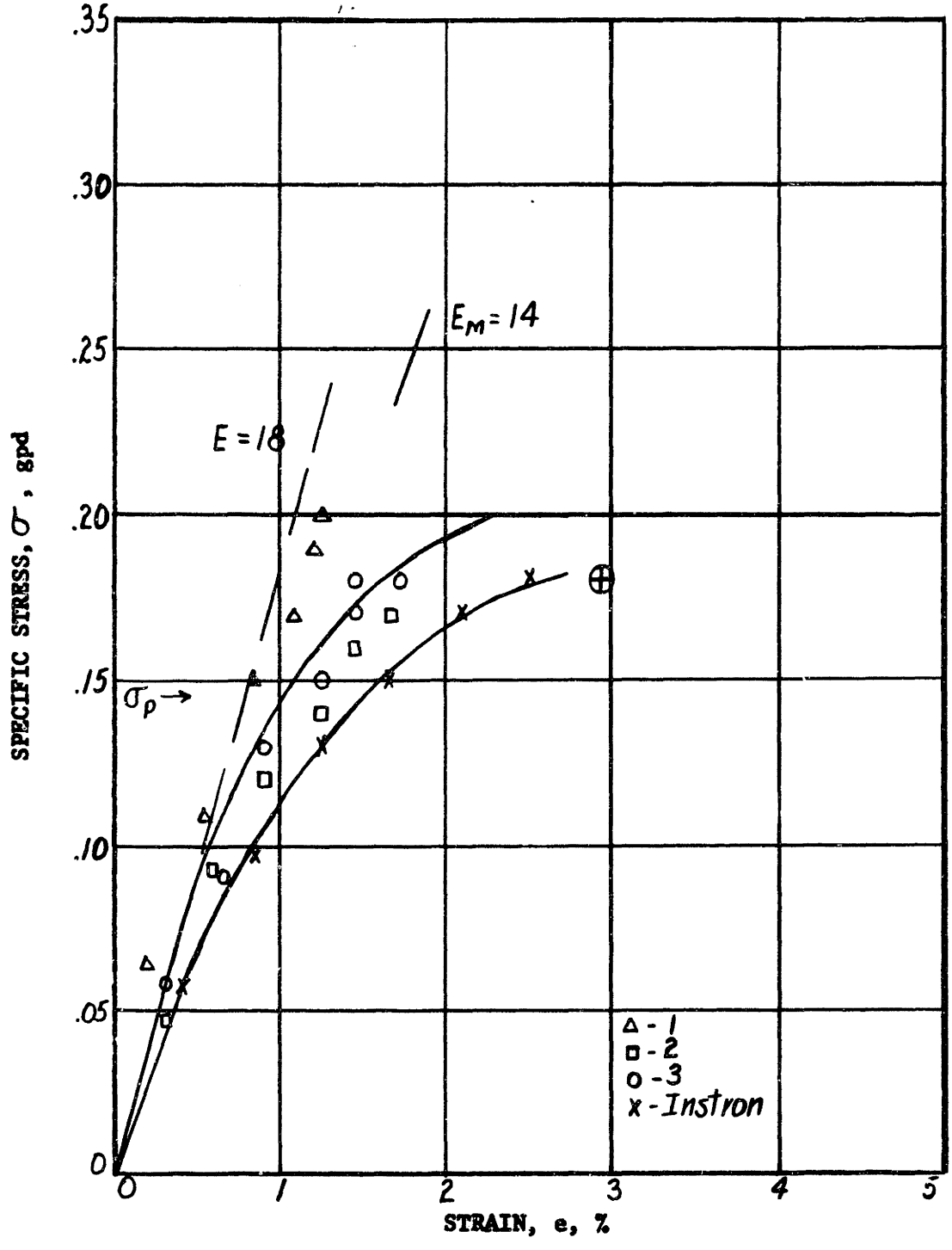

FIGURE 3.12

FABRIC A, STRESS-STRAIN CURVE, $\theta = 75^{\circ}$

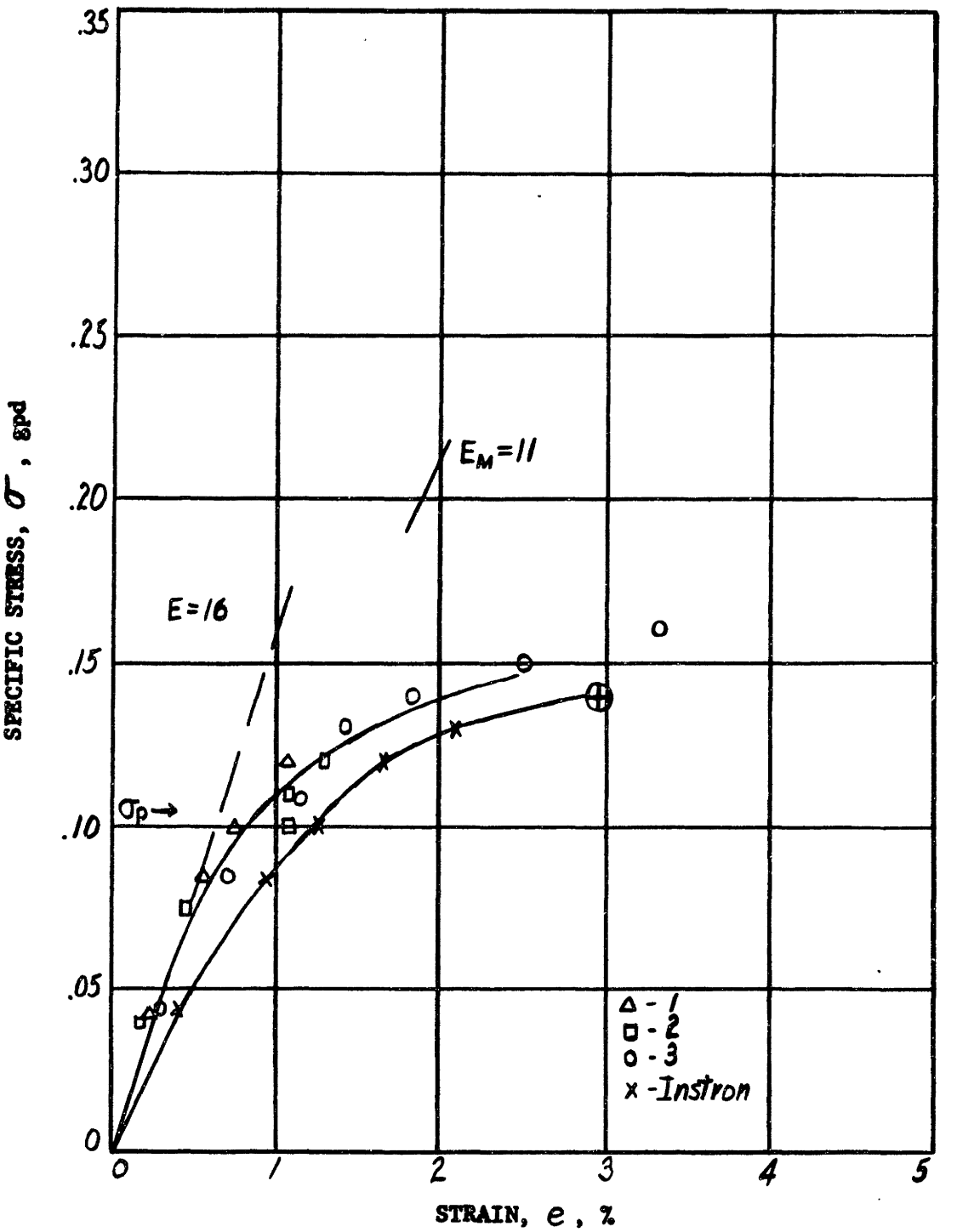

FIGURE 3.13

FABRIC A, STRESS-STRAIN CURVE, $\theta = 90^\circ$ (T)

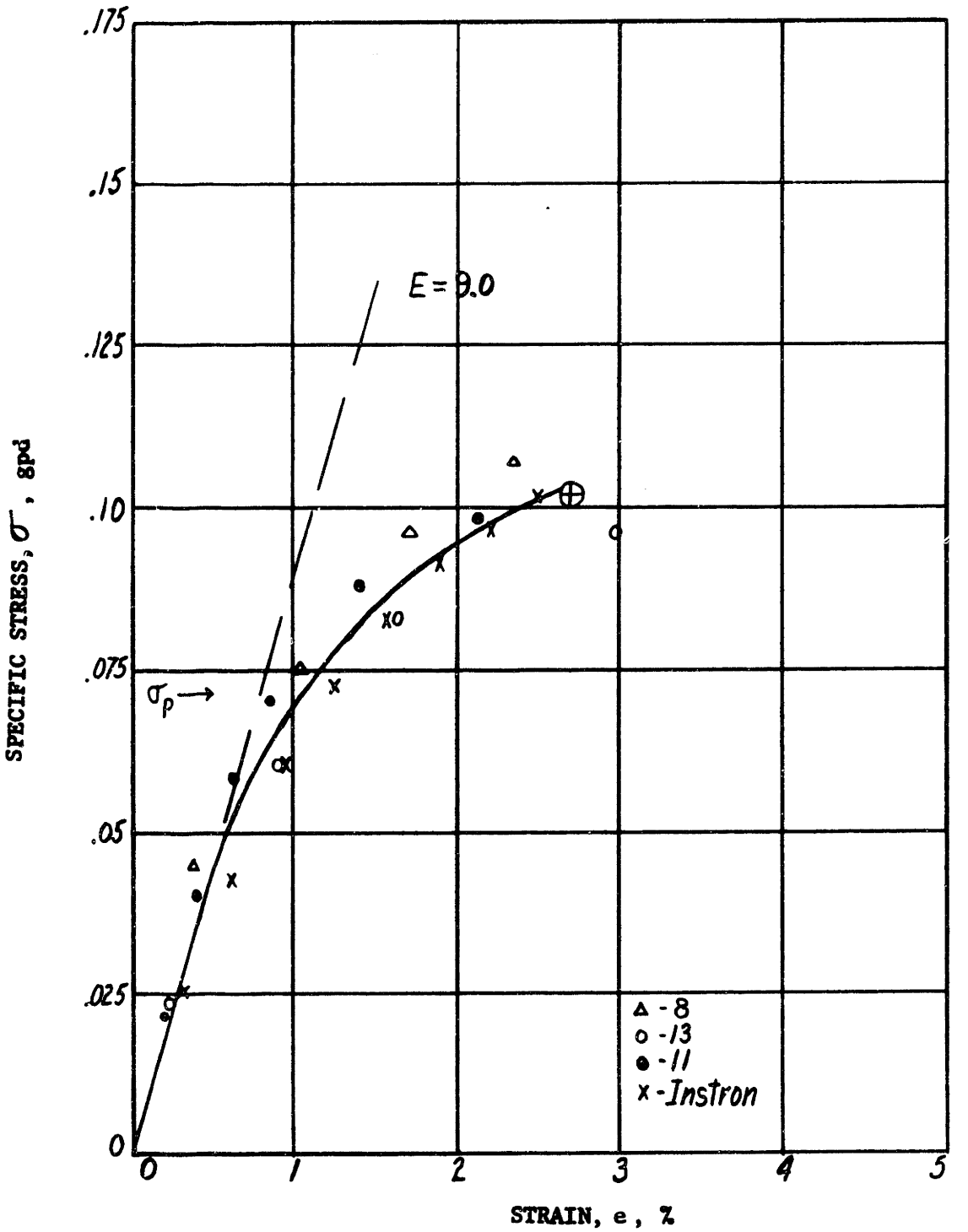

and 75° (Figure 3.11 and 3.12). The average of the two curves is used in the composite smooth curves at all seven angles given by Figure 3.14.

Figure 3.14 shows behavior typical of unbalanced ($E_L/E_T \neq 1$) orthotropic materials, i.e. a decrease in specific modulus and rupture stress as θ increases from 0° to 90°, or from the strong axis (L) to the weak axis (T). There is no consistent change in rupture elongation. However, if the photographic rupture strains were used in the cases where $\theta = 60^{\circ}$ and 75°, (see dotted terminals) rupture strain might appear to decrease from the orthotropic axes L and T and approach a minimum near 45°.

FIGURE 3.14

FABRIC A, COMPOSITE STRESS-STRAIN CURVES

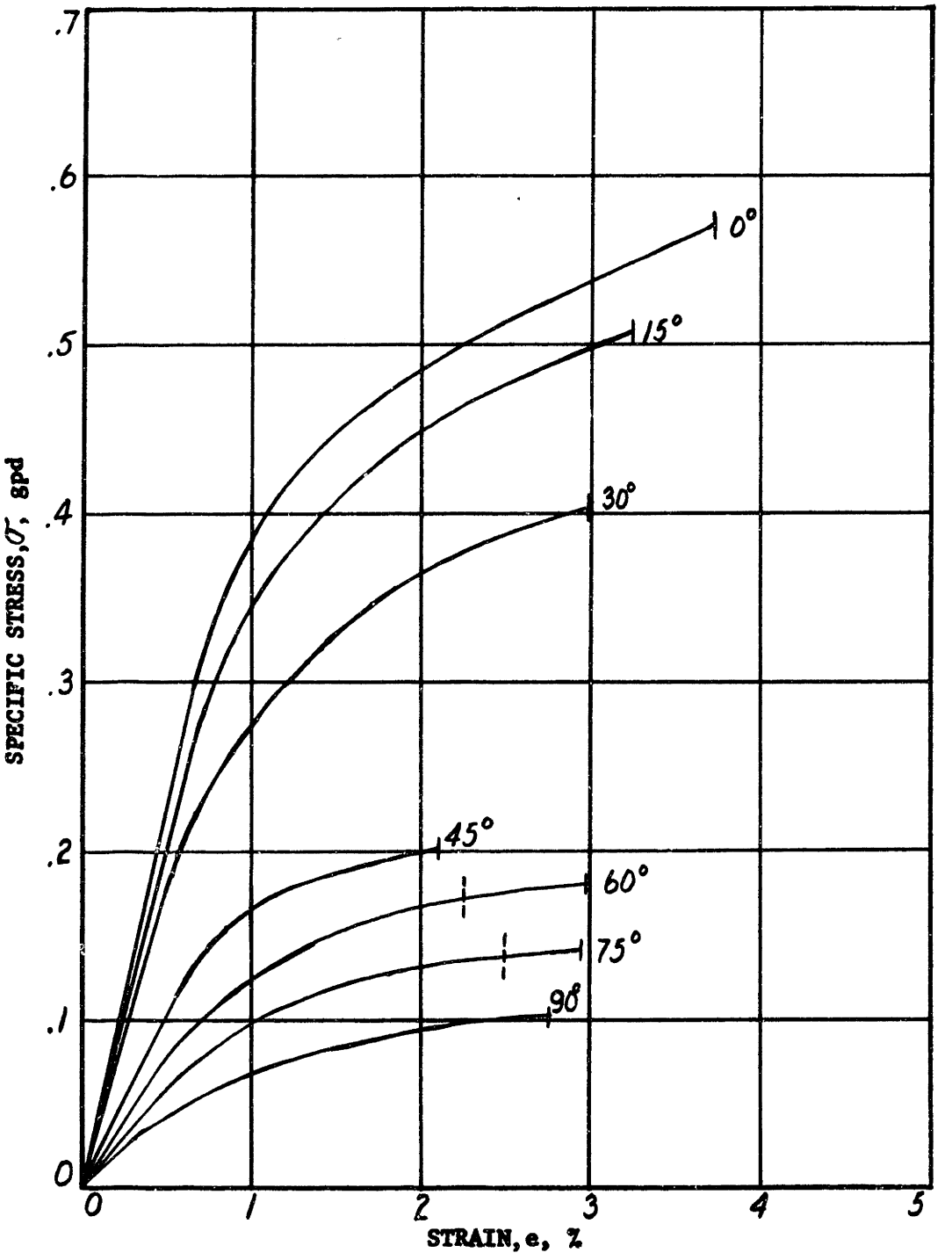

3. Poisson's Ratio at Various Angles θ

The data of ε_x and ε_y obtained from the photographic measurements, as exemplified by Tables 3.1 and 3.2, can be used to determine the Poisson's ratio. This ratio is defined in the usual manner as the ratio of the percentage contraction in the x direction to the percentage elongation in the y direction due to a stress in the y direction. Thus when the transverse strain contraction is plotted versus the longitudinal elongation, the slope of the curve gives Poisson's ratio ν_{yx}. Such a plot is given for $\theta = 0^\circ$ (L), or ν_{LT} in Figure 3.15. The function described by the observed data has been approximated by two straight lines giving $\nu_{LT} = 1.25$ for ε_L less than 1.25% and $\nu_{LT} = 2.30$ for ε_L greater than 1.25%. In actuality, Poisson's ratio is practically constant up to the specific proportional limit stress and continually increases thereafter. However, in the use of orthotropic theory, the calculations will be restricted to the region of constant modulus, or the Hookean portion of the stress-strain curve.

Figures 3.16 - 3.19 inclusive give the same information for $\theta = 15^\circ$, 30°, 45°, 60°, 75°, and 90°. The results for angles of θ from 0° to 45° are quite satisfactory. For $\theta = 60^\circ$, 75° and 90°, the scatter in the data is quite large, and only approximate values are given, obtained by averaging all the ratios over the entire stress-strain curve. As previously mentioned, the observational error involved in strain measurements is about 0.1% strain. For small lateral contractions, the one inch gauge is not satisfactory for determining Poisson's ratio to a high degree of accuracy.

FIGURE 3.15

FABRIC A, POISSON'S RATIO, $\theta = 0^{\circ}$ (L)

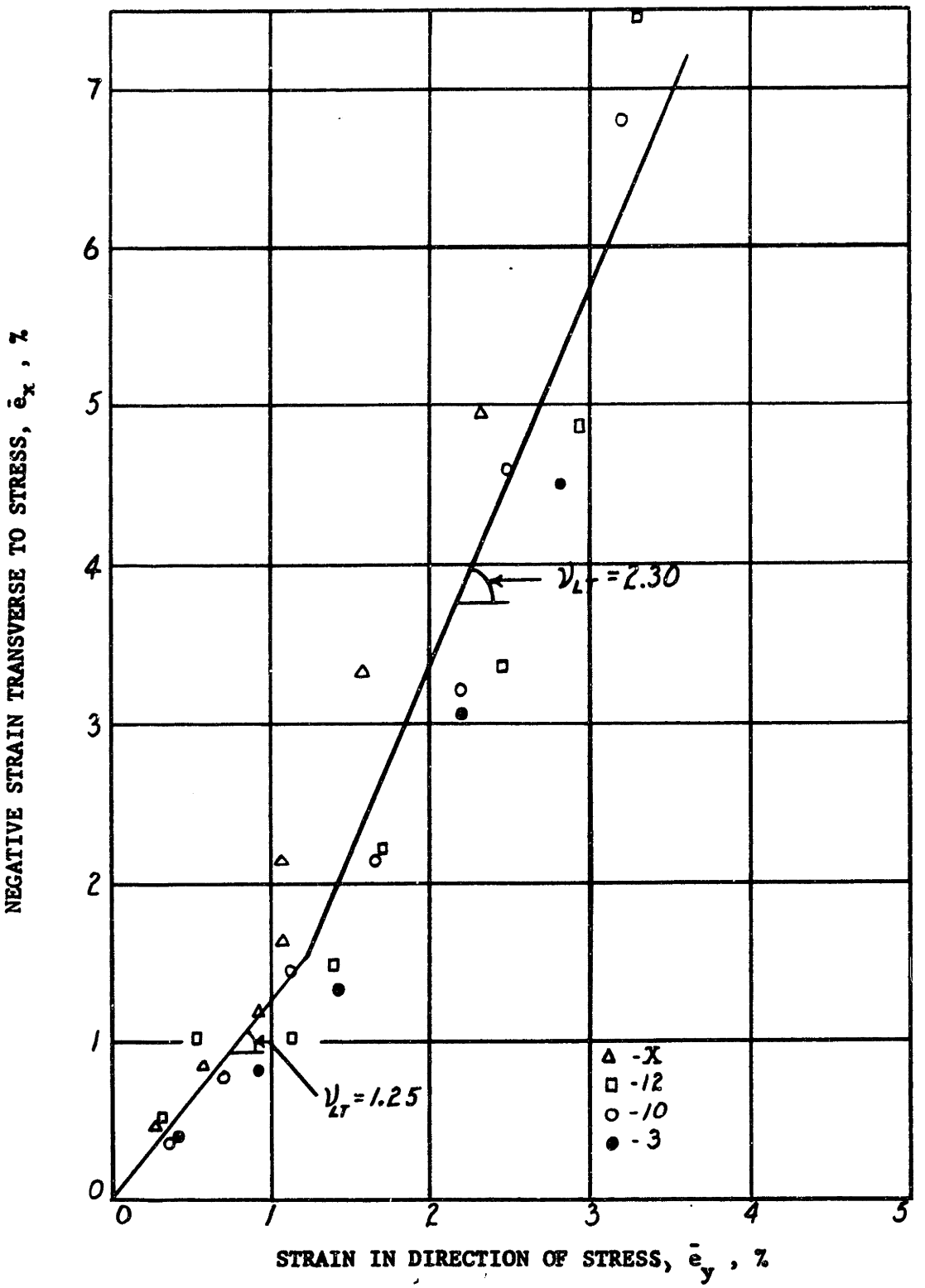

FIGURE 3.16

FABRIC A, POISSON'S RATIO, $\theta = 15^{\circ}$

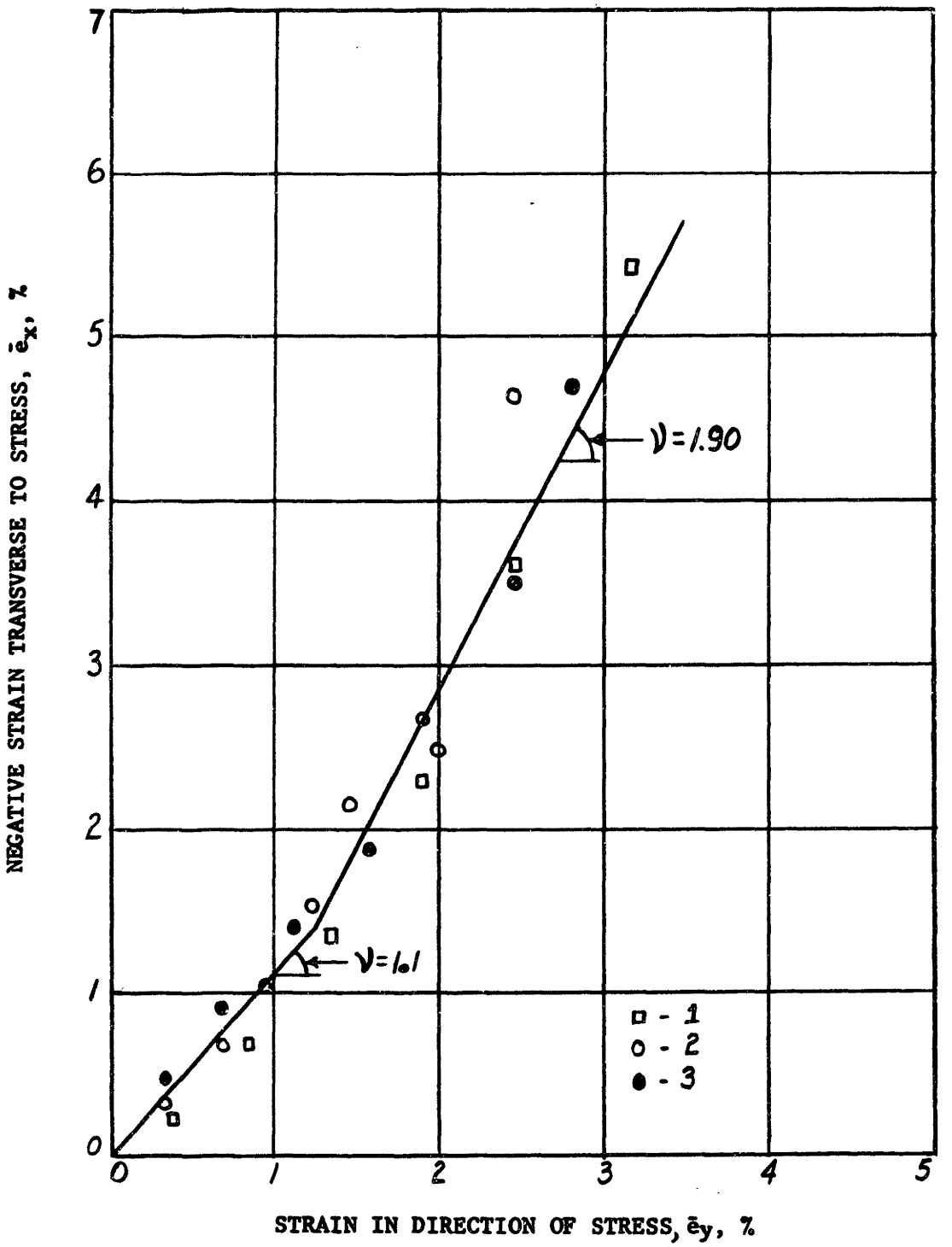

FIGURE 3.17

FABRIC A, POISSON'S RATIO, $\theta = 30^{\circ}$

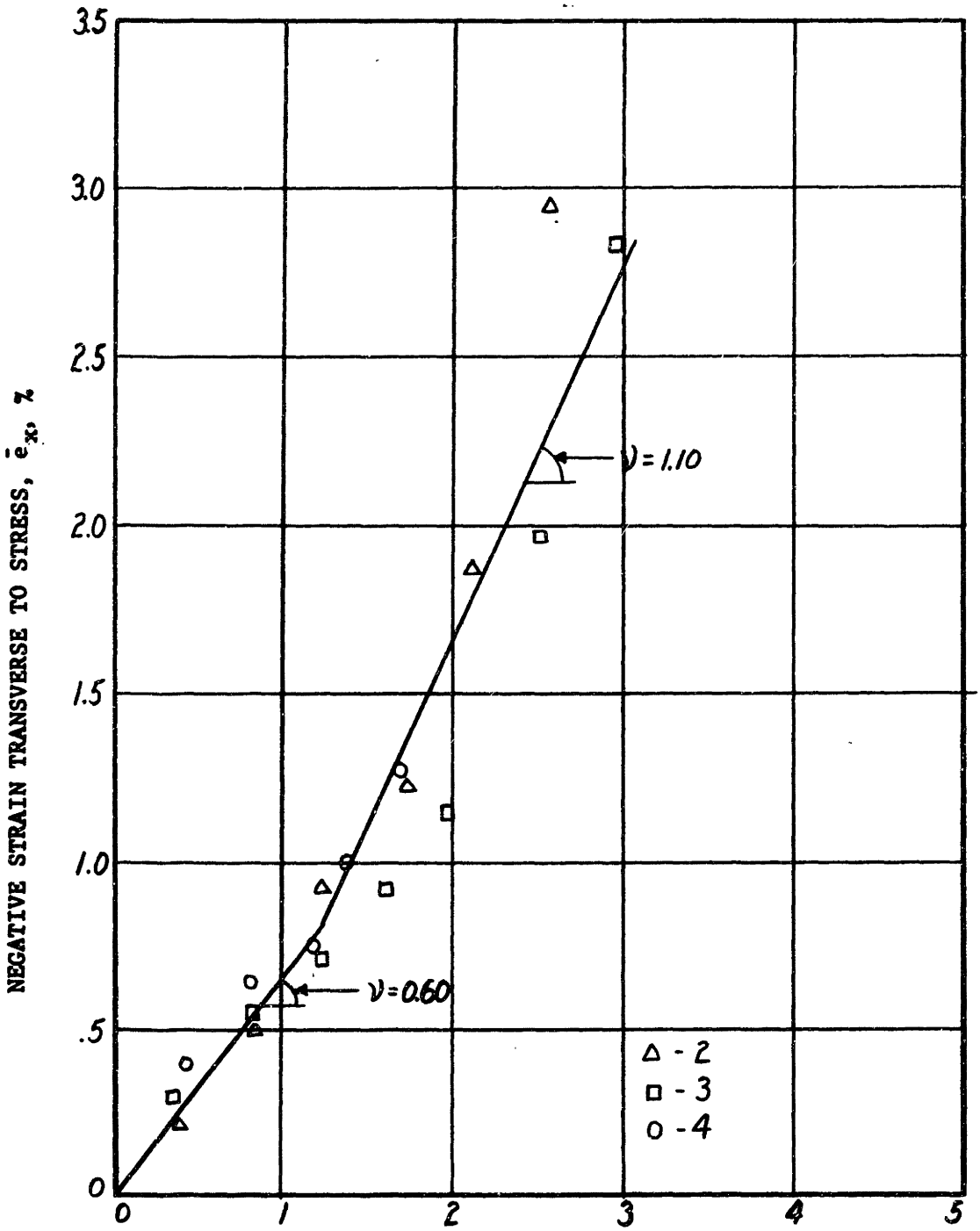

FIGURE 3.18

FABRIC A, POISSON'S RATIO, $\Theta = 45^{\circ}$ & 60°

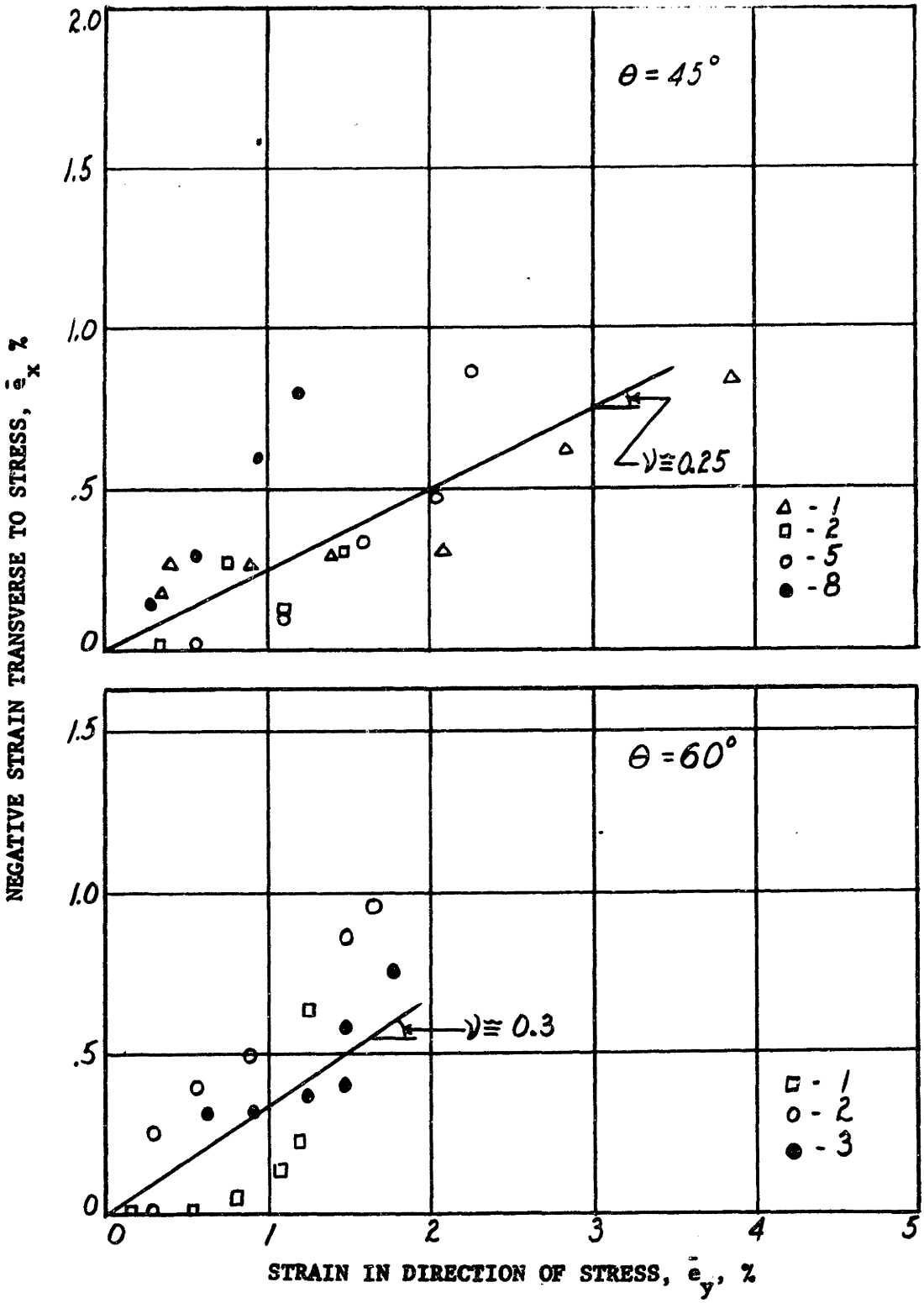

FIGURE 3.19

FABRIC A, POISSON'S RATIO, $\theta = 75^\circ$ & 90°

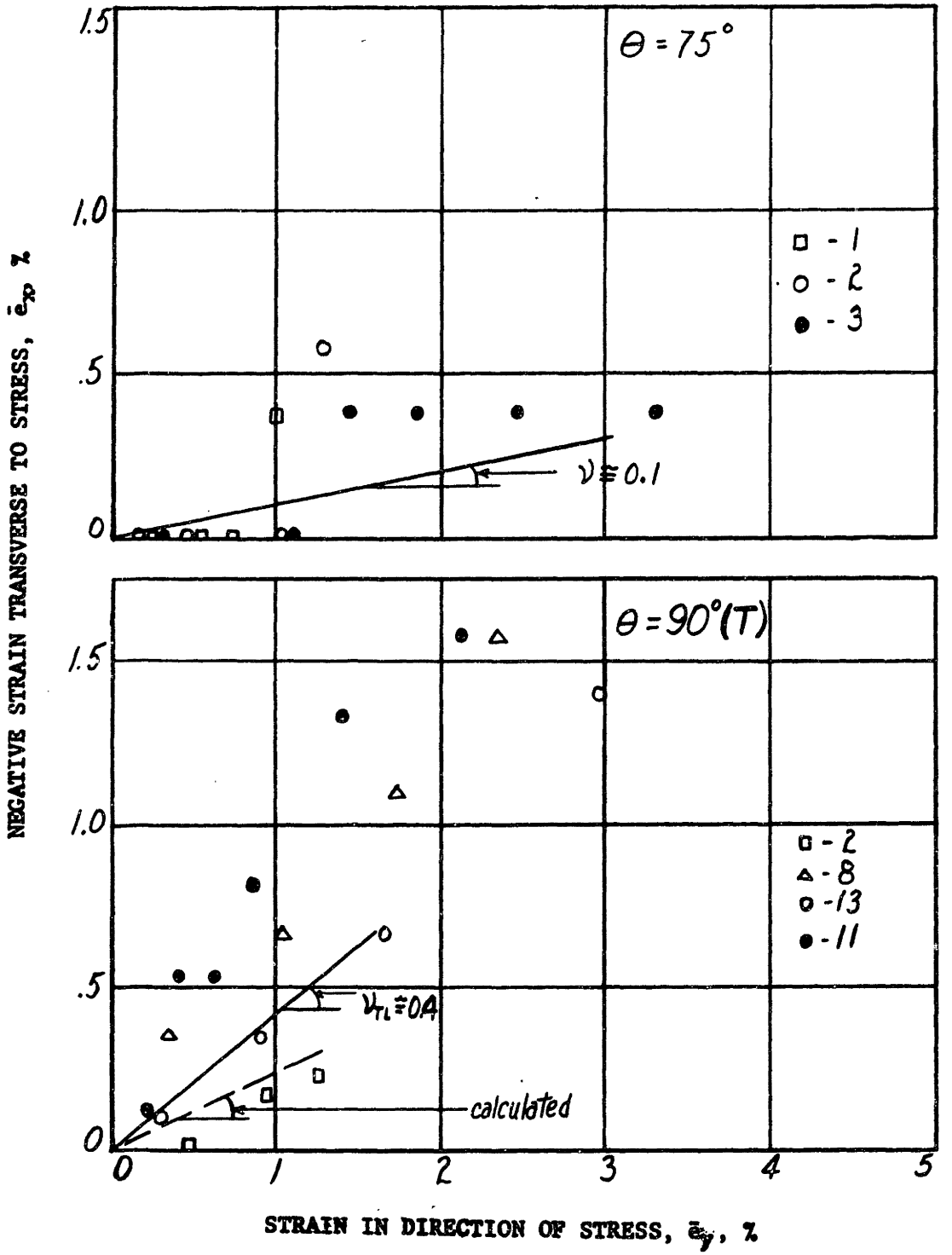

D. Gross Material Properties, Predicted and Measured

The experimental method has given directly four of the five material constants; namely E_L, E_T, ν_{LT} and ν_{TL}. As they are related by equation 3.13

$$\frac{\nu_{LT}}{E_L} = \frac{\nu_{TL}}{E_T} \qquad (3.13)$$

one check is immediately available. With the values $\nu_{LT} = 1.25$, $E_L = 45$ gpd; the ratio ν_{LT}/E_L is $1.25/45 = .028$. With the values $\nu_{TL} = .4$, $E_T = 9.0$ gpd, the ratio ν_{TL}/E_T is $.4/9.0 = 0.044$. Of these four measured values, ν_{TL} is the least accurate as seen by the scatter of data, Figure 3.19. Since the relation 3.13 has been used in simplifying the equation group 3.12; the calculated value of ν_{TL} will be used.

Thus

$$\nu_{TL} = \nu_{LT} \frac{E_T}{E_L} = 0.25$$

This value is indicated by the dashed line for $\theta = 90^\circ$ (T) on Figure 3.19.

As mentioned previously, a direct measure of G_{LT} is very difficult, if not impossible. The procedure adopted at Forest Products Laboratory (9) of calculating G_{LT} from equation 3.12a when $\theta = 45^\circ$ is used here.

$$\frac{1}{E_\theta} = \frac{\cos^4\theta}{E_L} + \frac{\sin^4\theta}{E_T} + \left[\frac{1}{G_{LT}} - \frac{2\nu_{LT}}{E_L}\right]\sin^2\theta\cos^2\theta \qquad (3.12a)$$

Substituting the measured value $E_{45^\circ} = 21$ gpd and $\theta = 45^\circ$; $G_{LT} = 9.0$ gpd.

With all five constants determined, values of E_y (at any test angle θ) can be calculated. The computations are given in Table 3.3. The calculated moduli, and the measured moduli are plotted in Figure 3.20. A smooth curve has been drawn through the calculated values, indicated by solid dots. In the case of $\theta = 60^\circ$ and 75°, both experimental moduli values are given (indicated by the vertical line); the lower value in each case being the specific modulus as obtained from the Instron chart. The agreement is seen to be good.

Calculated values of ν_{yx} can be obtained from Equation (3.12b). Thus

$$\nu_{yx} = E_y \left[\frac{\nu_{LT}}{E_L} - \left(\frac{1}{E_L} + \frac{1}{E_T} + \frac{2\nu_{LT}}{E_L} - \frac{1}{G_{LT}} \right) \sin^2\theta \cos^2\theta \right] \quad (3.12b)$$

These computations are given in Table 3.4 and the calculated and measured Poisson's ratio ν_{yx} plotted in Figure 3.21. Again a smooth curve has been drawn through the calculated points, indicated by solid dots. The measured data are indicated by open circles. Again the agreement is relatively good. The large errors associated with $\theta = 45^\circ$ to 90° (or small values of ϵ_x) are directly attributable to the use of a one inch gauge for the measurement of transverse contractive strains. Nevertheless, the measured data appear to follow the calculated values quite satisfactorily.

Two additional calculations can be made; 1) for the specific proportional limit stress at any angle (σ_{p_y}) and 2) for the specific rupture stress at any angle (σ_{m_y}). Calculations for proportional

TABLE 3.3

PREDICTED VALUES OF MODULUS, Ey, FABRIC A

$$\frac{1}{E_y} = \frac{\cos^4\theta}{E_L} + \frac{\sin^4\theta}{E_T} + \left[\frac{1}{G_{LT}} - \frac{2\nu_{LT}}{E_L}\right]\sin^2\theta\cos^2\theta$$

$E_L = 45$ gpd. ; $E_T = 9.0$ gpd. ; $\nu_{LT} = 1.25$; $\nu_{TL} = .25$; $G_{LT} = 9.0$ gpd.

θ°	$\cos^4\theta$	$\sin^4\theta$	$\frac{\cos^4\theta}{E_L}$	$\frac{\sin^4\theta}{E_T}$	$\sin^2\theta\cos^2\theta$	$.0558\times\sin^2\theta\cos^2\theta$	$\frac{1}{E_y}$	E_y
0	1.00	0	.0222	0	0	0	.0222	45
15	.87	.0045	.0193	.0005	.063	.0035	.0233	43
30	.56	.063	.0124	.0070	.19	.0106	.0300	33
45	.25	.25	.0056	.0277	.25	.014	.0473	21
60	.063	.56	.0014	.0621	.19	.0106	.0741	14
75	.0045	.87	.0001	.0966	.063	.0035	.1002	10
90	0	1.00	0	.111	0	0	.111	9.0

FIGURE 3.20

FABRIC A, PREDICTED & MEASURED SPECIFIC MODULI

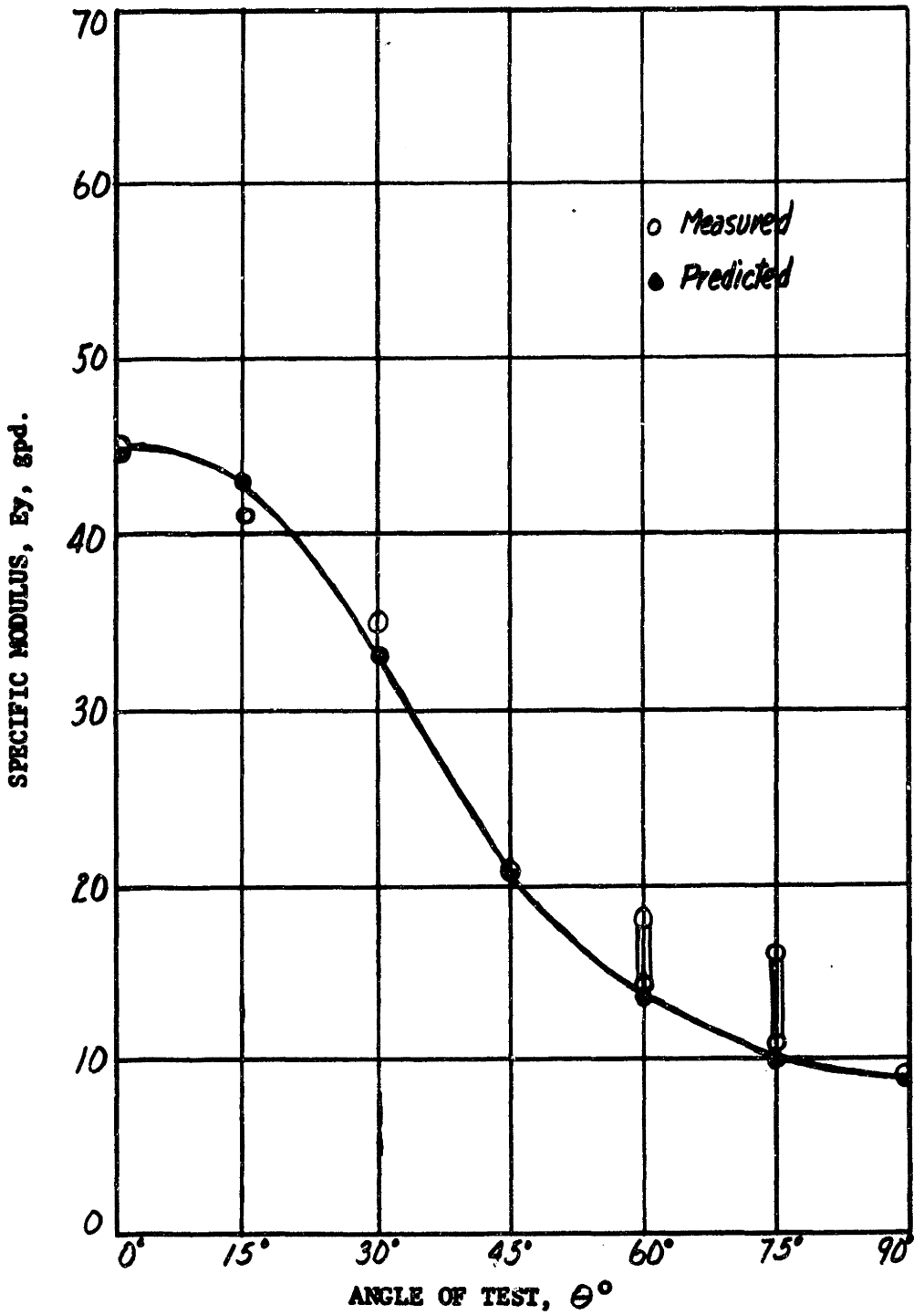

TABLE 3.4

FABRIC A, PREDICTED POISSON'S RATIOS

$$\frac{\nu_{yx}}{E_y} = \frac{\nu_{LT}}{E_L} - \left[\frac{1}{E_L} + \frac{1}{E_T} + \frac{2\nu_{LT}}{E_L} - \frac{1}{G_{LT}}\right] \sin^2\theta \cos^2\theta$$

θ°	(1) $\sin^2\theta\cos^2\theta$	(2) $.778 \sin^2\theta\cos^2\theta$	$.0278 - (2)$	Orthotropic Pred. E_y	ν_{yx}
0	0	0	.0278	45	1.25
15	.063	.0049	.0229	43	.99
30	.19	.0148	.0130	33	.43
45	.25	.0194	.0084	21	.18
60	.19	.0148	.0130	14	.18
75	.063	.0049	.0229	10	.23
90	0	0	.0278	9	.25

FIGURE 3.21

FABRIC A, PREDICTED & MEASURED

POISSON'S RATIO

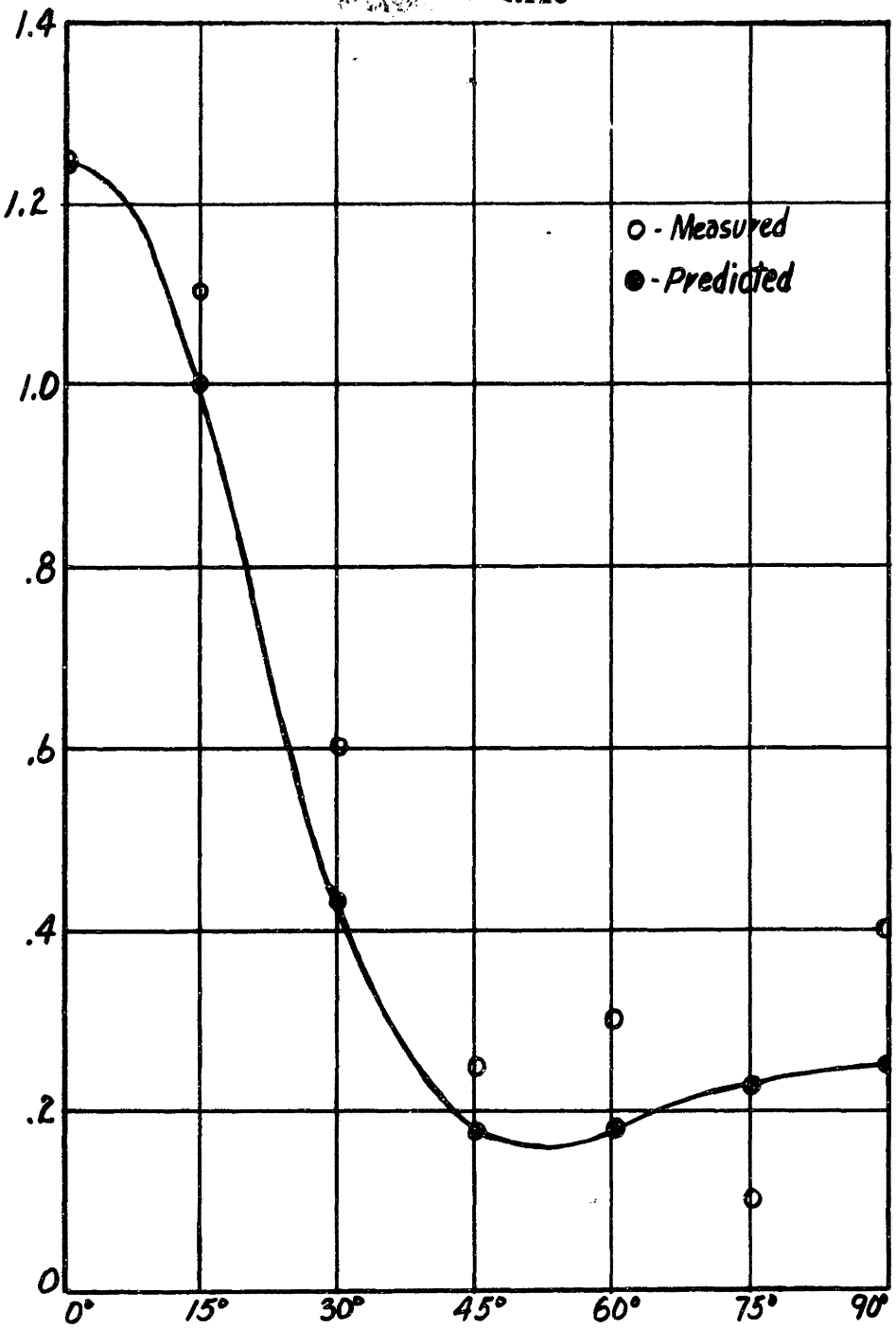

limit and failure are based on additional assumptions of behavior and are not as exact as the expressions for moduli and Poisson's ratio. (9) Calculations for proportional limit are based on the following reasoning. (9). If the material is under a uniaxial stress acting in the direction y, the proportional limit stress in that direction is determined by that proportional limit stress in any of the three principal directions (L, T, LT) which is first exceeded.

Since $\sigma_L = \sigma_y \cos^2\theta$, the stress σ_y necessary to cause $\sigma_L = \sigma_{p_L}$ is given by $\sigma_y = \frac{\sigma_{p_L}}{\cos^2\theta}$. Similarly, $\sigma_y = \frac{\sigma_{p_T}}{\sin^2\theta}$ and $\sigma_y = \frac{\sigma_{p_{LT}}}{\sin\theta\cos\theta}$. The lowest value of σ_y given by the above three equations will be σ_{p_y}.

The difficulty lies in obtaining a realistic value of $\sigma_{p_{LT}}$ in the absence of shear stress experiments. As the failure of specimens at $\theta = 45^\circ$ seems to be predominately shear in the L direction, $\sigma_{p_{LT}}$ has been taken as $\frac{1}{2}\sigma_{p_{45^\circ}}$, or .085 gpd. The values of σ_y obtained from the three conditions are given in Table 3.5 with the smallest of the three values entered as the predicted specific proportional limit stress (Column 5). The calculated and measured data are plotted in Figure 3.22, again with solid dots indicating predicted data, and open circles experimental data. The vertical lines at $\theta = 60^\circ$ and 75°, again indicate the difference between photographic and Instron proportional limit. The influence of the arbitrary selection of $\sigma_{p_{LT}}$ is easily seen, for the experimental agreement would be much improved were $\sigma_{p_{LT}}$ taken as .125 gpd. There is very little justification of either procedure in the absence of actual measurements in shear.

The specific rupture stress can be calculated by the method suggested by Erickson and Norris (9) in the following form;

$$\frac{1}{(\sigma_m)_y^2} = \frac{\cos^4\theta}{(\sigma_m)_L^2} + \frac{\sin^4\theta}{(\sigma_m)_T^2} + \left[\left\{\frac{1}{(\sigma_m)_{LT}^2} - \frac{1}{(\sigma_m)_L(\sigma_m)_T}\right\}\sin^2\theta\cos^2\theta\right] \qquad (3.14)$$

TABLE 3.5

FABRIC A, PREDICTED SPECIFIC PROPORTIONAL LIMIT STRESSES

$$\sigma_{p_y} = \frac{\sigma_{p_L}}{\cos^2\theta} \quad or \quad \frac{\sigma_{p_T}}{\sin^2\theta} \quad or \quad \frac{\sigma_{p_{LT}}}{\sin\theta\cos\theta}$$

θ°	$\sigma_{p_L}/\cos^2\theta$	$\sigma_{p_T}/\sin^2\theta$	$\sigma_{p_{LT}}/\sin\theta\cos\theta$	Predicted σ_{p_y}	Measured σ_{p_y}
0	.41	∞	∞	.41	.41
15	.45	1.03	.34	.34	.37
30	.55	.28	.20	.20	.29
45	.82	.14	.17	.14	.17
60	1.63	.094	.20	.094	.18 - .12
75	6.1	.075	.34	.075	.14 - .09
90	∞	.07	∞	.07	.07

FIGURE 3.22

FABRIC A, PREDICTED & MEASURED

SPECIFIC PROPORTIONAL STRESS LIMIT

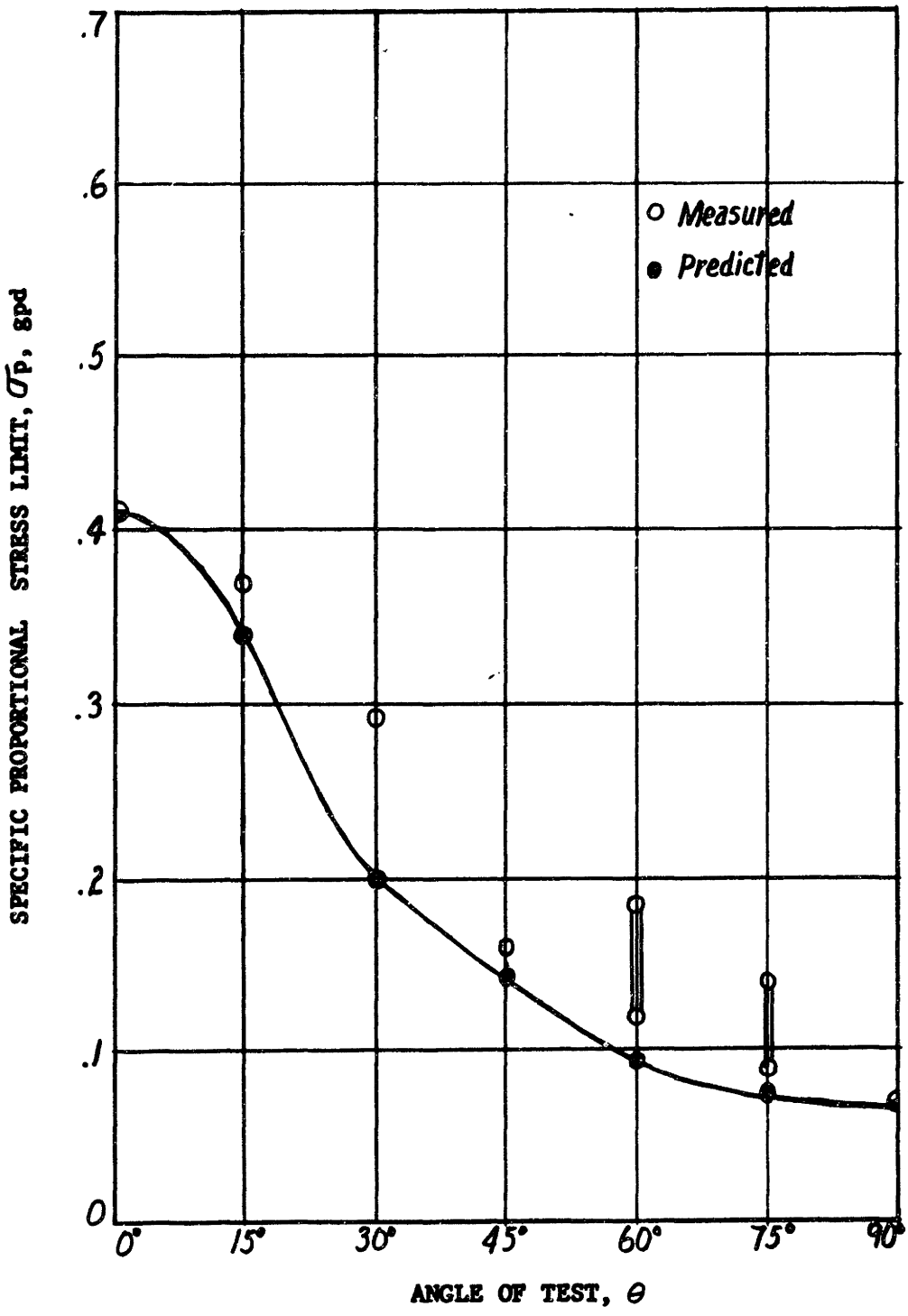

where σ_m is the specific rupture stress in the direction indicated by the subscript.) The calculated data in Table 3.6 and plotted along with the experimental data in Figure 3.23. The agreement between predicted and measured is quite good.

E. Conclusions on Fabric A.

The orthotropic theory developed for rigid materials appears to predict well the behavior of this flexible fibrous nonwoven structure. The material tested, Fabric A, was selected for its low binder content (2% on weight of fiber) and the corresponding existence of free, unsupported, fiber lengths between bonds. Presumably, as the amount of binder increased, the predicted and measured properties would agree even more closely.

Since Fabric A represents about the minimum in binder add-on to give a mechanically functional structure, the differences between predicted and measured results are probably at their maximum for this material, as follows:

1. Initial Moduli, maximum difference of 30% of predicted at $\theta = 75^\circ$ and average difference of about 10%.
2. Poisson's ratio, maximum difference of 40% of predicted at $\theta = 90^\circ$ (a large part of this difference due to experimental uncertainty).

Using the approximations given by Norris (9):

3. Specific proportional limit stress, maximum difference of 30% at $\theta = 60^\circ$. (Some of this difference due to the arbitrary selection of $\sigma_{p_{LT}}$).
4. Specific rupture stress, maximum difference of approximately 15% of predicted at $\theta = 60^\circ$.

TABLE 3.6

FABRIC A, PREDICTED SPECIFIC RUPTURE STRESSES

$$\frac{1}{(\sigma_m)_y^2} = \frac{\cos^4\theta}{(\sigma_m)_L^2} + \frac{\sin^4\theta}{(\sigma_m)_T^2} + \left[\left\{\frac{1}{(\sigma_m)_{LT}^2} - \frac{1}{(\sigma_m)_L(\sigma_m)_T}\right\}\sin^2\theta\cos^2\theta\right]$$

$(\sigma_m)_L$ = .57 gpd; $(\sigma_m)_T$ = .105 gpd; $(\sigma_m)_{LT} = (\sigma_m)_{45^o}$ = .20 gpd

θ^o	$\frac{\cos^4\theta}{(\sigma_m)_L^2}$	$\frac{\sin^4\theta}{(\sigma_m)_T^2}$	[ ]	$\frac{1}{(\sigma_m)_y^2}$	$(\sigma_m)_y$	$(\sigma_m)_{meas.}$
15	2.68	.41	.52	3.61	.53	.50
30	1.72	5.72	1.57	9.01	.33	.40
45	.77	22.7	2.07	25.54	.195	.20
60	.19	51.0	1.57	52.76	.14	.18
75	.01	79.	.52	79.53	.11	.14

FIGURE 3.23

FABRIC A, PREDICTED & MEASURED RUPTURE STRESS

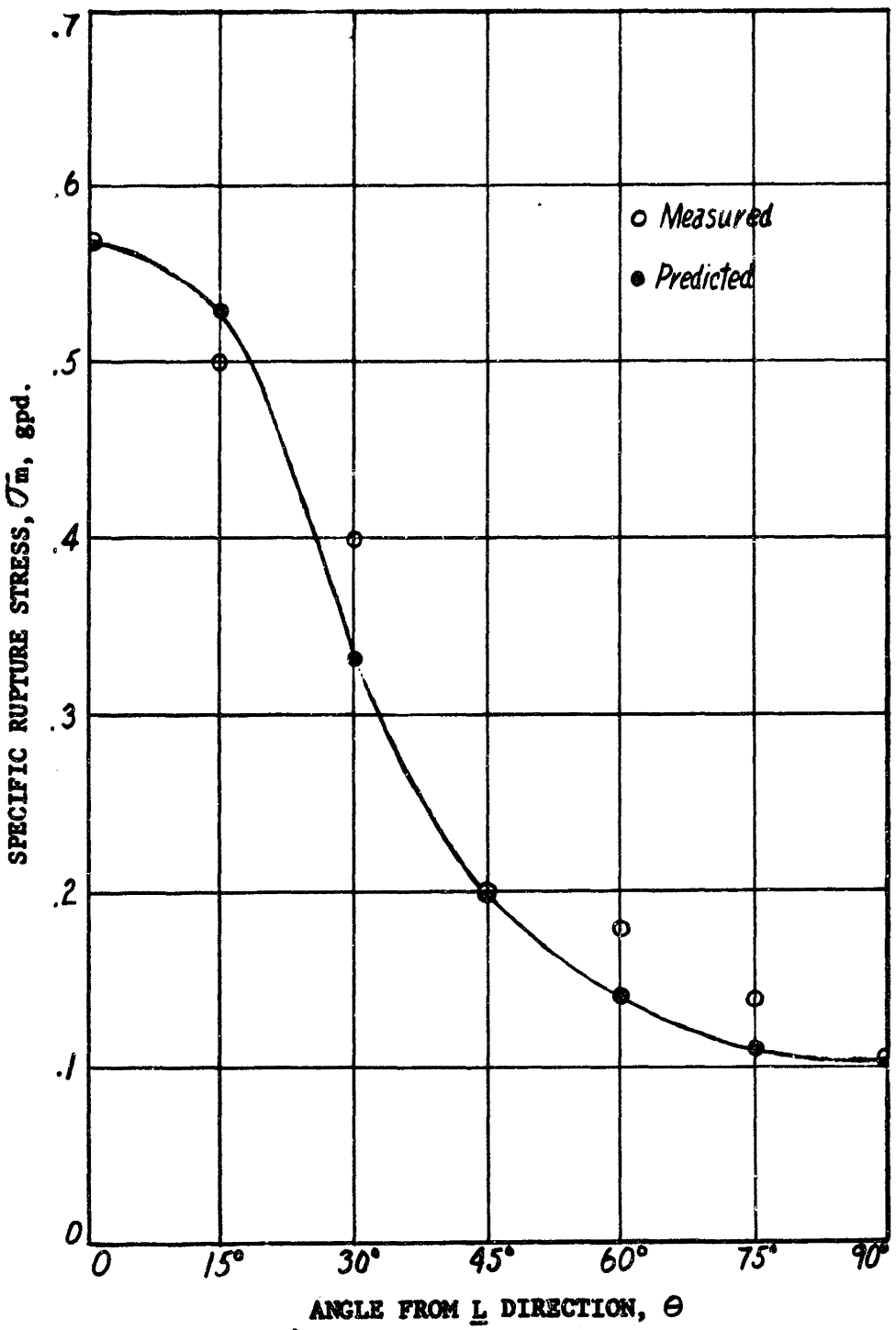

The figures given above might appear to indicate poor agreement, but actual comparison of the predicted vs. measured data in Figures 3.20 - 3.23 inclusive will show the average deviation from predicted to be in the order of 10%. This is quite reasonable agreement, and is perhaps twice the deviation experienced in applying the same equations to the analysis of plywood and multi-layer glass fabric laminates (5,9). This analytical procedure provides a basis for an engineering approach to the mechanical properties of fibrous non-woven structures in the Hookean region.

IV. THE CONCEPT OF THE UNIT CELL

A. The Boundary Conditions of the Unit Cell

In a perfectly homogeneous material under uniform stresses, the state of strain is the same for large or small areas, provided these areas are far enough from the loaded edges to eliminate any of the restraints of loading.

In homogeneous materials under non-uniform stress, a differential or very small element is chosen for analysis. The stresses can be considered constant over each boundary of this small element, but stresses on opposite faces will differ in magnitude by a small amount. With the stresses along opposite boundaries uniform, the material homogeneous, and its deformation to stress known, the strain within the differential element can be calculated. The size of the differential element can be taken small enough to consider the stress uniform along any boundary of that element and the stresses on opposite faces almost equal.* Consequently the strain within that element is also uniform. This is the analytical approach found in any text on the Theory of Elasticity (4, 15), and the same assumptions are implicit in the orthotropic theory given previously (III.A.).

These assumptions are not valid on the matrix of fibers which constitute a non-woven fabric such as shown in Figure 4.1. This element is not homogeneous, and taking the element smaller and smaller only serves to increase the non-homogeneity. Consider a simplified element as the square ABCD in Figure 4.1. The internal forces balancing any external

*The element is small enough to meet the assumptions given, yet is large enough to permit the element to have uniform properties. Thus, in metals, the differential element can be very small and yet contain millions of molecules, or thousands of agglomerated crystals.

FIGURE 4.1

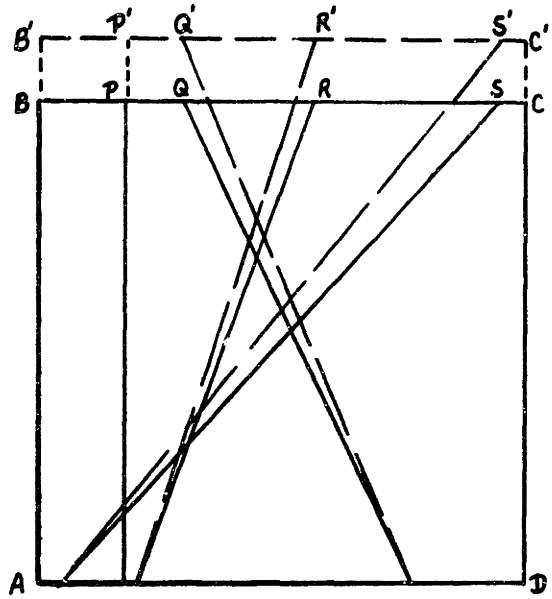

PHOTOMICROGRAPH AND SCHEMATIC OF UNIT CELL

load are concentrated in the fibers P, Q, R, & S. Regardless of what happens within the element, only forces in these fibers can balance any external force.

It is desired to determine the strains in the fibers as a result of the deformations of this element. These fiber strains can be converted to fiber forces, and the components of these forces can be summed to balance the external force causing the deformation of the element ABCD. This represents the goal of this investigation: to translate fiber stresses and strains into the stresses and strains of a non-woven assembly of these fibers. In order to accomplish this, the behavior of a small element of the fabric must be described.

Consider the photographed matrix of fibers and its simplification in Figure 4.1; and assume that the fabric, of which this element is a part, is under stress. In order to accomplish the stated goal, either the fabric stress must be related to fiber stress, or fabric deformation to fiber strain. This can be done by defining what happens at the boundaries of the element ABCD, irrespective of what might occur within the element. The element boundaries are defined by the loci of points on the fibers crossing that boundary, the loci lying originally in a straight line.

There are four possibilities, under the action of uniaxial tension, by which relationships can be established between fiber and fabric behavior. These are as follows:

a. Parallel displacement of boundaries parallel and perpendicular to the direction of stress. (Straight line boundaries remain straight lines)*

*More generally, the boundaries are to remain straight, of infinitely small width, and opposite boundaries parallel; through translation and rotation. Restricting the boundaries to be perpendicular or parallel to the direction of stress eliminates rotation of the element boundaries, and leaves only translation as boundary motion.

b. All fibers in the element have the same vertical force component.

c. All fibers in the element have the same fiber force.

d. All fibers in the element have the same fiber strain.*

If the element ABCD is considered alone, any of these four possibilities is satisfactory. However, the element is not an entity, but only one of many such elements with common boundaries which, together, constitute the fabric. In order to describe the behavior of the fabric in terms of the behavior of one of these elements; the common boundaries (given by points on the fibers lying in a straight line) must remain common. This means that points on the fibers must remain common to the two coincident straight line boundaries. This restriction, termed "compatibility", limits the action of the boundaries of the element to case a, i.e., parallel displacement of the straight boundary loci of the fibers in the element (Parallel Boundary Displacement). Thus in Figure 4.1, the locus of the boundary BC given by points P,Q,R,S, on their respective fibers moves to B'C'. The new boundary is the locus of the same fiber loci P,Q,R,S, which have taken new positions P',Q',R',S'--again lying in a straight line.

With the element restricted to deformation according to parallel boundary displacement the change in the length of the fibers P,Q,R,S, can be expressed in terms of the deformation or strain of the element. These changes in fiber length become strains, the fiber strains are converted into forces, and the vertical components of these forces summed to find the force acting on the element. This presents a feasible analytical procedure. However, several other factors must be considered.

*c and d are equivalent for Hookean behavior

B. The Geometrical Form of the Unit Cell

The previous discussion has been illustrated by the use of a square element containing a number of fibers. Yet the only condition which has been postulated is parallel straight line boundary displacement, and this might be satisfied by almost any non-curvilinear boundary configuration or size of element. Since the analysis to be carried out should be as general as possible, a list of element criteria appears useful. The following factors should be satisfied in order to eliminate as many a priori assumptions as possible. The basic element, or unit cell should:

1. Satisfy the parallel uniform boundary displacement concept.
2. Account for changes in the absolute number of fibers within the selected boundaries (weight variation)
3. Account for the effect of fibers ending within the boundaries.
4. Account for changes in fiber orientation between unit cells.
5. Satisfy the practical consideration of free fiber lengths between bond points
6. Not be influenced greatly by the addition or subtraction of a small number of bond points.

Two postulated unit cells were analyzed and rejected. (See Appendix B). The first of these was a unit cell consisting of two fibers bonded together. It became evident that this arrangement would depend more on the properties of the binder, and did not conform to the observed structure of the non-woven fabric. The second approach was to consider the fabric as a matrix of bond points, with fibers radiating outward to other matrix points. This approach will not satisfy uniform displacement if the number or orientation of fibers at various points changes.

The listed criteria, together with the experience obtained on the two postulated unit cells, indicated a finite-sized unit cell--one in which

weight variation and fiber orientation variation might be measured. A finite element allows certain assumptions about the number of bonds per fiber, and the subsequent influence of fibers ending within the unit cell. Also such unit cells (changing in weight and fiber orientation) will provide experimental information about the effect of small-scale non-uniformity on the matrix of unit cells which is the fabric. Thus it appeared that a finite-sized unit cell should be selected to contain a number of fibers, and be of proper or sufficient size to satisfy the requirement of parallel boundary displacement.

The fabrics to be considered are orthotropic, with two axes of symmetry. One of the axes, the L axi , is in the direction of manufacture of the fabric, or Machine Direction. The other axis, the T axis, is perpendicular to the Machine Direction, and is called the Cross-Machine Direction, or simply Cross Direction. The unit cell was chosen for measurement as a square with sides parallel to these two axes. For tests in the direction $y(\theta = 0^{\circ})$, the unit cell boundaries will be considered parallel and perpendicular to the direction of stress. With the shape of the unit cell chosen, it remains to show what size of unit cell in the fabric will, in fact, satisfy the uniform boundary displacement condition.

C. The Size of the Unit Cell

Examination of Fabric A under the microscope and in photo-micrographs (as in Figure 4.1), showed that a majority of the intersections appeared bonded. Thus if the unit cell is selected so as to include sufficient bonds along each fiber between the boundaries, the influence of fibers ending within the unit cell boundaries will be greatly reduced. Also if the number of bond points is large, small variations in their absolute number should have only a small effect at the boundaries of the unit cell.

Both weight variation and fiber orientation variation are to be measured on the unit cell. For this reason, an adequate sized unit cell was desired to facilitate measurements. It was found experimentally that an area containing from 25-75 fibers was the most practical size. On Fabric A (previously described) this represents a square with edges approximately 0.015" to 0.030" in length. In Figure 4.1, the square ABCD has sides 0.020 inches in length. It can be observed on the photograph, Figure 4.1, (and confirmed by many other observations) that each fiber is bonded from three to eight times within the boundaries of the unit cell. Also the fibers are relatively straight within the boundaries of this unit cell.

The large number of bond points per fiber would indicate that any local non-uniformity of strain along any fiber would average out at the boundaries. Also any non-uniform displacement of the bond points within the unit cell would not be reflected in the behavior of the straight boundaries described by the loci of points on the fibers crossing that boundary. The movement of bond points within the unit cell will follow the principle of minimum potential or strain energy. This will act to further equalize the strain along any particular fiber.

It would appear from the above reasoning that a unit cell of this size should satisfy the parallel boundary displacement concept. Further, the displacement of the unit cell boundaries is also the displacement of the loci of the individual fibers. Thus the average strain on any fiber can be determined from the unit cell strain <u>as if the fiber were bonded only at the boundaries of the unit cell</u>.

Thus a definition of the unit cell is as follows:

"A flexible non-woven fabric consists of a matrix of individual square unit cells oriented in the direction of stress, whose boundaries always move parallel under uniaxial stress; the unit cells of sufficient size (containing enough bond points) to allow the average strain developed in each fiber to be approximated by the strain that fiber would have if it were bonded only at the boundaries of the unit cell."

D. Experimental Justification of the Unit Cell

The arguments for the selected unit cell require that points on the fibers locating the original straight line boundary of the cell be displaced equally in the direction of stress. It is of considerable importance to determine if this is a correct assumption. A procedure was desired which would place a very fine line on the fibers in the fabric. This line could then be observed under stress to determine if the fiber points stayed in a straight line, or if the boundary line became jagged.

Slots 0.020" wide, two inches long, and 0.040" on centers were milled through a brass plate 1/32" thick, Figure 4.2. Two fabric samples were placed under the slotted brass plate with the slots parallel to the T direction. The assembly was placed in a bell-jar equipped for vacuum sputtering of silver, as commonly used for electron microstope specimens.*

*This technique of silver deposition is commonly used in the preparation of specimens for electron microscopy. The specimens were prepared by Dr. C. D. Hall of the Biology Department. Other methods might have been used to obtain a very narrow boundary marking on the fibers.

FIGURE 4.2

SPECIMEN AND MASK FOR EXPERIMENTS ON PARALLEL

BOUNDARY DISPLACEMENT

The result was a specimen as shown in Figure 4.2 with stripes of deposited silver. If this material is immersed in an oil of slightly different refractive index than the fiber, the edge of the silver stripe shows quite distinctly in transmitted light. A narrow strip of such coated material was placed on the vertical microscope stage and photographed under loads of 0.01 gpd and 0.40 gpd. The results are shown in Figure 4.3, A and B. There is no individual fiber motion observable at the boundary. If this were not the case, the boundary indicated by the edge of the silver deposit would become jagged, with fiber loci on both sides of the average displacement. There is no indication of jagged discontinuities and thus a unit cell of this size (.020") or larger appears to satisfy the condition of parallel boundary displacement.

Obviously, the size of the unit cell will depend upon the specific non-woven to be analyzed. Also, the unit cell selected could be larger without any loss in generality, but there is a practical limit as to the number of fibers which can be counted conveniently. There will be undoubtedly a lower limit or minimum size below which parallel boundary displacement will not be satisfied. It will be shown later that the actual area of the selected unit cell can vary by a factor of two or three without changing appreciably the results of the analysis. However, the real significance of unit cell size is concerned with the effect of variation between unit cells and its influence upon the rupture stress of the actual fabric. Before discussing rupture, an analysis based on the Average Unit Cell will be used to predict the mechanical properties of the fabric in the elastic and early plastic region of the stress-strain curve.

FIGURE 4.3

FABRIC A, PHOTOMICROGRAPHS OF UNIT CELL BEHAVIOR

STRESS DIRECTION - VERTICAL

MAGNIFICATION: 40X (ONE INCH ON PHOTOGRAPH IS

0.04 INCHES ON FABRIC)

STRAIN AT 0.40 pgd IS APPROXIMATELY 3 %

V. THE PREDICTION OF FABRIC PROPERTIES FROM THE AVERAGE UNIT CELL

A. The Average Unit Cell

In the previous section, a structural element, the unit cell, was defined. This section will present a numerical procedure for predicting fabric properties from unit cell behavior; considering the fabric as a matrix of identical uniform unit cells, each of average area density (weight/unit area) and average fiber orientation.

Two perpendicular axes of the non-woven fabric have been specified; the L or Machine Direction; and the T or Cross Direction. Assuming for the moment that the fibers are straight, their direction with respect to the L axis can be specified by the angle β between the L axis and the fiber axis with the angle β measured positively clockwise from the L axis. The "Orientation Distribution" expresses the manner in which the fibers are grouped around the L axis according to the angle β . In order to eliminate the absolute number of fibers present (a function of the area density), an "Orientation Distribution", $\phi(\beta)$, will be defined in terms of the relative number of fibers grouped; i.e., the ratio of the number of fibers in an angular interval with mid-point angle β_i to the total number of fibers in the cell. Since $\phi(\beta)$ is in terms of the relative number of fibers at angle β per unit width perpendicular to the fiber direction

$$\int_{-\pi/2}^{\pi/2} \phi(\beta)\, d\beta = 1^{*} \qquad \text{and } \phi(\beta)$$

*If the Orientation Distribution were based on actual number of fibers grouped at an angle, $\int \phi(\beta) d\beta$ would be the actual fiber density. Thus it would represent the total number of fibers of unit length per unit area. However, in a uniform structure, the fiber or area density merely determines the scale of the load-strain relationship and has no influence on the specific stress-strain relationship. For a complete discussion, see VIII.B.

can be expressed independently of the actual number of fibers present. The orientation distribution of the fabric can be taken as the mean fiber orientation distribution of all unit cells and as such, is designated, $\overline{\phi(\beta)}$. Since $\overline{\phi(\beta)}$ will be determined by the $\phi(\beta)$ of a number of unit cells, $\overline{\phi(\beta)}$ is also the fiber orientation distribution of the average unit cell. The area density of the average unit cell can be taken as the area density of the fabric.

1. Measurement of $\phi(\beta)$

It appeared, from observation of the fabric, that ten unit cells, or approximately 500 fibers would give a reasonable value for $\overline{\phi(\beta)}$. Accordingly, photomicrographs were taken at magnifications of 20 to 100 times directly on enlarging paper with the vertical microscope arrangement as shown in Figure 5.1.

The size of the unit cell has been selected as a square of edge length 0.0225 inches. The definition of $\phi(\beta)$ requires the relative frequency of fibers per unit width perpendicular to the fiber direction. This means that for the purpose of determining $\phi(\beta)$, only fibers that lie within a circle 0.0225 inches in diameter will be counted.

A uniform area of Fabric A was selected and a one inch wide strip cut from that area. This strip was mounted on a microscope slide (with the L direction parallel to the length of the slide). Near the center of this slide, two very small black yarns were placed across the slide and fabric, spaced one millimeter apart. A second microscope slide was placed over the fabric and marking yarns, and the two slides cemented together at the ends. The complete slide and a 20 times enlargement of a portion of the marked area are shown in Figure 5.2.

FIGURE 5.1

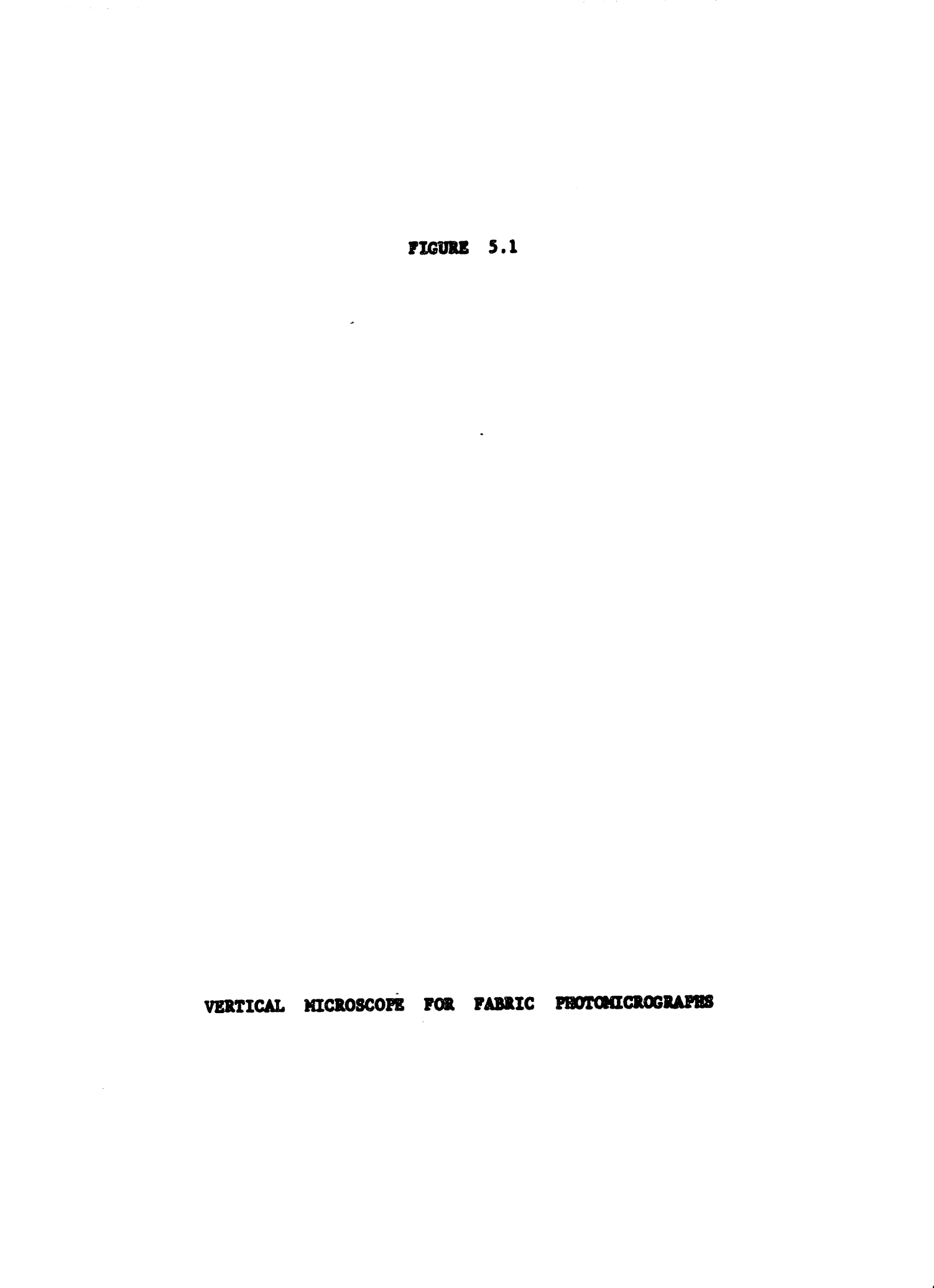

VERTICAL MICROSCOPE FOR FABRIC PHOTOMICROGRAPHS

FIGURE 5.2

SLIDE AND 20X ENLARGEMENT OF FABRIC A.

The slide was mounted in the vertical microscope set-up (as shown in Figure 5.1) with adjustable stage. Direct prints were made of the area of the fabric bounded by the two marking yarns. This gave a series of 21 overlapping photographs, which could be assembled into a composite strip representing the complete section of fabric bounded by the yarns. About 1/3 of that strip is reproduced as Figure 5.3. For ease in mounting, the continuous strip has been broken into thirds, starting at the top of Figure 5.3. Thus the right edge of the top row of photographs matches the left edge of the middle row; and the right edge of the middle row matches the left edge of the bottom row. The light edges along the top and bottom of each row of photographs are the marking yarns. The exact photographic procedure is as follows:

Objective - 16 mm. focal length

Ocular 8 x plano

Condenser yes

Filter No. 1, Varigram

Exposure Two seconds

Distance from ocular to image plane - 15 inches

Total Magnification - 100 x

Since the magnification is 100x, 0.022" on the fabric represents 2.2 inches on the original photographs or 5.7 centimeters (Figure 5.3 is a slightly reduced reproduction). The twelve circles have diameters of 5.7 cm. The horizontal line joining the centers of the circles was placed in the center of the area bounded by the marking yarns. Thus the circles locate 12 adjacent unit cells running in the T direction (horizontal), with

FIGURE 5.3

TWELVE ADJACENT UNIT CELLS, FABRIC A

the Machine Direction or L axis vertical.

In measuring the orientation of the fibers in any unit cell, a large plastic protractor was used. The fiber axis was located, and the angle between this fiber axis and the L axis noted (actually the angle between the fiber axis and the horizontal line was measured, and β taken as 90° minus this angle.) Since β can vary, by definition, from minus 90° to plus 90°, angular intervals of 10° were selected. Measurements started at one edge of the horizontal "diameter", and as the angle of each fiber crossing that diameter was determined, a scratch was made over the length of that fiber. Thus each counted fiber was identified. After completing a traverse of the diameter, all fibers which did not cross the horizontal diameter were measured. A summary of the data for ten cells is shown in Table 5.1. The symbol $\sum_R$ (the next to last column of Table 5.1) is the total number of fibers in a particular angular interval for the ten cells. The symbol $\sum_C$ (the last row of Table 5.1) is the total number of fibers in each cell. The sum of $\sum_R$ and $\sum_C$ are the same, and is the total number of fibers counted in the ten cells, $\sum\sum$. The relative frequency of fibers in any angular internal is $\sum_R / \sum\sum$ and is given by the last column of Table 5.1. These relative frequencies are plotted in Figure 5.4. This relative frequency curve is symmetrical about the L axis, within the experimental error. Thus the two axes of symmetry of the fiber orientation are also the axes of the fabric; i.e. the L and T axis.

Prior to establishing this procedure, measurements had been made at larger magnification on square areas with edges of 0.020 to 0.040 inches. This data can be converted to equivalent information for circular cells in the following way. Assume that all fibers are uniformly spaced, depending

TABLE 5.1

ABSOLUTE AND RELATIVE FIBER FREQUENCIES, FABRIC A,

TEN CELLS, 0.0225 INCHES IN DIAMETER

Angular Interval, °	Absolute Frequency Cell Number											Average Relative
	1	2	3	4	5	6	7	8	9	10	Σ_R	Freq.
-85 to +85	1	0	1	3	1	0	0	1	0	2	9	.0182
-75 to -85	4	0	2	0	2	1	2	0	0	0	11	.0222
-65 to -75	2	1	3	0	1	0	2	2	2	0	13	.0252
-55 to -65	1	4	2	2	2	1	2	0	2	3	19	.0384
-45 to -55	3	1	2	2	1	3	1	3	1	3	20	.0404
-35 to -45	2	2	2	1	1	1	0	0	2	3	14	.0283
-25 to -35	2	3	2	0	1	2	4	2	2	2	20	.0404
-15 to -25	3	3	6	2	1	1	3	5	3	1	31	.0525
- 5 to -15	7	5	6	6	7	4	7	2	7	5	56	.113
5 to - 5	10	6	7	9	9	10	8	6	5	13	83	.168
15 to 5	9	6	2	6	7	6	8	5	8	10	67	.135
25 to 15	3	2	3	4	4	4	4	2	4	3	33	.0667
35 to 25	2	3	5	2	0	4	3	1	5	3	28	.0566
45 to 35	2	1	3	2	2	4	0	1	3	4	22	.0444
55 to 45	2	2	1	3	2	3	2	1	0	0	16	.0323
65 to 55	2	3	2	4	3	1	2	2	1	2	22	.0444
75 to 65	2	3	2	1	2	3	3	3	3	1	23	.0465
85 to 75	0	1	2	1	1	2	1	2	0	2	12	.0242
Σ_C	57	46	53	48	50	46	52	38	48	57	$\Sigma\Sigma$ 495	

FIGURE 5.4

FIBER ORIENTATION RELATIVE FREQUENCY vs. ANGULAR INTERVAL

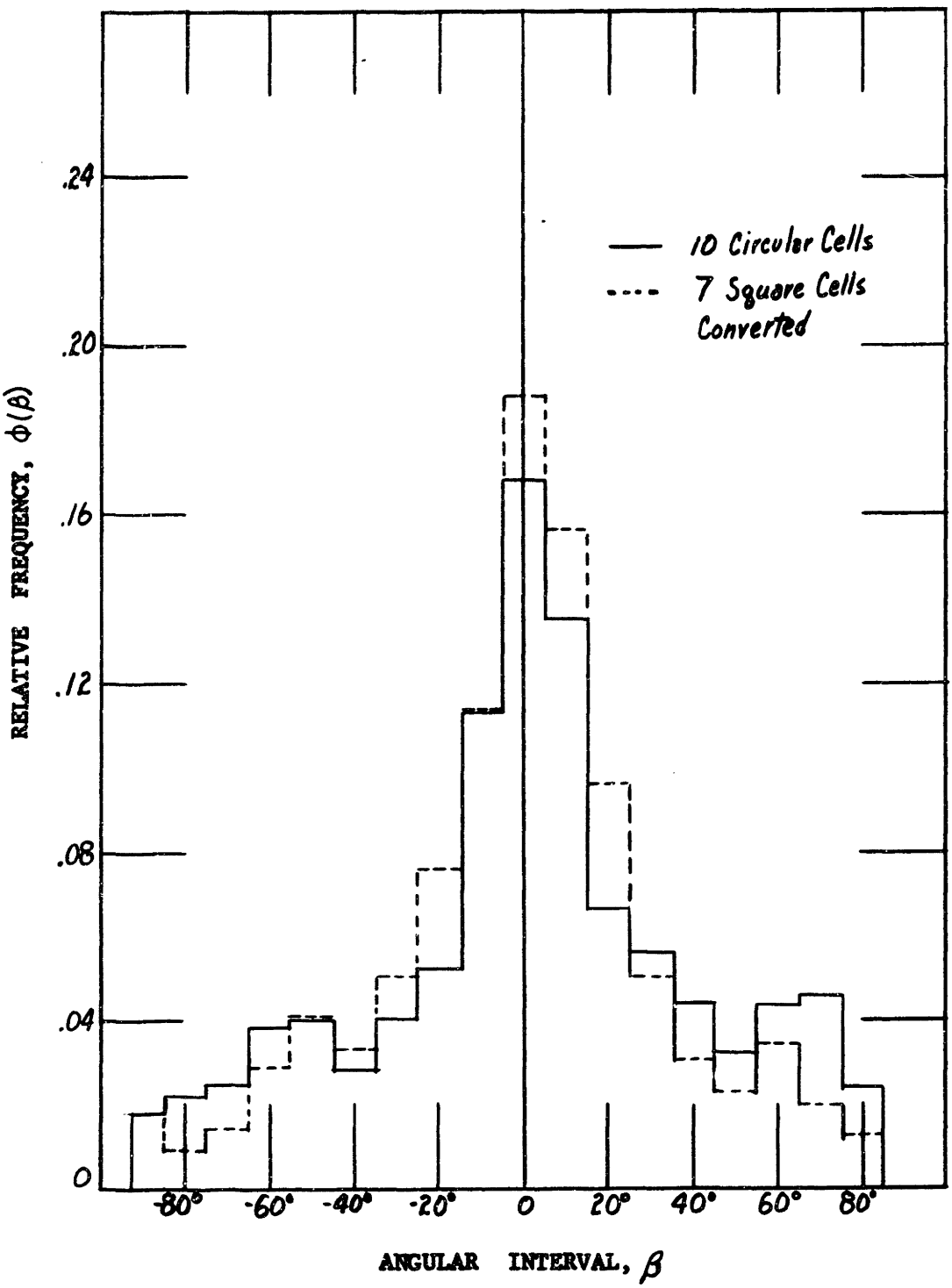

on their frequency of occurrance in any angular interval. Then referring to the sketch below, consider the fibers lying at the angle β_i . For fibers at β_i lying within the circle of diameter D, the correct value of number of fibers <u>per unit width perpendicular to these fibers</u> is obtained. But when counting in a square cell, the width perpendicular to those fibers is Y, not D. Since

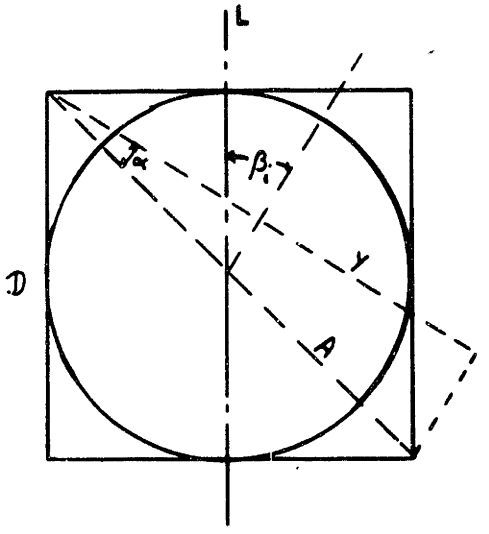

$$Y = A \cos\alpha$$
$$\alpha = \pi/4 - \beta_i \qquad 0 \le \beta \le \pi/2$$
$$A = D/\sin\pi/4$$

Then

$$Y = \frac{D}{\sin\pi/4}\cos\left(\frac{\pi}{4} - \beta_i\right) = D(\cos\beta_i + \sin\beta_i)$$

Assume that at angle β_i , the number of fibers counted over Y was n_i . What is desired is the number of fibers counted over D, and call this N_i . Assuming that the relative spacing of fibers over D and Y is the same, then

$$\frac{N_i}{n_i} = \frac{D}{Y} \quad ; \qquad N_i = \frac{n_i}{\cos\beta_i + \sin\beta_i}$$

The data are converted from fiber orientation in a square cell to fiber orientation per unit width perpendicular to the fiber axis, in Table 5.2. The fourth column, relative frequency, is the one of interest, and is also plotted in Figure 5.4 as a dashed line.

TABLE 5.2

FIBER ORIENTATION MEASUREMENTS FOR SQUARE AND CIRCULAR CELLS, FABRIC A

Angular Interval,	n_i	N_i	Relative Frequency	$N_i + \text{Sum}$	Relative Frequency	Average $\pm\beta$ Rel. Frequency
-85 85	5	5	.0181	14.0	.0180	.0180
-75 -85	4	3.45	.0088	14.4	.0186	.0192
-65 -75	5	3.90	.0141	16.9	.0218	.0293
-55 -65	11	8.05	.0291	27.0	.0348	.0378
-45 -55	16	11.35	.0411	31.3	.0404	.0346
-35 -45	13	9.22	.0334	23.2	.0299	.0346
-25 -35	19	13.90	.0504	33.9	.0437	.0489
-15 -25	27	21.00	.0761	52.0	.0671	.0720
- 5 -15	36	31.08	.1126	87.0	.1123	.1272
5 15	52	52.00	.1885	135.0	.1743	.1743
5 15	50	43.17	.1565	110.17	.1422	
15 25	34	26.50	.0960	49.5	.0768	
25 35	19	13.90	.0504	41.9	.0540	
35 45	12	8.51	.0308	30.5	.0393	
45 55	9	6.38	.0231	22.3	.0288	
55 65	13	9.51	.0344	31.5	.0406	
65 75	7	5.46	.0198	28.4	.0367	
75 85	4	3.45	.0125	15.4	.0199	
		$\Sigma = 275.8$		Σ 774.6		

Both sets of data are combined to give fiber orientation measurements on 775 fibers as shown in Table 5.2. Since the fiber orientation is symmetrical about the L axis, the relative frequencies of the plus and minus angular intervals can be averaged to improve the estimate of fiber orientation. This is done in the last column of Table 5.2. The final relative frequency fiber distribution is given as Figure 5.5.

2. Measurement of Weight of Average Unit Cell.

As mentioned previously in Section III, C.1, the average weight of the fabric can be expressed in two ways. The first is area density, or weight per unit area. In this investigation, area density has the units grams/sq. inch, although much larger areas are generally weighed. The second method is to use the equivalent denier of a one inch strip of the fabric. The two are directly related by

Area density (gms/sq. inch) x 9000 x 39.4 = Equivalent denier, or

Area density x 354,000 = Equivalent denier.

Both of these measures of fabric weight will be used.

The average area density of a number of specimens of Fabric A of different sizes and from different sheets was 16 grams/sq.yd or .0123 grams/sq. inch (at 65% R.H.) This is equivalent to 4400 denier for a one inch wide strip.

3. The Fiber Stress-Strain Curve

The fibers which constitute Fabric A are standard 1.5 denier viscose rayon. These fibers are shipped generally in the form of tow (zero twist bundles of thousands of continuous filaments) for wet-formed non-wovens. The tow is cut by the non-woven manufacturers into the short lengths required. A specimen of tow was obtained from C. H. Dexter and Sons, Inc., the manufacturer of Fabric A. Twenty filaments, or fibers, were selected

FIGURE 5.5

FINAL FIBER ORIENTATION DISTRIBUTION vs. ANGULAR INTERVAL

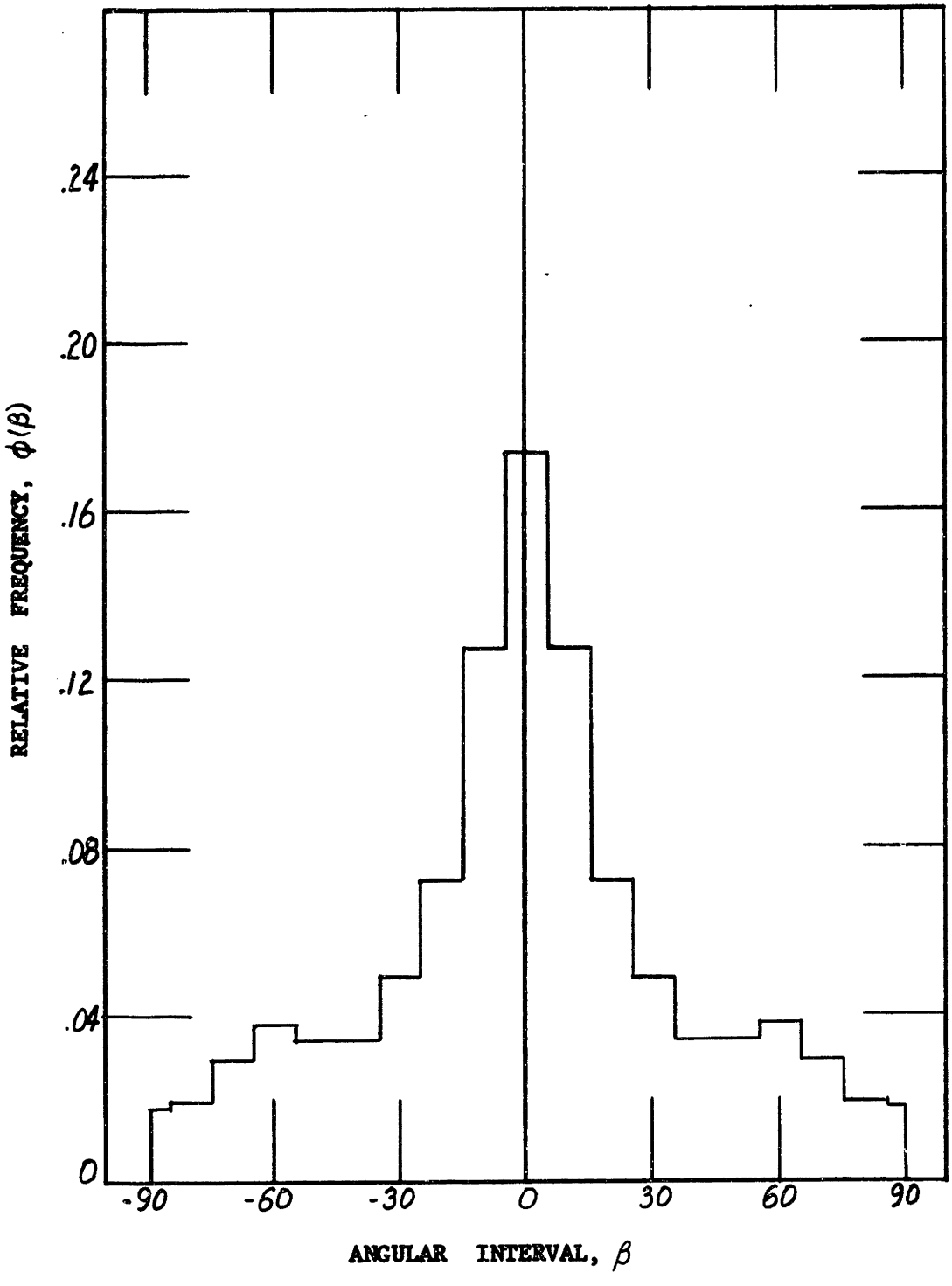

randomly from the tow, and tested.

The rate of strain used on the tests of Fabric A was 6.3%/min. In order to minimize rate effects, the fibers were tested with a gauge of 2 inches, and cross head rate of 0.12 inches/min. or a strain rate of 6%/min. These tests were also carried out at 60-65% R.H. The Instron curves are in terms of load vs. time. These were converted to strain using the strain rate; and to stress, by dividing the load in grams by the indicated denier of the fiber (1.5 denier). This gives stress in units of grams per denier, and a typical curve is shown in Figure 5.6, along with the straight line approximations. The straight line approximations are quite good for this fiber. Thus on each fiber load-elongation curve, four measurements were made: 1) Initial Modulus, 2) Rupture Load, 3) Rupture Elongation, and 4) Yield Point (the intersection of the two straight lines). This data is summarized for the twenty fibers in Table 5.3. The values given in Table 5.3 have been converted to stress units (grams/denier), and the equations of the average straight line approximations to the fiber stress-strain curve are:

$$\sigma_f = 72\, e_f \qquad e_f < 1.13\,\%$$
$$\sigma_f = .66 + 12.7 e_f \qquad e_f > 1.13\,\% \qquad (5.1)$$

B. Translation of Fiber Properties to Fabric Properties - Equations

Three distinct steps are necessary to translate fiber properties to fabric properties, as follows:

1) Translation of unit cell strains to fiber strains
2) Conversion of fiber strains to fiber stresses
3) Resolution of fiber stresses to component fabric stresses, and their summation.

These three steps will be considered separately.

FIGURE 5.6

SINGLE FIBER STRESS - STRAIN CURVE, VISCOSE RAYON,

1.5 DENIER, 65% R.H.

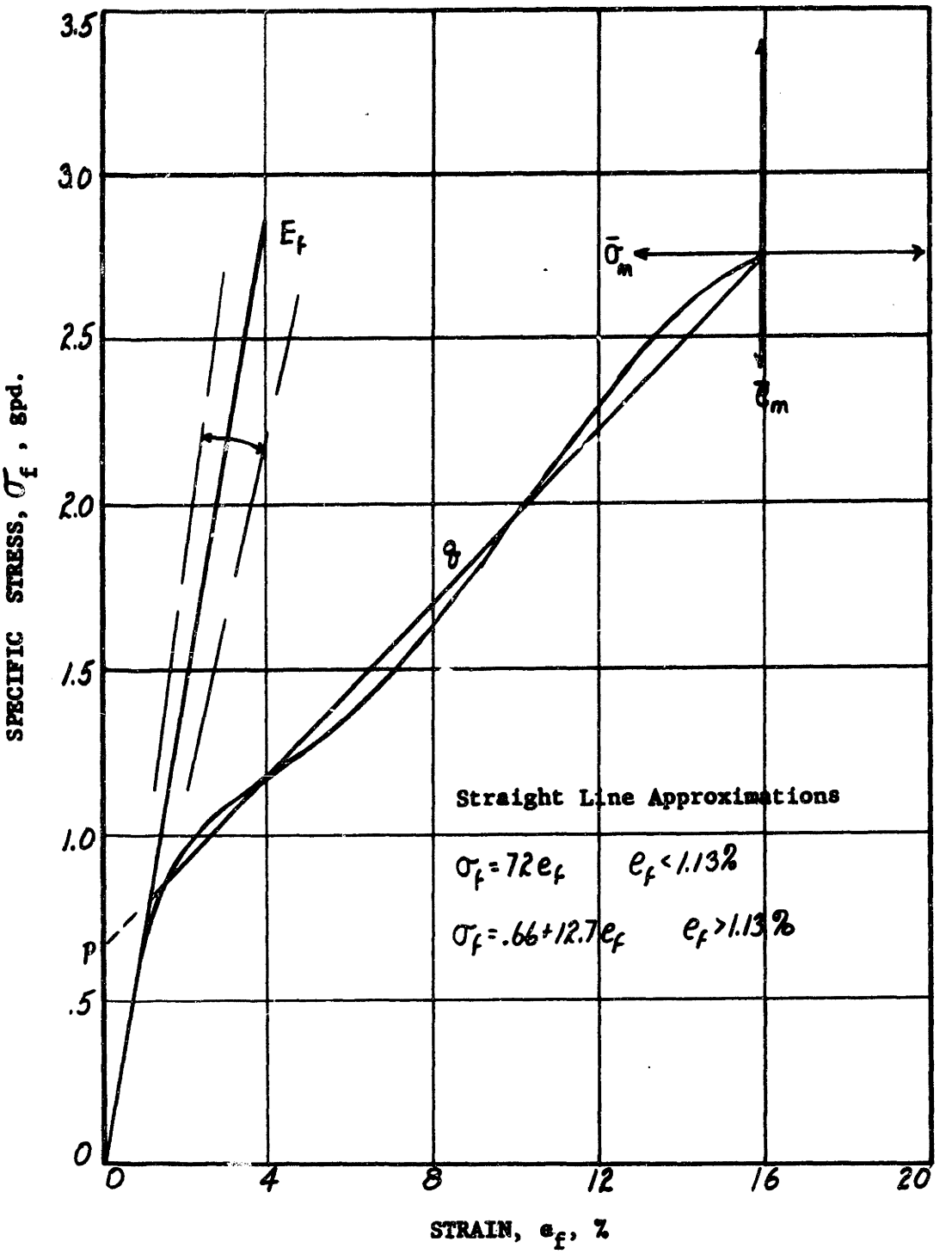

TABLE 5.3

VISCOSE RAYON, 1.5 DENIER, SINGLE FIBER PROPERTIES, 65% RH

Spec. #	Initial Modulus E_f, gpd.	Yield Point Y.P. gpd	Rupture Stress σ_m, gpd	Rupture Elongation e_m, %
1	74	.93	2.73	13.4
2	84	.80	2.60	14.3
3	67	.80	2.68	14.4
4	76	.87	3.00	14.5
5	60	.67	2.60	16.3
6	64	.73	2.40	15.4
7	-	.73	2.73	18.6
8	83	.93	3.40	19.8
9	-	.80	2.80	18.3
10	-	.87	2.80	18.5
11	54	.80	2.73	12.9
12	69	.73	2.53	15.7
13	95	.87	3.00	14.9
14	65	.73	2.53	18.0
15	73	.73	2.47	17.4
16	58	.70	2.40	16.2
17	85	.80	3.00	15.3
18	69	.73	2.47	16.2
19	73	1.07	3.13	17.4
Average	71.8	.805	2.74	16.13

1. Translation of Unit Cell Strains to Fiber Strains.

According to the definition of the unit cell, each fiber can be considered as straight, loaded only at the cell boundaries and these boundaries displaced parallel under stress. The fibers can be assumed individually clamped at the boundaries in accordance with the assumption of rigid bonds.

There are four possible relationships for the strain of the fibers in terms of the strain of the unit cell; - two for the case of small strain theory (where the fiber angle β does not change), and two for large strain theory (where β does change). The two sub-cases under the assumption of small or large strains concerns Poisson's ratio; i.e. whether it is considered to be zero or non-zero.

Small Strain Theory

Referring to Figure 5.7 and the diagrams for small strain, we will consider the cases where the change in fiber angle β is very small.

a. $\nu_{LT} = 0$. This requires point B, or the upper end of the fiber, to move vertically to B' just as the point A moves to A'. Then the unit cell strain e_c is the distance AA' = y divided by ℓ, an arbitrary unit cell length. At the same time, the change in length of the fiber is δ , or y cos β . Since the fiber length is $\frac{\ell}{\cos\beta}$, the fiber elongation $e_f = \delta/\ell/\cos\beta = \frac{y}{\ell}\cos^2\beta = e_c \cos^2\beta$. Since this is an average unit cell, the strain of the unit cell is identical with the strain of the fabric, e_L . Thus

$$e_f = e_L \cos^2\beta \qquad (5.2)$$

FIGURE 5.7

UNIT CELL STRAIN - FIBER STRAIN RELATIONSHIPS

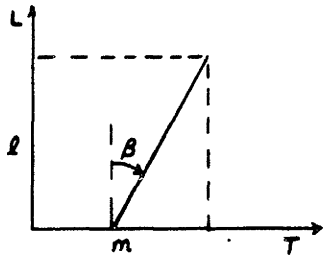

SMALL STRAIN THEORY:

a. $\nu_{LT} = 0$

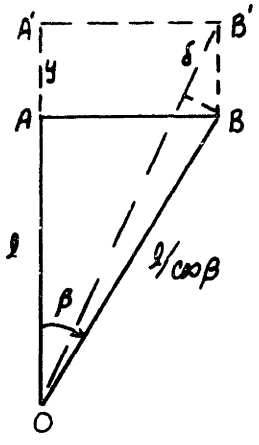

b. $\nu_{LT} \neq 0$

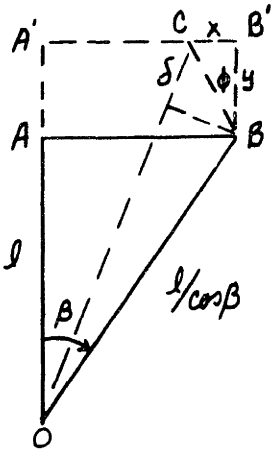

LARGE STRAIN THEORY:

c. $\nu_{LT} = 0$

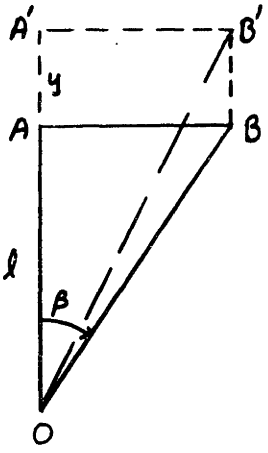

d. $\nu_{LT} \neq 0$

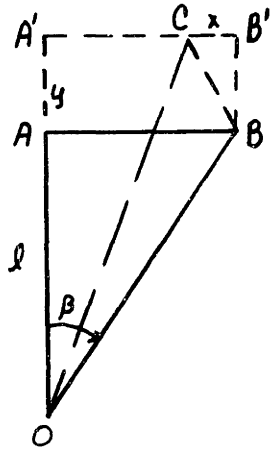

b. $\nu_{LT} \neq 0$. Point B moves vertically a distance y and horizontally a distance x. Then

$$\phi = \text{arc tan } x/y$$

$$\delta = \frac{y}{\cos\phi} \cos(\beta+\phi)$$

$$e_f = \frac{\delta}{\ell/\cos\beta}$$

$$= y/\ell \cos\beta [\cos\beta - \sin\beta \tan\phi]$$

Since $\tan\phi = x/y$

Strain in L direction $= e_L = y/\ell$

Strain in T direction $= e_T = x/\ell\tan\beta$

Thus

$$\tan\phi = \nu_{LT} \tan\beta$$

or

$$e_f = e_L [\cos^2\beta - \nu_{LT} \sin^2\beta] \qquad (5.3)$$

Large Strain Theory

In this case, the change of the fiber orientation angle β must be considered.

c. $\nu_{LT} = 0$. Again with uniform boundary displacement, B moves the distance y to B'. The original fiber length was OB $= \ell/\cos\beta$ and the new fiber length is

$$OB' = \sqrt{\overline{OA'}^2 + \overline{A'B'}^2} = \sqrt{(\ell+y)^2 + (\ell\tan\beta)^2}$$

The fiber strain is

$$e_f = \frac{OB' - OB}{OB}$$

$$e_f = \sqrt{\cos^2\beta\,(1 + y/\ell)^2 + \sin^2\beta} \; - 1$$

Since $e_L = y/\ell$;

$$e_f = \sqrt{\cos^2\beta\,(1 + e_L)^2 + \sin^2\beta} \; - 1 \qquad (5.4)$$

d. $\nu_{LT} \neq 0$. Now point B moves to point C, and the new fiber length OC is

$$OC = \sqrt{(\ell + y)^2 + (\ell \tan\beta - x)^2}$$

The fiber strain e_f is;

$$e_f = \frac{OC - OB}{OB} = \sqrt{\cos^2\beta(1 + y/\ell)^2 + \sin^2\beta(1 - x/\ell\tan\beta)^2} - 1$$

Since $e_L = y/\ell$, $e_T = x/\ell\tan\beta$, then

$$e_f = \sqrt{\cos^2\beta(1 + e_L)^2 + \sin^2\beta(1 - e_T)^2} \; - 1 \qquad (5.5)$$

In the above derivations, shear strain has been ignored. In an orthotropic material, stresses applied in the directions of the axes of symmetry, i.e., L and T, will not cause any shear strain or shear stress with respect to those axes. Thus both e_{LT} and σ_{LT} are zero when a normal stress is applied in the L or T direction. At other angles to the L axis, the normal stress can cause shear stress, or shear strain, depending on the boundary conditions assumed. This problem will be discussed in detail in Section VI.

2. Fiber Strains to Fiber Stresses

From V. A. 3. The two straight line approximations for the fiber stress-strain curve are

$$\sigma_f = 72\, e_f \qquad e_f < 1.13\% \qquad (5.1)$$

$$\sigma_f = .66 + 12.7\, e_f \qquad e_f > 1.13\%$$

The numerical data are for 65% RH on this particular fiber. In more general terms.

$$\sigma_f = E_f\, e_f \qquad 0 < e_f < e_p \qquad (5.6)$$

$$\sigma_f = p + q\, e_f \qquad e_f > e_p$$

where Ef is the Hookean fiber modulus (gpd), and e_p is the fiber proportional limit strain. The post-yield or plastic region is identified by the stress intercept p, and the secondary modulus q. (See figure 5.6). Substituting the values of fiber strain as obtained above for small strain theory.

a. $\nu_{LT} = 0$

$$\sigma_f = E_f\, e_f = E_f\, e_L \cos^2\beta \qquad 0 < e_L \cos^2\beta < e_p \qquad (5.7)$$

$$\sigma_f = p + q\, e_f = p + q\, e_L \cos^2\beta \qquad e_L \cos^2\beta > e_p$$

b. $\nu_{LT} \neq 0$

$$\sigma_f = E_f\, e_L \left[\cos^2\beta - \nu_{LT} \sin^2\beta\right] \qquad 0 < e_L\left[\cos^2\beta - \nu_{LT}\sin^2\beta\right] < e_p \qquad (5.8)$$

$$\sigma_f = p + q\, e_L \left[\cos^2\beta - \nu_{LT}\sin^2\beta\right] \qquad e_L\left[\cos^2\beta - \nu_{LT}\sin^2\beta\right] > e_p$$

Equations 5.7 and 5.8 give the stresses in each fiber (in gpd) due to a fabric or cell elongation .

3. Resolution of Fiber Stresses to Fabric Stresses. (Small Strain Theory)

The "Orientation Distribution", $\phi(\beta)$, has been defined as the relative frequency of fibers at an angle β per unit width $\perp$ to the direction of the fibers.

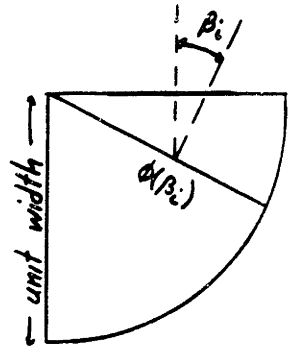

Referring to the diagram at left, the frequency of fibers at a particular angle β_i per unit width $\perp$ to β_i is $\phi(\beta_i)$. The relative frequency of these fibers which intersect a line of unit length $\perp$ to the L axis is $\phi(\beta_i) \times \cos \beta_i$. The contribution of any fiber at angle β_i to the specific stress in the L direction is the component of the specific fiber stress, $\sigma_f \cos\beta_i$. Thus the relative contribution of $\phi(\beta_i)\cos\beta_i$ fibers to the specific stress in the L direction is

$$\sigma_{L_i} = \sigma_f \, \phi(\beta_i) \cos^2\beta_i \quad * \qquad (5.9)$$

The total specific stress in the L direction is the summation of the relative contributions of all angular intervals or

*The specific fiber stresses can be converted to forces by multiplying by the fiber denier. The relative number of fibers can be converted to absolute numbers of fibers by multiplying the total number of fibers present in a unit area, (dependent on the area density). By this method, fiber forces are converted to fabric forces per unit width for this weight of fabric. Dividing the force per unit width by the area density leads to an identical expression for specific stress. The specific stress form is more convenient for later use in the introduction of unit cell variability.

$$\sigma_L = \sum_{i=1}^{i=n} \sigma_f \, \phi(\beta_i) \cos^2 \beta_i \qquad (5.10)$$

where each i interval is 10^o and therefore n = 18.

C. Predicted Fabric Properties in the L Direction

1. The Stress-Strain Curve

Referring to equations 5.7 and 5.10, knowledge of the fabric strain e_L, the orientation distribution $\phi(\beta)$, and the fiber constants, allows prediction of the fabric stress. However, equations 5.7 cannot be simply substituted into equation 5.10. For values of e_L slightly greater than e_p, $e_L \cos^2 \beta$ can be greater or less than e_p depending on the value of β. However by writing

$$\sigma_f = g(e_L, \beta)$$

equation 5.10 becomes:

$$\sigma_L = \sum_{i=1}^{i=18} g(e_L, \beta_i) \, \phi(\beta_i) \cos^2 \beta_i \qquad (5.11)$$

In practice, a value of e_L was selected, and e_f determined for each angular interval, β. The fiber stress σ_f was found for each interval and its component $\sigma_f \cos^2 \beta$, multiplied by its relative frequency $\phi(\beta)$, gave the contribution of this angular interval to the fabric stress. These contributions were summed to obtain the total fabric stress for the given strain e_L. This procedure is exemplified by Table 5.4 where e_L was taken as 1.5% strain. The fiber properties are taken from Figure 5.6 and $\phi(\beta)$ from Figure 5.5. Note that in the numerical calculation the plus and minus angular intervals were added, since $\phi(\beta)$ is symmetrical about the L axis.

TABLE 5.4

NUMERICAL CALCULATION OF FABRIC STRESS FOR FABRIC STRAIN OF 1.5%

	Angular Intervals, β									
	-5° to 5°	5° to 15°	15° to 25°	25° to 35°	35° to 45°	45° to 55°	55° to 65°	65° to 75°	75° to 85°	85° to 90°
Cell Midpoint, β_i	0°	10°	20°	30°	40°	50°	60°	70°	80°	90°
Relative Frequency[1], $\phi(\beta_i)$	.178	.255	.151	.103	.068	.068	.071	.052	.036	.018
$\cos^2\beta_i$	1.00	.970	.883	.750	.587	.413	.250	.117	.03	0
$-.54\sin^2\beta_i$[2]	0	.016	.064	.137	.226	.322	.411	-	-	
$e_f = 1.5(\cos^2\beta_i - .54\sin^2\beta_i)$	1.5	1.43	1.23	.92	.54	.13	— Compression			
σ_f[3]	.85	.84	.82	.663	.39	.09	—	—		
$\sigma_{L_i} = \sigma_{f_i}\cos^2\beta_i$	.85	.815	.725	.497	.228	.037	-	-		
$\sigma_{L_i} \times \phi(\beta_i)$	.154	.208	.110	.052	.015	.003	$\sum \sigma_{L_i} \times \phi(\beta_i) = \sigma_L = .54$ ppd			

1. $\phi(\beta_i)$ for plus and minus angular intervals added.

2. ν_{LT} calculated as 0.54

3. σ_f obtained from $\sigma_f = 7\ell e_f \quad e_f < 1.13\%$

$\sigma_f = .66 + 12.7 e_f \quad e_f > 1.13\%$

Numerical calculations at a number of values of e_L lead to a predicted fabric stress-strain curve. The fabric stress values obtained depend upon the particular case of strain transformation used. In Figure 5.8, four predicted curves are given together with the experimental data for fabric strains up to 3%. The lowest curve, A, is the measured stress - strain curve. Curves B, C and D are obtained from equation 5.10 using small strain theory: B assuming $\nu_{LT} = 0$; C assuming $\nu_{LT} = .54$*; and D using the measured value of $\nu_{LT} = 1.25$. The open circles along curve D are the results obtained using the measured value of ν_{LT} and large strain theory. The difference between small and large strain theory is negligible up to fabric strains of 4%. Beyond that point, the uncertainty in the value of ν_{LT} does not warrant the refinements of large strain transformation (equation 5.5). For instance, the measured value of ν_{LT} at $e_L = 3\%$ was approximately 1.80, and using this value lowered the calculated fabric stress from 0.64 to 0.62 gpd.

The general shape of the predicted curve is quite close to the measured fabric data, at least for small strains. Poisson's ratio affects the level of stress and the slope of the predicted curve in the so-called plastic region.

2. Predicted Initial Modulus

Since the fiber proportional limit strain e_p is greater than 1%, a fabric strain $e_L = 1\%$ can be used to determine the initial modulus E_L of the fabric. This can be done for the four cases described by

* ν_{LT} was calculated to be .54 on the basis of the measured $\phi(\beta)$ as described in the next section.

FIGURE 5.8

NUMERICALLY PREDICTED AND MEASURED STRESS-STRAIN CURVES, FABRIC A, $\Theta = 0^{\circ}$, (L)

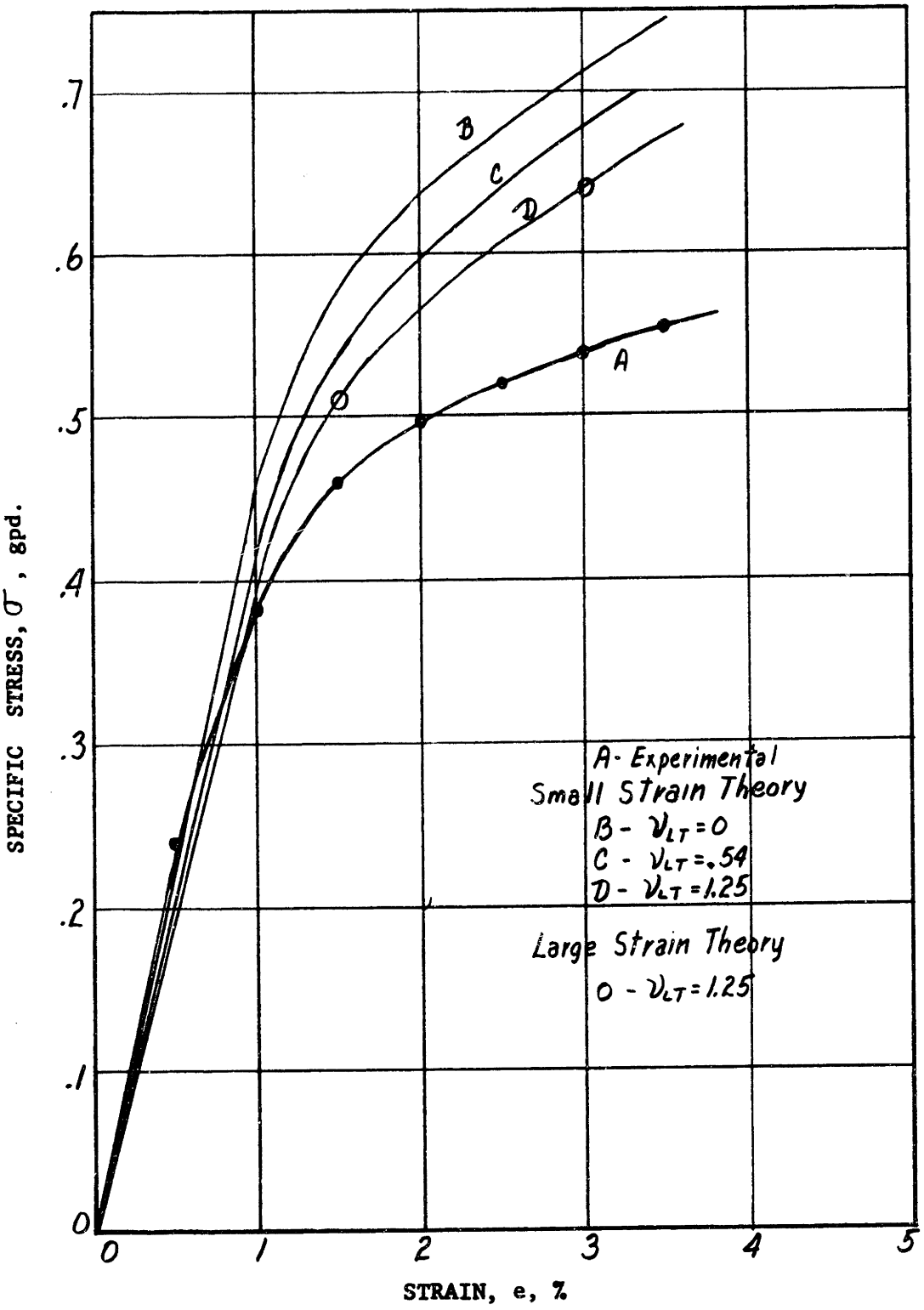

setting e_L = 1% in:

$$E_L = \frac{\sigma_L}{e_L}$$

These results are summarized as follows:

	E_L, gpd.
Measured on Fabric	45
Small Strain Theory, $\nu_{LT} = 0$	46
" " " , $\nu_{LT} = 0.54$	43
" " " , $\nu_{LT} = 1.25$	39
Large Strain Theory, $\nu_{LT} = 1.25$	39

All of the predicted values are within 20% of the measured modulus, and are quite satisfactory representations of the measured data.

All of the predicted stress-strain curves have proportional limits higher than the measured data. This is the result of two assumptions: 1) that the fibers all have the same proportional limit given by the average straight line approximations; and 2) that the strain in each fiber is uniform throughout the unit cell. Obviously both of these are idealizations, and in actuality, the predicted curve should show a lower proportional limit, and a more gradual change in slope from the Hookean to plastic modulus. This will tend to lower the stress level in the plastic region and bring the predicted curves into closer agreement with the measured data.

3. Measured and Calculated Poisson's Ratio

Equation 5.3 for the transformation of fabric strains to fiber strains was in the form

$$e_f = e_L\left[\cos^2\beta - \nu_{LT}\sin^2\theta\right] \qquad (5.3)$$

In the definition of uniaxial tension, the stress σ_L is the only acting stress, and σ_T is therefore equal to zero. Then if an equation for σ_T is formulated and set equal to zero, an initial value of ν_{LT} can be found. Thus

$$\sigma_f = E_f e_f = E_f e_L \left[\cos^2\beta - \nu_{LT} \sin^2\beta\right]$$

$$\sigma_T = \sum_{i=1}^{i=18} \sigma_{f_i}\, \phi(\beta_i) \sin^2\beta_i$$

$$= E_f e_L \sum_{i=1}^{i=18} \left(\cos^2\beta_i \sin^2\beta_i - \nu_{LT} \sin^4\beta_i\right) \phi(\beta_i) \qquad (5.12)^*$$

In order to set σ_T equal to zero in this form, the assumption must be made that the individual fibers can take compressive loads without buckling and that the compressive and tensile moduli are the same. Under these assumptions

$$\nu_{LT} = \frac{\sum_{i=1}^{i=18} \cos^2\beta_i \sin^2\beta_i\, \phi(\beta_i)}{\sum_{i=1}^{i=18} \sin^4\beta_i\, \phi(\beta_i)} \qquad (5.13)$$

and the calculated value of ν_{LT} is 0.54. The measured value of ν_{LT} was 1.25.

Of the two assumptions noted, the one involving fiber buckling is the most serious. While it has been stated that fibers were bonded from 3-8 times in a unit cell, observation of the fabric had shown that many

*The substitution can be made provided all fiber strains are less than e_p, or the fibers considered Hookean.

of the fibers oriented primarily in the T direction were on the surface of the non-woven and were poorly bonded. Since these fibers represent the largest terms in the $\sum \sin^4\beta_i\ \phi(\beta_i)$, the calculated ν_{LT} is not valid for this fabric. Preliminary calculations indicated that if every fiber intersection were bonded, then fiber buckling in this fabric would be small. Accordingly, sheets of Fabric A were returned to Dexter for re-impregnation with viscose. The measured ν_{LT} on this material was 0.47 (the procedure and data are given in VII.C.) Thus measurements of ν_{LT} on lightly bonded non-wovens will tend to exceed calculated values, primarily as a result of fiber buckling.

D. Predicted Fabric Properties in the T Direction

To obtain σ_T empirically from equations 5.8 and 5.10, the easiest procedure is to define a new angle

$$\beta' = \beta + 90^\circ$$

Then

$$\sigma_T = \sum_{i=1}^{i=18} \sigma_{f_i}\ \phi(\beta_i) \cos^2\beta_i'$$

$$e_f = e_T(\cos^2\beta' - \nu_{TL}\sin^2\beta')$$

and

$$\sigma_f = E_f e_f : \qquad \sigma_T = E_f e_T \sum_{i=1}^{i=18} (\sin^4\beta_i - \nu_{TL}\sin^2\beta_i\cos\beta_i)\,\phi(\beta_i)$$

Thus the same procedure can be used to find the predicted stress-strain curve by data similar to that of Table 5.4. The resulting calculations are plotted in Figure 5.9 for the calculated value of $\nu_{TL} = .134$. The divergence of the predicted and experimental curves is greater than in the

FIGURE 5.9

NUMERICALLY PREDICTED AND MEASURED STRESS - STRAIN CURVES, FABRIC A, $\theta = 90^{\circ}$(T)

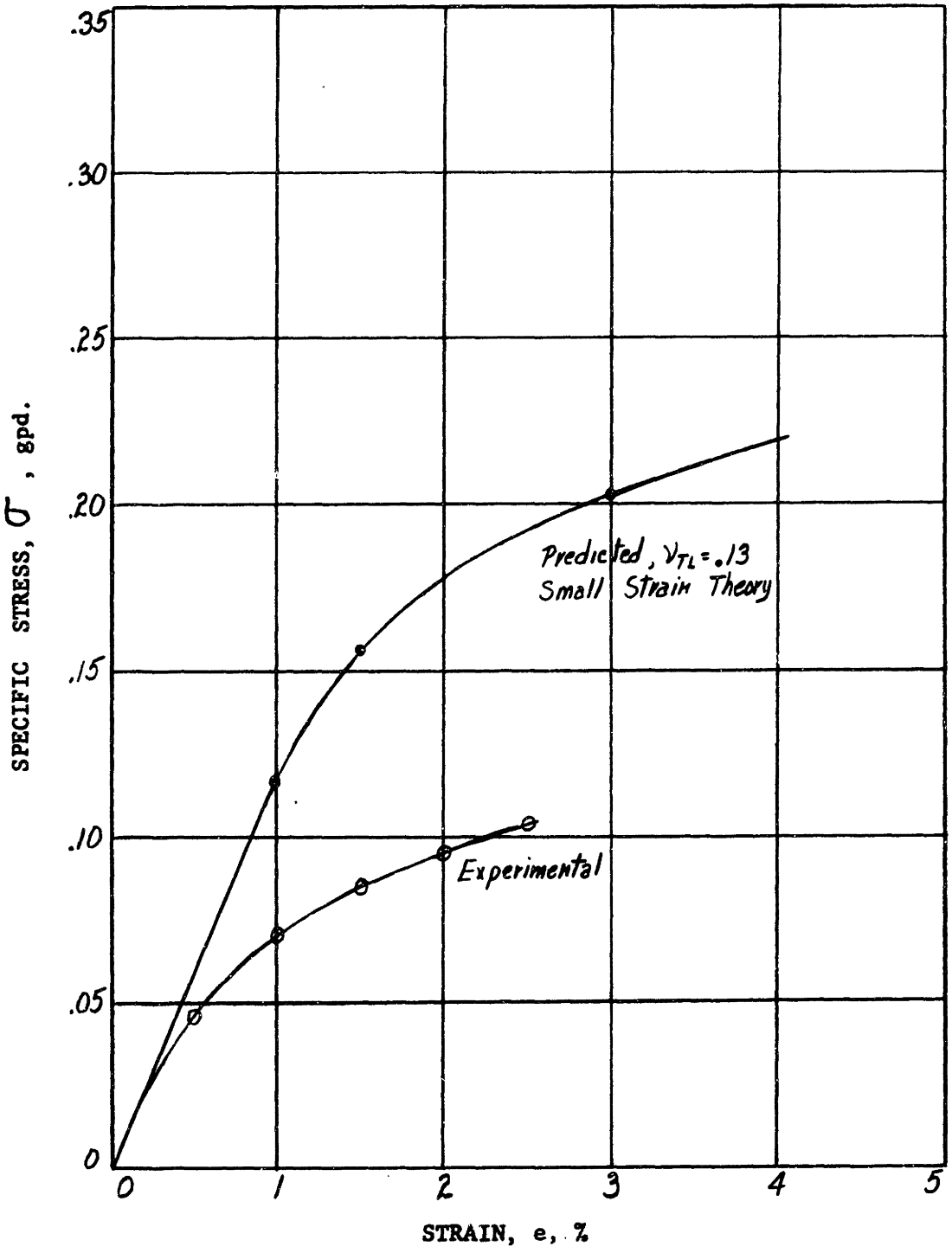

L direction. This was anticipated because of the poor bonding of the fibers oriented near the T direction. The predicted fabric modulus E_T = 11.6 gpd is in fair agreement with the measured value of 9.0 gpd.

The value of ν_{TL} = 0.13 was calculated by procedures identical with equation 5.13. This compares to the measured value of $\nu_{TL} \cong 0.24$. The reimpregnated fabric with more binder gave ν_{TL} = 0.15 (See VII.C), which is in excellent agreement with the predicted value.

E. Conclusions

The use of the average unit cell as a model to predict the initial part of the fabric stress-strain curves for the L and T directions is quite satisfactory. The agreement on initial modulus is good. However, the procedure is tedious and time consuming, and would be particularly slow if behaviour at test directions other than the symmetry axes were desired. A better procedure would be to replace the summation of stress components with an integratable $\phi(\beta)$; thus expressing the complete behaviour of the material in terms of continuous variables.

It might be pointed out that with a calculated value of $E_{45°}$ and subsequent solution of equation 3.12a for G_{LT} *, all of the required constants for use of the orthotropic equations have been obtained. Thus it is possible to use the numerical procedure to obtain E_L, E_T, ν_{LT}, & G_{LT}; and determine the values of these constants at other angles. However such a procedure is limited to elastic behavior. Prediction of the complete fabric stress-strain properties of the fiber is desired.

*a derivation for G_{LT} is given in section VI, F.

VI. FIBER WEB THEORY

In the previous sections, fabric stresses have been found as a result of numerical summation of the components of fiber stress from each angular interval, at various levels of fabric strain. It is proposed to represent $\phi(\beta)$ by a continuous function, such that the prior summations can be replaced by an integration. Thus equation 5.10

$$\sigma_L = \sum_{i=1}^{i=18} \sigma_f \, \phi(\beta_i) \cos^2 \beta_i$$

can be replaced by

$$\sigma_L = \int_{-\pi/2}^{\pi/2} \sigma_f \cos^2\beta \, \phi(\beta) \, d\beta \qquad (6.1)$$

A. The Empirical Fit of $\phi(\beta)$

Examination of the $\phi(\beta)$ distribution (Figure 5.5) shows a function periodic over the range of 180° or π, and symmetrical about the L axis, or $\beta = 0^\circ$. This suggests a Fourier series of cosine terms such as

$$\phi(\beta) = k\left(1 + a_1 \cos 2\beta + a_2 \cos 4\beta + a_3 \cos 6\beta + \cdots\right)$$

This series was examined and it was found that the function did not fit the experimental data well, and terms such as cos 10β and cos 12β were necessary to smooth the curve. A second type, combining cosines of multiples of β and powers of the cosine was tried; such as

$$\phi(\beta) = k(a + b\cos 3\beta + d\cos^{10}\beta)$$

This appeared more promising, but as cos 3β is a combination of cosβ and cos$^3\beta$, a series in powers of the cosine was selected. This proved

to be more easily handled, and thus $\phi(\beta)$ was taken in the form:

$$\phi(\beta) = k(a + b\cos\beta + c\cos^3\beta + d\cos^8\beta + e\cos^{16}\beta) \quad (6.2)$$

This was an arbitrary selection of powers of the cosine designed to keep the number of terms to five or less and obtain a good fit of the experimental data. As the integration procedure is rather long, a most general expression for $\phi(\beta)$ is desired. The function should be capable of describing an isotropic orientation, a moderate orientation and a severe orientation.

The expression for $\phi(\beta)$ has five arbitrary constants, which must be determined by solving five simultaneous equations. The conditions establishing these equations are

1. $\int_{-\pi/2}^{\pi/2} \phi(\beta)\, d\beta = 1$
2. $\beta = 0^\circ$; $\phi(\beta)$ = measured relative frequency
3. $\beta = 20^\circ$; $\phi(\beta)$ = " " "
4. $\beta = 40^\circ$; $\phi(\beta)$ = " " "
5. $\beta = 90^\circ$; $\phi(\beta)$ = " " "

The selection of $\beta = 20^\circ$ and $\beta = 40^\circ$ is arbitrary, and the use of 10° and 30° for the empirical fit will give slightly different results. Figure 6.1. shows the smoothed experimental data and two empirical fits of $\phi(\beta)$.*

*Note that in Figure 6.1, the abscissa is plotted in radians, not degrees, accounting for the change in scale of the ordinate. This scale factor is the angular interval with respect to the range or

$$\frac{\text{new relative frequency}}{\text{old relative frequency}} = \frac{1/\pi}{10^\circ/180^\circ} = \frac{18}{\pi}$$

This value was used to replot the measured data of Figure 5.5 in Figure 6.1.

FIGURE 6.1

EMPIRICALLY FITTED AND EXPERIMENTAL $\phi(\beta)$ vs. FIBER ANGLE β

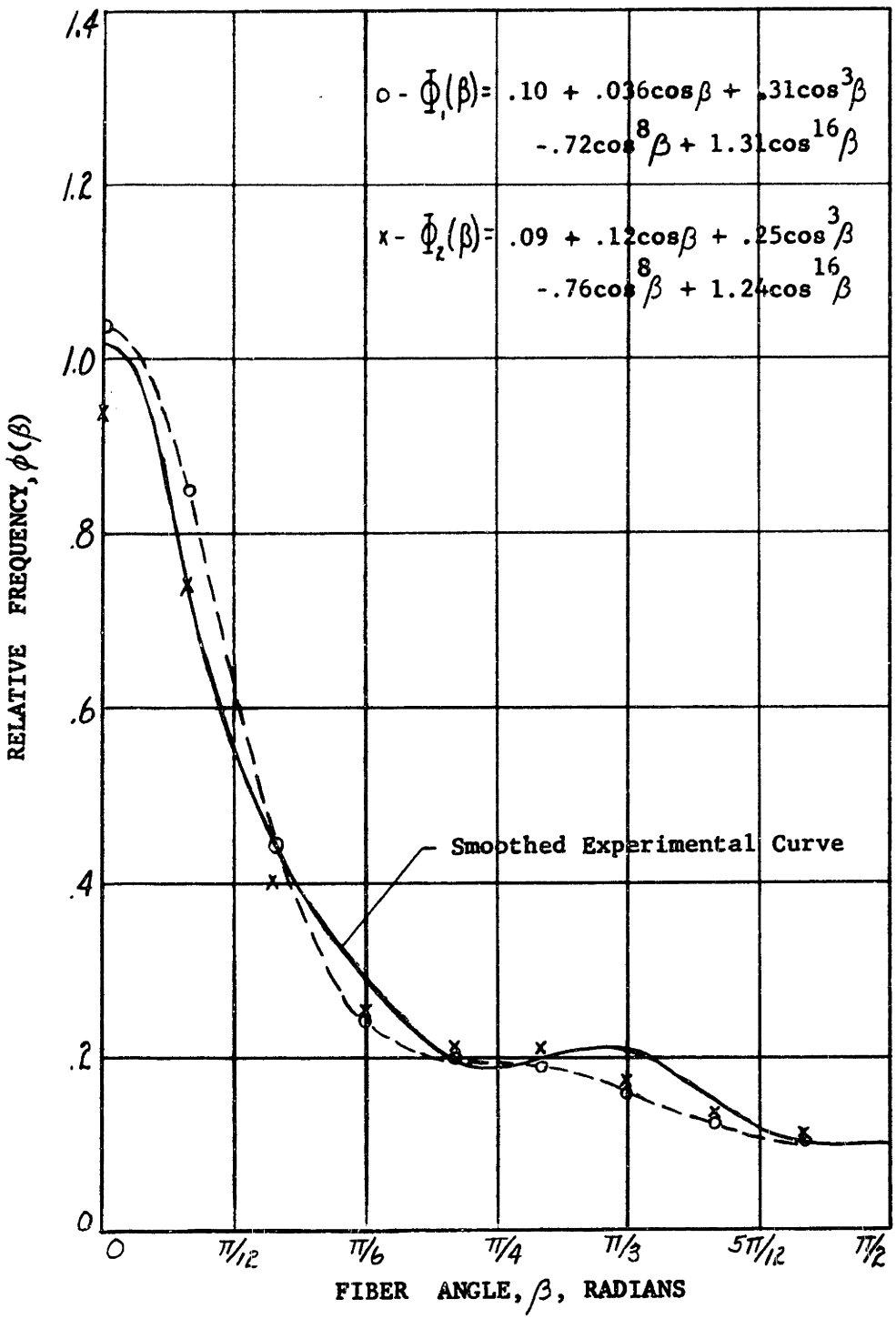

B. The Fiber Web Equations: Hookean Fiber

With the function $\phi(\beta) = a + b\cos\beta + c\cos^3\beta + d\cos^8\beta + e\cos^{16}\beta$, the expression for σ can be integrated, provided the fiber stress-strain curve is divided into two parts. These two parts are the Hookean region, where $\sigma_f = E_f e_f$ and the plastic, where $\sigma_f = p + q e_f$. While this procedure introduces some anomalies, these can be eliminated by a later transfer of axes. Thus the two solutions can be discussed separately.

Since the Hookean region involves small strains with a real Poisson's ratio, the strain transformation $e_f = e_L[\cos^2\beta - \nu_{LT}\sin^2\beta]$ will be used (equation 5.3). Then with $\sigma_f = E_f e_f$

$$\sigma_L = E_f e_L \int_{-\pi/2}^{\pi/2} [\cos^2\beta - \nu_{LT}\sin^2\beta]\cos^2\beta\ \phi(\beta)\, d\beta \qquad (6.3)$$

where E_f and σ_L are in grams per denier, and $\phi(\beta)$ is the relative fiber orientation distribution.

Since $E_L = \sigma_L / e_L$, we have

$$\frac{E_L}{E_f} = \int_{-\pi/2}^{\pi/2} [\cos^2\beta - \nu_{LT}\sin^2\beta]\cos^2\beta\ \phi(\beta)\, d\beta \qquad (6.4)$$

Poisson's Ratio ν_{LT} was shown to be a function of β only (V.C.3) as given by equation 5.13

$$\nu_{LT} = \frac{\sum_{i=1}^{i=18} \sin^2\beta_i \cos^2\beta_i\ \phi(\beta_i)}{\sum_{i=1}^{i=18} \sin^4\beta_i\ \phi(\beta_i)}$$

and this can now be put into integral form as

$$\nu_{LT} = \frac{\int_{-\pi/2}^{\pi/2} \sin^2\beta\cos^2\beta\ \phi(\beta)\, d\beta}{\int_{-\pi/2}^{\pi/2} \sin^4\beta\ \phi(\beta)\, d\beta} \qquad (6.5)$$

Combining 6.4 and 6.5

$$\frac{E_L}{E_f} = \int_{-\pi/2}^{\pi/2} \left[\cos^4\beta - \cos^2\beta \sin^2\beta \frac{\int_{-\pi/2}^{\pi/2} \sin^2\beta \cos^2\beta \, \phi(\beta) d\beta}{\int_{-\pi/2}^{\pi/2} \sin^4\beta \, \phi(\beta) d\beta} \right] \phi(\beta) d\beta \qquad (6.6)$$

The equations 6.5 and 6.6 give expressions for the fabric modulus, E_L and Poisson's ratio, ν_{LT} in terms of E_f and the five constants characterizing $\phi(\beta)$.

However, the equations are not general, since they will not yield any information about the properties of the fabric at angles other than $\theta = 0^\circ (L)$. If equations are to be developed to predict properties at all intermediate angles of θ, consideration must be given to the conditions of test. The orthotropic equations, simplified for uniaxial stress (equations 3.11, 3.12) imply that only one stress, σ_y , is acting, and that $\sigma_x = \sigma_{yx} = 0$. In an actual test, this would be the case if the jaws rotated freely, at the center point of clamping, such that the specimen was free of shear away from the restrained area near the jaws. An alternative would be to use an extremely long specimen, such that any shear stress imposed on the specimen by restricting the motion of the jaws would be very small.

A second test is where, not the shear stress, but the shear strain, e_{yx} , is zero. This is not the usual case found in textbooks, and will be discussed in more detail. The interesting point is that this latter condition seems to be a better representation of the actual experimental test. In the test procedure described in Section IIIB, the fabric specimen was distorted into an S or Z pattern, yet the gauge marks on the fabric remained almost orthogonal, or perpendicular. This implies that in the center of the specimen, $e_{yx} \cong 0$. Thus over the entire specimen length, a mixed

case exists with neither σ_{yx} or $e_{yx} = 0$.

Both cases will be analyzed, yet in slightly different fashion. The rather lengthy integration will be carried out for $e_{yx} = 0$, yielding E_y^* and ν_{yx}^* where the asterisk marks the conditions of a real σ_y, with $\sigma_x = e_{yx} = 0$. The true modulus in the y direction is defined for σ_y real, $\sigma_x = \sigma_{yx} = 0$, and will be denoted as Ey.

1. Boundary Conditions: $\sigma_x = 0,\ e_{yx} = 0$

Referring to the sketch below, consider a fiber which lies at the angle $(\theta + \beta)$ from the y axis (the axis of stress) and whose relative frequency is characterized by $\phi(\beta)$. The function $\phi(\beta)$ itself describes only the relative frequency of fibers with respect to the L axis $(\beta = 0^\circ)$ and is therefore independent of θ. However, the strains and stresses of the fiber, and the stress component in the y direction depend upon the angle $\theta + \beta$. Thus (for $e_{yx} = 0$)

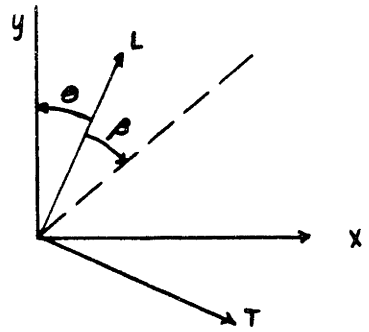

$$e_f = e_y \left[\cos^2(\theta+\beta) - \nu_{yx} \sin^2(\theta+\beta) \right]$$

$$\sigma_{yi} = \sigma_f \cos^2(\theta+\beta)$$

and the general equation for stress in the arbitrary direction y is:

$$\sigma_y = E_f e_y \int_{-\frac{\pi}{2}}^{\frac{\pi}{2}} \left[\cos^4(\theta+\beta) - \nu_{yx} \sin^2(\theta+\beta) \cos^2(\theta+\beta) \right] \phi(\beta)\, d\beta \qquad (6.7)$$

The same substitution of $\theta + \beta$ for β in equation 6.5 yields,

$$\nu_{yx} = \frac{\int_{-\pi/2}^{\pi/2} \cos^2(\theta+\beta) \sin^2(\theta+\beta)\, \phi(\beta)\, d\beta}{\int_{-\pi/2}^{\pi/2} \sin^4(\theta+\beta)\, \phi(\beta)\, d\beta} \qquad (6.8)$$

Subatitution of $\phi(\beta) = a + b\cos\beta + c\cos^3\beta + d\cos^8\beta + e\cos^{16}\beta$ in equations 6.7 and 6.8 leads to expressions in β and θ, which integrate to a function of θ and the five constants, a, b, c, d, and e.

Integration of ν^*_{yx}

Consider the numerator of equation 6.8, and expand to find

$$\begin{aligned}\cos^2(\theta+\beta)\sin^2(\theta+\beta) = {} & \sin^2\beta\cos^2\beta\left[\sin^4\theta - 4\sin^2\theta\cos^2\theta + \cos^4\theta\right] \\ & + \sin^4\beta\left[\sin^2\theta\cos^2\theta\right] \\ & + \cos^4\beta\left[\sin^2\theta\cos^2\theta\right] \\ & + 2\sin\beta\cos^3\beta\left[\sin\theta\cos^3\theta - \sin^3\theta\cos\theta\right] \\ & + 2\sin^3\beta\cos\beta\left[-\sin\theta\cos^3\theta + \sin^3\theta\cos\theta\right]\end{aligned}$$

Then the numerator consists of separate integrations of the five expanded terms multiplied by $\phi(\beta)$. The first of these is, upon integration;

$$\left[\frac{\pi}{8}a + \frac{4}{15}b + \frac{16}{105}c + \frac{21\pi}{1024}d + .0292e\right]\left[\sin^4\theta - 4\sin^2\theta\cos^2\theta + \cos^4\theta\right]$$

The second and third terms also result in real answers, but the indicated odd powers of sine and cosine of the last two terms integrate to zero. Thus the complete numerator of ν^*_{yx} becomes

$$\begin{aligned}& [.393a + .267b + .152e + .0645d + .0292e]\left[\sin^4\theta - 4\sin^2\theta\cos^2\theta + \cos^4\theta\right] \\ + & \left[1.18a + .400b + .114e + .0215d + .00514e\right]\left[\sin^2\theta\cos^2\theta\right] \\ + & \left[1.18a + 1.067b + .914c + .709d + .554e\right]\left[\sin^2\theta\cos^2\theta\right]\end{aligned}$$

Since each of the three terms in the brackets is a constant for any particular fiber orientation distribution, they can be designated A_1, A_2, and A_3, and the numerator of ν^*_{yx} becomes

$$A_1 \sin^4\theta + A_1 \cos^4\theta + (A_2 + A_3 - 4A_1)\sin^2\theta\cos^2\theta$$

Similar expansion of the denominator leads to identical bracketed terms, for a, b, etc., and thus

$$\nu^*_{yx} = \frac{A_1 \sin^4\theta + A_1 \cos^4\theta + (A_2 + A_3 - 4A_1)\sin^2\theta\cos^2\theta}{A_3 \sin^4\theta + A_2 \cos^4\theta + 6A_1 \sin^2\theta\cos^2\theta} \qquad (6.9)$$

where

$$\begin{aligned} A_1 &= .393a + .267b + .152c + .0645d + .0292e \\ A_2 &= 1.18a + .400b + .114c + .0215d + .00514e \\ A_3 &= 1.18a + 1.067b + .914c + .709d + .554e \end{aligned} \qquad (6.10)$$

Integration of E^*_y/E_f

Referring to equation 6.7, it can be seen that the second part of this expression is the same as the numerator of ν^*_{yx}. The first part involves the expansion of $\cos^4(\theta+\beta)$ and thus

$$\frac{E^*_y}{E_f} = \left[A_3\cos^4\theta + A_2\sin^4\theta + 6A_1\sin^2\theta\cos^2\theta - \nu_{yx}\left\{A_1\sin^4\theta + A_1\cos^4\theta + (A_2+A_3-4A_1)\sin^2\theta\cos^2\theta\right\}\right]$$

Substitution of equation 6.9, after simplification using the identity $\sin^2\theta + \cos^2\theta = 1$ yields:

$$\frac{E_y^*}{E_f} = \frac{(A_2A_3 - A_1^2) + \sin^2 2\theta\,(A_1A_2 + A_1A_3 - A_2A_3 + 3A_1^2)}{A_3\sin^4\theta + A_2\cos^4\theta + 6A_1\sin^2\theta\cos^2\theta} \qquad (6.11)$$

where the constants A_1, A_2, A_3, are as before.

Equations 6.9 and 6.11, with the equation set 6.10, provide equations for a modulus of elasticity, E_y^*, and a Poisson's ratio, ν_{yx}^*, in the arbitrary direction y, with the conditions $\sigma_x = e_{yx} = 0$. These equations are restricted to the case of Hookean fibers.

2. Boundary Conditions: $\sigma_x = \sigma_{yx} = 0$

As pointed out previously, when the applied normal stress acts in the direction of one of the orthotropic axes, no shear strain is produced. Thus for E_L, E_T, ν_{LT}, & ν_{TL} the boundary conditions $\sigma_{LT} = 0$ and $e_{LT} = 0$ are identical. Referring to equations 6.9 and 6.11, it can easily be seen that

$$E_L^* = E_L = E_f\frac{A_2A_3 - A_1^2}{A_2} \qquad \nu_{LT}^* = \nu_{LT} = \frac{A_1}{A_2}$$

$$E_T^* = E_T = E_f\frac{A_2A_3 - A_1^2}{A_3} \qquad \nu_{TL}^* = \nu_{TL} = \frac{A_1}{A_3} \qquad (6.12)$$

The boundary conditions $\sigma_x = \sigma_{yx} = 0$ are the same as those given in the simplified orthotropic theory for uniaxial tensile tests. Thus substitution of the above relations into equations 3.12a - 3.12d is correct. However, no derived expression for G_{LT} has been found in terms of the constants of the integrated fiber orientation distribution. This

derivation is given in sub-division F of this section and equation 6.30 gives

$$G_{LT}^{*} = G_{LT} = A_1 E_f$$

Substitution of equations 6.12 and 6.30 into equation 3.12a

$$\frac{1}{E_y} = \frac{\cos^4\theta}{E_L} + \frac{\sin^4\theta}{E_T} + \left[\frac{1}{G_{LT}} - \frac{2\nu_{LT}}{E_L}\right]\sin^2\theta\cos^2\theta \qquad (3.12a)$$

gives

$$\frac{E_y}{E_f} = \frac{A_1 A_2 A_3 - A_1^3}{A_1 A_2 \cos^4\theta + A_1 A_3 \sin^4\theta + (A_2 A_3 - A_1^2)\sin^2\theta\cos^2\theta} \qquad (6.13)$$

Similarly, for Poisson's ratio:

$$\nu_{yx} = \frac{A_1^2 - (A_1 A_2 + A_1 A_3 - A_2 A_3 + 3A_1^2)\sin^2\theta\cos^2\theta}{A_1 A_3 \sin^4\theta + A_1 A_2 \cos^4\theta + (A_2 A_3 - 3A_1^2)\sin^2\theta\cos^2\theta} \qquad (6.14)$$

Again a discussion of G_{yx} will be deferred until the end of this section, since no experimental verification can be made.

For those mathematically inclined, the equations given above for both sets of boundary conditions can be derived from the orthotropic theory, and this proof is given in Appendix D.

C. Predicted Properties with the Fiber Web Equations: Hookean Region

The use of the function $\phi(\beta)$ and subsequent integration has led to a general expressions for E_y^*, ν_{yx}^*, E_y and ν_{yx}, based on Hookean Fibers. The values given by these equations can be compared to the experimental data.

1. Predicted and Measured Ey.

The general equation for the modulus is given by equation 6.11 with the constants defined by equation set 6.10. Using the empirically fitted $\phi(\beta)$ function indicated as $\Phi_1(\beta)$ (Figure 6.1).

$$\Phi_1(\beta) = .10 + .036\cos\beta + .31\cos^3\beta - .72\cos^8\beta + 1.31\cos^{16}\beta$$

the constants A_1, A_2, A_3 are:

$$\begin{aligned} A_1 &= .393a + .267b + .152c + .0645d + .0292e = .0891 \\ A_2 &= 1.18a + .400b + .114c + .0215d + .00514e = .1624 \\ A_3 &= 1.18a + 1.067b + .914c + .709d + .554e = .6645 \end{aligned} \qquad (6.15)$$

Then equations 6.11 and 6.13 become

$$\frac{E_y^*}{E_f} = \frac{.0988 - .0420\sin^2\theta\cos^2\theta}{.665\sin^4\theta + .1624\cos^4\theta + .535\sin^2\theta\cos^2\theta} \qquad (6.16)$$

$$\frac{E_y}{E_f} = \frac{.0988}{.665\sin^4\theta + .1624\cos^4\theta + .96\sin^2\theta\cos^2\theta} \qquad (6.17)$$

and the results are tabulated below for various values of θ as both the ratios E_y/E_f and as absolute values of Ey, using the measured E_f = 72 gpd.

θ	0°	10°	20°	30°	40°	50°	60°	70°	80°	90°
E_y^*/E_f	.608	.577	.495	.390	.296	.230	.188	.164	.153	.148
E_y^*	43.7	41.5	35.6	28.0	21.3	16.6	13.5	11.8	11.0	10.6
E_y/E_f	.608	.54	.422	.325	.247	.203	.175	.159	.151	.148
E_y	43.7	38.	30.3	22.6	17.8	14.6	12.6	11.4	10.8	10.6

These predicted moduli are plotted in Figure 6.2 along with the experimental data and the values obtained using the orthotropic theory, equation 3.12a, with experimental E_L, E_T, ν_{LT}, & G_{LT}. The agreement is

FIGURE 6.2

INITIAL SPECIFIC MODULI, FABRIC A: MEASURED;

ORTHOTROPIC AND FIBER WEB THEORY

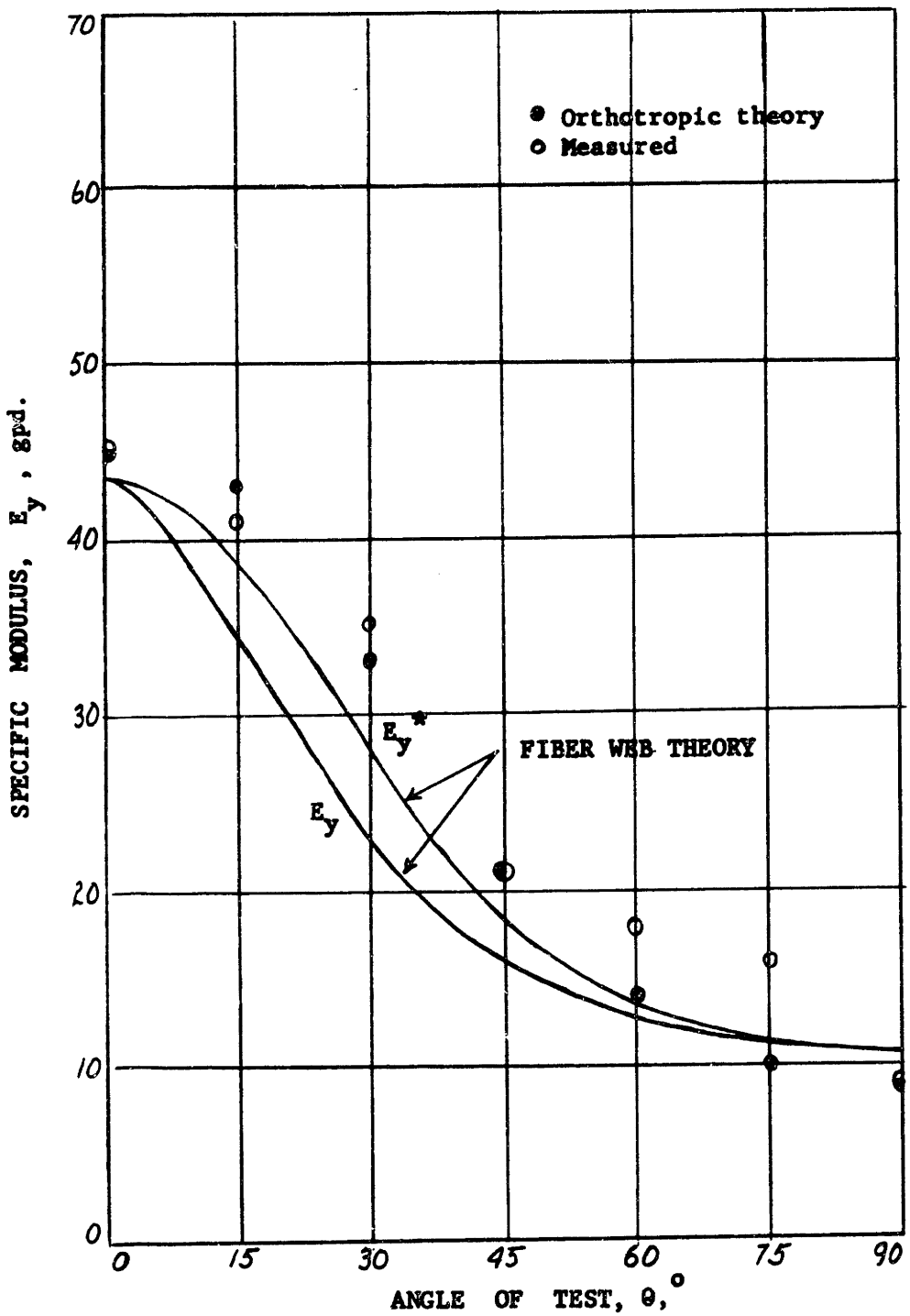

good, with Ey* appearing slightly better in agreement. Thus the initial moduli of an orthotropic flexible nonwoven can be predicted by knowledge of the fiber distribution and the fiber properties, under the assumption of uniform unit cells, or uniform fabric.

2. Predicted and Measured ν_{yx}

The general equations for Poisson's ratio ν^*_{yx} (equation 6.9) or ν_{yx} (equation 6.14) depend only on the values of A_1, A_2 and A_3 as given by equation set 6.15, or

$$\nu^*_{yx} = \frac{.0891 + .293 \sin^2\theta \cos^2\theta}{.665 \sin^4\theta + .1624 \cos^4\theta + .535 \sin^2\theta \cos^2\theta} \qquad (6.18)$$

and

$$\nu_{yx} = \frac{.0891 + 1.18 \sin^2\theta \cos^2\theta}{.665 \sin^4\theta + .1624 \cos^4\theta + .96 \sin^2\theta \cos^2\theta} \qquad (6.19)$$

The values of ν^*_{yx} and ν_{yx} are plotted in Figure 6.3 together with the measured data and the values calculated from the orthotropic theory by equation 3.12b, again with the experimental values of E_L, E_T, ν_{LT}, and G_{LT}.

The agreement between the two methods is not good. The explanation for the large discrepancy near $\theta = 0^\circ$ is fiber buckling, as has been discussed previously. The experimental data is not accurate from $\theta = 45^\circ$ to 90°, because of the errors involved in measuring transverse contraction on a one inch gauge. Thus the difference between the two curves in this region is probably not significant.

The points indicated on Figure 6.3 by small squares are experimental data obtained on High Viscose Fabric A, as detailed in Section VII. It would appear that the equation for ν^*_{yx} gives a better prediction of Poisson's ratio. This might be explained by the considerably greater flexual (and probably bias) stiffness of the material. In the preceding

FIGURE 6.3

POISSON'S RATIOS, FABRIC A, MEASURED;

ORTHOTROPIC AND FIBER WEB THEORY

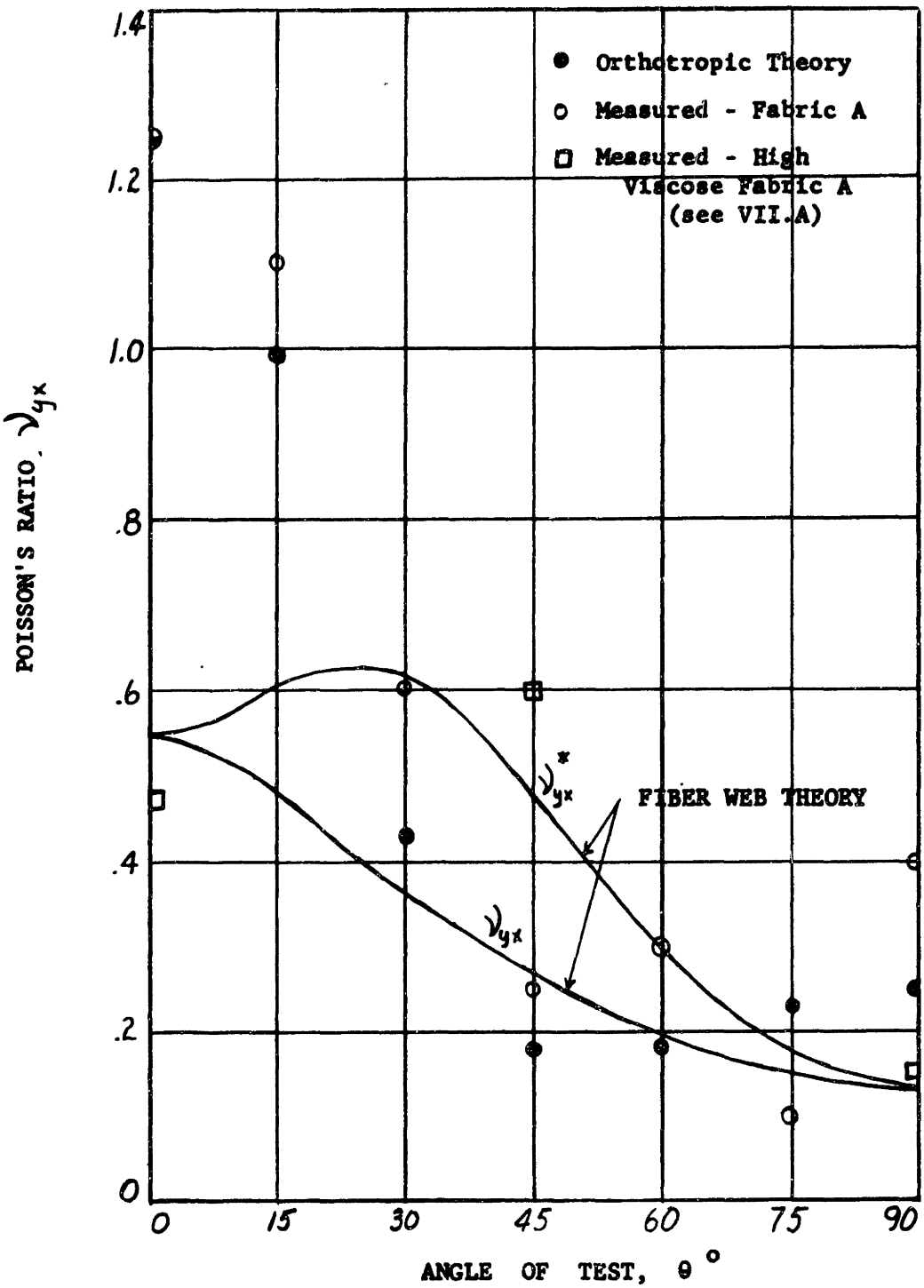

Figure 6.2 for specific modulus, the predicted values of E_y^* were also in better agreement. Thus the conditions of test will be assumed to conform more closely to $\sigma_x = e_{yx} = 0$ and the equations for E_y^* and ν_{yx}^* will be used in the remainder of the investigation.

D. The Fiber Web Equations: Plastic Fiber

All fibers are now represented by the fiber stress-strain equation $\sigma_f = p + q e_f$, where p is the stress intercept at zero strain and q is the plastic modulus. Using the small strain transformation for the boundary conditions $\sigma_x = e_{yx} = 0$ leads to:

$$\sigma_y = \int_{-\pi/2}^{\pi/2} \left[p + q\, e_y \left\{ \cos^2(\theta+\beta) - \nu_{yx} \sin^2(\theta+\beta) \right\} \right] \cos^2(\theta+\beta)\, \phi(\beta)\, d\beta$$

$$= p \int_{-\pi/2}^{\pi/2} \cos^2(\theta+\beta)\, \phi(\beta)\, d\beta + q e_L \int_{-\pi/2}^{\pi/2} \left[\cos^4(\theta+\beta) - \nu_{yx} \sin^2(\theta+\beta) \cos^2(\theta+\beta) \right] \phi(\beta)\, d\beta \qquad (6.20)$$

Integration of equation 6.20 yields:

$$\sigma_y = p\left[A_4 \cos^2\theta + A_5 \sin^2\theta\right] + q e_y \left[\frac{(A_2 A_3 - A_1^2) + \sin^2 2\theta \left(A_1 A_2 + A_1 A_3 - A_2 A_3 + 3A_1^2\right)}{A_3 \sin^4\theta + A_2 \cos^4\theta + 6A_1 \sin^2\theta \cos^2\theta} \right]$$

or

$$\sigma_y = p\left[A_4 \cos^2\theta + A_5 \sin^2\theta\right] + q\, e_y \frac{E_y^*}{E_y} \qquad (6.21)$$

where

$$A_4 = 1.708a + 1.33b + 1.067c + .773d + .583e \qquad (6.22)$$

$$A_5 = 1.708a + .667b + .266c + .086d + .0325e$$

and A_1, A_2, and A_3 are again given by equation set 6.10.

The first term of equation 6.20 is nothing more than the transformation of a fixed fiber stress, p. Therefore it is independent of the boundary condtions of the test. For the boundary conditions $\sigma_x = \sigma_{yx} = 0$, substitute E_y/E_f for E_y^*/E_f in equation 6.21 or

$$\sigma_y = p\left[A_4 \cos^2\theta + A_5 \sin^2\theta\right] + q\, e_y\, E_y/E_f \qquad (6.23)$$

E. The Predicted Stress-Strain Curve

At this point, distinct and spearate equations for the prediction of the stress-strain behavior of the fabric. These equations are based on all fibers being Hookean; or all fibers plastic. The fiber is actually a combination of these two cases, as shown diagramatically below:

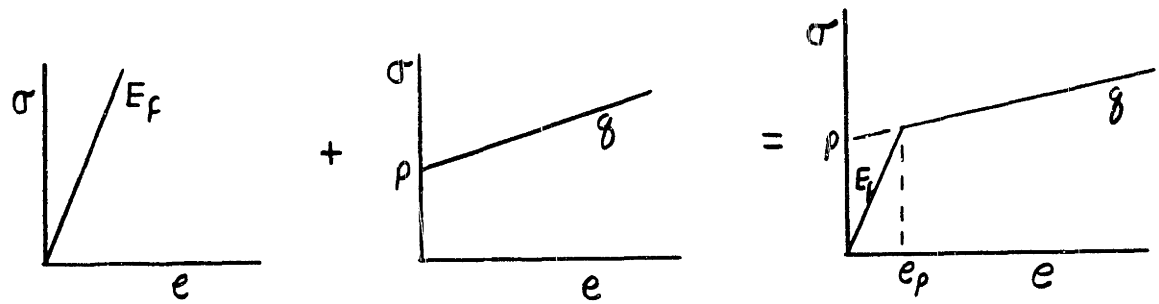

However, the fabric cannot be represented by this simple linear combination. At fabric strains just beyond the fiber proportional limit strain ep, some of the fibers will act Hookean and some plastic, depending on the value of β . This will tend to reduce the value of the stress intercept for the plastic case. By comparing the solutions of the general equations to the numerical prediction of the fabric stress-strain curve, a simple combining method can be found. Replot the data for the fabric stress-strain curve numerically calculated with $\nu_{LT} = .55$ (curve C in Figure 5.8) in Figure 6.4. The initial modulus E_L predicted by the general equation is shown as the line E_L . The modulus E_2 is the line given by the general equation for the plastic region, obtained from equations 6.21 and 6.22 with $\theta = 0^{\circ}$ and

(6.24)

$$A_4 = .763$$

$$A_5 = .264$$

FIGURE 6.4

COMBINING HOOKEAN AND PLASTIC SOLUTIONS OF THE FIBER WEB THEORY

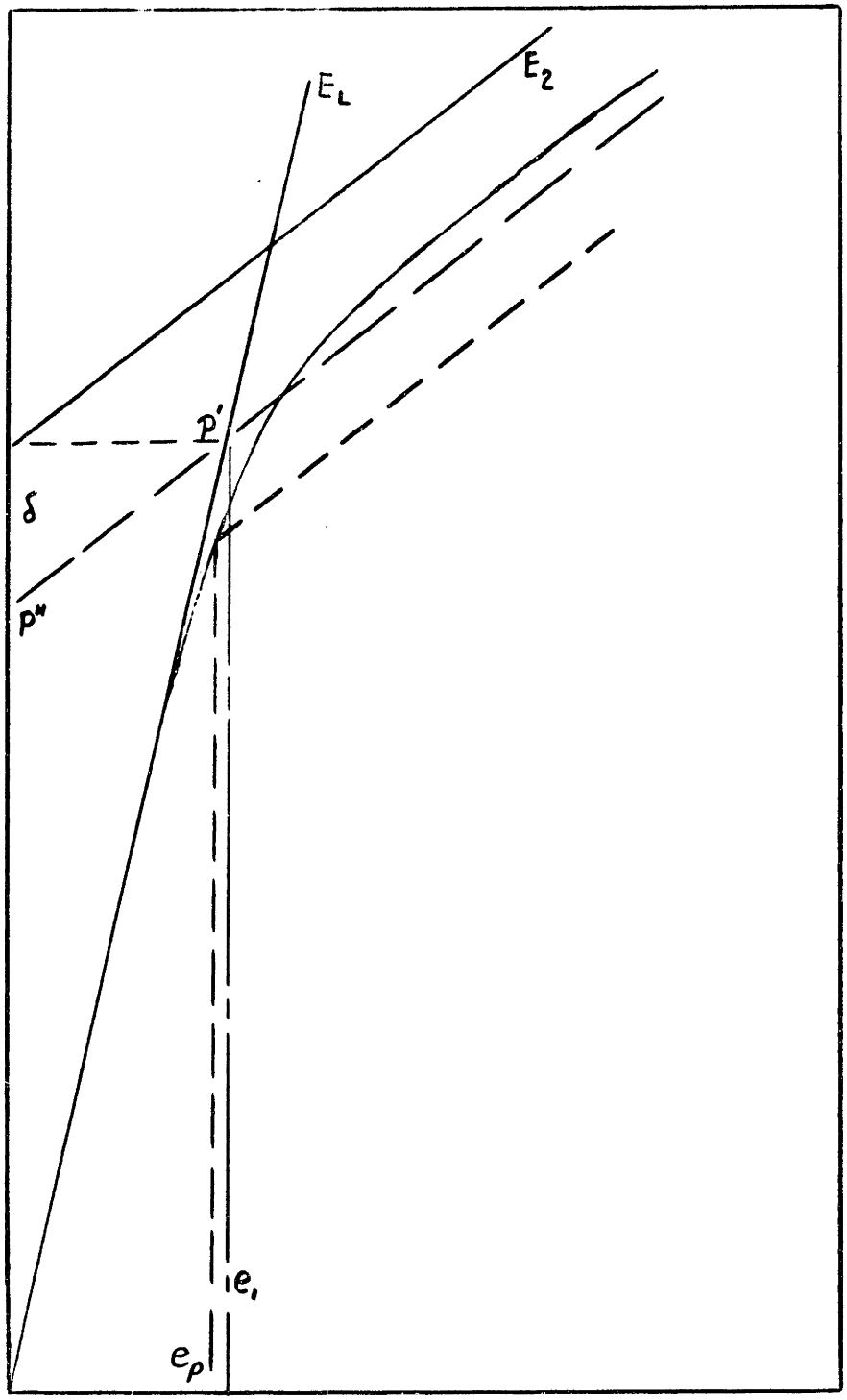

Therefore

$$\sigma_L = p A_4 + q e_L^{E_L/E_f}$$

and with p = .66 gpd and q = 12.7 gpd (equation 5.1)

$$\sigma_L = .511 + 7.73\, e_L$$

Two simple methods can be used to transpose the plastic curve to the Hookean curve. The first of these is to move the stress intercept P to the point P' on the Hookean curve and draw the plastic curve with the same slope $E_L = 7.73$ gpd. This agrees well with the numerical procedure. The second is to place the intercept of the plastic region and the elastic region at the proportional limit strain of the fiber, ep. This implies that all fibers at all angles enter the plastic region when the fabric strain reaches the fiber strain ep. This is not true and will give too low a value for the intersection, as shown.

The first of these methods was selected, i.e., to translate the stress intercept of plastic curve to the Hookean modulus line. This gives a new stress intercept p" where $P - p'' = \delta$, and $\delta = E_2 e_1$. Since $e_1 = P/E_L$

$$p'' = P - \delta = P - \frac{E_2}{E_L} P$$

From equation 6.25,

$$E_2 = q^{E_L/E_f}$$

and the equation for the plastic region, with this translation, becomes

$$\sigma_y = p\left[1 - q/E_f\right]\left[A_4 \cos^2\theta + A_5 \sin^2\theta\right] + q\, e_y^{E_y^*/E_y} \qquad (6.26)$$

$$\sigma_y = p'' + E_2 e_y \qquad (\sigma_x = e_{yx} = 0) \qquad (6.27)$$

Then with

$$p = .66 \text{ gpd.}, \quad q = 12.7 \text{ gpd.}, \quad E_f = 72 \text{ gpd.}$$

A_4 and A_5 given by 6.24 and E_4^*/E_f by 6.16, σ_4 can be tabulated as below.

θ	0	10	20	30	40	50	60	70	80	90
ρ''	.42	.41	.38	.35	.30	.26	.21	.18	.15	.157
E_2	7.73	7.4	6.3	5.0	3.8	2.9	2.4	2.1	1.9	1.9

Figure 6.5 shows the results of equations 6.16 and 6.27 (dashed lines) for $\theta = 0^\circ$, 45°, and 90° with the numerically predicted curves as solid lines.

The straight line approximations are in good agreement with the numerical procedure, and provide a simpler method of predicting the complete stress-strain behavior of a flexible non-woven fabric from the orientation distribution of the fibers and the fiber properties under either of two sets of boundary conditions.

F. The Modulus of Rigidity, G

If the unit cell provides a true representation of the fabric, then a modulus of rigidity should be predicted by the assumptions of the unit cell. The engineering modulus of rigidity, G_{LT}, is defined

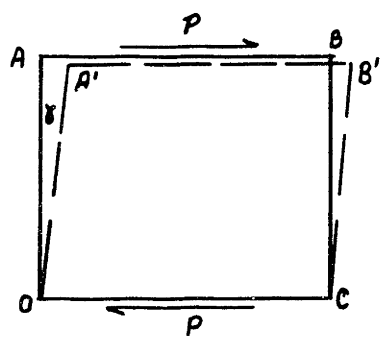

$$\gamma_{LT} = \frac{\tau_{LT}}{G_{LT}} \qquad (6.28)$$

where γ_{LT} is the angular rotation of the line OA about 0, under the influence of the force couple P, where the element OABC is of unit volume. Thus the stress τ_{LT} = P/unit thickness x unit edge length = P; and $G_{LT} = P/\gamma$.

FIGURE 6.5

PREDICTED FABRIC A STRESS STRAIN CURVES, NUMERICAL AND FIBER WEB THEORY

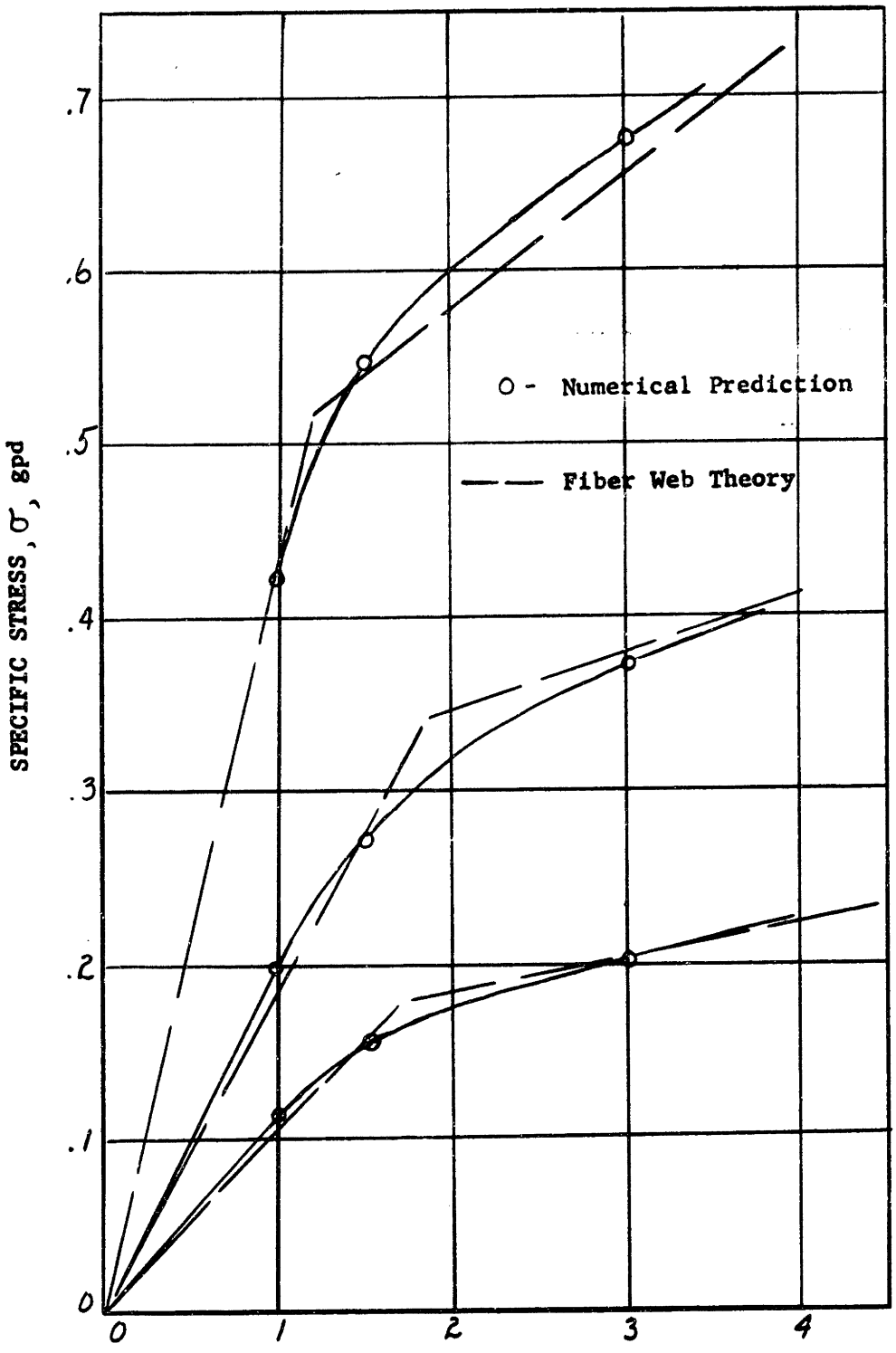

Consider the sketch below as a unit cell with the fibers loaded only at the boundaries of this cell and the strained state greatly magnified. The cell OABC is deformed to OA'B'C and the fiber DE deformed to DE'. Assuming the vertical displacements of points A, B, and E small compared to their horizontal displacement;*

original fiber length DE = $1/\cos\beta$

change in fiber length $\delta = 1 \cdot \gamma \cdot \sin\beta$

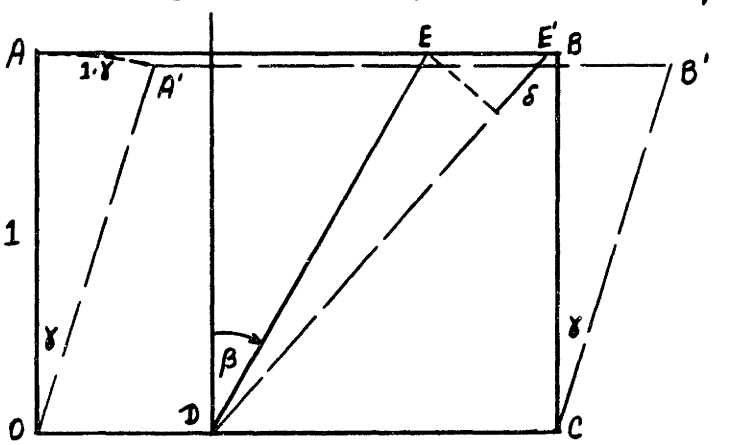

Then the fiber strain e_f is

$$e_f = \frac{\delta}{DE} = \gamma \sin\beta \cos\beta \qquad 0 < \beta < +\pi/2$$

For distortion of the element as shown, all fibers lying at angles $0 < \beta < \pi/2$ will be elongated, and their stresses positive, or tensile. All fibers lying at angles $-\frac{\pi}{2} < \beta < 0$ will be compressed (assuming no fiber buckling occurs). However, since $\sin(-\beta) = -\sin\beta$;

$$e_f = \gamma \sin\beta \cos\beta \qquad -\pi/2 < \beta < \pi/2 \qquad (6.29)$$

Representing all fibers as Hookean, or $\sigma_f = E_f e_f$, then

$$\sigma_f = E_f \gamma \sin\beta \cos\beta$$

*If the vertical displacements are included, e_f is a function of both and , which does not lend itself to prediction of Gyx by integration.

The previous equations for the total component of fiber stress in the L direction per unit width perpendicular to the L direction;

$$\sigma_L = \int_{-\pi/2}^{\pi/2} \sigma_f \cos^2\beta \, \phi(\beta) \, d\beta$$

$$= E_f \gamma \int_{-\pi/2}^{\pi/2} \sin\beta \cos^3\beta \, \phi(\beta) \, d\beta$$

Similarly, for the T direction

$$\sigma_T = \int_{-\pi/2}^{\pi/2} \sigma_f \sin^2\beta \, \phi(\beta) \, d\beta$$

$$= E_f \gamma \int_{-\pi/2}^{\pi/2} \sin^3\beta \cos\beta \, \phi(\beta) \, d\beta$$

Both of these integrals are identically equal to zero. Thus σ_L and σ_T are zero, and the only acting force is P. This conforms to the boundary conditions for the definition of G_{LT}, i.e., only a shear stress real, with normal stresses zero. The shear stress τ_{LT} is the component of fiber stress in the direction of P ($\sigma_f \sin\beta$) per unit width parallel to the P direction (or perpendicular to the L direction), $\phi(\beta)\cos\beta$. Thus

$$\tau_{LT} = \int_{-\pi/2}^{\pi/2} \sigma_f \cos\beta \sin\beta \, \phi(\beta) \, d\beta$$

$$= E_f \gamma \int_{-\pi/2}^{\pi/2} \sin^2\beta \cos^2\beta \, \phi(\beta) \, d\beta$$

Thus

$$G_{LT} = \frac{\tau_{LT}}{\gamma} = E_f \int_{-\pi/2}^{\pi/2} \sin^2\beta \cos^2\beta \, \phi(\beta) \, d\beta$$

This integral has been evaluated in VI.B, as the constant A_1, and

$$G_{LT} = A_1 E_f \qquad (6.30)$$

With $A_1 = .0891$ and $E_f = 72$ gpd; $G_{LT} = .0891 \times 72 = 6.4$ gpd. This compares to the value of $G_{LT} = 9.0$ gpd obtained by the orthotropic theory by predicting G_{LT} from E_{45^0} by equation 3.12a. A general derivation for Gyx becomes more complicated. Since G_{LT} is known, equation 6.30, the orthotropic solution of equation 3.12d. can be used with the boundary conditions $\sigma_y = \sigma_x = 0$, giving values of Gyx. A corresponding solution can be obtained for the conditions e_{yx} real and $e_y = e_x = 0$. This is implied when the fiber strain is written

$$e_f = \gamma \sin\beta \cos\beta$$

Then substitution of $\theta + \beta$ for β gives

$$G^*_{yx} = E_f \int_{-\pi/2}^{\pi/2} \sin^2(\theta+\beta)\cos^2(\theta+\beta)\,\phi(\beta)\,d\beta$$

This integral has been evaluated for equation 6.9, and

$$G^*_{yx} = E_f\left[A_1 + (A_2 + A_3 - 6A_1)\sin^2\theta\cos^2\theta\right] \qquad (6.31)$$

for the boundary conditions $e_y = e_x = 0$ 0. Thus the two predicting equations with their boundary conditions are:

For $e_y = e_x = 0$;

$$G^*_{yx} = E_f\left[A_1 + (A_2 + A_3 - 6A_1)\sin^2\theta\cos^2\theta\right] \qquad (6.31)$$

For $\sigma_y = \sigma_x = 0$;

$$\frac{1}{G_{yx}} = \frac{1}{G_{LT}}\cos^2 2\theta + 4\left[\frac{1}{E_L} + \frac{1}{E_T} + \frac{2\nu_{LT}}{E_L}\right]\sin^2\theta\cos^2\theta \qquad (3.12d)$$

A number of curves can now be plotted to determine the difference in form of the two expressions. Using the values of A_1, A_2 and A_3 for Fabric A, G^*_{yx} is plotted in Figure 6.7 from equation 6.31. Using the experimental values of E_L, E_T, ν_{LT} and G_{LT} obtained from E_{45^0}; the curve of Gyx is plotted in Figure 6.7 and labeled Gyx (3.12d). The difference

FIGURE 6.6

SPECIFIC MODULI OF RIGIDITY, FABRIC A,

ORTHOTROPIC AND FIBER WEB THEORY

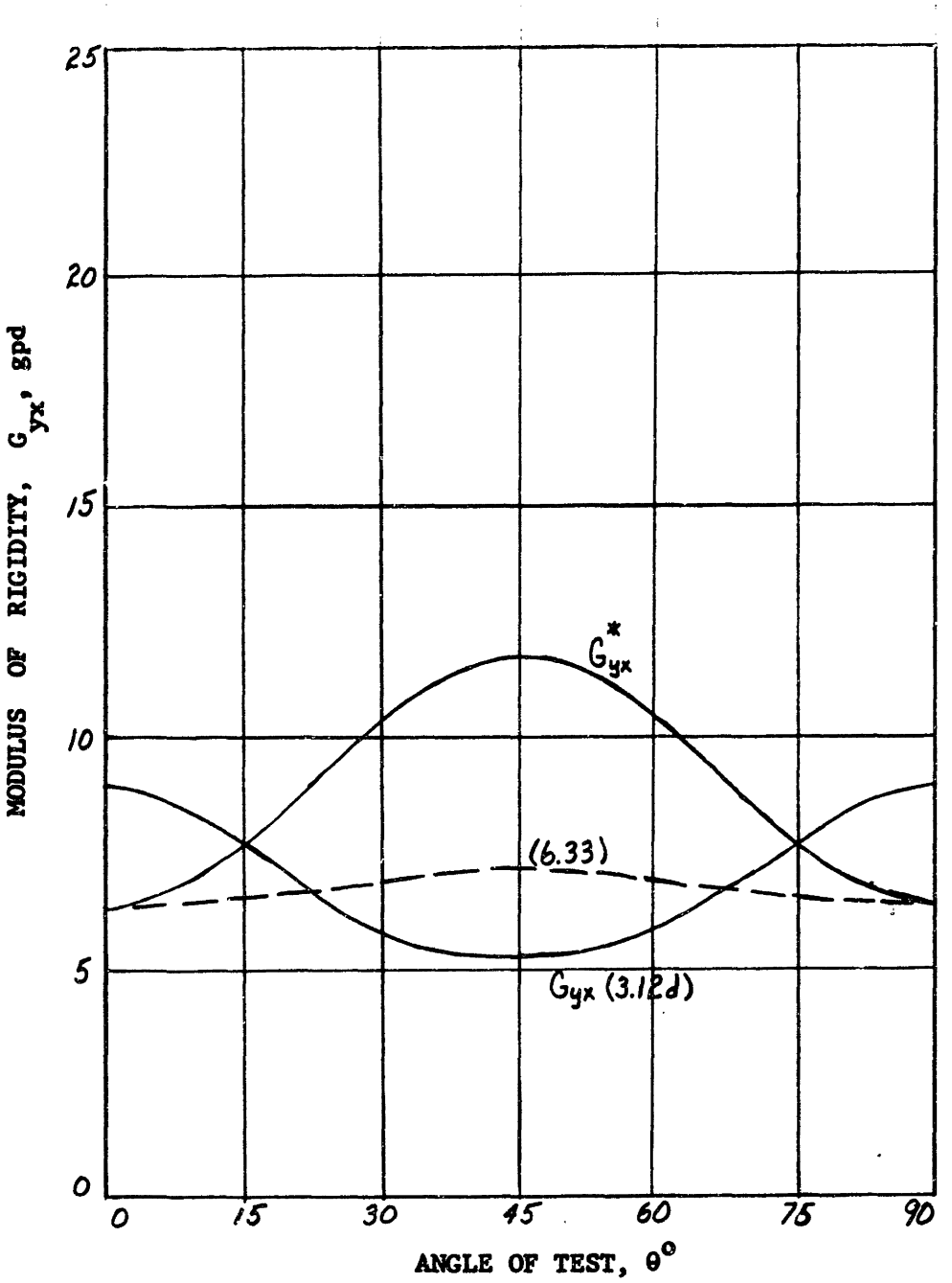

in form of the two expressions is easily seen. Again, the influence of the boundary conditions are most important. Previously, experimental data have aided in deciding which boundary conditions are better satisfied. No experimental data on Gyx has been obtained. The experimental difficulties are great. The non-woven fabric buckles in the third dimension (wrinkles) at the slightest provocation, and it would appear that biaxial stresses will have to be applied to prevent this wrinkling. It was impossible to include biaxial stress conditions in this investigation, and thus verification of the equations for Gyx must remain for other investigators.

One further comment appears worthwhile. If the relations $E_L = E_f \frac{A_2 A_3 - A_1^2}{A_2}$, (6.12), etc. are substituted into equation 3.12d, there results

$$\frac{G^*_{yx}}{G_{LT}} = 1 + \left[\frac{A_2}{A_1} + \frac{A_3}{A_1} - 6\right] \sin^2\theta \cos^2\theta \qquad (6.32)$$

$$\frac{G_{yx}}{G_{LT}} = \frac{1}{1 + 4\left[\frac{A_1 A_2 + A_1 A_3 - A_2 A_3 + 3A_1^2}{A_2 A_3 - A_1^2}\right] \sin^2\theta \cos^2\theta} \qquad (6.33)$$

Equation 6.33 is plotted in Figure 6.7 using the values of A_1, A_2, and A_3. The influence of the different boundary conditions is quite large, and should caution future investigators to carefully design the experimental test in accordance with one or the other set of conditions.

VII. ADDITIONAL EXPERIMENTS IN JUSTIFICATION OF FIBER WEB THEORY

While the general agreement of measured and predicted non-woven fabric properties has been satisfactory, certain discrepancies exist for the early region of the stress-strain curve. This section will examine certain of these differences, postulate as to their cause, and confirm, where possible, these postulates by experiment.

A. Difference in Poisson's Ratio - Predicted and Measured

On Fabric A the experimental and predicted values of ν_{yx} & ν_{yx}^{*} (by the fiber web theory) are given in Figure 6.3. The large discrepancy in ν_{LT} has been postulated as the result of buckling of fibers under compressive stresses i.e., those fibers being oriented closer to the T direction of the fabric. The critical force necessary to cause buckling of a slender column varies inversely with the square of the free length of the fiber between the assumed rigid bonds. These fibers oriented primarily in the T direction are not bonded well (as previously noted). The application of additional binder will increase the number of bonds per unit length of fiber and thus increase the fiber's resistance to buckling. If additional binder is incorporated without any other changes in the fabric structure, then any observed change in ν should be the result of increased bonding of the individual fibers. This should tend to lower the observed value of ν toward the value calculated from the fiber orientation distribution $\phi(\beta)$.

To evaluate this postulation, two sheets of Fabric A were returned to Dexter for reimpregnation with additional viscose solution and subsequent regeneration. Four small sheets (8x11) were returned, which were sufficient for a few experiments.

The original material, Fabric A, contained about 2% binder on the weight of fiber and the area density of the fabric was taken as the area density of fiber without any correction for the binder. In the reimpregnation, the area density at 65% RH changed from 16 gm/sq. yd (or 4400 equivalent denier) to 20 gm/sq. yd (or 5600 equivalent denier). While there was a small amount of shrinkage of the sheet during reimpregnation and drying, Dexter estimates that the shrinkage was small and represented only about 10% of the change in area density. Since the area density of fibers is required in the analysis, the fiber area density of both materials, low and high viscose Fabric A will be taken as 16 gm/sq. yd or 4400 equivalent denier*. The reimpregnated material will be identified as high viscose Fabric A (H. V. Fabric A). Specimens 1½" wide by 8" long were used for photographic measurement. Strains in the L and T direction were measured with specimens oriented in both the $\theta = 0^{o}$ (L direction) and $\theta = 90^{o}$ (T direction). For the L direction, ν_{LT}, two measurements of e_L and e_T were made at five fabric strains and the results averaged for each photograph. The averaged data at each stress level (or elapsed time) yield, when plotted, a straight line for values of e_L up to 1.5%. The slope of this line is 0.47, or Poisson's ratio $\nu_{LT} = 0.47$. This is in close agreement with the calculated value of $\nu_{LT} = .54$ (numerical method using angular intervals of fiber distribution, equation 5.13) and $\nu_{LT} = .55$ (integrated $\phi(\beta)$ value given by equation 6.18).

The same procedure was followed for determination of ν_{TL}, except that only the control photograph, and a photograph at 15 elapsed seconds were measured. The transverse strain, even on 1½" was too small to measure at smaller elapsed times.

The result of averaged measurements on this specimen gave $\nu_{TL} = 0.15$

*There may also be a change due to differences in moisture pickup between viscose fiber and viscose binder. In the absence of data, the two are assumed to be the same.

FIGURE 7.2

STRESS-STRAIN CURVES, FABRIC A AND HIGH VISCOSE FABRIC A EXPERIMENTAL: FIBER WEB THEORY

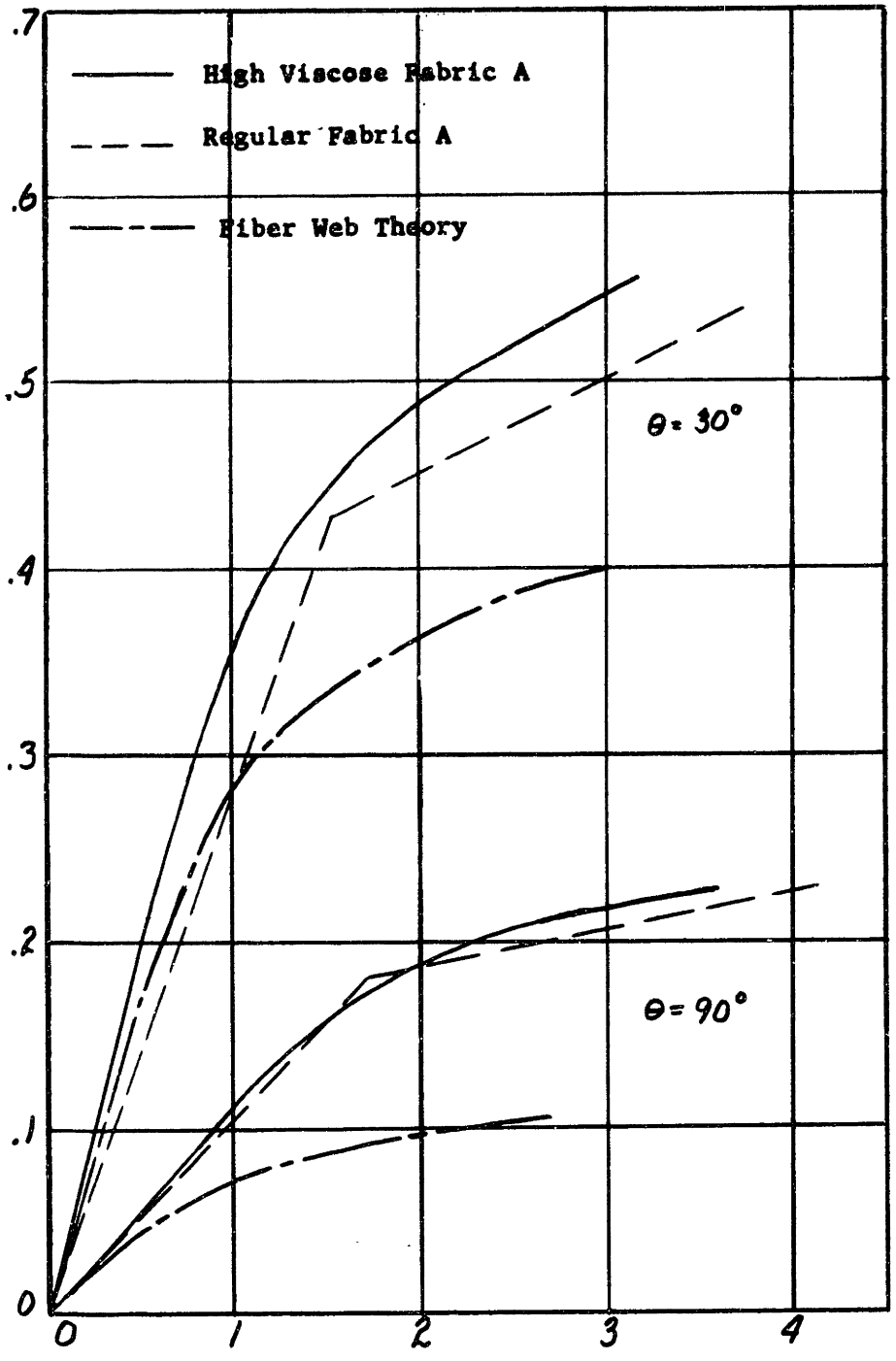

This is also in close agreement with the calculated values of 0.148 (numerical method) and 0.134 (integrated $\phi(\beta)$). One measurement of $\nu_{,}\ \theta = 45^{\circ}$ was made on a one inch wide specimen, and gave an average value of $\nu_{450} = 0.6$. This is also plotted in Figure 6.3.

The addition of more bond points to the fiber (thereby shortening the free length between bonds and lessening the fibers' ability to buckle) brings the measured ν_{yx} and predicted Poisson's ratio ν^{*}_{yx} within close agreement. This confirms the observation that the discrepancy in Figure 6.3. was due to fiber buckling and unbonded fibers. Since the measured moduli of Fabric A and High Viscose Fabric A were the same (next section), predicted Poisson's ratio ν_{yx} with the boundary conditions $\sigma_x = \sigma_{yx} = 0$ and $\nu_{LT} = 0.47$ will give the same shape of curve as obtained in Figure 6.3. It would appear that the experimental values of ν_{yx} conform more closely to $\nu^{*}_{yx}\ (\sigma_x = e_{yx} = 0)$ than to $\nu_{yx}\ (\sigma_x = \sigma_{yx} = 0)$. The analysis provides a good estimate of Poisson's ratio for the case of non-buckling fibers, as would be the case in a rigid or resin filled non-woven.

B. <u>Changes in Secondary Fabric Modulus With Increased Bonding</u>

As noted in Figure 5.8, the experimental secondary modulus (the general slope in the plastic region) is smaller than the value predicted by the numerical procedure. In addition, the measured data shows curvature towards rupture. The level of stress in this region cannot be critically examined due to the approximations made in translating the plastic portion of the stress-strain curve. However, the slopes might be expected to correspond more closely. One explanation has already been offered: namely the increase in Poisson's ratio with increasing strain. A second possibility is based on the assumption that the bonds between fibers are non-extensible and stronger

FIGURE 7.3

STRESS-STRAIN CURVES, HIGH VISCOSE FABRIC A,

θ 0 , 50 , 60 , 90 , 50%

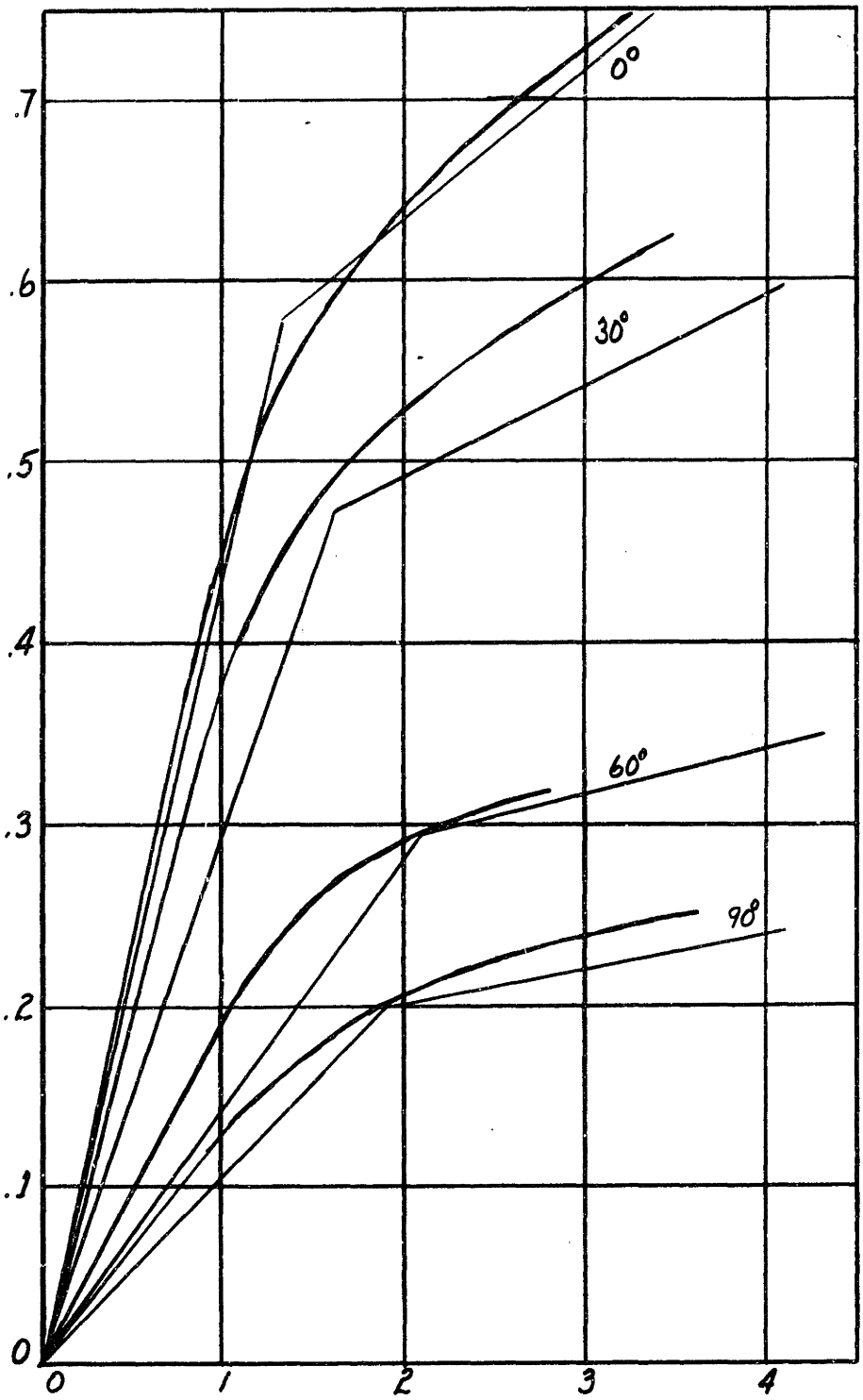

than the fiber. If some bonds fail, curvature in this region of the stress-strain relationship is quite possible. The addition of more binder to the fabric might establish the importance of this assumption.

Accordingly, tests were run on high viscose Fabric A at angles of $\theta = 0^{\circ}, 30^{\circ}, 60^{\circ}$, and 90°. Since the amount of fabric was very limited, the gauge length of the specimens was taken as 6.25 inches and the rate of strain as 8% per minute. The Instron curves were used for the stress-strain data, with strain based on the original jaw separation. Two specimens were tested in the T direction ($\theta = 90^{\circ}$) and one each at 0°, 30°, and 60°. The equivalent denier of the fabric was taken as 4400 denier, and the data are plotted in Figures 7.1 and 7.2. The solid curves at each angle are the data for high viscose Fabric A, the dashed curves for regular Fabric A, and the dotted straight lines the predicted approximations based on equations 6.16 and 6.27. Two effects are quite noticeable. The first is that all high viscose curves are above the regular Fabric A and are much closer to the predicted values. Also, the secondary moduli of the high viscose bonded material show better agreement with the predicted. The level of specific stress given by the high viscose Fabric A is probably as much as 10% too high, from the assumption of 4400 equivalent denier (no shrinkage in reimpregnation and no correction for added binder). Thus each curve might be lowered by as much as ten percent, but this would still leave the experimental data in excellent agreement with the predicted approximation. Since only one specimen was tested, the actual curve is probably subject to 10% error in any event. It would appear that the addition of more binder causes the fabric to follow more closely the predicted behavior, and the mechanical properties of this non-woven fabric are well predicted.

C. Predicted and Experimental Stress-Strain Curves With Change In Fiber Properties

As noted by equations 6.9, 6.11 and 6.22; for the identical fabric, any change in the properties of the fiber is directly reflected in the properties of the fabric. Since the viscose rayon fiber is sensitive to changes in humidity, a change in the % Relative Humidity should lead to changes in both fiber and fabric properties. Such an experiment should provide excellent confirmation of the previous behavior of the high viscose Fabric A. The fiber distribution $\phi(\beta)$ is the same and the same test angles θ will be used. Thus any change in stress-strain behavior from Figures 7.1 and 7.2 will be the result of changes in fiber properties only (provided, of course, that the assumption of stronger, rigid bonds is still valid).

Ten fibers were measured at 50% RH, with a gauge of two inches, and a strain rate of 6%/min. The straight line approximations to these curves give the following average data.

$$\sigma_m = 2.67 \text{ gpd.} \quad E_f = 72 \text{ gpd.} \quad Y.P. = .91 \text{ gpd.} \quad e_m = 15\%$$

This yields a fiber plastic modulus, q, of $\frac{2.67 - .91}{.15 - .91/72} = 13.0$ gpd, very close to the value of 12.7 obtained at 65% RH. The stress intercept, p, of the plastic modulus, q, is $0.91 - q\frac{.91}{72} = 0.75$ gpd. The initial or Hookean modulus is the same, i.e., Ef = 72 gpd. Thus the only significant shift in fiber properties occurs in the stress intercept of the plastic fiber modulus, which increased from 0.66 gpd at 65% RH to 0.75 gpd at 50% RH.

The only additional calculation is for new values of the stress intercept, p", of the fabric plastic modulus, where

$$p'' = p\left(1 - \delta/E_f\right)\left(A_4 \cos^2\theta + A_5 \sin^2\theta\right) \qquad (6.26)$$

The values of A_4 and A_5 given by Equation 6.24 give:

θ	0	30	60	90
E_y^*	43.7	28	13.5	10.6
p''	.47	.39	.24	.165
E_2	7.7	5.0	2.4	1.9

The predicted stress-strain relationships are plotted in Figure 7.3.

Again, one inch wide specimens of H.V. Fabric A were measured on 6.25 inch gauge, at 8%/min. Two specimens were tested in the L and T directions, and one each at $\theta = 30^\circ$ and 60°. The Instron curves of these tests, converted to grams/denier on the basis of a fiber area density of 4400 equivalent denier, are plotted in Figure 7.3. The predicted and experimental stress-strain relationships agree well, particularly as regard the secondary or plastic modulus and the level of stress in the plastic region. The change in % RH, which increased the yield point of the fiber, also increased the yield point of the fabric. Thus variations in fiber properties are directly related to changes in fabric properties. The largest discrepancy in initial modulus, Ey, again occurs at $\theta = 60^\circ$. This difference is about the same at both Relative Humidities, indicating consistency in the samples, and is of about the same magnitude as obtained with the orthotropic theory. This would indicate about the same degree of precision in predicting initial moduli Ey. However, the orthotropic theory is limited to Hookean behavior. The fiber web theory

takes into account the non-Hookean behavior of most textile fibers, and provides a more general analysis adaptable to the study of rupture conditions.

FIGURE 7.1

STRESS-STRAIN CURVES; FABRIC A AND HIGH VISCOSE FABRIC A EXPERIMENTAL: FIBER WEB THEORY

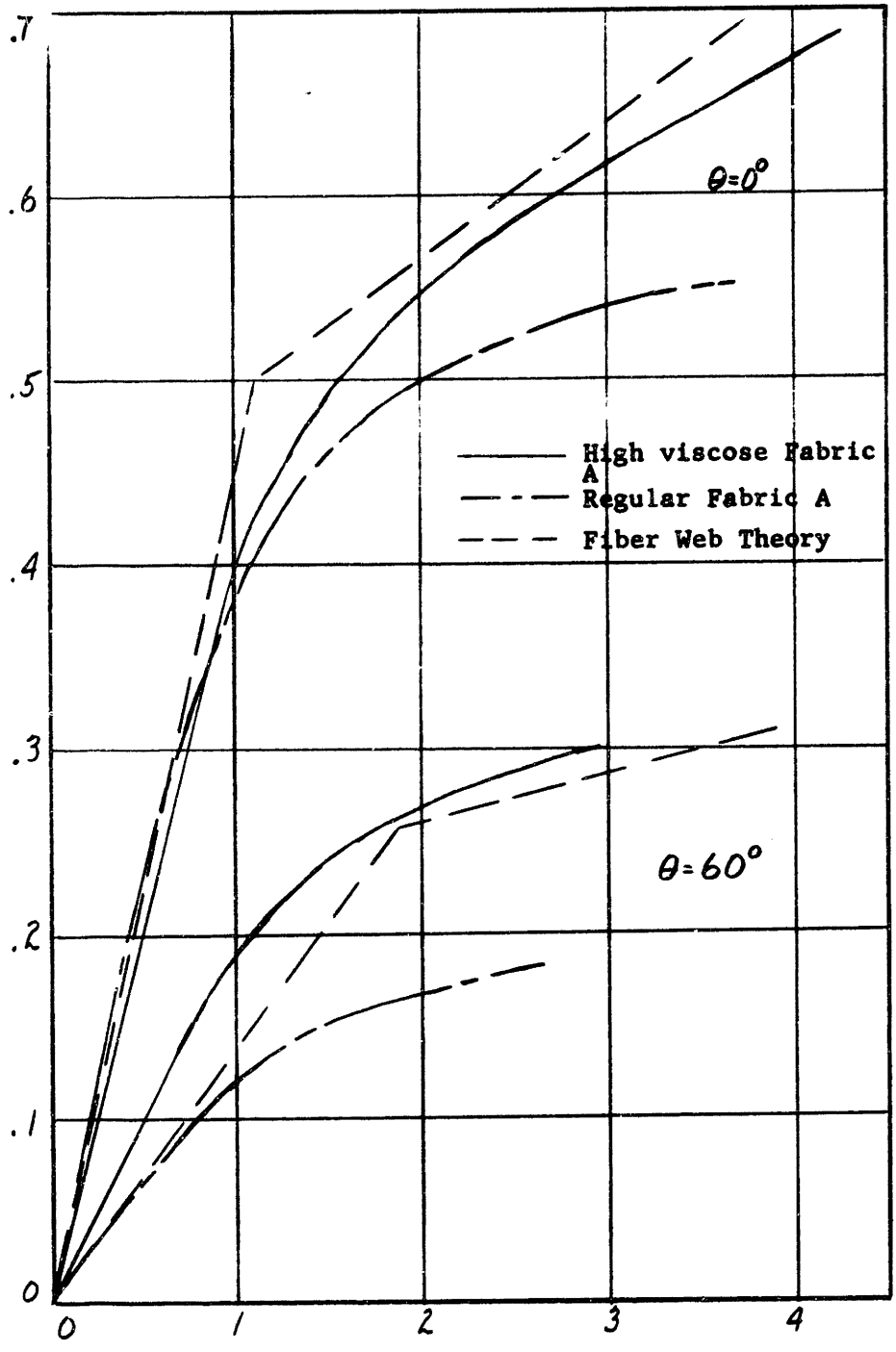

VIII. RUPTURE CONDITIONS AND THE VARIABLE UNIT CELL

A. Assumptions of Unit Cell and Fabric Rupture

Previously, the general theory has assumed a uniform fabric, i.e., one made up of a matrix of identical unit cells, all of the same area density and fiber orientation distribution, $\overline{\phi(\beta)}$. This approach has proven quite satisfactory for the early region of the stress-strain curve. Yet the experimental data on the unit cells (V.A.) indicate that the assumption of uniformity is not correct. In order to consider rupture, the behavior of a matrix of variable unit cells must be described. This requires consideration of rupture of the individual unit cells and supsequently of the group of unit cells which is the fabric. The failure behavior of the unit cell will be assumed to be as follows:

1. That only fibers fail (a reasonable assumption on Fabric A, and an excellent one for the High Viscose Fabric A).
2. That the failure of any cell occurs when the first fiber in that cell ruptures. This happens when the elongation of this cell reaches the lowest fiber rupture elongation of any of the fibers in that cell lying in the direction of strain. (The lowest fiber elongation, rather than the average, is used to account for the presence of a number of fibers lying in the direction of stress and the fact that their rupture elongations are distributed about the average).

The failure behavior of a fabric of variable unit cells will be assumed to be as follows:

1. That each cell acts as an independent unit.
2. That in a uniaxial tensile test (long gauge length compared to width), the fabric can be thought of as a number of long chains

of unit cells. Thus the force on each chain, and consequently on each unit cell, will be the same.

3. That the failure of the weakest cell in any one of the long chains of cells causes complete failure of the fabric.

Combination of these two groups of assumptions states that fabric failure will occur when, under the action of some load on the specimen, the stress on one unit cell causes that unit cell elongation e_c in the direction of stress to reach the lowest fiber rupture elongation of any of the fibers lying in the direction of stress. The failure of this first fiber leads to rupture of that unit cell, and consequently the fabric sample. Obviously, this is an assumption of minimum fabric rupture conditions where bonds are stronger than fibers; for it is conceivable that a number of fibers could fail before fabric failure occurred. This latter type of behavior (progressive fiber failure) can result in stress increase, equality or decrease; depending on the number of fibers involved, the slope of their stress-strain curve near rupture, and the distribution of fiber rupture elongations. An analytical procedure has been developed by Platt (14) for this behavior in yarns. However, the assumptions concerning the strain of fibers within the unit cell do not justify the use of this refinement. Further, the type of failure observed on Fabric A indicates very rapid rupture, without the typical saw-tooth curve characteristic of progressive fiber failure for yarns.

The assumptions of fabric failure appear to be reasonable ones, and thus failure of the fabric depends upon the failure of the weakest unit cell within the stressed area. The weakest unit cell is the one containing the fewest fibers and the least favorable fiber orientation distribution for that stress direction.

B. Variability of the Unit Cell

For the uniform fabric of uniform fibers, the rupture stress of the fabric (or the average unit cell) can be calculated from the fiber properties (E_f, p, q) and the average fiber orientation distribution, for the average fiber rupture elongation $\bar{e}_m$. The average rupture force/unit width on this fabric, $\bar{F}$, is the rupture stress $\bar{\sigma}_m$ times the average area density, D, in denier, or, in the L direction,

$$\bar{F} = D \int_{-\pi/2}^{\pi/2} (p + q\,\bar{e}_m \cos^2\beta)\, \overline{\phi(\beta)} \cos^2\beta \, d\beta \qquad (8.1)$$

For the variable or non-uniform fabric, the rupture force F depends upon the weakest unit cell; defined as the cell having a combination of

a) a fiber with the smallest rupture elongation, $(e_m)_{min}$

b) the fewest fibers, or lowest area density, d_{min}

c) the poorest fiber orientation distribution, $[\phi(\beta)]_{min}$

for that direction to give the smallest rupture force.

Then the fabric rupture force/unit width is the force/unit width necessary to rupture this weakest unit cell or

$$F = d_{min} \int_{-\pi/2}^{\pi/2} \left[p + q\,(e_m)_{min} \cos^2\beta\right] \left[\phi(\beta)\right]_{min} \cos^2\beta \, d\beta \qquad (8.2)$$

All three of these parameters - d, e_m, and $\phi(\beta)$ - have distributed values about their averages. The rupture stress will be related to the probability that minimum values of all three occur in the same unit cell. The probability distributions for e_m and d can be reasonably assumed as normal. The variability of $\phi(\beta)$ presents difficulty, since $\phi(\beta)$ is itself a relative frequency distribution of fibers with respect to β . The average fiber orientation distribution $\phi(\beta)$ has been fitted with an empirical function. For this function

$$\phi(\beta) = a + b\cos\beta + c\cos^3\beta + d\cos^8\beta + e\cos^{16}\beta$$

to describe variations in fiber orientation would require that each constant be distributed according to some probability function. Such a procedure is almost impossible to handle analytically. Instead, consider the variations in stress of a number of unit cells as a result of changes in $\phi(\beta)$ alone, (all cells of average area density, D). This can be written

$$\sigma_c = \int_{-\pi/2}^{\pi/2} (\rho + q e_c \cos^2\beta)\,\phi(\beta)\cos^2\beta\, d\beta \qquad (8.3)$$

For some arbitrary strain on the unit cell e_c, the stress σ_c is a function of $\phi(\beta)$. The distribution of σ_c can be considered as a variable, independent of the area density of the unit cell.* Thus the rupture force of the fabric, F , depends upon the variables e_m, d, and σ_c . Each of these is discussed separately.

1. Variability of fiber rupture elongation, e_m

According to the assumptions for rupture, the fabric fails when the first fiber fails. Since the unit cell is under uniform strain, those fibers parallel

*Provided that area density and $\phi(\beta)$ are independent variables. This is true for Fabric A as will be shown in the next section.

to the stress direction are elongated an amount equal to the cell strain. Those fibers not parallel to the stress direction are elongated less, depending upon the value of β . A formulation for the strain of the unit cell when the first fiber ruptures is possible, as given in Appendix F. The solution of this problem involves the assumption of certain configurations of fiber rupture strain distribution and fiber orientation distributions. Further, it is questionable whether the original assumptions of average fiber strain within the cell boundaries warrants the effort involve.

A simple alternative argument can be presented. Assume for the moment that the fiber properties E_f, p and q are constant; i.e., all fibers have identical stress-strain curves and differ only in their elongation to break.* The fiber rupture elongation is assumed to be distributed normally. Further, the minimum fiber rupture elongation will be considered to lie three standard deviations below the average value or $(e_m)_{min} = \bar{e}_m - 3 S_{e_m}$. This is not strictly correct for less than twenty fibers parallel to the unit cell strain. However, it represents a reasonable approximation for the lowest fiber rupture elongation of the fibers in the unit cell, taking into account the variable nature of their stress-strain curves, and the original assumptions on average fiber strain within the unit cell boundaries.

From the data of Table 5.5, the average fiber rupture elongation $\bar{e}_m$ was 16.2% and the standard deviation $S_{e_m} = 1.9\%$. Thus the lowest fiber rupture elongation $(e_m)_{min}$ is 10.4%. When any unit cell reaches an elongation equal to 10.4%, the unit cell, and consequently the fabric, ruptures. This applies for any arbitrary stress direction $\underline{y}$.

* See discussion at end of VIII. C.

2. Variability of Area Density of the Unit Cells

The area density of finite sized areas of fabric will be assumed to be normally distributed.

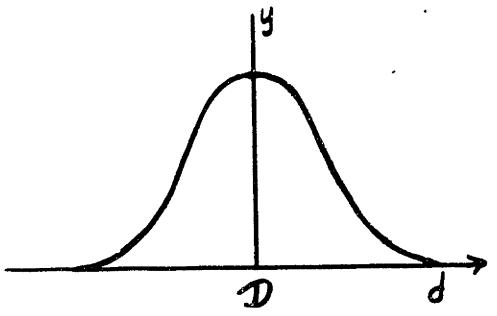

Thus, by the figure at the left, the probability of occurrence of a finite area of a certain area density d is given by the height of the curve. The equation for the curve is given by $y = \frac{1}{\sqrt{2\pi}S} e^{-\frac{(d-D)^2}{2S}}$ where D is the mean or average area density and S is the standard deviation of the normal distribution. With a change in the size of area considered, the true mean value, D, will not change, but the standard deviation S can and does change. The standard deviation for the distribution of area density of unit cells, denoted as S_d, is desired. Since the unit cell is quite small, it is expected that S_d will be greater than the measured standard deviation of larger areas, such as one square inch. The two methods available for estimating S_d are:

a. from the number of fibers counted in each cell, a standard deviation in number of fibers about the average number of fibers, converted to area density by the simple proportion

$$\frac{\text{std. dev. of counted fibers in unit cell}}{\text{Average number of fibers in unit cell}} = \frac{Sd}{D} \left\{ \begin{array}{l} \text{in either denier or} \\ \text{grams/square inch} \end{array} \right\}$$

b. From the standard deviation of area density of a series of different sized areas, an extrapolated S_d can be obtained by plotting the standard deviation versus the area of the unit cells.*

*or a ratio of standard deviations vs. the equivalent number of areas in the weighed area, as shown in Figure 8.1.

The first of these methods, using the total number of fibers in each of the ten counted cells (Table 5.1) gives a standard deviation S_d of 5.65 fibers. Thus with the average number of fibers per cell, 49.3, and the average area density, .0123 gm/sq. in., or 4400 denier;

$$S_d = 4400 \cdot \frac{5.65}{49.3} = 500 \text{ denier}$$

The second of the methods requires weighing a number of specimens of the same size to obtain the standard deviation of area density for that size of fabric sample, and repeating this procedure for a number of different sized areas.

The results of such an experiment are shown in Table 8.1. The specimens were cut simultaneously from four sheets of Fabric A, and were 7 3/4" long (L direction). Eight specimens were obtained for each of the four widths; 1/4", 1/2", 1" and 1½". The pattern of specimens is shown below:

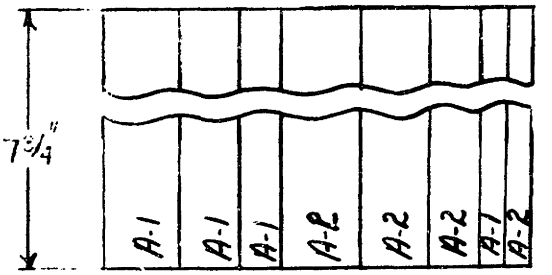

Each of the specimens was weighed individually. The specimens were also combined where possible to obtain a larger number for the calculation of the standard deviation of area density for that number of square inches of area. Thus for 7.75 square inches, the eight specimens 1" wide were used; and also the weights of the two ½" wide specimens (A-1 and A-2) were added together to give four more specimens of 7.75 square inches. The second column in Table 8.1 gives the number of specimens upon which the standard deviation is based. The last row in the column is for 12 specimens 2 " long and 1/4" wide cut from the original 1/4 inch wide specimens. The next to last column

TABLE 8.1

STANDARD DEVIATION OF AREA DENSITY AS A FUNCTION OF SAMPLE AREA, FABRIC A

Area in Square Inches	No. of Samples	Weight in Grams		Area Density gm/sq. in.		Ratio of Areas, n	Ratio of Std.Dev., S/S_{min}
		Mean	Std.Dev.	Mean	Std.Dev.		
50.375	4	.637	.0066	.01265	.00013	1	1
25.19	8	.3185	.00335	.01265	.000133	2	1.02
11.63	16	.1471	.00206	.01263	.000177	4.3	1.36
7.75	16	.0981	.00127	.01266	.000164	6.5	1.26
3.88	12	.0487	.000778	.01255	.00020	13	1.54
1.94	8	.0242	.00043	.01250	.00022	26	1.71
0.50	12	.0063	.00024	.01260	.00048	100	3.7

is the ratio of the largest area to the area of the specimens considered. The last column is the ratio of the standard deviation of that area to the smallest standard deviation measured (the largest area).

In the present use of statistics, there is little discussion of the change in standard deviation with sample size when sampling from a continuous non-random population. The usual argument for the change in standard deviation with multiple sampling is

$$S_n = \frac{S}{\sqrt{n}} \qquad (8.4)$$

where S is the standard deviation of the population of individuals and S_n the standard deviation of the means of n samples at a time. This assumes that the samples are drawn randomly. In the actual fabric, consecutive fabric areas cannot be assumed independent or randomly selected. The previous equation suggests that the ratio of standard deviations might follow a log-log relation. Thus

$$\frac{S}{S_{min}} = n^a \quad \text{or} \quad \log \frac{S}{S_{min}} = a \log n \qquad (8.5)$$

The data of Table 8.1 is plotted in Figure 8.1 on log-log scales. The data indicate a reasonable straight line relationship with a approximately equal to 0.20 ($0.16 < a < 0.24$) and equation 8.5 can be taken as

$$n^{.16} < \frac{S}{S_{min}} < n^{.24} \quad \text{and} \quad \frac{S}{S_{min}} \cong n^{1/5} \qquad (8.6)$$

The measured unit cell was 0.0225 inches on edge or an area of 5×10^{-4} square inches. The largest measured areas were 50 square inches. Thus $n = \frac{50}{5 \times 10^{-4}} = 100{,}000.$* Then

* This represents an extrapolation through a physical boundary - the fiber length. Further experimentation is needed to justify the use of the procedure in lieu of counting fibers in the unit cell.

FIGURE 8.1

RATIO OF STANDARD DEVIATIONS VS. RATIO OF WEIGHED SPECIMENS, FABRIC A

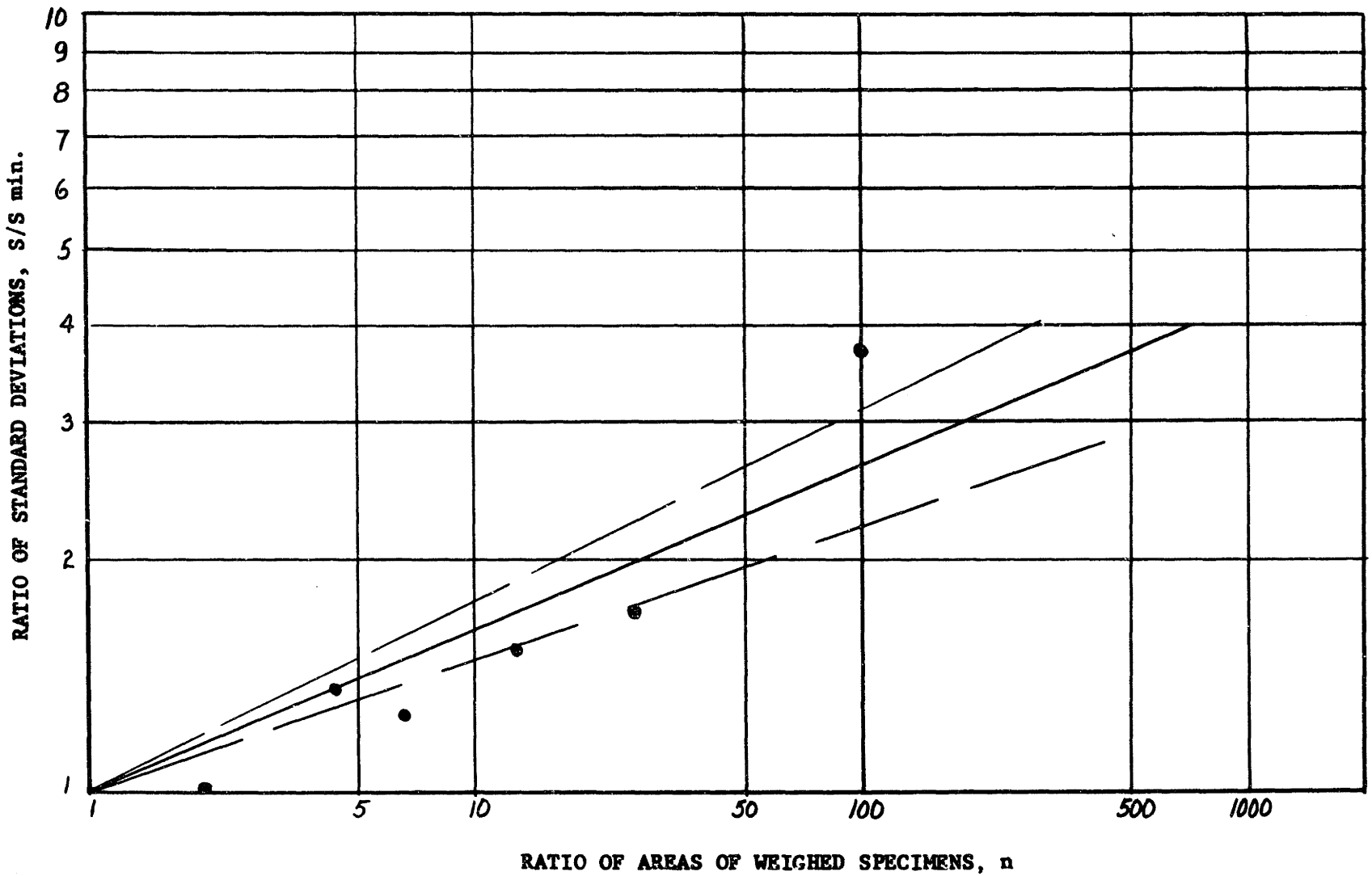

$$(100,000)^{.16} = 6.3$$

$$(100,000)^{.20} = 10$$

$$(100,000)^{.24} = 15.8$$

With the value of S_{min} taken from fifty square inches, or .00013 gm/sq. inch, the predicted standard deviation of area density of the unit cell, S_d, is $S_d = 10 \times .00013 = .0013$ gm/sq. inch. This can be converted to equivalent denier by

$$\text{Area density (gm/sq. inch)} = \frac{\text{Equivalent denier}}{354,000}$$

and the predicted S_d is 460 denier, where the average equivalent denier of the fabric is 4400 denier. The value of S_d obtained from counted fibers was 500 denier. The two estimates of the area density standard deviation for the unit cell are in excellent agreement.

3. Variability of Unit Cell Rupture Stress

The specific stress of the average unit cell in the L direction (plastic region) is given by

$$\sigma_c = \int_{-\pi/2}^{\pi/2} \left[p + q\, e_c(\cos^2\beta)\right] \overline{\phi(\beta)}\, \cos^2\beta\, d\beta \qquad (\gamma_{LT} = 0)$$

The value of unit cell strain which causes the first fiber to rupture, e_c, is 10.4%. Substitution of this value in the equation above gives the average specific rupture stress of the unit cell of average area density $(\overline{\sigma_c})_m$. This value of e_c, together with the measured $\phi(\beta)$ for each cell, can be used in the numerical method to obtain ten values of $(\sigma_c)_m$. These ten values will be distributed about $(\overline{\sigma_c})_m$ and the distribution will be assumed normal. The calculations are shown in Table 8.2 and the ten values used to obtain an estimated standard

TABLE 8.2

VARIABILITY OF UNIT CELL RUPTURE STRESS AS A FUNCTION OF CHANGES IN FIBER ORIENTATION DISTRIBUTION, FABRIC A

$$\sigma_{cm} = \sum \left[.66 + 12.7(.104)\cos^2\beta_i\right] \phi(\beta_i) \cos^2\beta_i$$

Unit Cell#	$\phi(\beta_i)$ 0	10	20	30	40	Stress Components 0	10	20	30	40	Σ
1	.176	.281	.106	.07	.07	.350	.530	.171	.087	.060	1.20
2	.130	.239	.108	.130	.065	.259	.452	.174	.161	.056	1.10
3	.132	.151	.169	.132	.094	.261	.285	.272	.164	.081	1.06
4	.187	.250	.125	.042	.063	.373	.473	.201	.052	.054	1.15
5	.180	.280	.160	.020	.060	.358	.529	.258	.025	.052	1.22
6	.217	.217	.109	.131	.109	.432	.410	.176	.163	.094	1.28
7	.154	.289	.135	.135	-	.307	.546	.218	.168	.000	1.24
8	.158	.183	.183	.079	.026	.315	.346	.296	.098	.022	1.08
9	.104	.312	.146	.146	.104	.207	.590	.235	.181	.089	1.30
10	.224	.259	.069	.086	.121	.446	.490	.111	.107	.104	1.26
								Average			1.19

deviation S_σ of this assumed normal distribution. Thus from the data,

Mean unit cell specific rupture stress = $(\overline{\sigma_c})_m$ 1.19 gpd

Standard deviation of $(\sigma_c)_m$ = S_σ = 0.086 gpd

4. Combining the Three Distributed Parameters

The independent parameters e_m, σ_c, and $\underline{d}$ have been discussed separately. A unit cell rupture strain, e_c, of 10.4% has been assumed - based upon three standard deviations of the fiber rupture strain. This strain level is assumed to cause rupture of any unit cell, and thus the joint influence of variations in σ_c and d will determine the fabric rupture stress. For the particular value of e_c = 10.4%, the fabric rupture stress for the unit cell of average area density is given as

$$\sigma_m = \sum_{i=1}^{i=18} \left[\rho + g e_c(\cos^2\beta_i - \nu_{LT}\sin^2\beta_i)\right]\cos^2\beta_i\ \phi(\beta_i)$$

If this stress (in gpd) is multiplied by the actual area density of this unit cell, $\underline{d}$; the force (in grams/unit width) required to rupture this unit cell is obtained, or

$$f_c = d\,(\sigma_c)_m$$

Then the rupture force (in grams/inch width) of the fabric, is given by the lowest value of f_c of all the cells within the stressed area, or

$$F = (f_c)_{min} = d\left[(\sigma_c)_m\right]_{min} \qquad (8.7)$$

Considering the average unit cell to rupture at e = 10.4% also, then the rupture stress of the average unit cell $(\overline{\sigma_c})_m$ times the average area density D gives the rupture force of the average unit cell, or the rupture force of the fabric.

$$\bar{F} = \bar{f}_c = D(\overline{\sigma_c})_m \qquad (8.8)$$

Dividing equation 8.7 by 8.8 gives

$$F = \frac{d_{min} \cdot (\sigma_{cm})_{min}}{D \cdot \overline{\sigma_{cm}}} \cdot \bar{F} \qquad (8.9)$$

where the rupture force of the variable fabric F is given by the rupture force of the average fabric reduced by the variability of d and σ_c (or $\phi(\beta)$). The ratios $\frac{d_{min}}{D}$ and $\frac{(\sigma_{cm})_{min}}{(\overline{\sigma_{cm}})}$ suggest the use of the coefficients of variation, defined as the ratio of the standard deviation to the mean of a distribution or

$$C.V.(\%) = \frac{S}{Mean} \cdot 100 = C$$

The value of d_{min} and $(\sigma_{cm})_{min}$ depend upon the size of the stressed area and the size of the unit cell, as reflected in the total number of unit cells under the stress, n. Thus the ratio d_{min}/D will depend upon the value of the Coefficient of Variation, C_d, and some function of n, possibly in the form

$$\frac{d_{min}}{D} = [1 - C_d \cdot f(n)] \qquad (8.10)$$

where f(n) expresses the probability of d_{min} occurring in the n cells.

C. The Analysis of Peirce

In 1926, F. T. Peirce published a mathematical treatment of the tensile rupture of textile yarns, in which he introduced the concept of "The Weakest Link" (13). The work is recognized as a most important contribution to textile research, and initiated greater application of statistical theory to

textile problems. It represents the only definitive work on the influence of variability along a specimen to the obtainable rupture strength. The following analysis is taken from his work.

Consider specimens of length ℓ whose distribution of rupture loads, f, can be expressed by a frequency curve $y_\ell = \phi(f)$. Then the probability that the strength of any given specimen will lie between f and f + df = y_ℓ df.

The probability that the rupture load of any specimen of length ℓ should not be less than f is

$$\int_f^\infty \phi(f)\,df$$

The probability that one of r lengths has a rupture strength between f and df is $r\,\phi(f)df$ and that the strength of the r-1 specimens has a strength greater than f is

$$\left[\int_f^\infty \phi(f)\,df\right]^{r-1}$$

Thus the probability that the breaking load of any specimen of length rℓ lies between f and f + df is y_r df where

$$y_r = r\,\phi(f)\left[\int_f^\infty \phi(f)\,df\right]^{r-1}$$

As Peirce states, the expression is completely independent of the form of $\phi(f)$, and he gives a procedure for numerical application when r is small.

To obtain an analytical expression for the variation in rupture strength with length, some form of $\phi(f)$ must be assumed. Peirce applied the normal distribution, remarking that while the majority of observed data gave irregular and possibly skew distributions, the normal distribution appeared to be the most general case. To follow through to his conclusions, the normal distribution

$$\phi(f) = \frac{1}{\sqrt{2\pi}\,S}\, e^{-\frac{(f-a)^2}{2S^2}}$$

together with the substitutions $x = f-a$, and $h = \frac{1}{\sqrt{2}\,S}$ (the "modulus of precision"), yield

$$y_r = r\frac{h}{\sqrt{\pi}}\, e^{-h^2x^2}\left[\frac{1}{\sqrt{\pi}}\int_0^{\infty} e^{-h^2x^2}\cdot h\,dx - \frac{1}{\sqrt{\pi}}\int_0^{x} e^{-h^2x^2}\cdot h\,dx\right]^{r-1}$$

$$= \frac{h}{\sqrt{\pi}}\, e^{-h^2x^2}\, r\left[\frac{1-\phi(hx)}{2}\right]^{r-1}$$

where

$$\phi(x) = \frac{2}{\pi}\int_0^{x} e^{-x^2}dx$$

The function $\phi(x)$ cannot be obtained in integrated forms. However, it is in published tables, and from these, curves of the form as shown in Figure 8.2 were given by Peirce. Since the curves must be obtained by rather lengthy procedures, Peirce also analyzed the change in the distribution and average rupture strength in the following way.

"If a_ℓ be the mean from lengths ℓ, S_ℓ the standard deviation then

$$a_\ell - a_{r\ell} = v_r\, S_\ell$$

$$S_{r\ell}/S_\ell = u_r$$

FIGURE 8.2

CHANGES IN DISTRIBUTION OF STRENGTHS FROM PEIRCE (13)

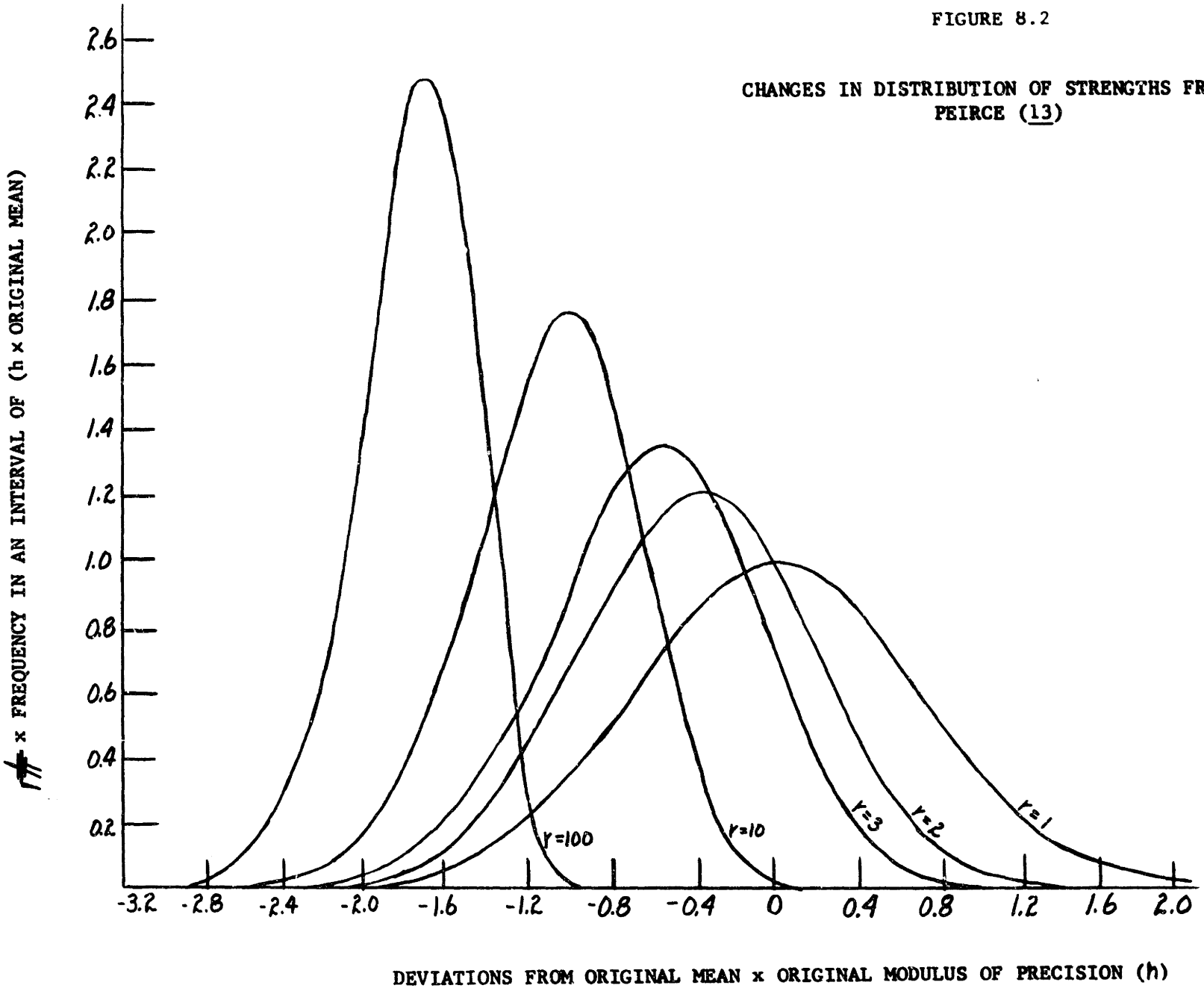

where v_r and u_r are independent of the variability and are known functions of the multiple r, if the curve for lengths l be normal. . .To obtain a general expression for the effect of length on strength, small changes in v_r and u_r due to skewness must be ignored and simple relations between them then appear
For--

$$a_l - a_{rsl} = v_{rs}\, s_l$$

and

$$s_{rsl}/s_l = u_{rs}$$

Also

$$a_{rl} - a_{rsl} = (v_{rs} - v_r)\, s_l$$

$$s_{rsl}/s_{rl} = u_{rs}/u_r$$

Whence

$$v_r\, s_{rl} = (v_{rs} - v_r)\, s_l$$

$$\frac{s_{rsl}}{s_{rl}} = \frac{u_{rs}}{u_r}$$

or

$$v_s = \frac{v_{rs} - v_r}{u_r}$$

and

$$v_{rs} = v_r + v_s \cdot v_r = v_s + v_r \cdot u_s$$

$$\therefore \frac{v_r}{1-u_r} = \frac{v_s}{1-u_s} = \text{constant} = C$$

or

$$v_r = C(1 - u_r)$$

But $u_{rs} = u_r u_s$, whence by continuing to factorize r and s comes the relation that u for any value of r is equal to the product of u for the factors of r or to the nth power of u for the nth root of r.

$$\therefore\ u_r = u_l^{\log_e r} = r^b$$

and

$$v_r = C(1 - r^b)\ ;\ u_r = r^b$$ "

The last two constants change slowly with the increase in skewness but a good approximation was given by Peirce where b = -1/5 and C = 4.2. The values given by these empirical contants are as close as the normal distribution assumption warrants.

Subsequently, Peirce discusses several cases of boundary conditions, two of which are pertinent to this work. These will be related to their equivalents on the non-woven fabric.

The first case is a series of parallel strands under uniform tension which, when one strand breaks, the remainder slip. To draw the analogy, the fabric is considered as a number of long strands of unit cells (independent from each other) and under uniform tension. Each cell is under the same load and when one cell ruptures, the remaining slip or rupture.* This is equivalent to the assumption of independent unit cells under equal loads. The rupture strength of the s parallel strands each of length rl, will depend upon the value of rs., or the total number of multiples of ℓ in the composite.

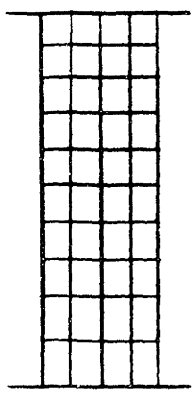

For the non-woven fabric, the total number rs will be the number of unit cells between the jaws. This case is fully covered by the analysis for long specimens.

The assumption of uniform tension on the individual strands and the independence of strands implies a considerable number of cell lengths between jaws. Perhaps 20 unit cell lengths, or for Fabric A, 20 x .0225 = 0.45 inches, is a reasonable value. For more than 20 cell lengths between jaws, the preceding analysis is valid. For less than 20 cell lengths, the fabric boundaries might be approximated better by uniform extension than uniform tension. This definitely would be the case for one cell length, and the region between one and 20 cell lengths becomes

*Whether slip or rupture occurs is inconsequential, since the load on the fabric will not increase in any event. This is the assumption which has been made concerning rupture.

a transition between the two boundary conditions.*

The second case is of strands of uniform original length uniformly extended until one breaks, when the remainder slip. If e_r be the mean breaking extension of a specimen of $\underline{r}$ strands, S the dtandard deviation,

$$e_r = e_1 - v S_1 \quad ; \quad \frac{S_r}{S_1} = u$$

According to Peirce, the mean ratio of the load to extension E (or in our case q Ey/Ef = E_2) may be taken as a first approximation as constant, for its variability decreases as $r^{1/2}$ against $r^{1/5}$ for the breaking extension of the whole specimen. Then

$$E_r = E e_1 - v E S_1$$

or

$$a_r = a_1\left(1 - v \frac{S_1}{e_1}\right) \quad ; \quad \frac{\sigma_r}{a_r} = \frac{S_r}{e_r} = \frac{S_1 u}{e_r} = u \cdot \frac{e_1}{e_r} \cdot \frac{S_1}{e_1}$$

or

$$\sigma_r = u E S_1 \qquad (8.11)$$

where σ_r here denotes the standard deviation of strength.

Equation 8.11 is approximate in so far as it neglects the variability of E. Peirce states, however, that the equation is nearly true when the variability of load is of the same order as that of extension.

This question of rupture elongation distribution has been eliminated previously by the selection of a particular unit cell rupture strain based on the variability of the fiber rupture elongation. Thus the assumption has been made that any cell will fail when its rupture elongation reaches 10.4% or $\bar{e}_m - 3 S_{e_m}$. This precludes any variation in unit cell rupture elongation. The importance of this assumption and the problems it raises

*There is also a physical testing problem in this region, as the distance between jaws becomes less than the fiber length employed in the non-wovens tested.

can be quickly shown. Consider the horizontal strip of s unit cells wide, and one unit cell length between parallel jaws. If the jaws remain parallel the extension of each unit cell is the same. Then when the elongation reaches

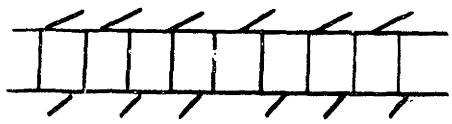

10.4% all cells fail simultaneously and the rupture stress on each cell is σ_{cm}, the rupture force $f_c = d\,\sigma_{cm}$ (in grams/unit width), and the rupture force of the entire specimen

$$F = \frac{1}{s}\sum_{i=1}^{i=s} d\,\sigma_{cm} \equiv \frac{1}{s}\sum d \sum \sigma_{cm}$$

$$\equiv \mathcal{D}\,\bar{\sigma}_{cm} \qquad (8.12)$$

Then for s cells so arranged, there is no reduction in rupture strength. However, if the same s cells were arranged vertically, as in one strand

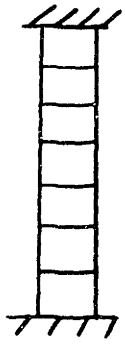

(ignoring edge effects), the rupture strength would be given by Peirce as

$$a_p = a - V_p\,S \qquad (8.13)$$

where a is the mean unit cell rupture strength, $\mathcal{D}\,\bar{\sigma}_{cm}$, and S is the standard deviation of the rupture strength, denoted as $S_{d\sigma}$. Rewriting

$$(F)_s = \mathcal{D}\,\bar{\sigma}_{cm} - V_p\,S_{d\sigma} \qquad (8.14)$$

and the rupture strength of the column of cells is less than that of the row. If there were only one column or row, the problem would not be difficult. Also when the number of cells in the column becomes large, the problem again reduces to that of Peirce's first case.

Designating the number of horizontal cells as j (or the number of strands) and the number of cells in a strand by h, two types of solutions exist.

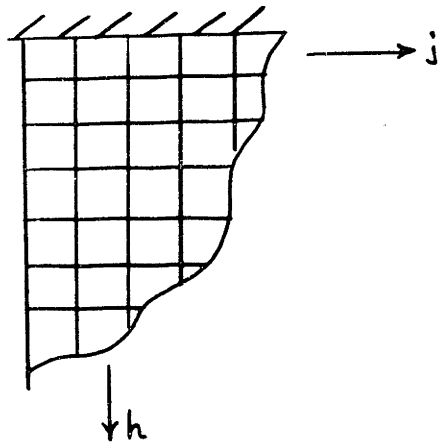

h very small; $1 \leq j \leq \infty$

$$F_{hj} = \mathcal{D}\,\bar{\sigma}_{cm}$$

h large; $1 \leq j \leq \infty$

$$F_{hj} = \mathcal{D}\,\bar{\sigma}_{cm} - V_{hj}\,S_{d\sigma}$$

These two formula are sufficient to permit prediction of the rupture strength of specimens of various sizes, provided the distribution of $d\sigma_{cm}$ is approximately normal and the standard deviation of this distribution, $S_{d\sigma}$ can be determined.

Several comments appear necessary at this point. The first concerns the assumptions of normal distributions of $\underline{d}$ and σ_c. For only ten samples, or unit cells, the use of any statistical method to justify normality (such as χ^2) is worthless. Further, the empirical relation of Peirce is also an approximation. Finally, fiber strain has been approximated by the assumptions of the unit cell. In view of these factors, consideration of the possible skewness of the $\underline{d}$, σ_c, and $d\sigma_c$ distributions is not warranted.

The question of constant modulus of the unit cells and the assumption that they act independently are interrelated. Even if the hypothesis of independent cells is accepted, the moduli of the individual unit cells are also distributed. If, in the case of parallel columns of many cells, the distributions of moduli are identical, then the

assumptions of equal force on each column and each cell is valid. If, on the other hand, two adjacent columns of unit cells have different distributions of moduli, the force on the two columns will be different for the same total extension of the columns. If this were the case, the rupture stress would be lower than the value given by Peirce, who assumed that the variability of the distributions of moduli was small compared to the variability of rupture stress. Provided there is no apparent periodicity to the variations in $\underline{d}$ and $\underline{\sigma_c}$ between the several columns (as would be evidenced by a "streaky" fabric), a specimen containing reasonably long columns - say 200 cells in each - might be expected to give equivalent distributions of moduli between columns. Thus for sufficiently long specimens, equal force on each independent unit cell appears to be a valid assumption. In fact, this could be experimentally verified by the measurement of a sufficient number of unit cells, but the work involved does not seem justified in view of the following arguments concerning "coupling" between cells.

"Coupling" here means the real consequence of fibers continuing from one cell to another, and thus preventing truly independent action. The cases of independent and dependent unit cells can be considered as two types of matrices of springs. If the unit cells are independent, the springs (of varying spring constants, or moduli) are series connected into columns--the columns being completely independent. If the unit cells, or springs are not independent, then cross springs must be added to account for their mutual influence, one on another. This alters the columns of springs to a two-dimension network of springs, as shown below. The analogy is similar to the claims of certain mattress manufacturers who assert that their springs act independently, and deride the typical bed springs which are

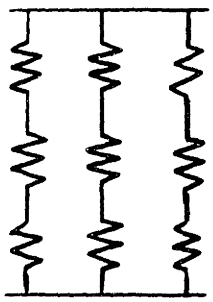

Independent

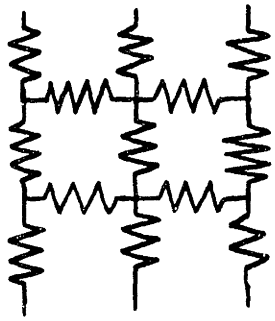

Dependent

tied together, or coupled. A solution of a two dimension spring network is extremely difficult. However, the results of this coupling are quite evident. Consider the weakest unit cell (or the one which would deform the most under a given load) surrounded by and connected to unit cells of high modulus and low deformation. Then these "stiff" unit cells prevent the"soft" unit cell from deforming as much as if it were independent. This is accomplished by the stiffer springs carrying a greater share of the load. In the fabric, this would result in a higher rupture stress.

The effects of these two assumptions are opposite, and an analysis of their combined influence will require a major investigation.

D. Predicted Rupture Stress

With the preceding equations of Peirce, rupture stress of varying fabric sample sizes can be predicted, provided the standard deviation of rupture stress, $S_{d\sigma}$, is known.

The area density of the unit cell, d, and the rupture stress, σ_{cm} have both been assumed normally distributed. Thus the distribution of the product of the two normal distributions is desired, specified by the parameters of mean value and standard deviation.

The question arises as to whether the area density and fiber orientation distribution are dependent, i.e., having a real correlation coefficient. This can be determined by the use of a Spearman rank coefficient. Consider the distribtuion of unit cell rupture stress, σ_{cm}, given in Table 8.2. Rank the ten unit cells in order of decreasing rupture stress using the cell number. Then rank the unit cells by the counted number of fibers in the cell, also in order of decreasing number of fibers, or area density.

	High									Low
Strength Rank	6	9	10	5	7	4	1	2	3	8
Weight	1	10	3	7	5	4	9	2	6	8
Difference in Rank, d	5	1	7	2	2	0	8	0	3	0
d^2	25	1	49	4	4	0	64	0	9	0

The Spearman Rank Coefficient

$$R = 1 - \frac{6 \Sigma d^2}{n^3 - n} = 1 - \frac{6 \times 156}{990} = 0.06 \qquad (8.15)$$

The significance of R can be tested using Students' "t" test, as

$$t = R \frac{n-2}{1-R^2} = 0.17 \qquad (8.16)$$

Since the value of "t" significant at the 5% level with 8 degrees of freedom is 2.3, the two are definitely not correlated. Therefore, the distributions of area density, d, and unit cell rupture stress, σ_{cm}, can be considered independent.

1. The Standard Deviation of the Joint Distribution

The problem of the product of two normally distributed independent variables has been considered by Craig (3), Aroian (1), and Haldane (10). The analysis of Haldane will be used here.*

If x and y be reduced normal variates, that is to say, variates whose mean is zero and standard deviation = 1, it is required to find the distribution of XY, where $X = m_1(1+k_1^{1/2}x)$, $Y = m_2(1+k_2^{1/2}y)$, $k_1^{1/2}$ & $k_2^{1/2}$ are the coefficients of variation of x and y respectively. Then Haldane gives the moments of XY about zero as (See Appendix E).

$$\mu_1' = m_1 m_2$$
$$\mu_2' = m_1^2 m_2^2 (1+k_1)(1+k_2)$$
$$\mu_3' = m_1^3 m_2^3 (1+3k_1)(1+3k_2)$$
$$\mu_4' = m_1^4 m_2^4 (1+6k_1+3k_1^2)(1+6k_2+3k_2^2)$$

So the moments about the mean m_1, m_2 are

$$\mu_2 = m_1^2 m_2^2 (k_1 + k_2 + k_1 k_2)$$
$$\mu_3 = 6 m_1^3 m_2^3 (k_1 k_2)$$
$$\mu_4 = 3 m_1^4 m_2^4 [k_1^2 + k_2^2 + 2k_1 k_2 + 6k_1 k_2^2 + 6k_1^2 k_2 + 3k_1^2 k_2^2]$$

As μ_2 (the second moment about the mean) is defined as the standard deviation, S

$$S_{xy}^2 = m_1^2 m_2^2 (k_1 + k_2 + k_1 k_2) \qquad (8.17)$$

*Haldane considers other cases of products of both independent and dependent variables and provides the only explicit treatment of the third and fourth moments of the product distribution. A more detailed treatment is given in Appendix E.

Recalling that $k = C^2$, where C is the coefficient of variation;

$$C_{xy}^2 = C_1^2 + C_2^2 + C_1^2 C_2^2 \qquad (8.18)$$

Substituting σ_c, d, for x and y gives

$$S_{d\sigma}^2 = (D\bar{\sigma})^2 [C_d^2 + C_\sigma^2 + C_d^2 C_\sigma^2]$$

or

$$C_{d\sigma}^2 = C_d^2 + C_\sigma^2 + C_d^2 C_\sigma^2 \qquad (8.19)$$

Multiplying through by $(D\bar{\sigma})^2$ gives

$$S_{d\sigma}^2 = \bar{\sigma}^2 S_d^2 + D^2 S_\sigma^2 + S_d^2 S_\sigma^2$$

a form arrived at by Aroian (1). However, the method of Haldane also gives the third and fourth moments of $g(d\sigma_{cm})$ about the mean, indicative of the skewness of the distribution.*

Numerically, for Fabric A, in the L direction;

$\bar{\sigma} = 1.19$ gpd $\qquad S_\sigma = 0.086$ gpd

$D = 4400$ denier $\qquad S_d = 500$ denier

$$S_{d\sigma}^2 = (1.19)^2 \times (500)^2 + (4400)^2 \times (0.086)^2 + (500)^2 \times (0.086)^2 = 500350$$

$S_{d\sigma} = 707$ grams/inch width

or $\qquad \frac{707}{4400} = 0.16$ gpd

2. <u>The Predicted Gauge Length Effect</u>

Consider a specimen one inch wide and of various lengths. With the unit cell of 0.0225", the number of horizontal cells (or strands), $j_1 = 44.5$. Then the total number of unit cells (hj) in the specimen of gauge length J is

*The presence of skewness states that the joint distribution of $d\sigma$ is no longer normal. Thus Peirce's analysis is not exactly valid. In the interest of simplicity and considering the prior assumptions, Peirce's solution will be used as an approximation without change.

$\frac{J}{.0225} \times 44.5 = 1960J$, where the length J is in inches. Using equation 8.14 for uniform tension ($J > 0.45$")

$$F_{hj} = D\,\bar{\sigma}_{cm} - V_{hj}\,S_{d\sigma} \qquad (8.21)$$

Dividing through by $D\bar{\sigma}_{cm}$, and converting F_{hj} to σ_{hj} by dividing by D, gives, in terms of stress in gpd;

$$\frac{(\sigma_m)_{hj}}{\bar{\sigma}_{cm}} = 1 - V_{hj}\frac{S_{d\sigma}}{D\bar{\sigma}_{cm}} = 1 - V_{hj}C_{d\sigma} \qquad (8.22)$$

Substituting the values for Fabric A gives

$$(\sigma_m)_{hj} = 1.2\left[1 - .56(hj)^{-1/5}\right] \qquad (8.23)$$

Then the minimum strength of the fabric will occur when $hj \to \infty$, and $(\sigma_m)_\infty =$ 1.2-.67 = .53 gpd. Rewriting equation 8.22 in terms of the gauge length J for the unit cell = .0225" of Fabric A (one inch wide) gives

$$(\sigma_m)_J = 1.2\left[1 - .56(1960\,J)^{-1/5}\right] \qquad (8.24)$$

Figure 8.3 gives the values of rupture stress plotted versus gauge length, J. The solid line joins these predicted values for $J > 0.45$ inches. The dotted line from $0 < J < 0.45$ indicates the area in which the boundary conditions probably change from uniform tension to uniform extension, the latter given by the horizontal straight line at 1.2 gpd, $0 < j < 0.45$ inches. The circles indicate experimental points from tests of Fabric A at J = 0.10, 0.25, 0.625, 2.5, 6.25 and 8 inches, all at the same rate of strain (6.25 %/min).

FIGURE 8.3

PREDICTED SPECIFIC RUPTURE STRESS vs. GAUGE LENGTH, FABRIC A

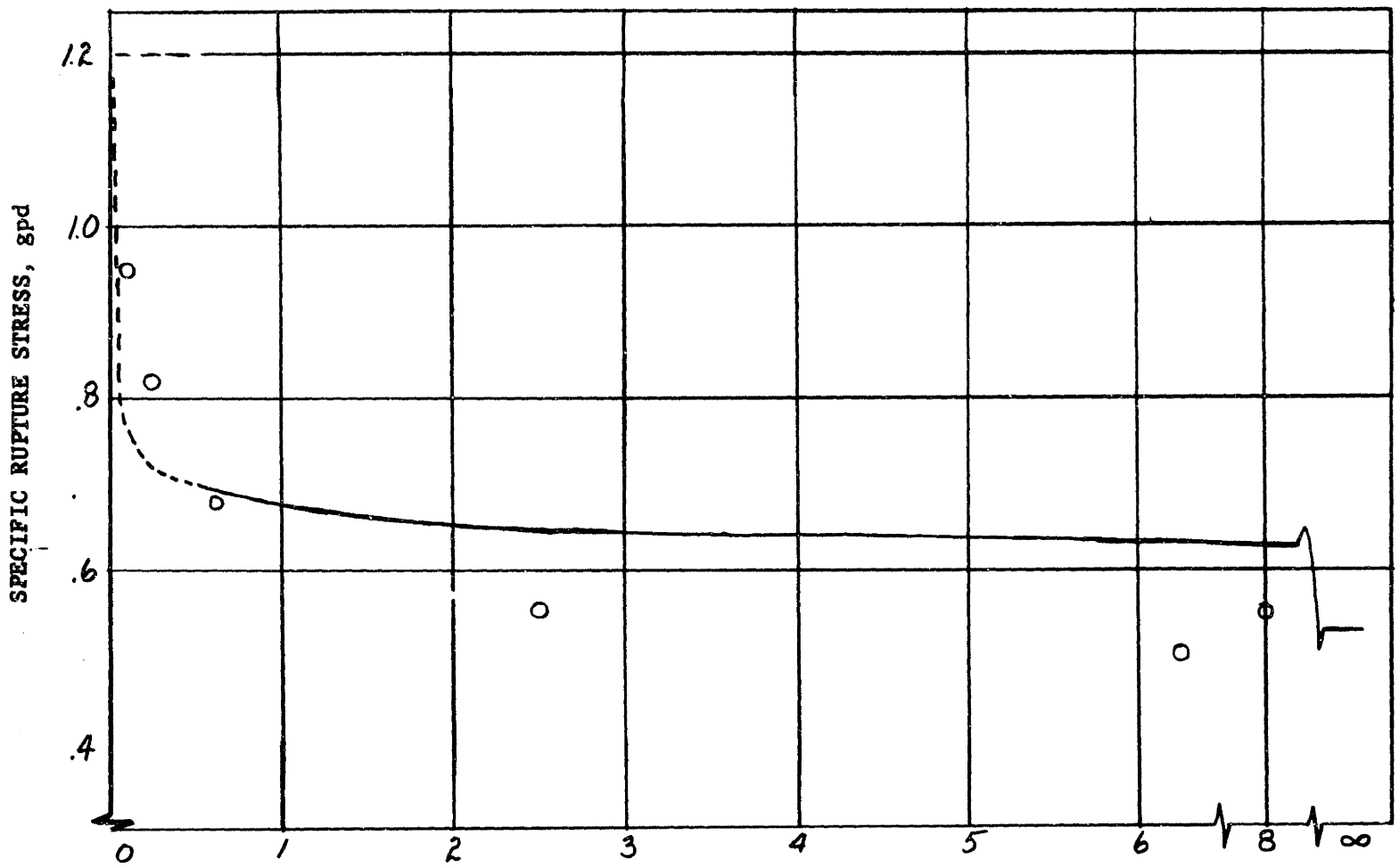

Since the measured stress strain curves fall below those predicted by the general theory, Figure 8.4 shows the average stress-strain curves of four of the gauge length tests. The agreement in form with the predicted curve is excellent, disregarding the initial modulus for J = 0.25". At that jaw spacing, mounting a one inch wide specimen so as to preserve uniform tension across the specimen becomes almost impossible.

Assuming that $C_{J\sigma}$, the coefficient of variation of rupture strength of the unit cell due to changes in $\phi(\beta)$ and d, is constant for all angles of θ*; then predictions can be made of the rupture stress at angles of θ for the 8 inch gauge specimens. Recalling that

$$\sigma = p'' + E_2 e$$

with the values for p'' and E_2 from Section VI.D and e = 10.4%, we have for Fabric A;

Predicted	θ°	0°	10°	20°	30°	40°	50°	60°	70°	80°	90°
$\overline{\sigma_{cm}}$		1.22	1.17	1.05	.87	.69	.56	.46	.40	.36	.34
σ_J		.63	.60	.54	.45	.36	.29	.24	.21	.19	.18
Measured (Fabric A)	θ°	0°	15°	30°	45°	60°	75°	90°			
	σ_m	.55	.51	.39	.20	.18	.135	.11			
Measured σ_m, H.V. Fabric A		.69	-	.56	.37	.30	-	.25			

These results are plotted in Figure 8.5. The prediction is excellent with deviations on the order of 10-20%.

With this discussion of rupture, the original goal of the project is complete. With the fiber web theory and the analysis of Peirce, the mechanical

*A valid argument on Fabric A, but invalid on Fabric B, as shown in Section IX.E.

FIGURE 8.4

STRESS-STRAIN CURVES AT VARIOUS GAUGE LENGTHS
FABRIC A, $\theta = 0^{\circ}$ (L)

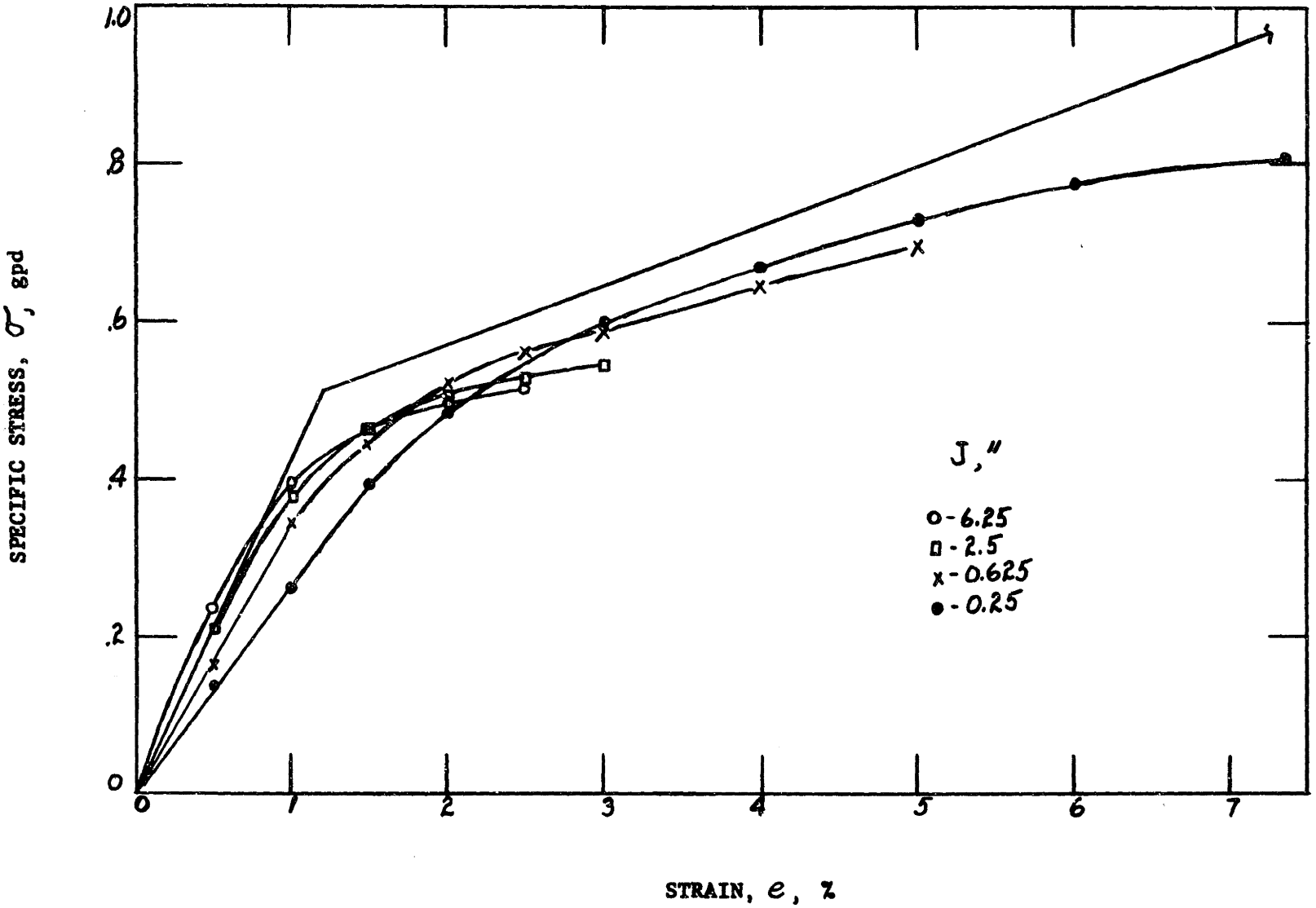

FIGURE 8.5

FABRIC A, PREDICTED AND EXPERIMENTAL RUPTURE STRESS

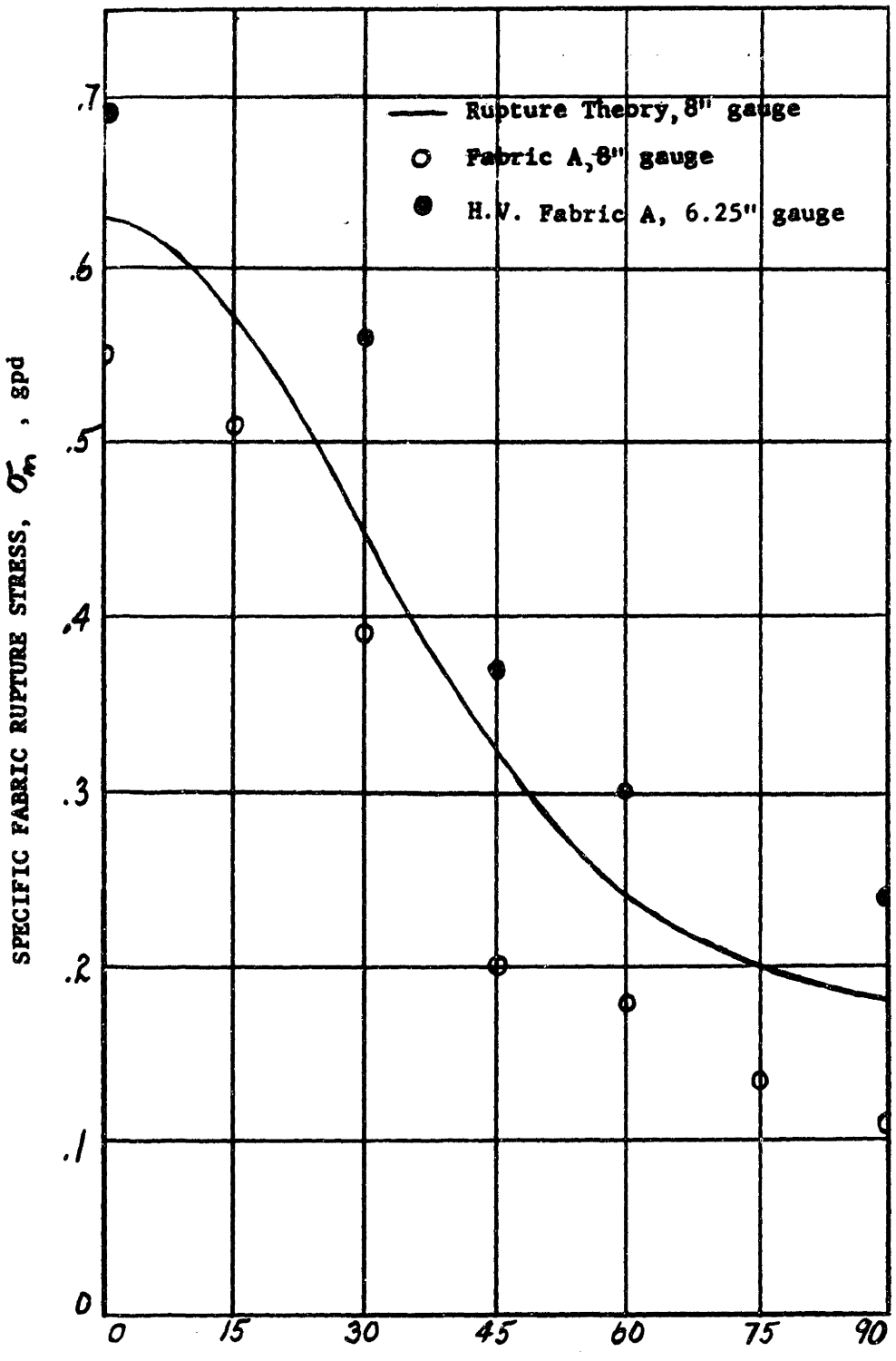

properties and rupture stress of this flexible non-woven structure can be predicted very satisfactorily from the properties of the fiber, the fiber orientation distribution, and the inherent variability of the fabric.

IX. THE SECOND NON-WOVEN FABRIC

The previous sections have all been confined to experimental data on one non-woven material, Fabric A; and the development of a general analytical procedure for the prediction of fabric properties. It is desirable to select another non-woven structure for experimental work, in order to verify the fiber web theory and the assumptions concerning the unit cell.

A. The Relative Importance of Variables and the Selection of Fabric B.

Certain parameters are available for study, and the most important are as follows:

a. Change in Fiber Properties

b. Change in Fiber Orientation Distribution

c. Change in Fiber Length

d. Change in Binder System

e. Change in Fabric Weight

f. Change in Process, with change in Coefficient of Variation of Unit Cell Weight and Strength.

As all of these cannot be changed easily at the same time, the most important should be studied. The theory is based on fiber properties, a and fiber orientation b; and the rupture conditions are based on unit cell variability, f. Fiber property changes, a, with % RH have been examined briefly. This leaves two variables, of perhaps equal importance. With the assistance of C. H. Dexter and Sons, Inc. the fiber orientation distribution and the process equipment were both changed.

A small run of non-woven fabric was made on the pilot-stage machine in Windsor Locks. The fiber and binder were again viscose, and the fiber length was unchanged. Understandably, the process control on short runs

of this type is different than on production equipment, and the variability of the fabric could be expected to be different. The fiber orientation distribution was changed to give as high a directionality to the fabric as possible, or greatest E_L/E_T ratio. This material, Fabric B, has the following specifications and is shown in Exhibit IV.

Fabric B. (Dexstar #202)

Nominal Weight - 7#/ream or 7#/380 sq. yds.

Actual Weight at 65% RH - 10.8 gm/sq. yd.

Fiber - Regular tenacity viscose rayon, 1½ denier, 1/4" - 3/8" in length

Binder - Regenerated viscose solution, approximately 5% on weight of fiber

Formation - Poor, with considerable thin streaks and heavy clumps. Fiber orientation fairly uniform, but with fibers agglomerated into bundles, increasing the open appearance of the fabric. Fibers highly oriented in machine direction.

Furnished 24" wide roll.

If the Fabric B properties can be predicted with any degree of accuracy then the analytical approach can be considered a success. Referring to Exhibit IV, the material is quite open, with considerable free length of fiber between intersections and bond points. This means that fiber buckling will be pronounced, and the behavior of the unit cell may have to be modified.

B. The Orthotropic Measurements and Theory

From the roll of Fabric B, five sheets thirty inches long were cut; each sheet separated from its adjacent area by approximately 18 inches of discarded fabric. The five sheets were selected for uniformity of formation, and were trimmed to 18 inches wide. The sheets were cut in half, yielding

ten sheets, each 15 inches long (L direction) and 18 inches wide. Five of the sheets were reversed sidewise, to reduce edge to edge variation. The average weight of the ten sheets was 10.82 grams/sq. yd, or an equivalent denier of 3050.

Ten specimens, one from each sheet, were cut 8" long x 1" wide, at the angles of $\theta = 0^\circ$, 15°, 30°, 45°, 60°, 75°, and 90°. The specimens were tested at 6.25 inch jaw separation, and a strain rate of 8%/min. Four major points were taken from the Instron curve and averaged. As in III C., these points were the Initial Modulus, the rupture load/inch width, the proportional limit load, and the maximum strain. The loads are converted to specific stress and the data presented in Table 9.1. For each of the four entries at each test angle θ, the average value is given first, followed by the observed range of data.

Figure 9.1 gives the shapes of the seven stress-strain curves. Obviously the fabric is of much higher orientation than Fabric A. Also, the rupture strain increases markedly after $\theta = 30^\circ$, reaching a maximum for $\theta = 75^\circ$. Observation of the specimens ($\theta = 30^\circ - 90^\circ$) during test indicated that the straining became localized after the yield point, and that the deformation appeared to be shear between planes parallel to the L direction, rather than uniform distortion of the fabric.

One specimen, $1\frac{1}{2}$" wide, and supported by the backing plate, was used to determine ν_{LT}. Two measurements of e_L and e_T were made on each photograph and the data, plotted in Figure 9.2, gives $\nu_{LT} = 2.71$.

With the measured values of $E_L = 59$ gpd, $E_T = 1.69$ gpd, we have, by equation 3.13:

TABLE 9.1

MEASURED STRESS-STRAIN CURVE CHARACTERISTICS, FABRIC B

Angle of Test, θ	E, gpd Avg.	E, gpd Range	σ_p, gpd Avg.	σ_p, gpd Range	σ_m, gpd Avg.	σ_m, gpd Range	e_m, % Avg.	e_m, % Range
0°	59	52/63	.52	.47/.56	.72	.65/.77	2.30	1.75/2.62
15°	39	35/41	.33	.28/.38	.43	.35/.47	2.22	1.67/2.64
30°	14.2	11/17	.14	.115/.17	.19	.145/.27	2.24	1.67/4.00
45°	5.8	4.3/7.4	.075	.059/.102	.12	.089/.175	4.13	3.3/6.0
60°	2.65	2.1/3.4	.039	.031/.050	.08	.049/.12	7.9	5.9/10.7
75°	1.45	1.1/1.7	.026	.019/.029	.065	.052/.089	~12.0	8.0/15.0
90°	1.6	1.5/1.7	.028	.023/.033	.06	.041/.072	7.4	6.2/11.0

FIGURE 9.1

FABRIC B; COMPOSITE STRESS-STRAIN CURVES

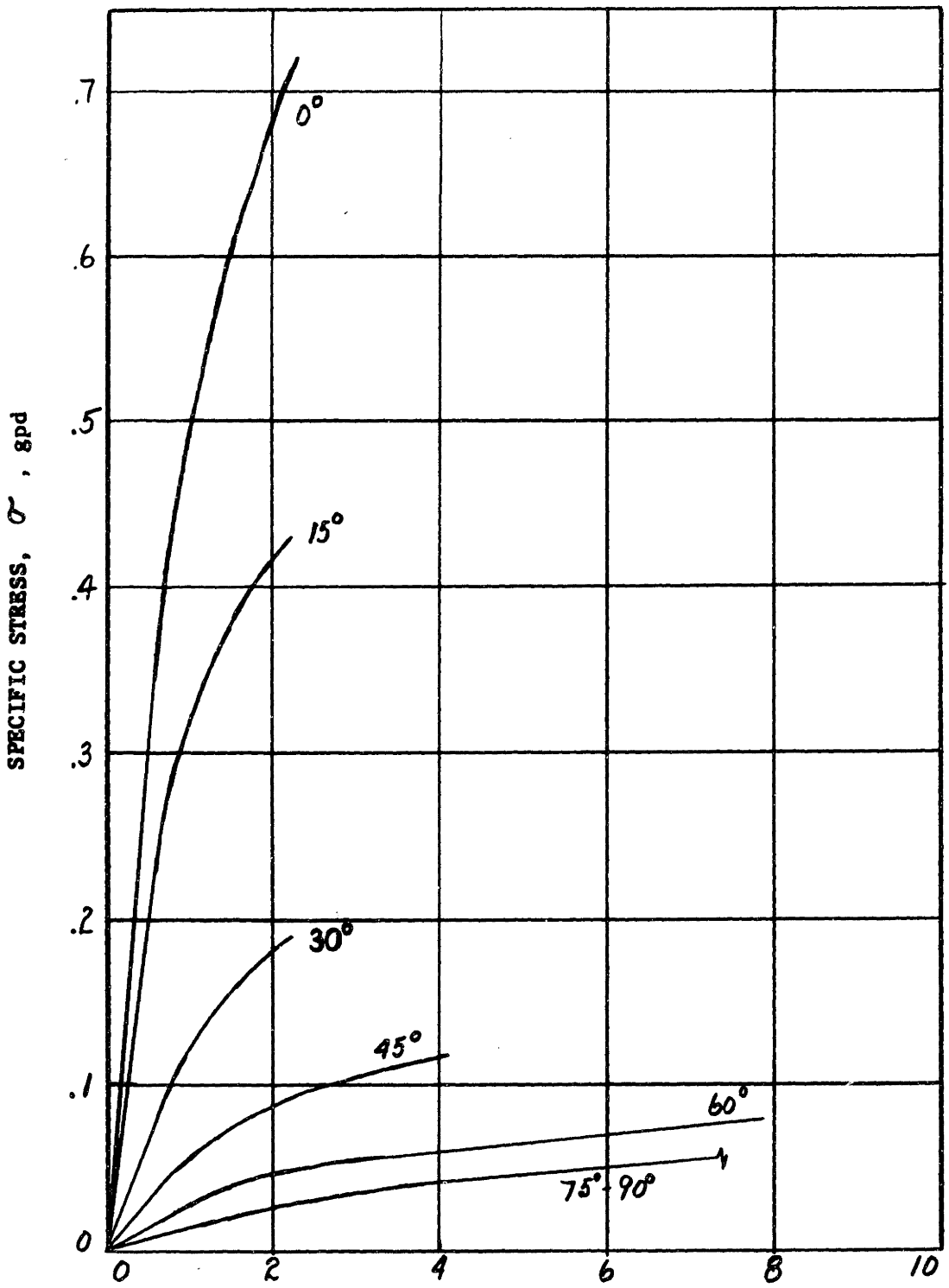

FIGURE 9.2

FABRIC B, POISSON'S RATIO, ν_{LT} ($\theta = 0^{\circ}$)

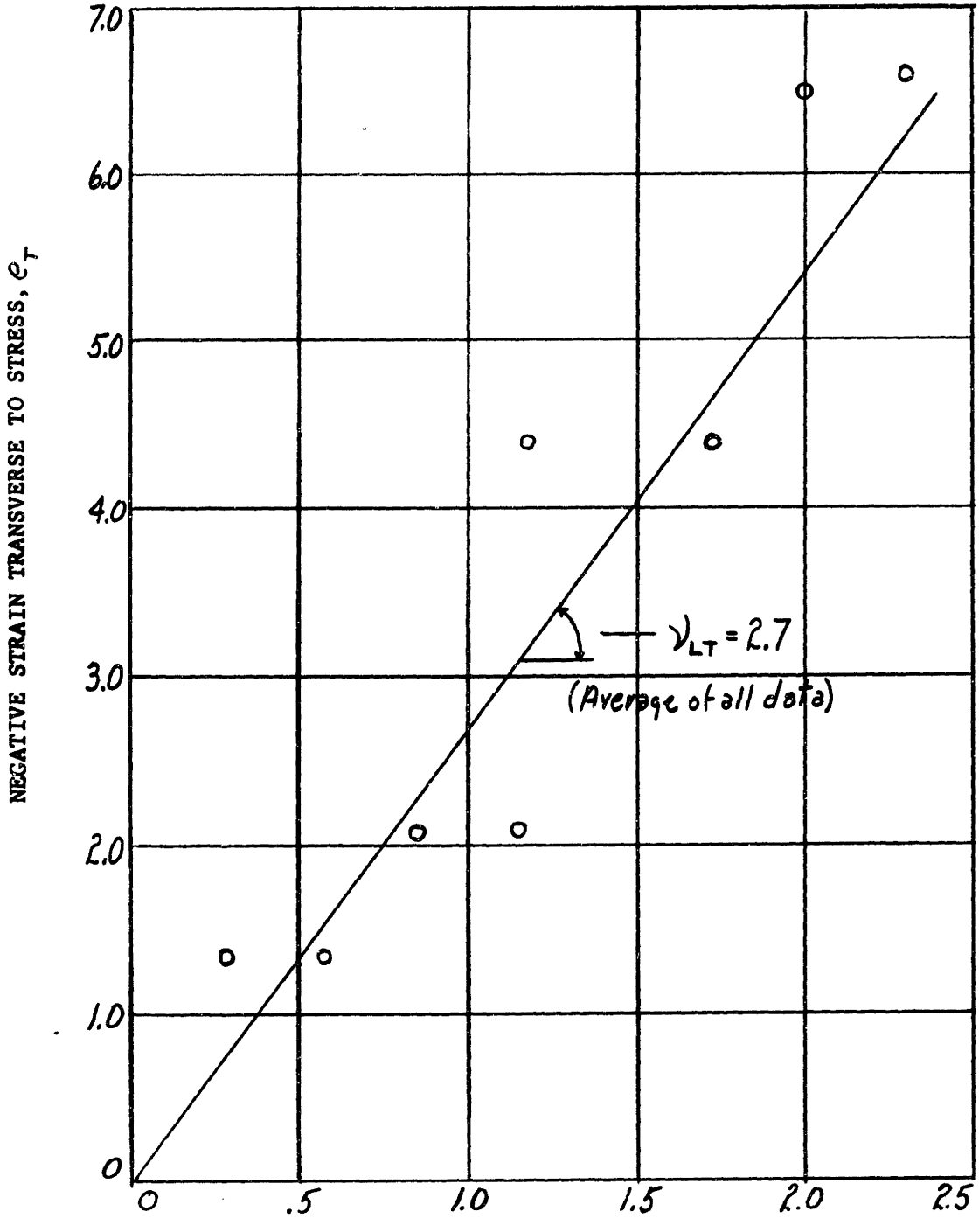

$$\nu_{TL} = \frac{E_T}{E_L}\nu_{LT} = 0.072$$

With the measured value of $E_{45^\circ} = 5.8$ gpd, and equation 3.12a, the modulus of rigidity, G_{LT} is

$$\frac{1}{E_{45^\circ}} = \frac{\cos^4 45^\circ}{E_L} + \frac{\sin^4 45^\circ}{E_T} + \left[\frac{1}{G_{LT}} - \frac{2\nu_{LT}}{E_L}\right]\sin^2 45^\circ \cos^2 45^\circ$$

$$G_{LT} = 7.9 \text{ gpd.}$$

The five orthotropic constants are determined and the equations of section III.A. can be used to predict the properties of Fabric B at intermediate test angles, θ.

The modulus of elasticity, Ey, is given by

$$\frac{1}{E_y} = \frac{\cos^4\theta}{E_L} + \frac{\sin^4\theta}{E_T} + \left[\frac{1}{G_{LT}} - \frac{2\nu_{LT}}{E_L}\right]\sin^2\theta\cos^2\theta$$

and the predicted behavior is shown with the experimental data in Figure 9.3. The agreement is fair. However, since the values of E_{45° and E_T are of the same order of magnitude, the portion of the predicted curve from $\theta = 45^\circ$ to 90° is forced into agreement. The difference between predicted and measured E_y at $\theta = 15^\circ$ and 30° is not excessive, but with both experimental points below the predicted values, some real causal effect might be expected. Note that in Figure 3.20 for Fabric A, experimental points lay on both sides of the predicted curve in this region, suggesting experimental error.

FIGURE 9.3

FABRIC B. ORTHOTROPIC PREDICTED AND MEASURED SPECIFIC MODULI

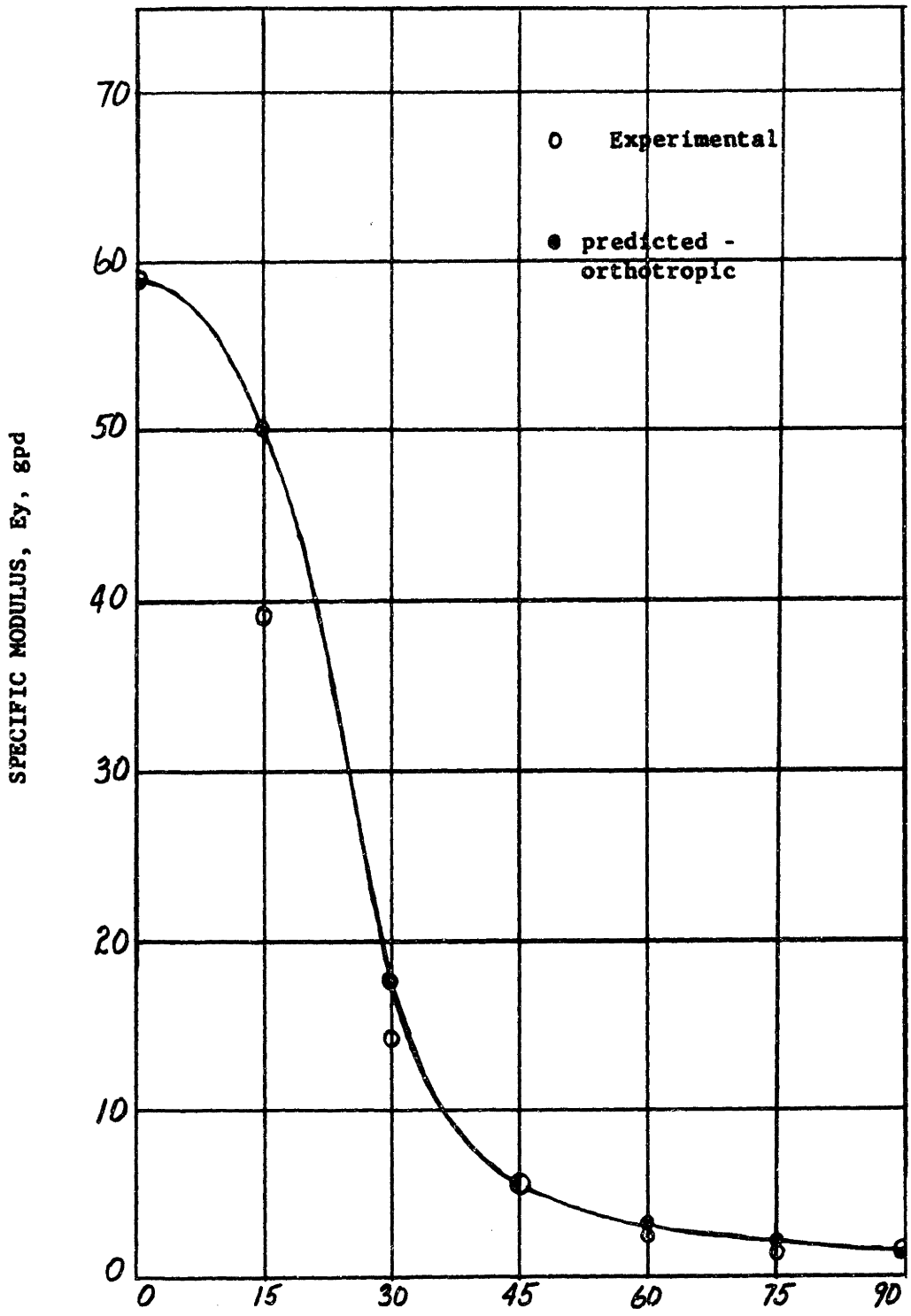

Experimental data on ν_{yx} was not obtained. It was felt that a comparison between orthotropic and fiber web theory would be more advantageous and this discussion will be delayed until the next section.

The predicted values of σ_p are given by the procedure described in Table 3.5, again defining $\sigma_{p_{LT}} = \frac{1}{2}\sigma_{p_{45}}$. These values are plotted as Figure 9.4A along with the experimental results. Again, if $\sigma_{p_{LT}}$ were twice its assumed value, the agreement would be satisfactory.

The specific rupture stress prediction is again given by equation 3.14 as

$$\frac{1}{(\sigma_m)_y^2} = \frac{\cos^4\theta}{(\sigma_m)_L^2} + \frac{\sin^4\theta}{(\sigma_m)_T^2} + \left[\frac{1}{(\sigma_m)_{LT}^2} - \frac{1}{(\sigma_m)_L(\sigma_m)_T}\right]\sin^2\theta\cos^2\theta$$

where σ_m is the specific rupture stress in the direction indicated by the subscript (and $(\sigma_m)_{LT} = (\sigma_m)_{45^\circ}$). The values obtained from this equation are plotted in Figure 9.4B along with the experimental data. The agreement is quite satisfactory, despite the non-Hookean fabric behavior.

In conclusion, it may be stated that the fabric properties predicted by the orthotropic theory are good, (with the exception of Poisson's ratio, discussed later). However, the use of experimental data at $\theta = 45^\circ$ to establish G_{LT}, $\sigma_{p_{LT}}$, and $(\sigma_m)_{LT}$ have <u>forced</u> this agreement to a large extent. Furthermore, even for moderate changes in G_{LT} and ν_{LT} the predicted curves do not change by appreciable amounts. This suggests that the orthotropic theory is valuable for examining the behavior of a fabric under test - to predict its performance at other angles of test; but is of little value in examining theoretical structures to determine if they offer improvement in properties at certain intermediate angles.

FIGURE 9.4

FABRIC B. PREDICTED AND MEASURED SPECIFIC PROPORTIONAL LIMIT AND RUPTURE STRESS

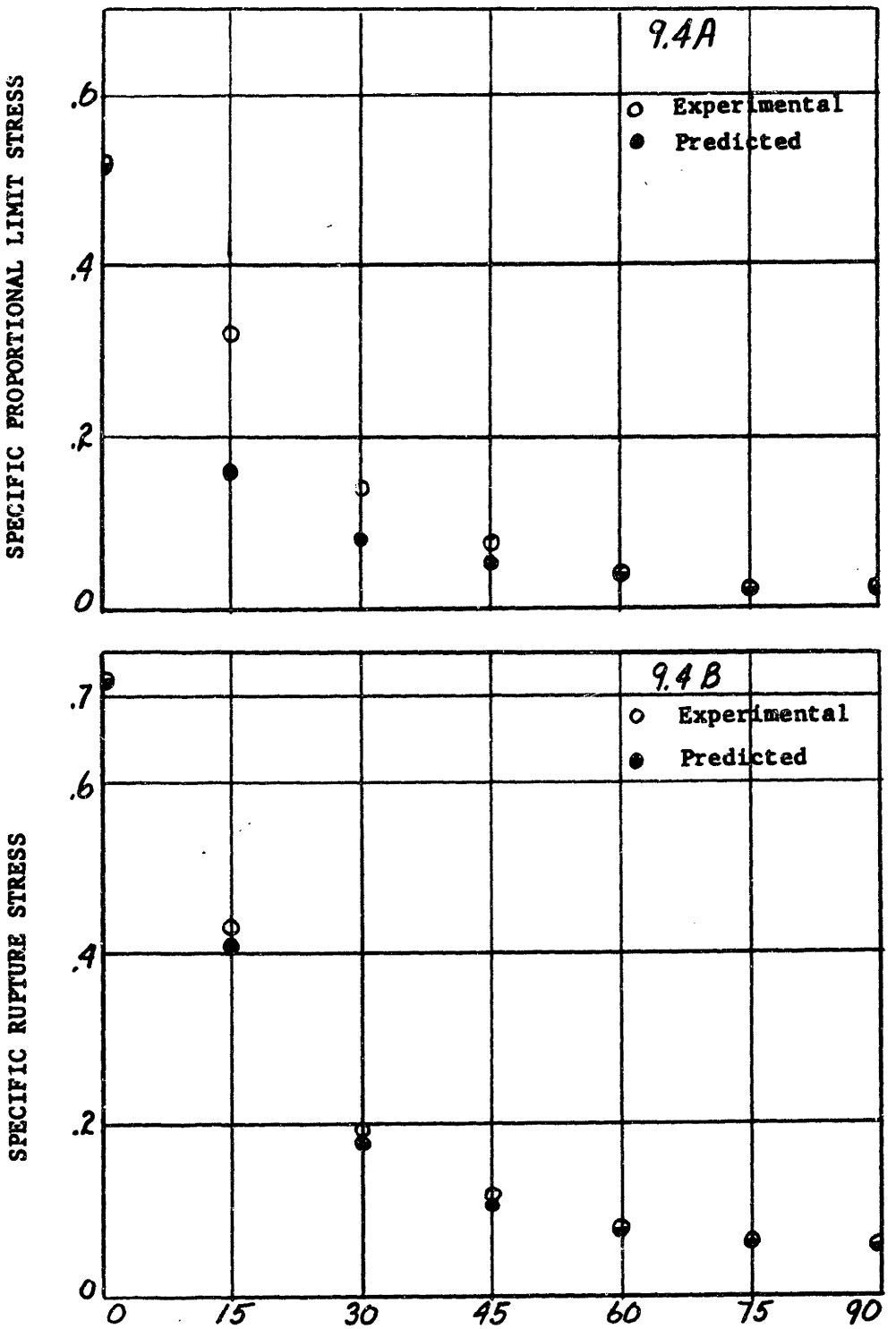

C. The Fiber Web Theory and the Unit Cell

1. The Average Unit Cell

A visually selected uniform area of Fabric B was mounted between two microscope slides as described in V.A. Since Fabric B was less dense than Fabric A, and the number of intersections smaller, it was assumed that a larger unit cell would be required to satisfy the uniform boundary displacement concept. Microscopic observation indicated a unit cell of approximately .060 inches on edge in order to have each fiber bonded from three to eight times. The unit cell was selected as 0.0625 inches square and the marking yarns on the slide were placed 2 mm or 0.080 inches apart, running in the T direction, similar to that shown in the photograph of the slide in Figure 5.3. Photomicrographs were made of one of these areas, providing a continuous strip photograph of the area at a magnification of 37.5 times. This is shown in Figure 9.5, again divided for purposes of display into three rows and with the L direction of the fabric vertical. The circles drawn between the marking yarns (horizontal bright bands) are 0.0625 inches in diameter on the fabric, or 2.34" on the actual photographs (Figure 9.5 is a slightly reduced reproduction of the original).

Measurement of $\phi(\beta)$

The counting procedure described in V.A.I. was again followed to determine the relative fiber orientation distribution, $\phi(\beta)$. However two problems arose. The first was fiber straightness - since the majority of fibers oriented away from the L direction have several bends or kinks within the bounding circle. This problem was arbitrarily solved by taking the angular orientation of these fibers as their average direction between the circle boundaries.

FIGURE 9.5

TWELVE ADJACENT UNIT CELLS, FABRIC B

The second problem involved fiber bunching, and the subsequent difficulty in determining exactly how many fibers were present in a bundle. This problem is discussed in Appendix C. in regard to the difference between area density obtained from counting fibers and by actual weighing. In Fabric A, this difference in area density was small. On Fabric B, the first countings of fibers for $\phi(\beta)$ gave only 40% of the number of fibers predicted by the weighed area density. Subsequent recounts (using a magnifying glass on the photographs) yielded better results, but the difference was still significant. Increasing the magnification means reducing the size of the unit cell, thus changing the estimates of coefficient of variation of weight and strength of the unit cell. This was not desirable and thus all of the data were averaged to obtain a best estimate of $\overline{\phi(\beta)}$. This is justified on the visual observation that bunching (and thus uncounted fibers) does not appear to depend on the angle of orientation. Consequently fibers at any angle β have the same probability of not being counted. If this were exactly true, then the measured $\overline{\phi(\beta)}$ would be an excellent estimate of the true $\overline{\phi(\beta)}$. This appears to be a valid assumption, and thus the data in Table 9.2 lists the original fiber counts of the twelve cells, and the recounts of six of these cells (with a magnifying glass) with the plus and minus angular intervals summed. The data for 18 counts of the angular intervals are averaged to give the estimated $\overline{\phi(\beta)}$ distribution shown as Figure 9.6 (corrected for the change in scale of β). The dashed line on Figure 9.6 is the empirical fit of the measured $\overline{\phi(\beta)}$ using the equation

$$\phi(\beta) = a + b\cos\beta + c\cos^3\beta + d\cos^8\beta + e\cos^{16}\beta$$

TABLE 9.2

FABRIC B, ABSOLUTE AND RELATIVE FIBER ORIENTATION DISTRIBUTION FREQUENCIES;

TWELVE UNIT CELLS, 0.0625 INCHES IN DIAMETER

Unit Cell No.	Angular Interval with Mid-point β_i									
	5-0-5	5-15	15-25	25-35	35-45	45-55	55-65	65-75	75-85	85-90
1	7	7	4	4	1	0	2	2	2	0
2	13	9	9	1	5	5	1	2	0	0
3	14	10	1	2	1	2	4	0	0	0
4	8	11	6	2	1	5	1	1	0	2
5	12	12	5	3	2	4	1	0	1	0
6	10	12	4	3	0	0	0	2	2	1
7	6	10	3	0	1	1	1	0	1	0
8	10	10	6	2	0	1	3	2	0	0
9	8	19	6	0	1	3	1	1	1	0
10	12	19	5	3	0	0	2	2	0	1
11	11	15	7	0	3	1	0	2	0	0
12	10	14	6	2	3	1	0	4	0	0
R.C.1	16	20	11	9	4	4	5	4	3	0
R.C.2	23	13	6	10	7	4	4	4	1	0
R.C.3	16	18	7	9	3	6	4	4	0	0
R.C.4	12	16	15	4	1	7	2	1	0	2
R.C.7	9	19	4	0	3	4	4	0	2	0
R.C.10	17	34	12	8	0	0	8	1	5	2
Σ_c	214	268	117	62	36	48	43	32	18	8
% of distribution	214	134	58.5	31	18	24	21.5	16	9	8
Relative Freq.	.256	.158	.069	.037	.021	.028	.024	.019	.011	.009

FIGURE 9.6

FABRIC B, FIBER ORIENTATION DISTRIBUTION

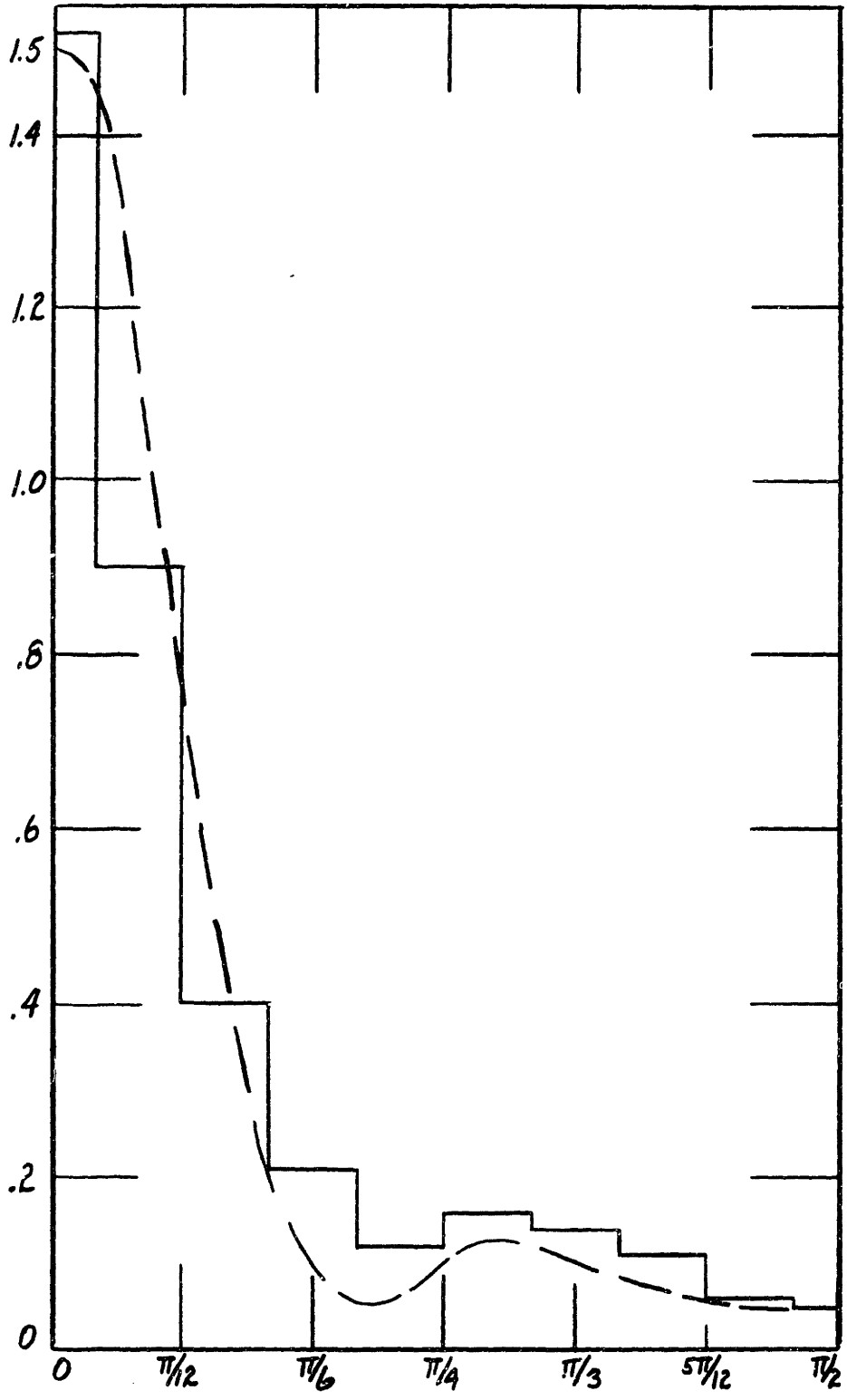

or

$$\phi(\beta) = 0.04 + 0.10\cos\beta + 0.10\cos^3\beta - 1.0\cos^8\beta + 2.26\cos^{16}\beta \quad (9.1)^*$$

Since the Fabric B experiments were also conducted at 65% RH, the fiber properties are the same, as given by

$$\sigma_f = 72\, e_f \qquad e_f < 1.13\%$$
$$\sigma_f = .66 + 12.7\, e_f \qquad e_f > 1.13\%$$

With the fiber properties and $\phi(\beta)$ known, the equations 6.9, 6.11 and 6.26 can be used to predict all of the early mechanical properties of Fabric B.

Before proceeding with this prediction based on the fiber web theory, a number of observations can be made about the unit cell of Fabric B. The theory is based on the assumption of straight fibers and uniform boundary displacement. The use of the average direction for kinked or curved fibers is satisfactory for determining $\phi(\beta)$. Figure 9.5 shows that the majority of bent or curved yarns are oriented primarily toward the T direction. Since these fibers do not contribute to properties in the L direction, no difficulty should be experienced in predicting the modulus of the fabric near $\theta = 0^\circ$. In the T direction, however, the presence of bent fibers will definitely reduce the modulus and proportional limit. Further, the number of fibers oriented toward the T direction is so small as to cause serious questions concerning the assumption of uniform boundary displacement in the T direction.

The presence of the bent fibers in the T direction, along with their relatively infrequent occurrence and greater lengths between intersections, precludes any assumptions about the absence of fiber buckling. These longer free lengths are a direct result of fiber bunching. Compare Figure 9.5 with Figure 5.3 for Fabric A. Although the magnification in Figure 5.3 is 2.5 times that for Fabric B in Figure 9.5., the free length of fiber between bonds is much smaller in Fabric A. If fiber buckling can occur easily, the

*This equation obtained by changing the values at $\beta = 0^\circ$, $\beta = 20^\circ$ in the five simultaneous equations to provide a better fit in the $\beta = 30^\circ - 60^\circ$ region.

predicted value of ν_{yx} has little meaning. Also, if fibers cannot bear compressive loads, then shear between bundles of longitudinal fibers will be borne solely by the fibers under tension. In the previous analysis of the unit cell, the use of the complete distribution is warranted on the assumption that fibers would take compression. If this is not true in Fabric B, then the properties at angles of θ intermediate to the L and T axes may depend only on the fibers oriented so as to be under tension. This calls for modification of the unit cell, as will be shown.

2. Prediction of Fabric Properties by the Fiber Web Equations

Modulus of Elasticity, Ey. The initial modulus of elasticity ($\sigma_x = e_{yx} = 0$) is given by

$$\frac{E_y^*}{E_f} = \frac{A_2A_3 - A_1^2 + 4(A_1A_2 + A_1A_3 - A_2A_3 + 3A_1^2)\sin^2\theta\cos^2\theta}{A_3\sin^4\theta + A_2\cos^4\theta + 6A_1\sin^2\theta\cos^2\theta}$$

The values of A_1, A_2 and A_3, as defined by equation set 6.10 with the constants given by $\phi(\beta)$, equation 9.1, are

$$A_1 = .0591 \quad A_2 = .0884 \quad A_3 = .787 \tag{9.2}$$

Solution of equation 6.11 yields the following data

θ	0°	10°	20°	30°	40°	50°	60°	70°	80°	90
E_y^*/E_f	.75	.70	.54	.37	.23	.16	.12	.097	.087	.084
$E_{y,gpd}^*$	54	50	39	27	17	11	7.8	7.0	6.3	6.0

These values are plotted in Figure 9.7, along with the experimental data. While the agreement is fair, the previous observations about the unit cell appear correct. The predicted values of Ey (30° - 90°) are too large, since they are based on the straight fiber assumption. An analytical treatment

FIGURE 9.7

SPECIFIC MODULI, FABRIC B, MEASURED;
ORTHOTROPIC AND FIBER WEB THEORY

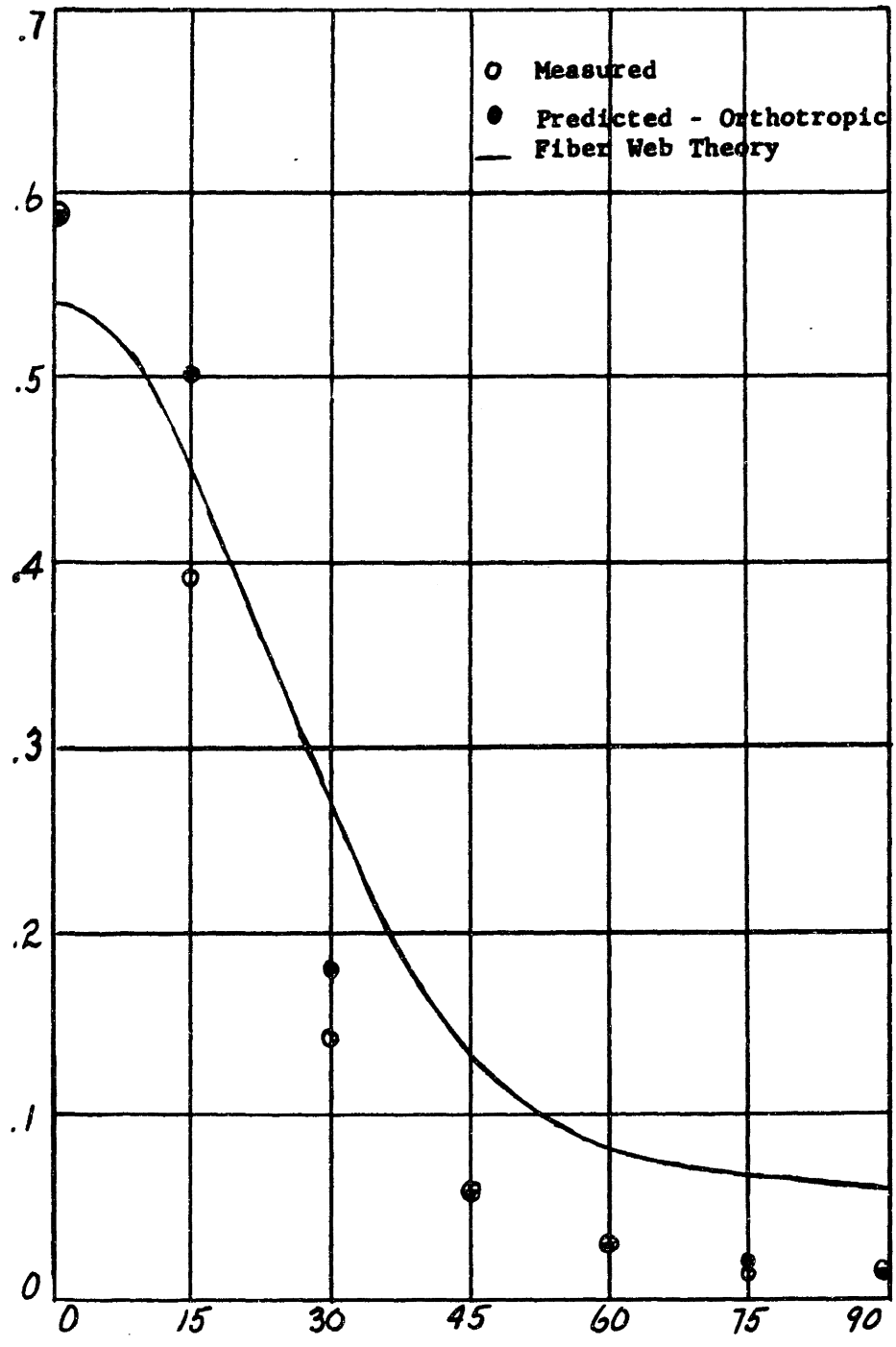

of the effect of fiber curvature is given later; but in any event, fiber curvature decreases the fabric modulus.

Poisson's Ratio ν_{yx} Predicted values of ν^*_{yx} are given by equation 6.9.

$$\nu^*_{yx} = \frac{A_1 + (A_2 + A_3 - 6A_1)\sin^2\theta\cos^2\theta}{A_3\sin^4\theta + A_2\cos^4\theta + 6A_1\sin^2\theta\cos^2\theta} \qquad (6.9)$$

With values of A_1, A_2, and A_3 given above; ν^*_{yx} can be calculated and are plotted in Figure 9.8, as the solid curve. The values obtained from the orthotropic theory are given as the dashed curve. Any semblance of agreement is purely coincidental. The large negative ν_{yx} predicted by the orthotropic theory are not correct. Measurement on Fabric B, $\theta = 45^0$, gave a Poisson's ratio equal to 0.6 - 0.8, indicated by the bar on figure 9.8. Writing the two equations

Orthotropic Theory ($\sigma_x = \sigma_{yx} = 0$)

$$\nu_{yx} = E_y\left[\frac{\nu_{LT}}{E_L} - \left(\frac{1}{E_L} + \frac{1}{E_T} + \frac{2\nu_{LT}}{E_L} - \frac{1}{G_{LT}}\right)\sin^2\theta\cos^2\theta\right]$$

Fiber Web Theory ($\sigma_x = e_{yx} = 0$)

$$\nu^*_{yx} = \frac{A_1 + (A_2 + A_3 - 6A_1)\sin^2\theta\cos^2\theta}{A_3\sin^4\theta + A_2\cos^4\theta + 6A_1\sin^2\theta\cos^2\theta}$$

certain conclusions can be drawn. As G_{LT} (7.9 gpd) approaches E_T (1.6 gpd) in value, then the second term in the orthotropic theory becomes smaller and ν_{yx} varies more with Ey without becoming negative. As $G_{LT} = A_1 E_F$ (equation 6.30), the fiber web theory predicts G_{LT} as 4.3 gpd. Using $G_{LT} = 4.3$, $\nu_{LT} = 2.7$ and $E_T = 6.0$ gpd in the orthotropic theory ($\sigma_x = \sigma_{yx} = 0$) will make all ν_{yx} positive, (as shown by the dotted curve in Figure 9.8), and the agreement with the theory is similar to that for Fabric A, Figure 6.4.

FIGURE 9.8

FABRIC B , PREDICTED POISSON'S RATIO, ν_{yx}

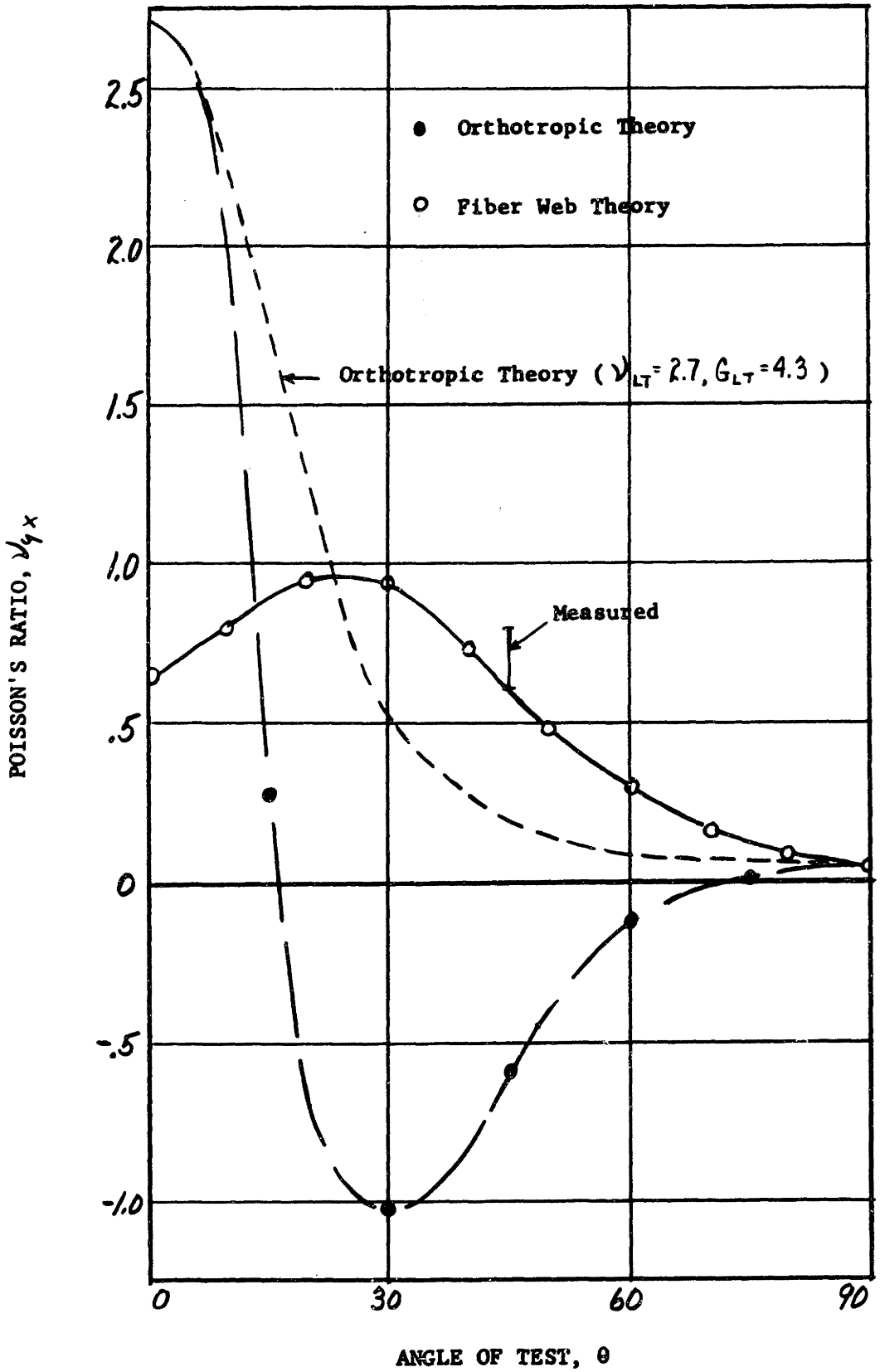

Stress-Strain Curve

Equation 6.26 gives the transposed plastic region of the fabric stress-strain curve as

$$\sigma_y = \rho\left[A_4 \cos^2\theta + A_5 \sin^2\theta\right]\left[1 - q/E_f\right] + q e_y E_y/E_f$$
$$= \rho'' + E_2 e_y$$

where $A_4 = .855$ and $A_5 = .149$ as given by equations 6.18. Thus

θ	0°	10°	20°	30°	40°	50°	60°	70°	80°	90°
ρ'	.465	.455	.42	.37	.31	.26	.18	.12	.09	.08
E_2	9.5	8.9	6.9	4.7	3.0	2.0	1.5	1.2	1.1	1.1

These values combined with the values of Ey are plotted as the predicted stress-strain behavior in Figure 9.9. As expected, the predicted behavior for $\theta = 0^\circ$ is in good agreement with the experiment; but the predictions are very poor at other angles. Based on our experience with Fabric A, we might expect some differences but not of the order of magnitude shown in Figure 9.9. The observation has already been made that the defined concept of the unit cell does not appear valid on this fabric. Thus the question arises as to how to deal with a real structure like Fabric B.

D. Revised Unit Cell for Bunched Fibers

The previous assumptions for the unit cell and strain transformation were as follows:

a. Uniform Boundary Displacement

b. Sufficient bonding to negate fiber ends

c. Sufficient bonding to average out strain variations within the unit cell

d. Fiber lengths between bonds short enough to permit compressive loading on the fibers without buckling.

e. Uniform Distortion of the Unit Cell (even in shear).

FIGURE 9.9

STRESS-STRAIN CURVES, FABRIC B, MEASURED AND FIBER WEB THEORY

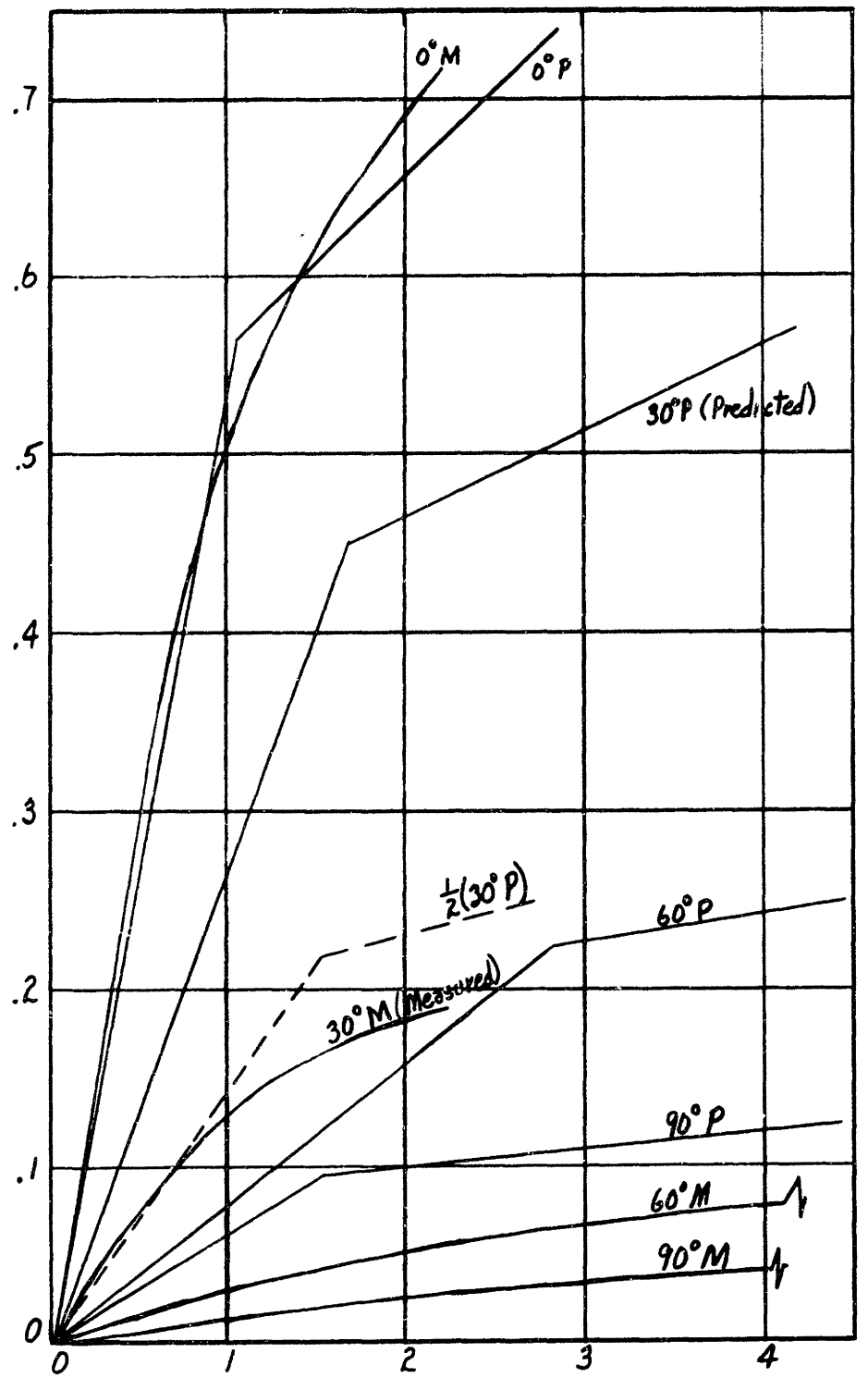

The unit cell of Fabric B does not satisfy d and e above. The postulated explanation has been the bunching or agglomeration of fibers in the fabric. Comparison of Figure 5.3 and Figure 9.5 makes this very evident. If fibers do not take compressive loads, then the deformation of the fabric structure under stress is changed.

Consider the two simulated unit cells shown in Figure 9.10, A and B; being schematic representations of Fabrics A and B respectively. The two figures have the same number and orientation of fibers, but differ only in the spatial placement of fibers at a particular orientation angle β. The schematic of Fabric A should deform uniformly under any stresses, as the fibers would not buckle under compressive loads. In Fabric B, buckling occurs almost immediately with the presence of any compressive stress component. The deformation does not involve straining of all the fibers, but rather consists almost entirely of shear between the bunched fiber groups. This is made very clear by considering the action of these two schematics under the action of shear forces, Q. In A, as the fibers take compression, all fibers except those parallel to Q resist the shear. In B, only the R and S groups (being in tension) resist the shear, while the U and T groups buckle and contribute practically nothing. Thus the change in the distance m between the fiber groups K and L is determined by the equilibrium state of only one-half the fibers of the $\phi(\beta)$ distribution. As only one-half the fibers are strained, then the resisting force for the same shear distortion is also only one-half. Consequently any measured property of the fabric at any angle other than $\theta = 0^{\circ}$ will be approximately one-half of the value predicted by the unit cell. This is a very idealized simplification. This shift in deformation behavior will occur probably between $\theta = 10^{\circ}$ and

FIGURE 9.10

TWO SCHEMATIC UNIT CELLS, WITH AND WITHOUT FIBER BUNCHING

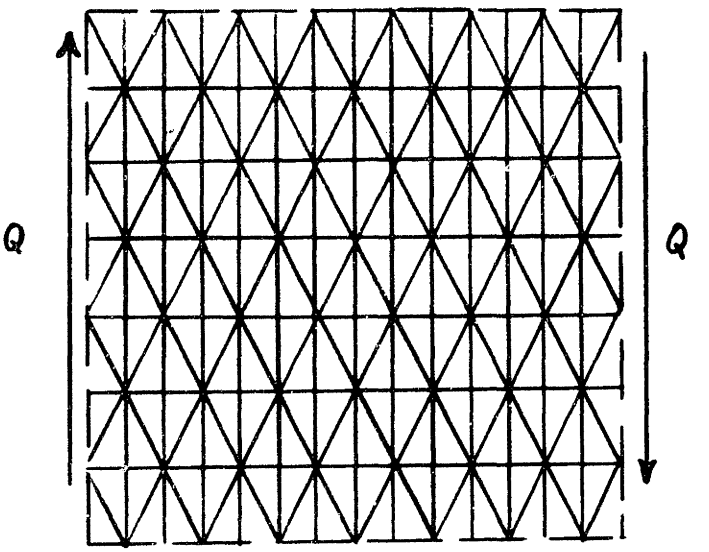

A.

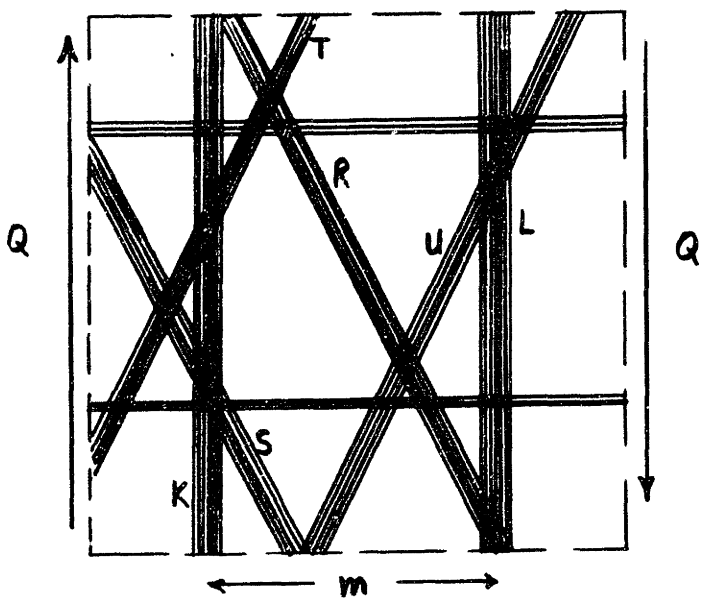

B.

$\theta = 30^\circ$ on the real fabric. While this is a very rough approximation, the result can be shown for $\theta = 30^\circ$ as the dotted lines in Figure 9.9. The reduction in the predicted stress-strain curve is quite drastic, and brings it into fairly good agreement with the experimental data.

The change in deformation behavior also can explain the large rupture strains obtained for $\theta = 45^\circ - 90^\circ$. The fabric deformation was observed to become localized and be primarily shear between planes parallel to the L axis. Refer to the sketch below, where A, B and C are bands of fibers, let us assume no shear, but only vertical displacement of the band A. Now

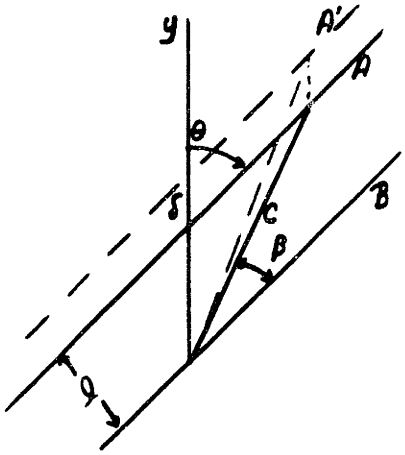

the fabric strain $e_y = \frac{\delta}{\ell/\sin\theta}$ and the fiber strain $e_f = \frac{\delta \cos(\theta-\beta)}{\ell/\sin\beta}$

Then

$$\delta = e_f \frac{\ell}{\cos(\theta-\beta)\sin\beta} = e_y \frac{\delta}{\ell/\sin\beta}$$

$$e_f = e_y \frac{\cos(\theta-\beta)\sin\beta}{\sin\theta}$$

$$= e_y \left[\sin^2\beta + \cot\theta \cos\beta \sin\beta\right] \quad (9.3)$$

Obviously, when $\theta = 0^\circ$, the $\cot\theta = \infty$ and the formula does not apply. At other values of θ, the fiber strain is reduced compared to the original analysis.

Thus two factors act to reduce the properties given by the general theory; 1) a change in the e_y to e_f transformation, and 2) the utilization of only one-half the fibers at intermediate angles of θ. A general analytical development for all angles of θ incorporating these two factors is very difficult, and does not seem warranted. However, a special case can be derived.

1. **Special Unit Cell Behavior**

The modification of the strain transformation has been given as

$$e_f = e_y\left[\cot\theta \cos\beta \sin\beta + \sin^2\beta\right]$$

valid for angles of θ where this type of deformation occurs, (presumably for $\theta > 20^\circ - 30^\circ$). Then assume that the change in behavior occurs at $\theta = \frac{\pi}{6} = 30^\circ$.

Then

$$e_f = e_y \cos^2(\theta+\beta) \quad 0 \le \theta \le 30^\circ$$

$$e_f = e\left[\cot\theta \cos\beta \sin\beta + \sin^2\beta\right] \qquad 30^\circ \le \theta \le 90^\circ \qquad (9.4)$$

allowing two calculations for the properties at $\theta = 30^\circ$.

Since all the fibers act at $\theta = 0^\circ$ and 90°, and only one-half (or less) at $\theta = 45^\circ$, the percentage acting can be approximated by

$$\% \text{ acting} = (1 - \tfrac{1}{2} \sin 2\theta) \times 100 \qquad (9.5)$$

This changes equation 6.9 to

$$\frac{E_y^*}{E_f} = \frac{.066 - .028 \sin^2\theta \cos^2\theta}{.787 \sin^4\theta + .0884 \cos^4\theta + .355 \sin^2\theta \cos^2\theta}\left[1 - \frac{\sin 2\theta}{2}\right] \qquad (9.6$$

For the remaining values of θ, substitution of 9.3 yields

$$\frac{\sigma_y}{e_y} = E_f \int_{-\pi/2}^{\pi/2} \cos^2(\theta+\beta)\,\phi(\beta)\left[\cot\theta \sin\beta \cos\beta + \sin^2\beta\right]\left[1 - \frac{\sin 2\theta}{2}\right] d\beta$$

and upon integration

$$\frac{E_y'}{E_f} = \left[A_2 \sin^2\theta + 3A_1 \cos^2\theta\right]\left[1 - \frac{\sin 2\theta}{2}\right] \qquad 30^\circ \le \theta \le 90^\circ \qquad (9.7)$$

With the values of $A_1 = .0591$, $A_2 = .0884$ and $A_3 = .787$, the results of the two equations are plotted in Figure 9.11. While this approach is only

FIGURE 9.11

PREDICTED SPECIFIC MODULI, MODIFIED UNIT CELL, FABRIC B.

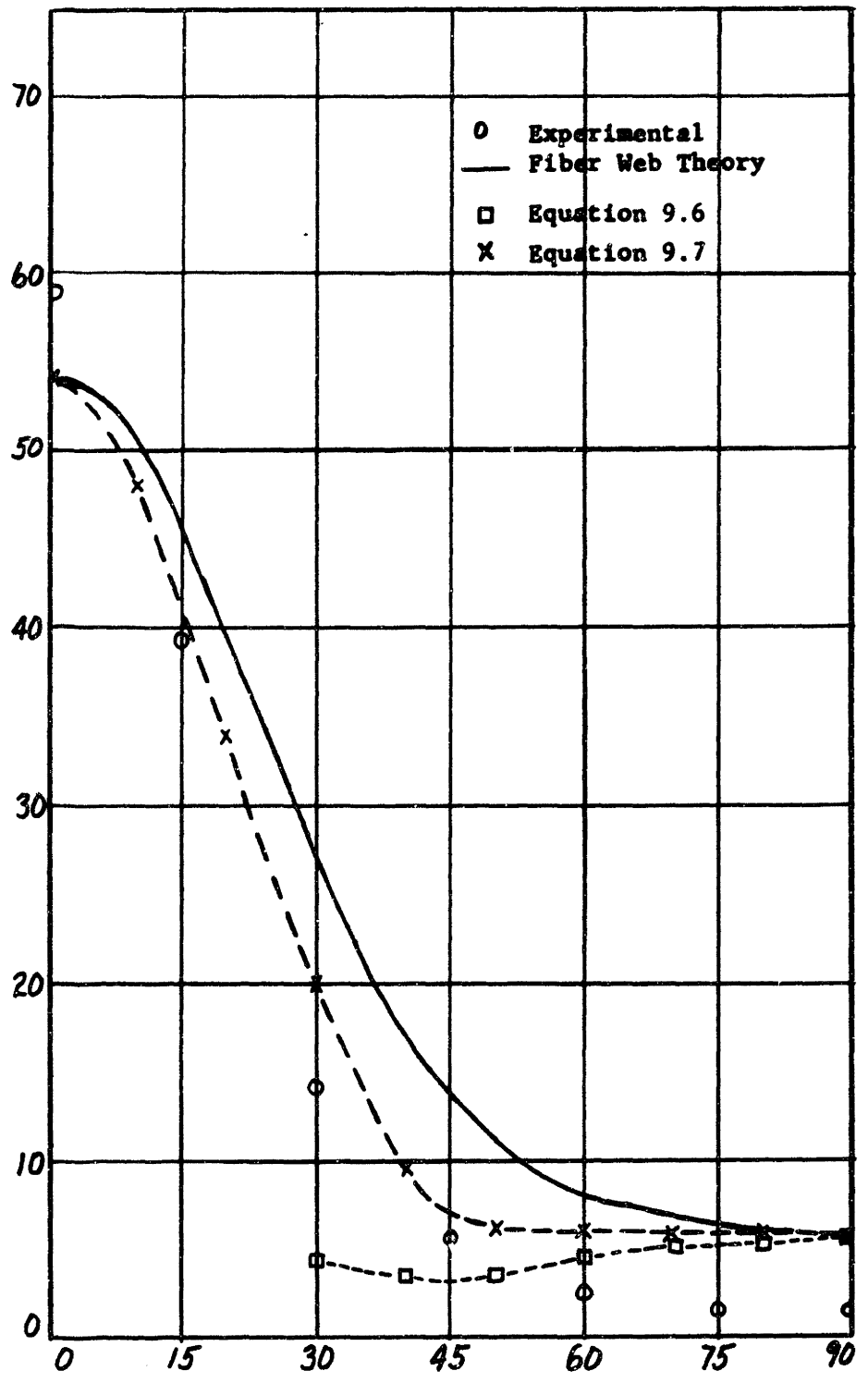

a rough approximation, it does show the effects of the bunching of fibers and their lack of compressional resistance on the predicted properties of a highly oriented non-woven structure. At $\theta = 90^{\circ}$, the higher predicted modulus results from the assumption of straight fibers. At $\theta = 30^{\circ}$, the average of the two predicted moduli is about equal to the experimental modulus, indicating a gradual shift in behavior of the fabric.

E. Variability of the Unit Cell and Predicted Rupture Stress

Following the analysis of Section VIII, the variable unit cell can be described by the mean and standard deviation of the two independent variables, σ_c and $\underline{d}$. An estimate of S_{σ} is made as before, by considering the rupture stress of a number of unit cells of average area density and varying fiber orientation distributions, $\phi(\beta)$. With the minimum unit cell rupture elongation = 10.4%, the rupture stresses are tabulated in Table 9.3 for twelve cells. The mean value of $(\overline{\sigma_m})_L$ is 1.39 gpd, and $S_{\sigma_L} = 0.084$ gpd for the L direction. Similar calculations in the T direction for ten cells gives $(\overline{\sigma_m})_T = .22$ and $S_{\sigma_T} = .05$. The coefficients of variation are

$$(C_{\sigma})_L = 6\%$$

$$(C_{\sigma})_T = 23\%$$

Since the latter figure is more probably in error, two procedures will be followed.

Observation of Fabric B indicated a tendency toward streakiness, with light and heavy areas running side by side in the machine direction. Thus the standard deviations of area density might well be expected to be different when weighing given areas of fabric. Two weighing experiments were made, one with samples whose long dimension was in the L

TABLE 9.3

VARIABILITY OF UNIT CELL RUPTURE STRESS AS A FUNCTION OF CHANGES IN FIBER ORIENTATION DISTRIBUTION $\phi(\beta)$, FABRIC B

$$\sigma_{cm} = \sum \left[.66 + 12.7(.104)\cos^2\beta_i \right] \phi(\beta_i) \cos^2\beta_i$$

Unit Cell Number	$\phi(\beta_i)$					σ_{Li}					$(\sigma_{cm})_L$
	0°	10°	20°	30°	40°	0°	10°	20°	30°	40°	
1	.24	.24	.14	.14	.03	.48	.45	.23	.17	.03	1.36
2	.29	.20	.20	.02	.11	.58	.38	.32	.02	.09	1.39
3	.41	.29	.03	.06	.03	.82	.55	.05	.07	.03	1.52
4	.21	.30	.16	.05	.03	.42	.57	.26	.06	.03	1.34
5	.30	.30	.13	.08	.05	.60	.57	.21	.10	.04	1.52
6	.29	.35	.12	.09	0	.58	.66	.19	.11	0	1.54
Recounted											
1	.21	.26	.14	.12	.05	.42	.49	.22	.15	.04	1.32
2	.32	.18	.08	.14	.10	.64	.34	.13	.17	.08	1.36
3	.24	.27	.10	.13	.04	.48	.51	.16	.16	.03	1.34
4	.20	.27	.25	.07	.02	.40	.51	.40	.09	.02	1.42
7	.20	.42	.09	0	.07	.40	.79	.14	0	.06	1.39
10	.20	.39	.14	.09	0	.40	.74	.23	.11	-	1.48
									Average		1.39

direction, and one with the long dimension in the T direction. Ten sheets of fabric were used to obtain ten specimens of each size oriented as shown at left. As the long dimension tends to average out variability in the L direction, such fabric samples are primarily a measure of the non-uniformity in the T direction and the resulting standard deviation of area density will be termed $(S_d)_T$. A similar experiment with the specimens parallel to the T axis, gives an estimate of $(S_d)_L$. The data from these two experiments are given in Table 9.4 and plotted in Figure 9.12. Again the log-log relationship appears satisfactory, with two different slopes. The base point, or minimum standard deviation was 10 specimens of 270 square inches each, 18" in the T direction, 15" in the L direction. Figure 9.12 gives the relationships.

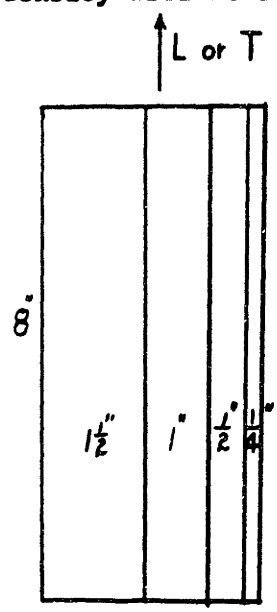

$$\left(\frac{S}{S_{min}}\right)_L = n^{.21} = \left[\frac{C}{C_{min}}\right]_L \qquad (9.8)$$

$$\left(\frac{S}{S_{min}}\right)_T = n^{.27} = \left[\frac{C}{C_{min}}\right]_T \qquad (9.9)$$

since the average area densities are the same, D.

The unit cell of Fabric B is 0.0625" square and 270 square inches contains 69,000 unit cells. With $(C)_{min}$ for 270 square inches equal 1.21%.

$$(C_d)_L \cong 1.21(69{,}000)^{1/5} \cong 12.6\%$$

$$(C_d)_T \cong 1.21(69{,}000)^{1/4} \cong 20\%$$

TABLE 9.4

STANDARD DEVIATION OF AREA DENSITY AS A FUNCTION OF SAMPLE AREA,

FABRIC B.

$(S_d)_L$ Specimens with long dimension in T direction

Area in Sq. Inches	No. of Samples	Area Density gm/sq.in Mean	Std. Dev.	Ratio of Areas, n	Ratio of Std. Dev., S/S min.
270	10	.0084	.000101	1	1
26	10	.0083	.000138	10.4	1.37
12	10	.0084	.000228	22.5	2.26
8	10	.0082	.000195	34.	1.93
2	10	.0084	.000265	135.	2.62
3/4	20	.0086	.00039	360.	3.85

$(S_d)_T$ Specimens with long dimension in L direction

270	10	.0084	.000101	1	1
26	10	.0084	.000190	10.4	1.88
12	10	.0084	.00030	22.5	2.97
8	10	.0083	.000265	34	2.62
4	10	.0083	.000312	68	3.1
2	10	.0086	.000485	135	4.8
3/4	10	.0086	.00065	360	6.4

FIGURE 9.12

RATIO OF STANDARD DEVIATIONS OF AREA DENSITY vs. RATIO OF AREAS OF WEIGHED SPECIMENS, FABRIC B.

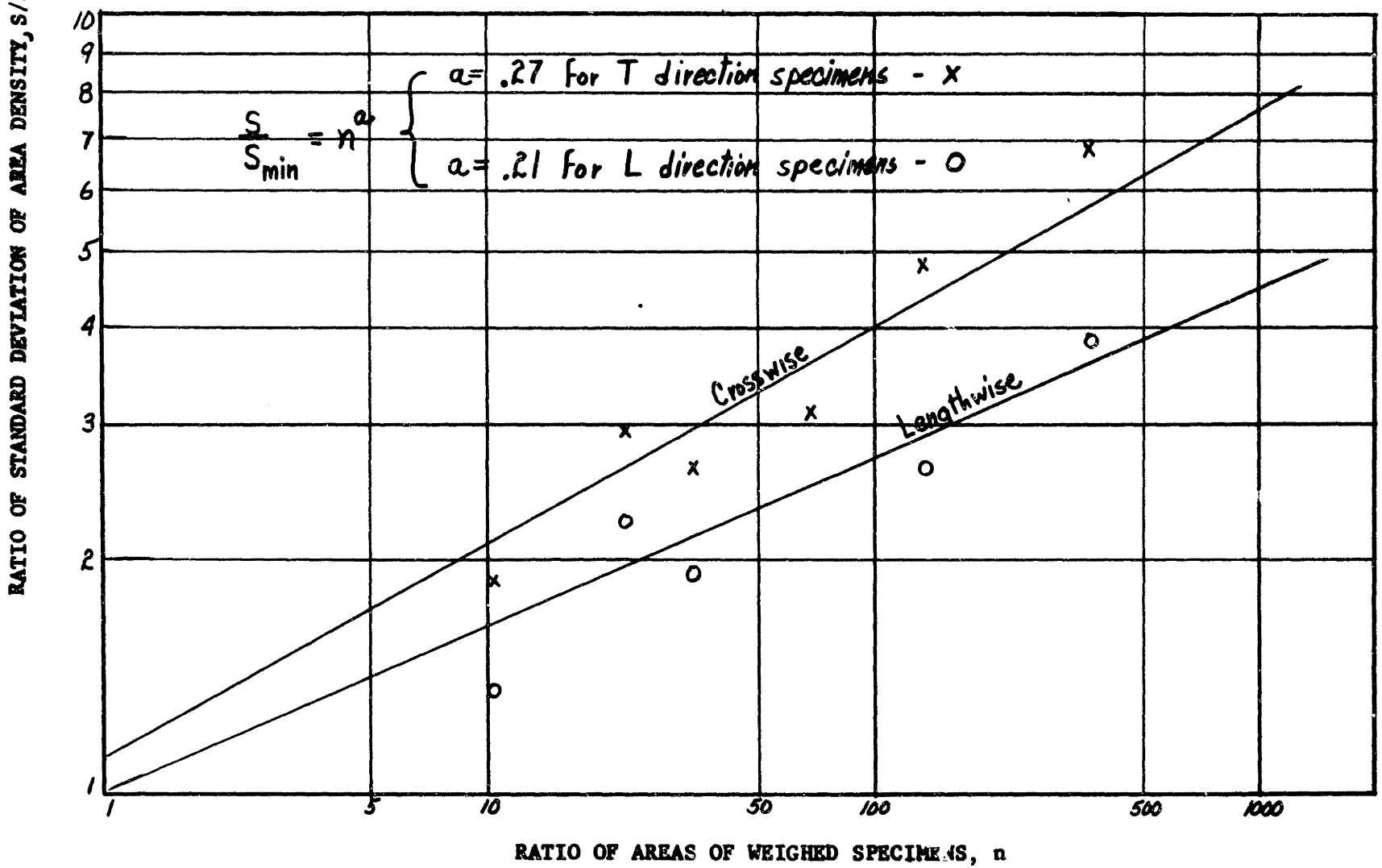

These compare with a value of $(Cd)_T = 17\%$ obtained from the standard deviation of the counted fibers in the twelve cells.

Using equation 8.18, as

$$(C_{d\sigma})^2 = (C_d)^2 + (C_\sigma)^2 + (C_d)^2(C_\sigma)^2 \qquad (8.18)$$

two values are obtained:

$$(C_{d\sigma})_L = 14\% \qquad (9.10)$$

$$(C_{d\sigma})_T = 29.6\% \qquad (9.11)$$

These values of $C_{d\sigma}$ can now be substituted into equation 8.22,

$$[\sigma_{hj}]_L = [\bar{\sigma}_{cm}]_L [1 - V_{hj}(C_{d\sigma})_L] \qquad (9.12)$$

$$[\sigma_{hj}]_T = [\bar{\sigma}_{cm}]_T [1 - V_{hj}(C_{d\sigma})_T] \qquad (9.13)$$

For an eight inch gauge length, and specimens one inch wide, hj = 2050, and $V_{hj} = 4.2\ (1-(2050)^{-1/5}) = 4.2(.78) = 3.28$. Thus

$[\sigma_g]_L = 1.39(1-3.28 \times .14) = .75$ gpd

$[\sigma_g]_T = .22(1-3.28 \times .296) = .03$ gpd

Assuming that $C_{d\sigma}$ varies linearly with θ*

$$(C_{d\sigma})_\theta = .14[1 + .00173\theta] \qquad (9.14)$$

where θ is in degrees. Referring to equation 6.26, and the correction for bunched fiber cells, as given in section IX.D.

*Obviously a very crude approximation, since (C_σ) and (C_d) are more likely to vary linearly and $C_{d\sigma}$ therefore varies in a quadratic form. However, the difference is small (See Figure 9.13).

$$\sigma_y = \sigma_\theta = \left[p'' + q^{E_y/E_f e_y}\right]\left[1 - \tfrac{1}{2}\sin 2\theta\right]$$

Using the data for p" and E given in IX.C, together with $(e_m)_{min}$ 10.4%, the following results are obtained.

θ	0°	10°	20°	30°	40°	50°	60°	70°	80°	90°
p"	.465	.455	.42	.37	.31	.26	.18	.12	.09	.08
$.104E_2$	.99	.92	.72	.49	.31	.21	.16	.13	.12	.115
Σ	1.46	1.38	1.14	.86	.62	.47	.34	.25	.21	.20
$1-\frac{\sin^2\theta}{2}$	1.0	.97	.88	.75	.58	.58	.75	.88	.97	1.0
$\bar{\sigma}_{cm}$	1.46	1.33	1.00	.64	.36	.27	.25	.22	.20	.20

Substituting equation 9.14 into equation 8.22 gives for 8" x 1" specimens

$$(\sigma_8)_\theta = \bar{\sigma}_{cm}\left[1 - 3.28\{.14(1+.00173\theta)\}\right] \qquad (9.15)$$

and these results are plotted in Figure 9.13. In the same Figure are plotted the results using $(C_J\sigma)_L$ for all angles of θ (the dashed curve). While the discrepancy in percent in the T direction is large, the absolute prediction is excellent over the entire curve.

The use of Peirce's theory together with the unit cell variability gives very good results for the prediction of fabric rupture stress on Fabric B, provided the proper modification of the unit cell is made.

FIGURE 9.13

FABRIC B, PREDICTED AND EXPERIMENTAL RUPTURE STRESS

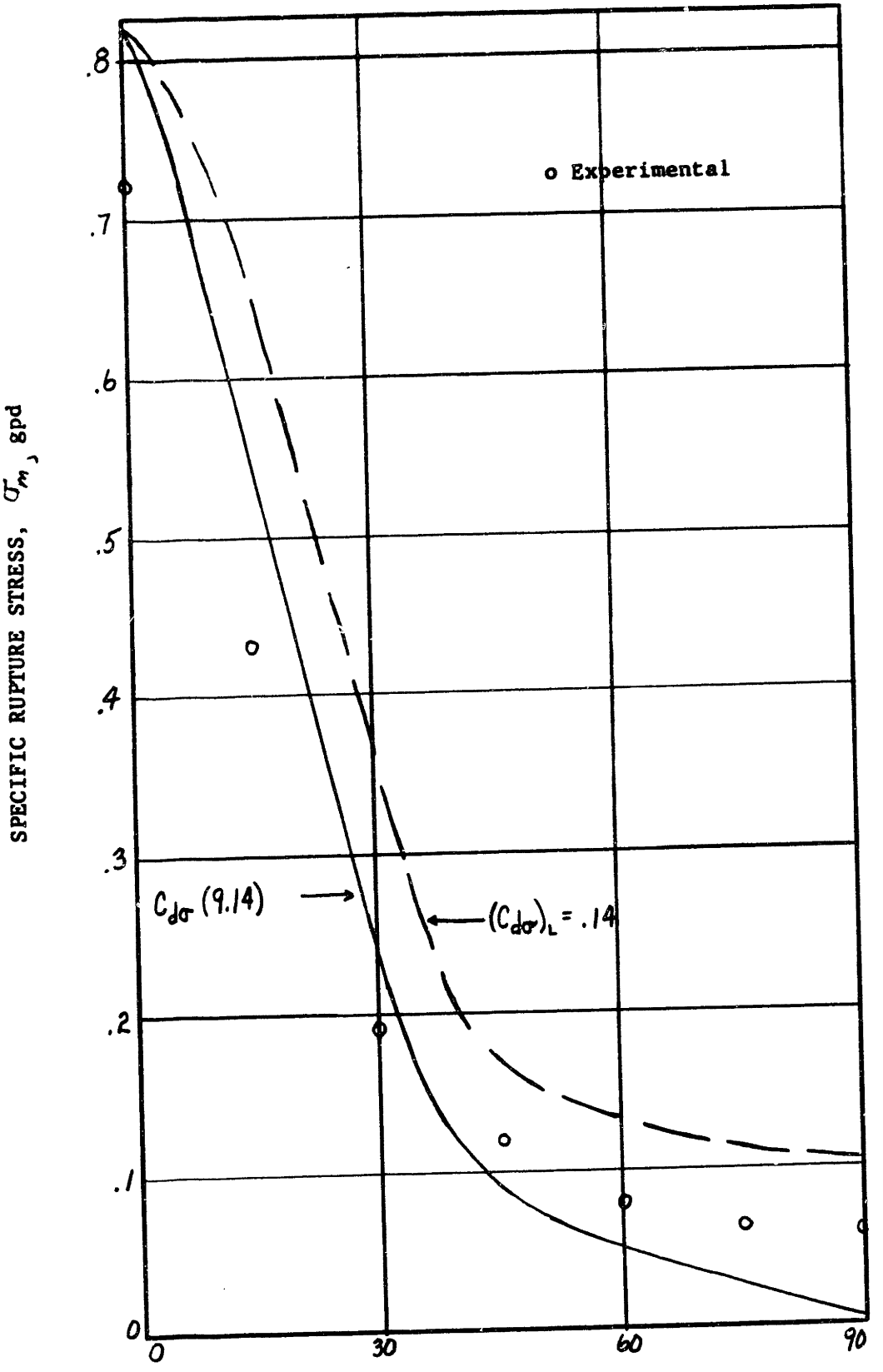

X. THE MECHANICAL PROPERTIES OF CERTAIN ASSUMED FIBER ORIENTATION DISTRIBUTIONS

Two non-woven materials, Fabric A and Fabric B, have been considered, both experimentally and theoretically. As the analytical prediction of fabric properties has proven good on two materials, certain other fiber orientation distributions can be examined. In particular, isotropic fabrics and parallel grouped fiber arrangements are of interest, primarily to determine the salient features of these "pure" distributions and to observe the changes in properties that occur when the fibers become distributed less perfectly.

A. Isotropic

Consider a fiber structure in which there is no preferential fiber orientation, or where $\phi(\beta)$ = constant. As

$$\int_{-\pi/2}^{\pi/2} \phi(\beta)\, d\beta = 1$$

the constant has the values $\frac{1}{\pi}$ as shown on the left

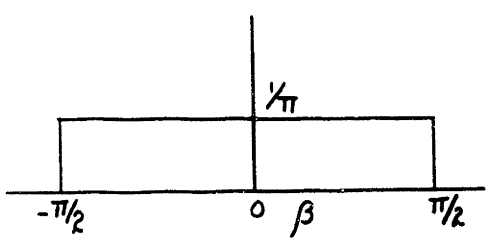

The mechanical properties may be quickly calculated from the equations of Section VI, when $\sigma_x = e_{yx} = 0$

$$e_f = e_y\left[\cos^2(\theta+\beta) - \nu_{yx}\sin^2(\theta+\beta)\right]$$

$$A_1 = .393/\pi \qquad A_4 = A_5 = 1.708/\pi$$

$$A_2 = A_3 = 1.18/\pi = 3A_1$$

Then

$$\frac{E_y^x}{E_y} = \frac{9A_1^2 - A_1^2 + 4\left(3A_1^2 + 3A_1^2 - 9A_1^2 + 3A_1^2\right)\sin^2\theta\cos^2\theta}{3A_1\sin^4\theta + 3A_1\cos^4\theta + 6A_1\sin^2\theta\cos^2\theta}$$

or

$$\frac{E_y^*}{E_f} = \frac{8A_1^2}{3A_1} = \frac{1}{3}$$

with E_y^* independent of θ. Poisson's ratio is

$$\nu_{yx}^* = \frac{A_1}{3A_1} = \frac{1}{3}$$

again independent of θ. For the modulus of rigidity, the relations become;

$$G_{yx}^* = E_f\left[A_1 + (A_2 + A_3 - 6A_1)\sin^2\theta\cos^2\theta\right]$$

$$= E_f A_1$$

$$= E_f/8$$

In the plastic region, the equation for stress is:

$$\sigma_y = \rho\left[1 - 8/E_f\right]\left[A_4\cos^2\theta + A_5\sin^2\theta\right] + q\,e_y^{E_y^*/E_f}$$

$$= \rho\left[1 - 8/E_f\right].543 + \frac{1}{3}q\,e_y$$

Using the values for the particular fiber tested:

$$\rho = 0.66 \text{ gpd} \; ; \; E_f = 72 \text{ gpd} \; ; \; q = 12.7 \text{ gpd} \; ; \; e_m = 16\%$$

substitution gives the specific rupture stress for a uniform fabric as:

$$\bar{\sigma}_m = 0.3 + 0.68 = 0.98$$

These results are plotted in Figures 10.1 - 10.4 inclusive.

B. Parallel Fiber Groups, Perpendicularly Arranged

Consider the distribution consisting of two groups of fibers, each group consisting of fibers parallel within $\pm 5^{\circ}$, and the two groups lying perpendicular. This is, then, a perpendicular cross-lay fabric, but one which meets the assumption of all fibers in one plane. This would be the case only if the two perpendicular groups were intimately blended. In present practice, the two groups are formed as distinct layers, and thus do not meet the planar assumption. However, a preliminary analysis of this idealized structure will be carried out.

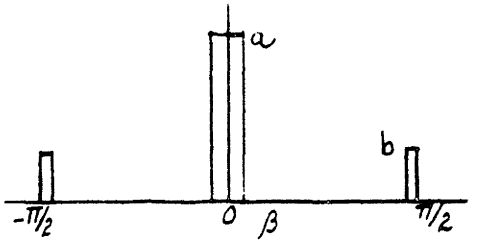

Then the $\phi(\beta)$ distribution can be pictured as at left. Then for 10° intervals; $a\frac{\pi}{18} + b\frac{\pi}{18} = 1$; or $c + d = 1$, where c and d are the relative frequency areas denoting the percentage of fibers in each of the two directions, or $c = a\frac{\pi}{18}$ and $d = b\frac{\pi}{18}$

Thus

$$\phi(\beta) = c(\beta = 0^{\circ}) + d(\beta = 90^{\circ})$$

Using the equations of Section VI, again with the boundary conditions $\sigma_x = e_{yx} = 0$:

$$\frac{E_y^*}{E_f} = \left[\cos^4(\theta+\beta) - \nu_{yx}\sin^2(\theta+\beta)\cos^2(\theta+\beta)\right]\left[c(\beta=0^{\circ}) + d(\beta=90^{\circ})\right]$$

$$= \frac{cd\,(\sin^4\theta - \cos^4\theta)^2}{c\sin^4\theta + d\cos^4\theta}$$

$$\nu^*_{yx} = \frac{\cos^2(\theta+\beta)\sin^2(\theta+\beta)\left[c(\beta=0^\circ)+d(\beta=\pi/2)\right]}{\sin^4(\theta+\beta)\left[c(\beta=0^\circ)+d(\beta=\pi/2)\right]}$$

$$= \frac{\sin^2\theta\cos^2\theta}{c\sin^4\theta + d\cos^4\theta}$$

Solving for the Modulus of Rigidity, with the boundary conditions

$e_y = e_x = 0$;

$$G^*_{yx} = E_f\left[\sin^2(\theta+\beta)\cos^2(\theta+\beta)\right]\left[c(\beta=0^\circ)+d(\beta=90^\circ)\right]$$

$$= E_f \sin^2\theta\cos^2\theta$$

independent of the ratio c/d, provided any bending resistance of the fibers is neglected.

In the plastic region

$$\sigma_y = \rho\left[\cos^2(\theta+\beta)\right]\left[c(\beta=0^\circ)+d(\beta=90^\circ)\right] + g\, e_y\, E^*_y/E_f$$

$$= \rho\left[1-g/E_f\right]\left[c\cos^2\theta + d\sin^2\theta\right] + g\, e_y\, E^*_y/E_f$$

Again with the measured fiber properties

$$\bar{\sigma}_m = .55\left[c\cos^2\theta + d\sin^2\theta\right] + 2.03\,\frac{cd(\sin^4\theta-\cos^4\theta)^2}{c\sin^4\theta + d\cos^4\theta}$$

The functions for $\frac{E_y^*}{E_f}$ & σ_y go to zero at $\theta = 45^\circ$ as a result of including ν_{yx}^* in the strain transformation. A second approximation can be made using

$$e_f = e_y \cos^2(\theta+\beta) \qquad \nu_{yx} \equiv 0$$

Thus, for the boundary conditions $e_x = e_{yx} = 0$;

$$E_y'/E_f = c\cos^4\theta + d\sin^4\theta$$

$$\bar{\sigma}_m' = .55\left[c\cos^2\theta + d\sin^2\theta\right] + 2.03\left[c\cos^4\theta + d\sin^4\theta\right]$$

The two cases of strain transformation will be denoted I; $\sigma_x = 0$ and II; $e_x = 0$.

Thus the equations are:

I; $\sigma_x = 0$

$$\frac{E_y^*}{E_f} = \frac{cd(\sin^4\theta - \cos^4\theta)^2}{c\sin^4\theta + d\cos^4\theta}$$

$$\nu_{yx}^* = \frac{\sin^2\theta\cos^2\theta}{c\sin^4\theta + d\cos^4\theta}$$

$$\bar{\sigma}_m = .55\left[c\cos^2\theta + d\sin^2\theta\right] + 2.03\left[E_y^*/E_f\right]_I$$

II; $e_x = 0$

$$\frac{E_y'}{E_f} = c\cos^4\theta + d\sin^4\theta$$

$$\frac{G_{yx}^*}{E_f} = \sin^2\theta\cos^2\theta$$

$$\bar{\sigma}_m' = .55\left[c\cos^2\theta + d\sin^2\theta\right] + 2.03\left[E_y'/E_f\right]_{II}$$

The functions are plotted for two ratios of c/d, i.e., c/d = 1, and c/d = 5, in Figures 10.1 - 10.4. The equation simplification for these two ratios are as follows:

If c = d = ½, then

I, $\nu_{4x} \neq 0$

$$\frac{E_y^*}{E_f} = \frac{1}{2}\frac{(\sin^4\theta - \cos^4\theta)^2}{\sin^4\theta + \cos^4\theta}$$

$$\nu_{4x}^* = 2\frac{\sin^2\theta\cos^2\theta}{\sin^4\theta + \cos^4\theta}$$

$$\bar{\sigma}_m = \frac{.55}{2} + 2.03\left[E_y/E_f\right]_I$$

II, $\nu_{4x} \equiv 0$

$$E_y'/E_f = \frac{1}{2}(\cos^4\theta + \sin^4\theta)$$

$$G_{yx}^*/E_f = \sin^2\theta\cos^2\theta$$

$$\bar{\sigma}_m' = \frac{.55}{2} + 2.03\left[E_y/E_f\right]_{II}$$

θ	I E_y^*/E_f	I ν_{4x}^*	I $\bar{\sigma}_m$	II E_y'/E_f	II G_{yx}^*/E_f	II $\bar{\sigma}_m'$
0	.50	0	1.28	.50	0	1.28
10	.47	.06	1.22	.47	.029	1.22
20	.38	.26	1.04	.39	.103	1.06
30	.20	.60	.68	.31	.188	.91
40	.03	.94	.34	.257	.242	.80
50	.03	.94	.34	.257	.242	.80
60	.20	.60	.68	.31	.188	.91
70	.38	.26	1.04	.39	.103	1.06
80	.47	.06	1.22	.47	.029	1.22
90	.50	0	1.28	.50	0	1.28

If c/d = 5; c = 5/6, d = 1/6

I, $\nu_{4x} \neq 0$

$$E_y^*/E_f = \frac{5/6(\sin^4\theta - \cos^4\theta)^2}{5\sin^4\theta + \cos^4\theta}$$

$$\nu_{4x}^* = \frac{6\sin^2\theta\cos^2\theta}{5\sin^4\theta + \cos^4\theta}$$

$$\bar{\sigma}_m = \frac{.55}{6}\left[5\cos^2\theta + \sin^2\theta\right] + 2.03\left[E_y^*/E_f\right]_I$$

II, $\nu_{4x} \equiv 0$

$$\frac{E_y'}{E_f} = \frac{1}{6}\left[5\cos^4\theta + \sin^4\theta\right]$$

$$\frac{G_{yx}^*}{E_f} = \sin^2\theta\cos^2\theta$$

$$\sigma_m' = \frac{.55}{6}\left[5\cos^2\theta + \sin^2\theta\right] + 2.03\left[E_y/E_f\right]_{II}$$

	I			II			III	
θ°	E_y^*/E_f	ν_{yx}^*	$\bar{\sigma}_m$	E_y/E_f	G_{yx}^*/E_f	$\bar{\sigma}_m'$	E_y/E_f	$\bar{\sigma}_m''$
0	.83	0	2.12	.83	0	2.12	.83	2.12
10	.75	.18	1.95	.78	.029	2.04	.78	2.03
20	.52	.72	1.45	.65	.103	1.73	.59	1.61
30	.23	1.3	.83	.48	.188	1.35	.37	1.12
40	.02	1.2	.35	.32	.242	.96	.18	.68
50	.013	.77	.26	.20	.242	.65	.12	.48
60	.098	.40	.38	.145	.188	.47	.11	.40
70	.12	.16	.40	.142	.103	.45	.13	.42
80	.15	.04	.40	.157	.029	.42	.15	.40
90	.16	0	.41	.16	0	.41	.16	.41

An approximate solution lying between these two assumptions of $\nu_{yx} \neq 0$ or $\nu_{yx} \equiv 0$ is given by the equations below, denoted as III.

$$E_y''/E_f = \frac{cd(\sin^4\theta + \cos^4\theta)}{c\sin^4\theta + d\cos^4\theta}$$

$$\bar{\sigma}_m'' = .55\left[c\cos^2\theta + d\sin^2\theta\right] + 2.03\left[E_y/E_f\right]_{III}$$

As the values of ν_{yx}^* and G_{yx}^* are not changed, the tabulated results are shown as III in the above data.

C. E_L/E_T Ratio = Five, Strong Orientation plus Isotropic

Two fabrics have been analyzed with E_L/E_T ratio of approximately 4.5; the first, as Fabric A; the second, as one example of the perpendicular fiber arrangement (X . B). It is of interest to examine an intermediate case, in which a strong orientation is superimposed over an isotropic structure.

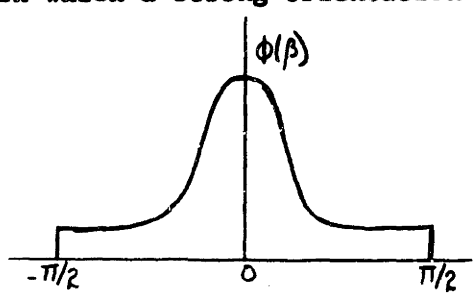

Such a $\phi(\beta)$ would be as at the left, given by $\phi(\beta) = a + e\cos^{16}\beta$.

Then with the conditions:

$$A_2 = 1.18\,a + .00514\,e$$

$$A_3 = 1.18\,a + .554\,e$$

$$\int_{-\pi/2}^{\pi/2} \phi(\beta)\, d\beta = 1$$

and

$$E_L/E_T = A_3/A_2 = 5$$

values of a and e are found to be

a = 0.116 e = 1.03

The constants of the general equations are:

A_1 = .0755 A_3 = .708 A_5 = .232

A_2 = .142 A_4 = .798

Substitution of these values into the equations of VI yield the following:

$$\frac{E_y^*}{E_f} = \frac{.095 - .0768 \sin^2\theta \cos^2\theta}{.708 \sin^4\theta + .142 \cos^4\theta + .453 \sin^2\theta \cos^2\theta} = \frac{N_1}{D}$$

$$\nu_{yx}^* = \frac{.0755 + .397 \sin^2\theta \cos^2\theta}{D} = \frac{N_2}{D}$$

$$G_{yx}^*/E_f = \left[.0755 + .397 \sin^2\theta \cos^2\theta\right] = N_2$$

$$\bar{\sigma}_m = .55\left[.798 \cos^2\theta + .232 \sin^2\theta\right] + 2.02\, E_y/E_f$$

The calculations are given in Table 10.1 and the data also plotted in Figures 10.2, 10.3, 10.5, and 10.6.

TABLE 10.1

PREDICTED FABRIC PROPERTIES, ASSUMED FIBER DISTRIBUTION C

θ	$.708 \sin^4\theta$	$.142 \cos^4\theta$	$.453 \sin^2\theta\cos^2\theta$	D	$.077 \frac{\sin^2\theta}{\cos^2\theta}$	N_1	$.397 \frac{\sin^2\theta}{\cos^2\theta}$	N_2	$\frac{N_1}{D}$	$\frac{N_2}{D}$
0°	0	.142	0	.142	0	.095	0	.076	.67	.54
10°	.001	.133	.013	.147	.002	.093	.011	.087	.63	.59
20°	.010	.111	.046	.167	.008	.087	.041	.117	.52	.70
30°	.045	.080	.085	.210	.014	.081	.074	.150	.39	.71
40°	.121	.049	.110	.280	.019	.076	.096	.172	.27	.62
50°	.244	.024	.110	.378	.019	.076	.096	.172	.20	.46
60°	.398	.009	.085	.492	.014	.081	.074	.150	.16	.30
70°	.553	.002	.046	.601	.008	.087	.041	.117	.15	.20
80°	.665	-	.013	.678	.002	.093	.011	.087	.14	.13
90°	.708	0	0	.708	0	.095	0	.076	.13	.11

θ	0°	10°	20°	30°	40°	50°	60°	70°	80°	90°
$.798 \cos^2\theta$	.798	.775	.707	.598	.468	.328	.199	.093	.024	0
$.232 \sin^2\theta$	0	.007	.027	.058	.096	.137	.174	.205	.224	.232
ρ''	.44	.43	.40	.36	.31	.26	.21	.16	.14	.13
$E_2\bar{e}_m$	1.37	1.28	1.06	.80	.55	.41	.33	.31	.29	.27
$\bar{\sigma}_m$	1.81	1.71	1.46	1.16	.86	.67	.54	.49	.43	.40

D. Comparison of Assumed Fiber Distributions

The polar diagrams of Figures 10.5 and 10.6 show certain behavior which might have been expected. The shape of the curves for E_y/E_f and $\bar{\sigma}_m$ are very similar, as would be expected. The only difference in the two functions is that p is modified by $\sin^2\theta$ and $\cos^2\theta$, whereas E_y is a function of $\cos^4\theta$ or $\sin^2\theta\cos^2\theta$ (trigonometric functions to the 4th power). Thus the modulus ratio E_y/E_f shows a small, sharp peak near the T axis, while $\bar{\sigma}_m$ shows a lesser effect. The Modulus of Rigidity G_{yx} is always symmetrical about $\theta = \frac{\pi}{4}2n$; $n = 0, 1, 2, etc$; with the maximum at $\theta = \frac{\pi}{4}2n$. The maximum value increases as the fiber orientation distribution changes from isotropic to oriented to perpendicularly grouped fibers (B), and the ratio of groups c/d has no effect. If fiber bending were taken into account for $G_{LT} \equiv G_{TL}$, these values would not be zero, but intermediate of zero and the value obtained for the distributed fibers, Case. C.

Poisson's ratio (under the restriction of compressional resistance without buckling) also has its highest value for grouped fibers (Case B), and is uniform for isotropic materials.

Obviously, many other types of distributions could be treated, but this section has been an attempt to characterize a few distributions under certain boundary conditions, and to compare their behavior. Any method of comparison is fraught with difficulty, since the end use of the structure should dictate the selection of $\phi(\beta)$ and fiber properties. However, one method is to compare the total E_y/E_f ratio for two different $\phi(\beta)$ by integrating E_y/E_f over $0 < \theta < 2\pi$.

For the isotropic case:

$$\left[E_y/E_f\right]_T = \int_0^{2\pi} \frac{1}{3}\,d\theta = \frac{2\pi}{3}$$

For the perpendicularly grouped case c/d = 1, II

$$\left[E_y/E_f\right]_T = \frac{1}{2}\int_0^{2\pi} (\sin^4\theta + \cos^4\theta)\,d\theta = \frac{3}{4}\pi$$

and for c/d = 5, II

$$\left[E_y/E_f\right]_T = \frac{1}{6}\int_0^{2\pi} (5\cos^4\theta + \sin^4\theta)\,d\theta = \frac{3}{4}\pi$$

Integration of Fabric A is not feasible, but by numerical summation

$$\left[E_y/E_f\right]_T = 4\cdot\frac{\pi}{18}\left[2.87\right] = .64\pi$$

It is important to note that these values should not be compared with 2π, but with the value of $\left[E_y/E_f\right]_T$ for all fibers parallel in the same direction, or

$$\left[E_y/E_f\right]_T = \int_0^{2\pi} \cos^4\theta\,d\theta = .75\pi$$

This assumes that when fibers are all grouped at $\beta = 0^\circ$ (L), there is no modulus or strength in the T direction. Obviously, even for weak resins, there will be some measurable properties.

The basic question is whether or not more orientation is advantageous; or alternatively, whether lack of specific orientation reduces the maximum utilization of the fibers. The suggested method does not appear sensitive enough to determine this. In any event, this question is subordinate to in actual fabrics to the problems of variability and its influence on rupture stress, as discussed in Section VIII.

FIGURE 10.1

ASSUMED DISTRIBUTIONS, SPECIFIC MODULI VS. ANGLE OF TEST

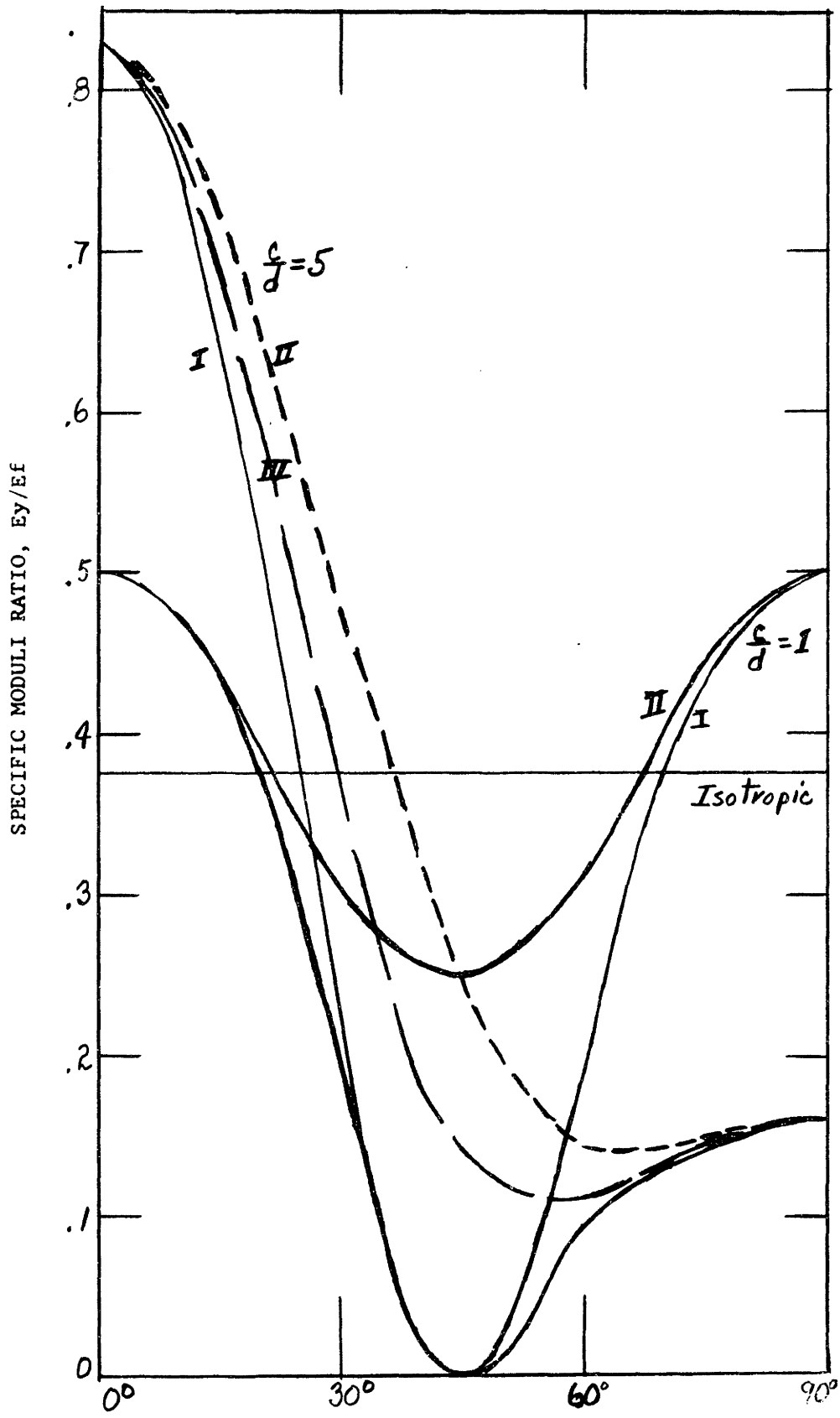

FIGURE 10.2

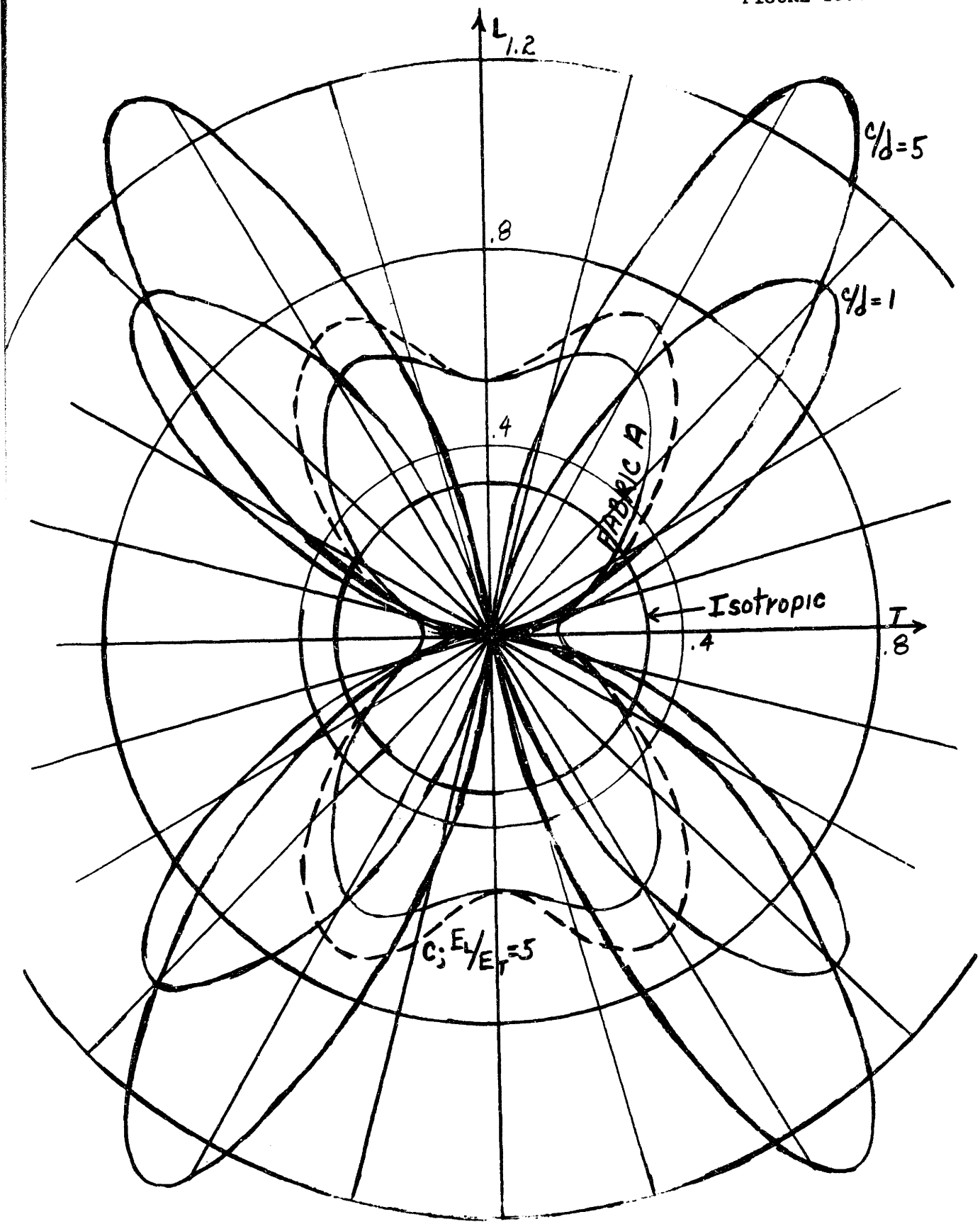

ASSUMED DISTRIBUTIONS, POISSON'S RATIO, ν_{yx}^{*} VS. ANGLE OF TEST

FIGURE 10.3

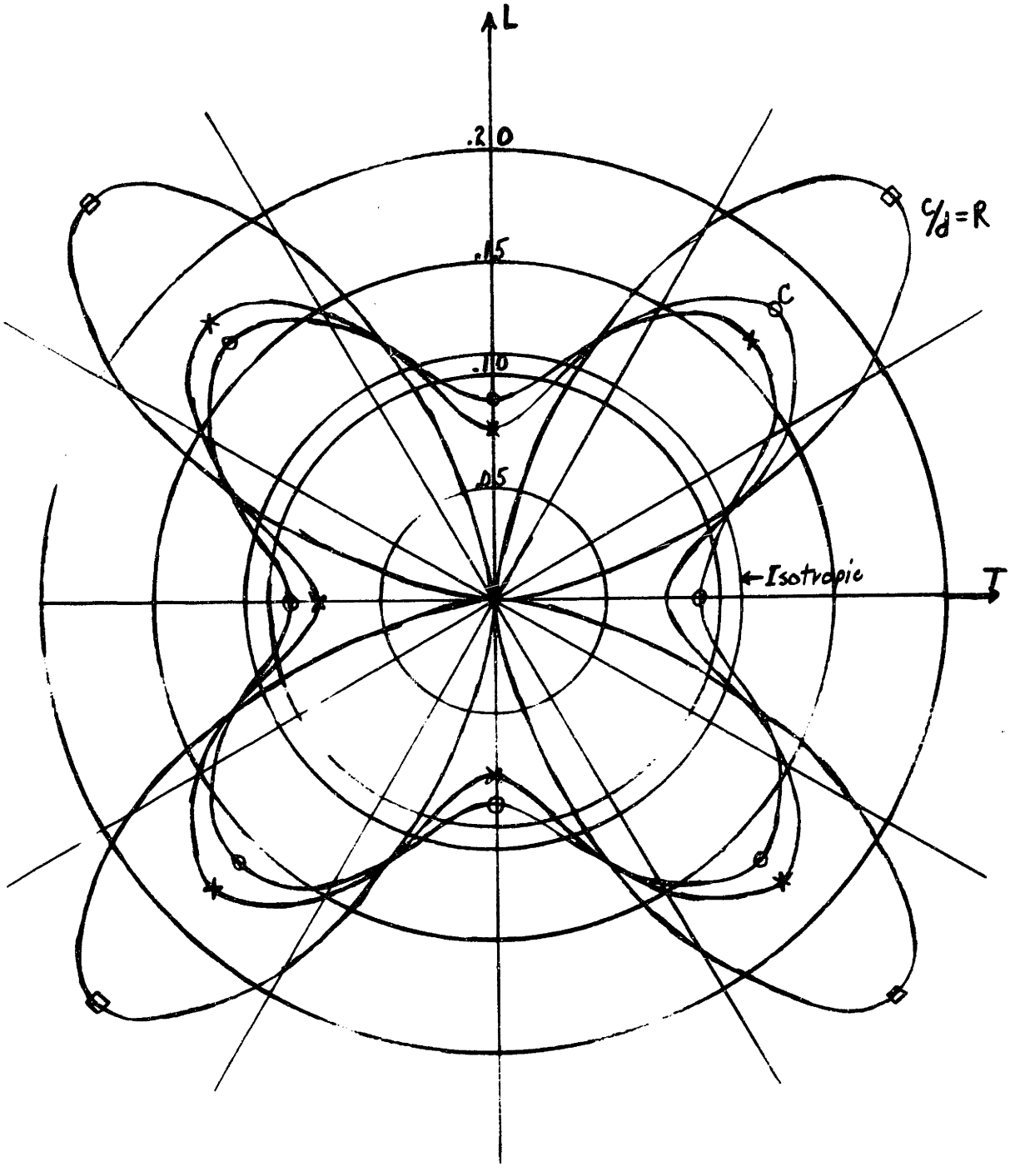

ASSUMED DISTRIBUTIONS, MODULI OF RIGIDITY VS. ANGLE OF TEST

FIGURE 10.5

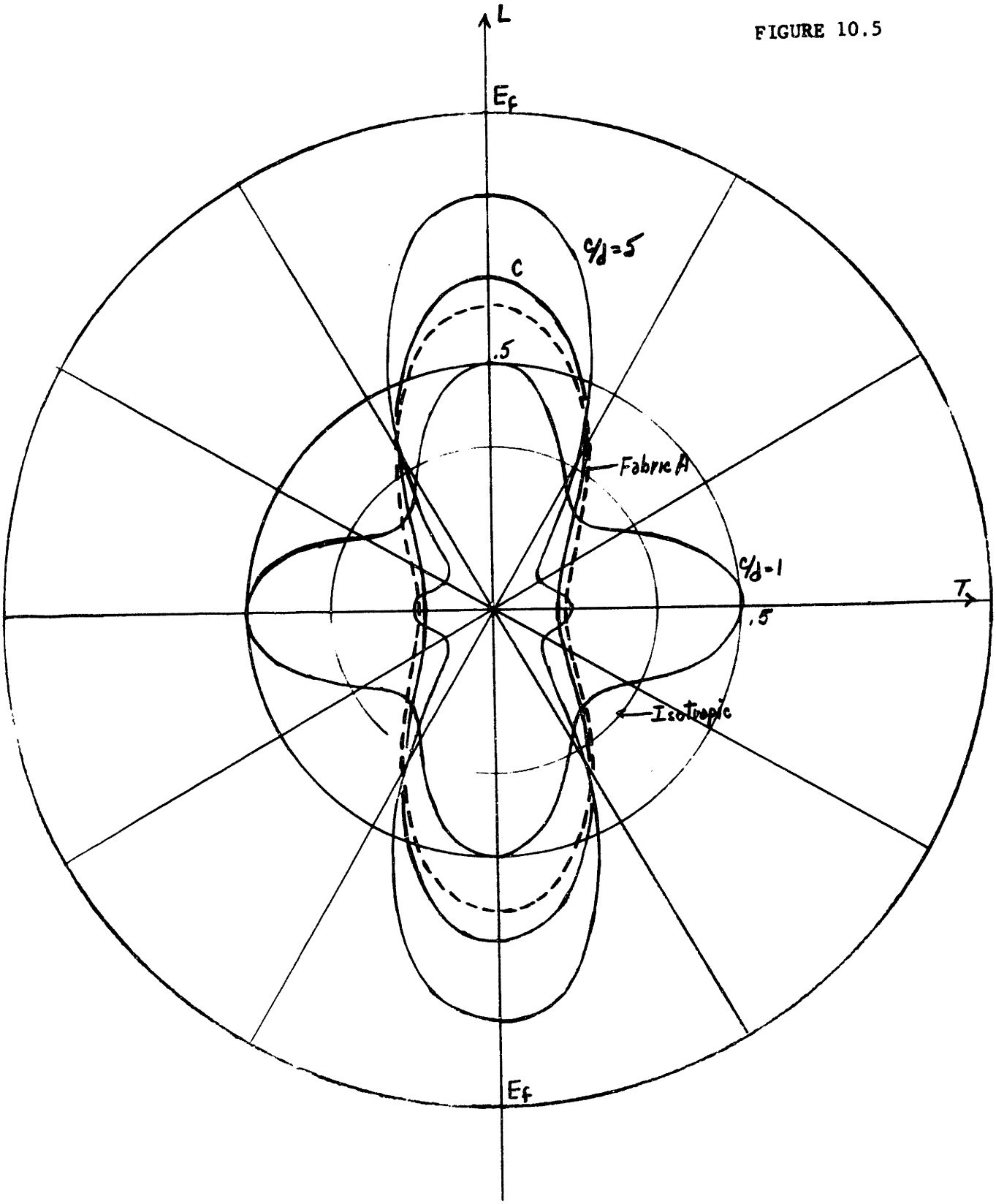

SPECIFIC MODULI OF ASSUMED DISTRIBUTIONS, VS. ANGLE OF TEST

FIGURE 10.6

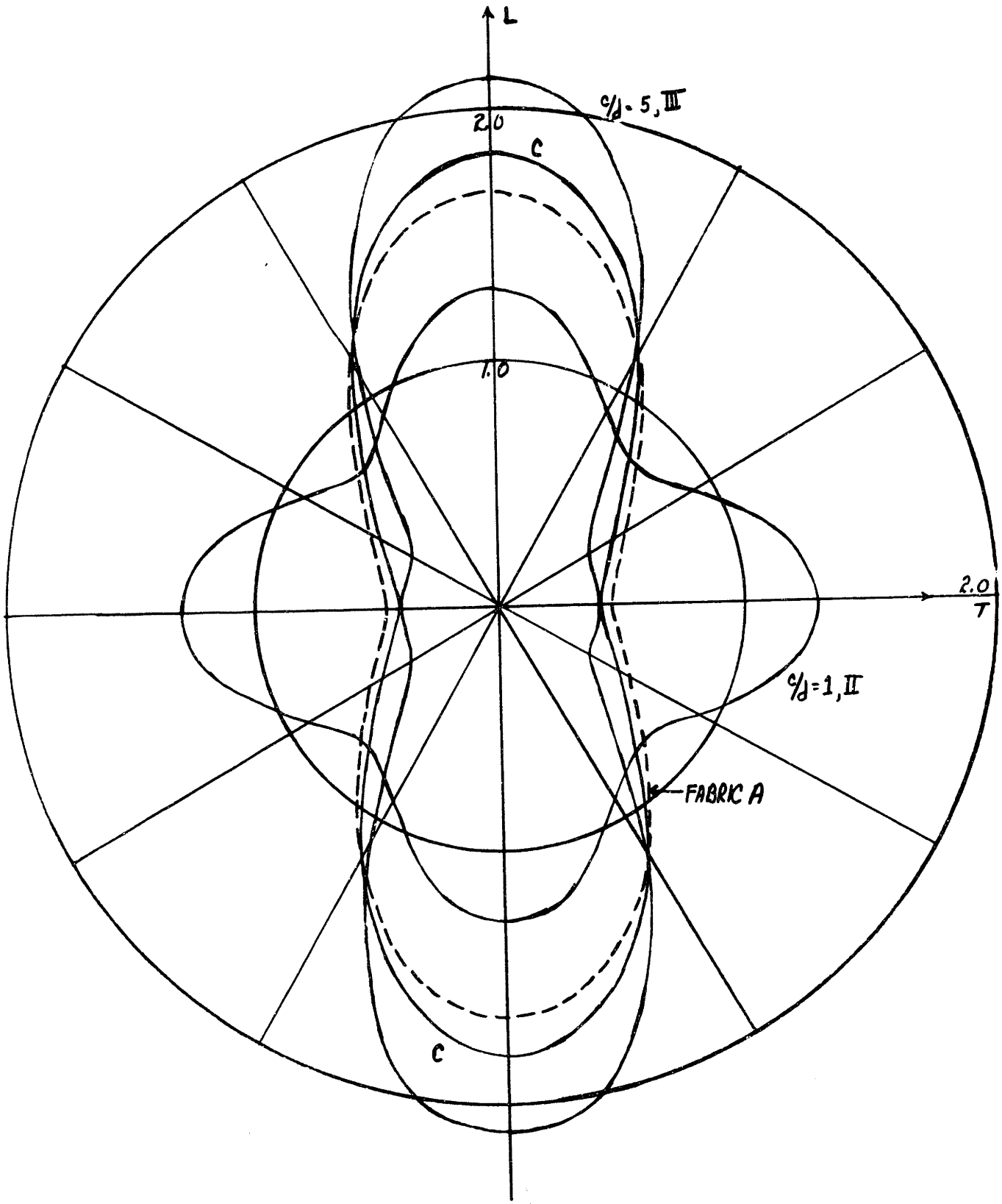

SPECIFIC RUPTURE STRESS OF ASSUMED DISTRIBUTIONS VS. ANGLE OF TEST

FIGURE 10.4

ASSUMED DISTRIBUTIONS, MEAN SPECIFIC RUPTURE STRESS VS. ANGLE OF TEST

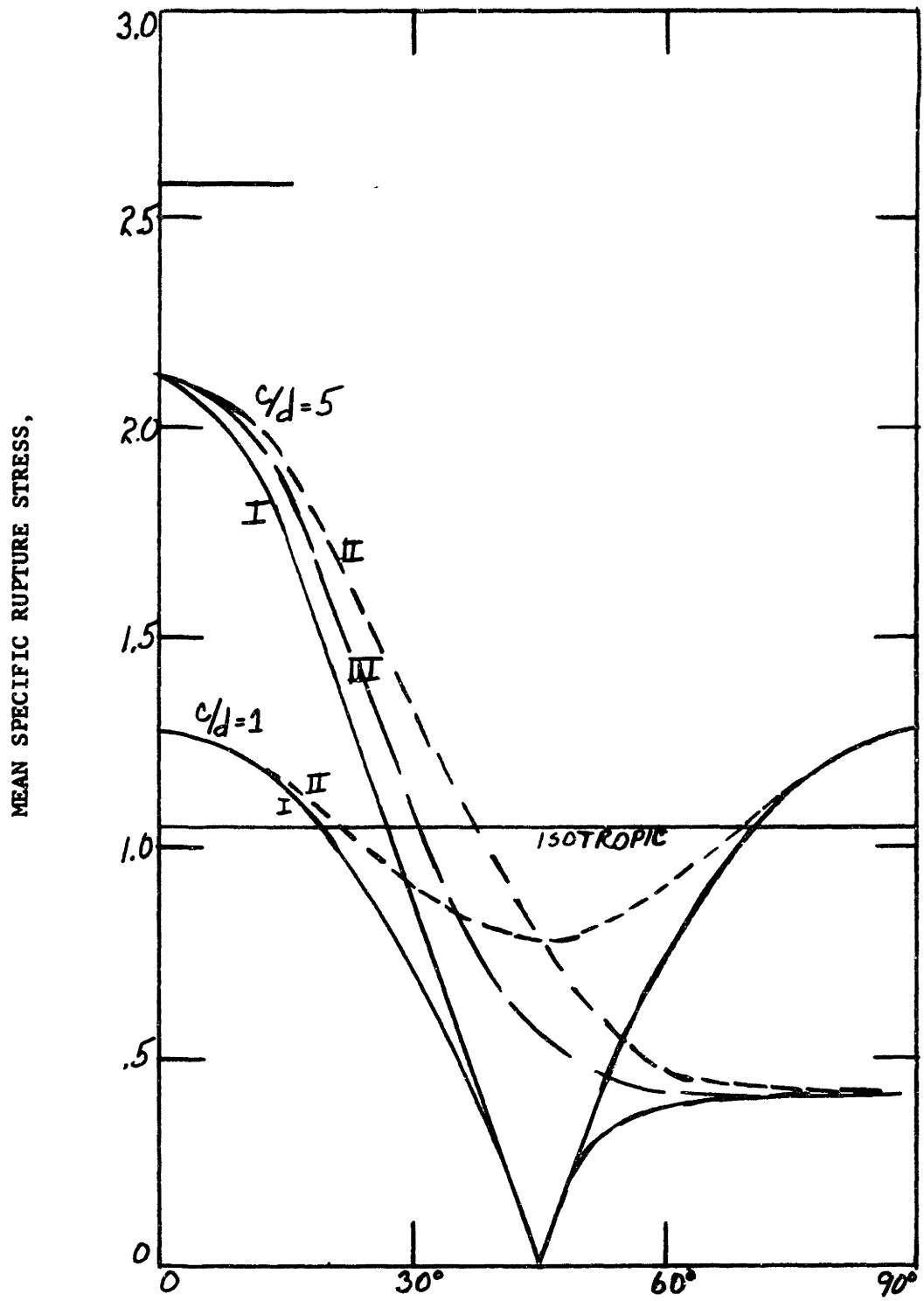

XI. CERTAIN PRACTICAL CONSIDERATIONS MODIFYING THEORY

Certain problems appear worthy of further discussion, in light of the important roles which they play in the translation of fiber properties to fabric properties. There are other considerations which might be investigated, but the following appear to warrant comment.

A. Effect of Fiber Length

Fiber Length has a real influence in any practical material, but not in the most obvious way. An increase in fiber length, in a structure of the same characteristics ($\phi(\beta), E_f$, etc.) and the same variability (S_σ, S_J) might be expected to increase the size of the unit cell. This argument is based upon the original definition, that the unit cell be of sufficient size to negate the influence of ends of fibers. At the same time, if the degree of bonding between fibers is the same, no change in unit cell size would be required. Presumably then, changes in fiber length will have no influence on the mechanical properties of the fabric, and very little, if any, influence on the specific rupture stress at any particular gauge length greater than the fiber length.

All of the preceding makes one very important assumption, namely, that long fibers or short fibers will both be straight within the fabric, (or at least within the unit cells).. Practically, this assumption is not valid. As pointed out in the Introduction (II), the major dividing line between wet-formed and air-or-machine-formed non-wovens has been fiber length and fiber straightness. The air processes of deposition are noted for their typical curled and kinked fiber structure. Thus any practical improvement which might result from increased fiber length will probably be lost in the property changes which usually occur in changing from water to air-or-machine formation. Thus, one question to be considered is the importance of the straight fiber assumption.

B. Effect of Fiber Curvature

Consider, in the figure below, the fiber segment ABA' as lying on a circle of radius ρ with center at 0, and the length ACA' cos β as the length of the unit cell. This implies that fiber curvature is constant within a unit cell, and that $\rho >$ ACA' cos β . Then the angle of the chord ACA' with the L axis is again β and the following relations appear.

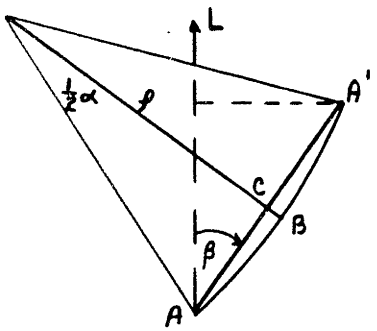

Denoting the length ABA' by ℓ , the chord length ACA' by K;

$$K = 2\rho \sin \tfrac{1}{2}\alpha \qquad \alpha \text{ in radians}$$

$$\ell = \rho\alpha$$

Now the simple strain transformation with $\gamma_{LT} = 0$

gives $e_K = \gamma/K \cos\beta$

and $e_K = e_L \cos^2\beta$

However, no strain will occur in the fiber (if A & A' are the first bonded intersections) until K' = ℓ . Thus

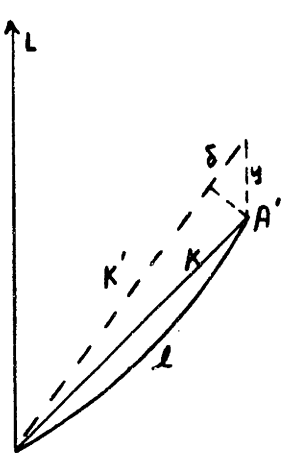

$$K' = K(1+e_K) = K(1+e_L\cos^2\beta) = \ell$$

$$2\rho \sin\tfrac{1}{2}\alpha(1+e_L\cos^2\beta) = \rho\alpha$$

$$e_L^* = \frac{1}{\cos^2\beta}\left[\frac{\alpha}{2\sin\frac{1}{2}\alpha} - 1\right]$$

where e_L^* is the <u>minimum</u> fabric strain necessary to straighten the curved fiber of length ℓ lying at angle β and introduce the first increment of tensile strain. Now neglecting any change in angle β, the fiber strain e_f is

$$e_f = (e_L - e_L^*)\cos^2\beta$$

$$= e_L\cos^2\beta - \left[\frac{\alpha}{2\sin\frac{1}{2}\alpha} - 1\right]$$

If $\sigma_f = E_f e_f$ and for one fiber $(\sigma_L)_i = \sigma_f \cos^2\beta$;

$$(\sigma_L)_i = E_f\left[e_L\cos^4\beta - \left(\frac{\alpha}{2\sin\frac{1}{2}\alpha} - 1\right)\cos^2\beta\right]$$

and summing all components according to the fiber orientation distribution, $\phi(\beta)$, the stress on the fabric is

$$\sigma_L = E_f\int_{-\pi/2}^{\pi/2}\left[e_L\cos^4\beta - \left(\frac{\alpha}{2\sin\frac{1}{2}\alpha} - 1\right)\cos^2\beta\right]\phi(\beta)\,d\beta$$

For an isotropic fiber orientation where $\phi(\beta) = 1/\pi$

$$\sigma_L = E_f/\pi\int_{-\pi/2}^{\pi/2}\left[e_L\cos^4\beta - \left(\frac{\alpha}{2\sin\frac{1}{2}\alpha} - 1\right)\cos^2\beta\right]d\beta$$

and several arguments for α can be considered.

<u>Constant α</u>

If α is constant for all fibers, then $\sigma_L = 0$ until first fiber is strained, and this will occur for fibers whose chords have angle $\beta = 0^\circ$ or

$$e_f = e_L - \left(\frac{\alpha}{2\sin\frac{1}{2}\alpha} - 1\right) = 0$$

$$[e_L] = \frac{\alpha}{2\sin\frac{1}{2}\alpha} - 1$$

This gives the minimum value of e_L for $\sigma_L > 0$ and for certain values of α, the following data result

α (rad.)	.10	.20	.40	.60	1.0
α°	5.7	11.5	22.9	34.3	57.2
$[e_L]$, %	.02	.17	.67	1.52	4.3

This is merely the initiation of stress, and does not give any information about the early modulus. A simple way to arrive at this early modulus is by the incremental method. Just before the $1/18$ relative fibers assigned to the angular interval of mid-point $\beta = 10^\circ$ act

$$e_L^* = \frac{1}{\cos^2\beta}\left[\frac{\alpha}{2\sin\frac{1}{2}\alpha} - 1\right] = 1.03\left[\frac{\alpha}{2\sin\frac{1}{2}\alpha} - 1\right] = [e_L]_2$$

and the value of $[e_L]_2$ is given by

α rad.	.10	.20	.40	.60	1.0
$[e_L]_2$	.021	.175	.69	1.57	4.4

and the stress is

$$\sigma_L = E_f \cdot \frac{\pi}{18} \cdot \frac{1}{\pi}\left[[e_L]_2 - [e_L]\right] \cos^4(\beta = 0^\circ)$$

$$\frac{\sigma_L}{[e_L]_2 - [e_L]} = \bar{E}_L = \frac{1}{18} E_f$$

This value of E_L will continue to increase with increasing strain, approaching $E_L = 3/8\ E_f$, given for straight fibers (provided all strained fibers are still in the Hookean region). Thus the stress-strain response would be as shown below asymtotically approaching the slope 3/8 Ef. To obtain the complete form, it would be necessary to complete

this argument for all nine intervals (since $\phi(\beta)$ is symmetrical). However, α is probably not constant, and thus a discussion of a distributed α is desired.

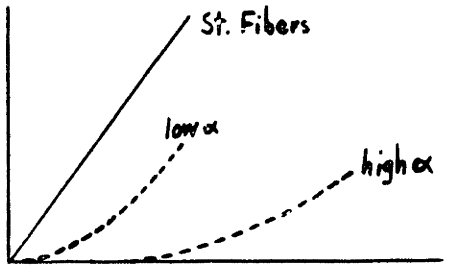

Distributed α

Consider that α and β are independent, which would appear likely in any air-formed isotropic fiber orientation; and that α is distributed in a Poisson frequency distribution with mean $\bar{z}$. Then

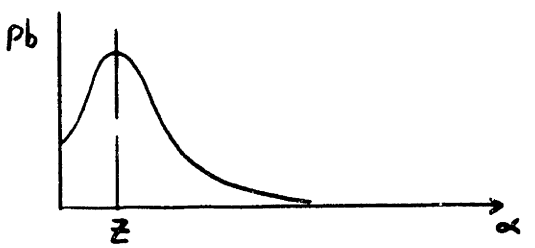

$$P_b(\alpha = 0) = e^{-\bar{z}}$$

$$P_b(\alpha = 1) = \bar{z}\, e^{-\bar{z}}$$

$$P_b(\alpha = 2) = \frac{\bar{z}^2 e^{-\bar{z}}}{2}$$

Handling this Probability distribution in the same way as above will also give an incremental solution to the early stress-strain curve.

The procedure is tedious and certain conclusions can be reached without any computation. The same general form as with α constant will be obtained, but with no initial delay of stress and a slower increase of modulus. With fibers of low proportional limit strains, the first fibers stressed will enter the plastic region before all of the fibers become stressed. Thus the modulus may never reach the value of 3/8 E_f predicted for a straight fiber isotropic web. The measured modulus may not increase and might appear constant. The stress-strain curve of such a material may give little information as to the fiber properties. If α and β are dependent, the measured fabric properties could also

give misleading information about the ratio of E_L/E_T or $\frac{(\sigma_m)_L}{(\sigma_m)_T}$. Fiber curvature must, of necessity, reduce the available rupture stress of the material. This occurs because of the progressive fiber involvement, and thus any straight fibers in the direction of stress will fail before any curved fibers in that direction reach their rupture strain. The larger the value of α, the more severe this strength loss.

As noted previously, if the fibers are already curved, they resist compressive stresses only by bending. Since the resistance to bending is much less than the tensile fiber modulus, Poisson's ratio will be greater than the value of 1/3 given by the general theory. One experiment on an air formed curled fiber isotropic web gave $\nu_{LT} = \nu_{yx} \cong 1.0$. The larger value of Poisson's ratio will also act to decrease the modulus of the fabric.

The above discussion is not intended to leave the impression that curved fiber structures are inferior. They have properties unique among textile materials. However, their analysis becomes less a function of tensile fiber properties and requires a more exhaustive treatment of the geometry of the structure and curved fiber properties; an analysis beyond the scope of this investigation.

C. Influence of Multiple Parallel Plies

In the previous section (X . B), consideration was given to perpendicular groups of parallel fibers and their predicted fabric properties. The comment was made that evaluation of their performance appears more a function of fabric variability than small differences in orientation. The purpose here is to examine the influence of multiple plies of the same fabric, all plies oriented in the same direction. Two cases can occur for the multiple layer fabric. The first is rigid bonding between plies, such that the local elongation in one ply is the local elongation of all the plies, or the composite, at that point. This meets the original limitation of the study; that fabrics will be considered as two-dimensional. The second case would be no bonding between plies (or bonding with a very flexible material) such that each unit cell of each ply can be considered to act independently.

According to the previous theory, the Hookean properties of either composite can be predicted by the average unit cell. Only the conditions of rupture require explanation. Consider each ply to consist of $\underline{h}$ cells wide, $\underline{j}$ cells long and the number of plies given by $\underline{k}$. Assuming no periodic variation in average area density of the individual plies, the coefficient of variation of specific rupture stress $(C)_{d\sigma}$ will be modified by the number of plies $\underline{k}$. For one ply, when area density and fiber orientation distribution are independent; $(C)^2_{d\sigma} = (C)^2_d + (C)^2_\sigma + (C)^2_d (C)^2_\sigma$,

Assume further that the conditions of fiber rupture strain are the same, i.e.

$$e_{rup} = \bar{e}_m - 3 s_{e_m}$$

When $\underline{k}$ unit cells are bonded together, the individual area density and fiber orientation distribution will tend to give smaller values of the $(C)_{d\sigma}$ for the unit cell of $\underline{k}$ layers. If the $\underline{k}$ unit cells are random, then the usual law will hold; that is, the standard deviation of the <u>average value</u> of the $\underline{k}$ specimens taken together is $1/\sqrt{k}$ times the standard deviation of the individuals, or

$$S_k = \frac{S}{\sqrt{k}}$$

The coefficient of variation of the individual plies is $\frac{S_{d\sigma}}{D\bar{\sigma}}$, while the coefficient of variation of the k specimens taken together is $(S_{d\sigma})_k / k D\bar{\sigma}$

Thus

$$\left[C_{d\sigma}\right]_k = \frac{\left[S_{d\sigma}\right]_k}{k D\bar{\sigma}} = \frac{S_{d\sigma}}{k^{3/2} D\bar{\sigma}} = \frac{1}{k^{3/2}} C_{d\sigma}$$

Thus the equation for the rupture force of k plies, as divided by the total area density in denier, kD, gives the specific rupture stress for the $\underline{k}$ plies as

$$(\sigma_{hj})_k = (\bar{\sigma})\left(1 - v_{hj} \frac{1}{\sqrt{k}} C_{d\sigma}\right)$$

This compares to

$$\sigma_{hj} = (\bar{\sigma})\left(1 - v_{hj} C_{d\sigma}\right)$$

for the individual plies. Thus, for rigid bonding of $\underline{k}$ plies, the coefficient of variation of $d\sigma$, $(C)_{d\sigma}$, is reduced by the factor $1/\sqrt{k}$. For $\underline{k} = 4$, the $(C)_{d\sigma}$ is halved. Then for Fabric A, by equation 8.24, the predicted strength of four plies tested one inch wide by 8 inches long would be

$$(\sigma_{hj})_4 = 1.2\left[1 - 4.2(8.5)\tfrac{1}{2}.13\right]$$

$$= 0.80 \text{ gpd}$$

compared to the predicted value of 0.64 gpd for each ply. If the plies were not bonded together the total number of unit cells is now hjk, and (assuming complete freedom between plies)

$$\sigma_{hjk} = \bar{\sigma}\left(1 - v_{hjk}\, C_{d\sigma}\right)$$

in which hjk = 15,800 x 4 = 63,000, Thus

$$\sigma_{hjk} = 1.2\left[1 - 4.2\left(1 - \{63{,}000\}^{-1/5}\right).13\right]$$

$$= 0.60$$

These two cases represent the extremes in the effects of multiple plies, and the practical values will lie between these two limits. However, the analysis definitely indicates an advantage to multiple plies when rigid bonding is to be used.

D. Dependent Area Density and Fiber Orientation Distribution

The rupture predictions are based upon the independence of area density d and unit cell stress σ_c (or fiber orientation distribution $\phi(\beta)$). In the event the two parameters are not independent, serious modification of the equations can result. Consider for the moment that high area density is correlated with high fiber orientation on one particular direction (say the L direction). Now the calculation of $\left[C_{d\sigma}\right]_D$ is not the same, and becomes larger, as given by Haldane (10) (See Appendix E)

$$\left[C_{d\sigma}^2\right]_D = \left[C_{d\sigma}\right]_I^2 + 2\rho C_d C_\sigma + \rho^2 C_d C_\sigma^2$$

where ρ is the correlation coefficient of d and σ_c, and $[C_{d\sigma}]_I$ is the coefficient of variation when d & σ_c are independent. When ρ is positive, the standard deviation of the joint $d\,\sigma_c$ population increases. Thus for failure predicted by the weakest link theory, the rupture stress of finite specimens will be reduced.

Assume, however, that ρ is negative, approaching - 1 in value; then the product $d\,\sigma = f$ will be almost constant, even for large individual variations in d or σ. The coefficient of variation $(C)_{d\sigma}$ will approach zero, and the rupture stress of the fabric in that direction will approach $\bar{\sigma}_m$. Thus, it would appear that one way of increasing the actual fiber strength utilization would be to make $\rho = -1$. However, this could only apply to one direction of stress, for in a continuous $\phi(\beta)$, negative correlation coefficient in one direction must have a positive correlation coefficient in some other direction, provided the fabric was made of only one ply all formed at the same time. If, however, the material was multilayed, with the layers oriented at various angles, each ply might be so constructed as to have a negative ρ in the direction of principle fiber orientation. Since, in such a multipli-oriented material, the rupture stress in any direction is most dependent on the variability of the fibers oriented in that direction, greater fiber strength utilization should result.

It might be pointed out, that it is conceivable to have a negative correlation coefficient in two perpendicular directions by sacrificing the properties intermediate to those directions. Thus, the rupture strength on finite specimens might be increased in the L and T directions with a corresponding decrease in the rupture stress at 45° to L and T.

E. Influence of Other Variables

In the course of the investigation, three other factors have been psotulated as having some possible influence on the properties of the fabric. These factors have to do with all properties in varying degrees, and are briefly discussed below.

Bunching Coefficient

In the unit cell study, the influence of non-uniform spacing of fibers oriented in the same direction was considered. Observation of the photomicrographs of Fabrics A and B will show two degrees of fiber bunching. In Fabric A, the spacing between fibers lying at some direction is fairly uniform. In Fabric B, a number of fibers lie side by side to form a bunch, with the bunches widely separated. The influence of this upon free fiber length between bonds and, consequently, Poisson's ratio, has already been discussed; and leads to the modification of the unit cell for Fabric B (Section IX). It was suggested that where bunching of fibers was quite severe that the proportion of fibers acting at angles away from the direction of bunching is less than the total number of fibers present. The form

$$\% \text{ acting} = 100 \left(1 - \tfrac{1}{2} \sin 2\theta \right)$$

was used, as an approximation, for severe bunching. Thus, the concept of a bunching coefficient, denoted B.C., is defined as follows. In any particular direction y, consider the number of fibers in the unit cell lying within some small angle of that direction. Dividing the unit cell dimension by the number of fibers gives the average space occupied by one fiber, as shown below. Now, if the spacing of fibers were perfectly uniform, each fiber space should contain one fiber. If the fibers are bunched, fewer spaces are occupied by fibers.

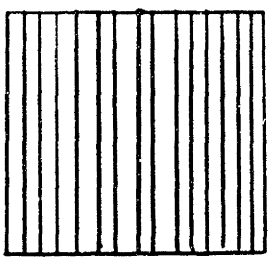

n fibers

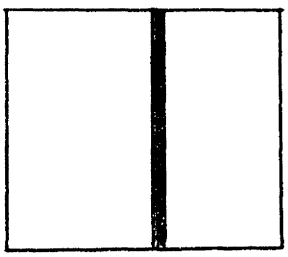

B.C. ~ 1

B.C = $\frac{1}{n}$

The Bunching Coefficient can be defined as

$$\text{B.C.} = \frac{\text{No. of fiber spaces containing fibers in the unit cell}}{\text{Total number of fiber spaces in the unit cell}}$$

and $0 < \text{B.C.} \leq 1$. When the B.C. equals unity, all fibers will act in any direction. When the B.C. $\longrightarrow$ zero, one-half of the fibers carry tension in an intermediate direction. Thus, the percent acting can be approximated by

$$\% \text{ acting fibers} = \frac{1-(1-\text{B.C})\sin 2\theta}{2}$$

Degree of Bonding

This factor, while quite important, is very difficult to specify. In the previous discussions of Fabric A with two amounts of binder, nearly all properties were changed by increasing the binder, but to varying degrees. No satisfactory procedure has been found for including this factor into the general equations, but the following comments are included in the hope of clarification.

The fabric properties have been based on the fabric weight or the weight of the fiber (neglecting the small amounts of binder in most of the materials tested). Presumably, bonding is best when the highest specific fabric properties are obtained, based on the total area density of the fabric. Also, bonding is best when only fibers fail. Yet, the analysis has been based on rigid bonds, and it is possible that a less rigid binder might allow greater equalization of fiber stress, and completely alter the postulated failure mechanism of the unit cell. If the material could be

altered so as to allow some fibers to fail while the fabric stress increased, the rupture stress might increase also. The investigation has not attempted to include binder variations. The question of the degree of bonding is more a function of the binder type and amount, and its influence on the mechanism of rupture, and the final equations do not consider degree of bonding.

Degree of Coupling

Among the assumptions of failure, was the condition that every unit cell is independent. This is, quite obviously, an oversimplification; for fibers do not end at the boundaries of a unit cell, but continue on through one or more adjacent unit cells. This interaction of unit cells has been termed "coupling". While the word is precise, the influence of its presence is not clear. Both coupling and degree of bonding seem interrelated. As bonding increases, the minimum size of the unit cell might be expected to decrease; but the added bond points probably increase the interaction of adjacent unit cells, effectively increasing their size. This appears to be a rational explanation of the behavior of high viscose Fabric A. The increased amount of binder causes the unit cell size to increase, thereby raising the rupture stress. Conversely, the unit cell size might have decreased, but the added binder changed the postulated mechanism of failure.

The study of these three factors becomes a major investigation. This has been an attempt only to introduce their concepts and suggest the manner in which they influence the actual fabric, and their clarification must be left to others.

XII. SUMMARY FOR FABRIC DESIGN

A. Orthotropic Theory and the Prediction of Fabric Properties

The predictions of four major fabric parameters, E_y, ν_{yx}, σ_ρ, and σ_m by the orthotropic theory are quite satisfactory on Fabrics A and B. Without experimental data on G_{yx}, no conclusions can be drawn concerning the validity of calculating G_{LT} from E_{45°. It is important to note that in every case, the use of experimental data at $\theta = 45^\circ$ to calculate a material constant is fraught with possible error. Such a procedure tends to force a closer agreement between experimental and predicted values than might occur in using experimental determinations. However, within the limitations of Hookean behaivor, and for initial loading response in relatively short times; the following conclusions appear justified. For an orthotropic, flexible straight fiber non-woven fibrous strucute, well bonded with a rigid binder, and available for testing; the orthotropic theory predicts the following properties quite well, under the assumptions of uniaxial tensile stress $\sigma_x = \sigma_{yx} = 0$.

a. The initial specific modulus, Ey.

b. The initial Poisson's ratio,

c. The specific rupture stress,

d. The specific proportional limit stress .

The final test of the orthotropic theory wi'l come with the introduction of experimental data on Gyx, $\sigma_{\rho_{LT}}$ and $\sigma_{m_{LT}}$. Until this information is available, alternative calculations leave the impression of having forced, to some extent, the agreement between experimental and predicted behavior. This question is referred to in Section XIII, in Recommendations.

B. Fiber Web Theory: Summary of Equations

This theory based on a number of assumptions, was not developed to improve the accuracy of the predictions of fabric behavior. Rather it is an attempt to formulate a logical analytical procedure to examine the influence of fiber properties and fiber orientation distributions on the mechanical characteristics of non-woven structures. It presents a method of examining the consequences of changes in these parameters without manufacturing the fabric. The analysis has achieved this goal, and is not restricted by the assumptions of Hookean behavior or of perfect uniformity.

The boundary conditions of test are quite important. Two sets of conditions have been used in the general analysis: a) σ_y real, $\sigma_x = \sigma_{yx} = 0$, and b) σ_y real, $\sigma_x = \epsilon_{yx} = \ldots$ The boundary conditions are established by the physical arrangement of test. The orthotropic equations have been given for $\sigma_x = \sigma_{yx} = 0$, and the material constants E_L, E_T, ν_{LT}, ν_{TL} and G_{LT} are independent of the boundary conditions and are given by equations 6.12. Thus equations 3.12a can be used to solve for the properties in any other direction under these boundary conditions.

The analysis has also been carried out for the boundary conditions $\sigma_x = \epsilon_{yx} = 0$. These conditions appear to be closer to the mixed case actually present in the testing. It may seem that the boundary conditions are somewhat contradictory. However, analytical procedures can be developed, following the techniques described, for any set of boundary conditions of stress or strain by the proper use of the strain transformation

$$\epsilon_y = \epsilon_y \cos^2\beta - \epsilon_x \sin^2\beta + \epsilon_{yx} \sin\theta \cos\theta$$

and the use of the boundary values of σ_y, σ_x and σ_{yx} in the area of the specimen under consideration (See Appendix D.)

The tensile test, as performed, appeared to be better approximated by the boundary conditions $\sigma_x = e_{yx} = 0$, and the summary given below is for these boundary conditions. The concept of Fiber Bunching has been included in the equations.

With the additional concepts introduced in Sections X and XI, the equations and symbolism are summarized below:

Fiber $\sigma_f = E_f e_f \qquad e_f < e_f$

$\sigma_f = p + q e_f \qquad e_f > e_p$

Fiber Orientation Distributions:

$$\phi(\beta) = a + b\cos\beta + c\cos^3\beta + d\cos^8\beta + e\cos^{16}\beta$$

Fabric Equations (Hookean Region)

For the defined material constants relative to the orthotropic axes (regardless of boundary or stress conditons)

$$E_L = E_f \frac{A_2 A_3 - A_1^2}{A_2} \qquad E_T = E_f \frac{A_2 A_3 - A_1^2}{A_3}$$

$$\nu_{LT} = \frac{A_1}{A_2} \qquad \nu_{TL} = \frac{A_1}{A_3} \qquad G_{LT} = A_1 E_f$$

For the boundary conditions, $\sigma_x = \sigma_{yx} = 0$ substitute the above in relations 3.12

$$C_{11} = \frac{1}{E_y} = \frac{\cos^4\theta}{E_L} + \frac{\sin^4\theta}{E_T} + \left[\frac{1}{G_{LT}} - \frac{2\nu_{LT}}{E_L}\right]\sin^2\theta\cos^2\theta$$

$$C_{12} = -\nu_{yx} = \frac{E_y}{E_L}\left\{-\nu_{LT} + \left[1 + \frac{E_L}{E_T} + 2\nu_{LT} - \frac{E_L}{G_{LT}}\right]\cos^2\theta\sin^2\theta\right\}$$

$$C_{13} = \frac{e_{yx}}{f_y} = \left[\frac{1}{G_{LT}} - \frac{2\nu_{LT}}{E_L} - \frac{2}{E_L}\right]\sin\theta\cos^3\theta - \left[\frac{1}{G_{LT}} - \frac{2\nu_{LT}}{E_T} - \frac{2}{E_T}\right]\sin^3\theta\cos\theta$$

$$C_{33} = \frac{1}{G_{yx}} = \frac{1}{G_{LT}}\cos^2 2\theta + 4\left[\frac{1}{E_L} + \frac{1}{E_T} + \frac{2\nu_{LT}}{E_L}\right]\sin^2\theta\cos^2\theta$$

For the boundary conditions $\sigma_x = e_{yx} = 0$.

$$\frac{E_y^*}{E_f} = \left[\frac{A_2A_3 - A_1^2 + 4(A_1A_2 + A_1A_3 - A_2A_3 + 3A_1^2)\sin^2\theta\cos^2\theta}{A\sin^4\theta + A_2\cos^4\theta + 6A_1\sin^2\theta\cos^2\theta}\right]\left[1 - \frac{1 - B.C._1}{2}\sin 2\theta\right]^*$$

$$\nu_{yx} = -\frac{A_1 + (A_2 + A_3 - 6A_1)\sin^2\theta\cos^2\theta}{A_3\sin^4\theta + A_2\cos^4\theta + 6A_1\sin^2\theta\cos^2\theta}$$

Where

$A_1 = .393a + .267b + .152c + .0645d + .0292e$

$A_2 = 1.18a + .400b + .114c + .0215d + .00514e$

$A_3 = 1.18a + 1.067b + .914c + .709d + .554e$

B.C. = Bunching Coefficient = $\frac{\text{No. of fiber spaces containing fibers}}{\text{Total number of fiber spaces}}$

Fabric Equations (Plastic Region)

$$\sigma_y = \left\{P\left[1 - 8/E_f\right]\left[A_4\cos^2\theta + A_5\sin^2\theta\right] + q\,e_y\,E_y^*/E_f\right\}\left\{1 - \frac{1 - B.C._1}{2}\sin 2\theta\right\}$$

where $A_4 = 1.708a + 1.33b + 1.067c + .773d + .583e$

$A_5 = 1.708a + .667b + .266c + .086d + .0325e$

$(1 - 8/E_f)$ = Arbitrary transposing of plastic stress intercept to Hookian Modulus

$\left(1 - \frac{1 - B.C.}{2}\sin 2\theta\right)$ = assumed form of reduction in acting fibers due to bunching of fibers (eliminating those fibers in compression)

Rupture $(\sigma_{hj}) = \bar{\sigma}_{cm}\left[1 - \nu_{nj}\,C_{d\sigma}\right]$

where $\bar{\sigma}_{cm}$ = rupture stress of average unit cell (first fiber fails at elongation $(\bar{e}_m - 3s_{em})$ and

$\nu_{nj} = 4.2\left[1 - (hj)^{-1/5}\right]$ in the form given by Peirce (13)

$C_{d\sigma}$ = coefficient of variation of rupture stress of the unit cells in

*The Bunching Coefficient (B.C.) has been introduced arbitrarily, and further work will be necessary before the proper form of the expression is justified However, as observed on Fabric B, the influence of fiber bunching can be quite large. The real importance lies in the interpretations of the abnormalities of the fiber structure, which can only be resolved by careful study of the fabric under the microscope.

the direction $y = \sqrt{C_\sigma^2 + C_d^2 + C_\sigma^2 C_d^2}$

(σ_{hj}) = predicted rupture stress of a specimen containing hj unit cells

The fiber web theory allows the calculation of the mechanical properties of a fabric with any fiber orientation distribution under the following limitations:

a. straight fibers, at least between the boundaries of the unit cell.

b. rigid bonds, or at least bonds with the same properties as the fibers.

c. Only fiber failure

d. All fibers in one plane.

All fiber bending has been neglected. For this reason ν_{yx} and E_y are predicted as zero for certain fiber orientation distributions (See Section X). The influence of several other factors were discussed (Section XI) but were not included in the formulation of the general equations.

In general, the experimental and predicted mechanical properties of Fabrics A and B are in excellent agreement. These two fabrics are fairly representative samples of straight-fiber non-woven structures. The fiber web theory should predict well the properties of any fabric of this type. Further the engineering properties of non-woven fabrics composed of blends or combinations of fibers can be predicted also.

XIII. CONCLUSIONS AND RECOMMENDATIONS

A. Conclusions

The goal of this investigation, within the limitations originally set forth, has been accomplished. The mechanical properties in tension of a flexible, straight fiber, non-woven bonded structure can be predicted from knowledge of the fiber properties and the fiber orientation distribution. The complete stress-strain curves can be predicted from knowledge of the fiber properties and the fiber orientation distribution. The rupture stresses can be predicted with information as to the local variability of area density and fiber orientation distribution. The analytical predictions are not dependent on the assumptions of Hookean behavior, nor of product uniformity and provide a more general approach to the problem.

The analytical procedures summarized by the equations of Section XII B allow abstract examination of the possible performance of specific non-woven structures. The important parameters can be varied independently to determine their individual influence. Further, the theory provides a tool for examining composite structures of fiber materials. The developed analytical procedure has been limited to uniaxial tension, and to rigid, stronger than fiber, bonds. However, the procedures can be adapted to account for such changes without serious modification.

The fiber web theory provides a means of predicting the performance of an ideal non-woven structure. Thus it gives a yard-stick by which present non-woven fabrics and processes can be measured. One of the major problems in any new field of technology is to know the theoretical limitations of the resulting product. Only then can research be properly guided into those areas offering the greatest improvement. The analytical

tools developed appear to have fulfilled this requirement.

The orthotropic theory, an extension of the simplest stress-theory, is limited by certain basic assumptions, notably the assumption of Hookean behavior without time effects. Further, orthotropic theory does not attempt to interpret the structure of the material, but is based upon knowledge of the material constants for the orthotropic axes. Then stresses imposed at certain angles to these axes can be resolved into their component stresses relative to the orthotropic axes. These orthotropic stresses are converted to orthotropic strains on the basis of Hooke's law and the known constants . These strains are then resolved into their components relative to the directions of the stresses.

The fiber web theory, on the other hand, is formulated from basic considerations of the structure and its most important member - the fiber.

The theory is based upon the assumption of a certain value of strain in the arbitrary directions $\underline{y}$ and $\underline{x}$. This strain results in fiber strains depending upon the position of the fiber relative to the direction of imposed strain. The fiber strains are converted to fiber stresses through the fiber stress-strain relationship. The fiber stresses are resolved to give a component of fabric stress resulting from this imposed strain. These components are weighed by the proportion of fibers geometrically placed at this position in the fabric, and those adjusted components summed to give the fabric stress at this particular strain. The fiber web theory explains rupture stresses in terms of characteristics of the fiber and the web formation. The reasoning behind certain assumptions has been carefully noted, in the hope that future investigators will thoroughly understand the significance of the assumptions.

To summarize, the analytical development provides a new approach to the design of specific non-woven materials. The parameters of the structure can be altered to obtain the optimum inherent properties to match the desired characteristics in specific directions. Further, the analysis provides a tool for examining the behavior of composities of different materials; such as blends of fibers, woven and non-woven laminates, combinations of plastic films and non-woven fabric, and multi-plied, multi-oriented non-woven materials. Since the treatment is based on the properties of the fiber, the analysis can be extended to include cyclic loading and time effects under constant load, based on the known behavior of the fiber. This investigation is but a start towards a complete understanding of the mechanics of the fibrous non-woven structure.

B. Recommendations

There are many areas for future investigations in the mechanics of non-woven structures. The more important ones are summarized below, with a brief discussion as to the goal and approach. The listing is not in order of decreasing importance.

1. Additional $\phi(\beta)$. Only two fiber orientation distributions have been examined extensively, with several others treated theoretically. Further experimental work is desirable, particularly with regard to bi-modal distributions.

2. Biaxial Stress Measurements The theory is readily expandable to biaxial stress conditions. Biaxial measurements designed to give properties in shear are highly desired. The final determination of the full usefulness of the fiber web theory will depend upon the exactness of the experimental boundary conditions.

3. Curved and Bunched Fibers The theory has been developed for straight fibers neglecting any bending resistance, and a very approximate correction made for buckling of fibers due to long free fiber lengths. In view of the large commercial importance of curved fiber isotropic webs, this generalization of the theory is most desirable.

4. Process Variables The small scale variability of area density and fiber orientation distribution appears to be a very important factor in the rupture stresses of the non-woven. A thorough investigation of these variables should include the most uniform structure, in order to examine closely the adaptation of Peirce's "Weakest Link" theory.

5. Multiple Plys The influence of plying identical structues parallel has been discussed. The question of plies at various angles to each other opens a tremendous area of investigation, one still not thoroughly understood on plywood and glass-fiber laminates. The questions of unequal strains in the plies and interlaminar shear become extremely important.

6. Different Bonding Systems A simple change in the properties of the binder can create many new problems requiring modification of the theory. If the binder becomes more extensible than the fiber, the response of the non-woven to stress must change, and the equa - tions suitably altered.

7. Bonding other than Impregnation The analysis has assumed a large number of bond points on each fiber. As the amount of bonding diminishes, the variability of number of bonds per unit area may become an important factor. Further, if the bonding is restricted to

certain finite areas, the entire concept of the unit cell may have to be altered to preserve the conditions of boundary compatibility.

8. Creep This concerns the behavior of the non-woven under continuing load or elongation, and its behavior with time. Since both the binder and fiber will have individual creep behavior, the performance of the fabric should be predictable under the usual assumptions.

XIV APPENDIX

Appendix A

Strain Energy Function and Maxwell Reciprocal Relations (9)

Starting with the stress-strain relations for the general axes 1, 2, and making the substitution of L for 1, T for 2, equations 3.5 become:

$$e_L = a_{11} f_L + a_{12} f_T + a_{13} f_{LT}$$

$$e_T = a_{21} f_L + a_{22} f_T + a_{23} f_{LT} \qquad (1)$$

$$e_{LT} = a_{31} f_L + a_{32} f_T + a_{33} f_{LT}$$

In the fibure below, consider the rectangle to be very small and of unit thickness, with the sides parallel to L and T direction of length a and b, respectively. Let the component, f_L increase slowly from zero to the final value f_L . At the same time, the total displacement of side a will increase from zero to $e_L \cdot a$.

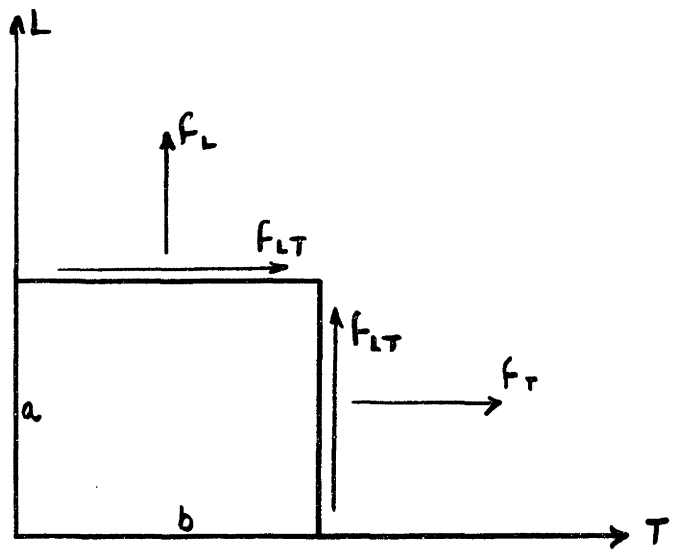

FIGURE 14.1

EQUIPMENT FOR SINGLE FIBER TESTS

The energy stored in the element due to this component will be equal to one-half the product of the final value of the force $f_L \cdot b$ and the final value of the displacement $e_L \cdot a$, or $\frac{1}{2} f_L e_L ab$. In like manner, the energy stored by the component f_T in increasing slowly from zero to a final value f_T is equal to $\frac{1}{2} f_T e_T ab$.

Let the component f_{LT} on the upper face increase slowly from zero to a final value f_{LT}, this final value of force being $f_{LT} \cdot b$. At the same time, the total angular distortion will increase from zero to a final value δ, where $\delta = a \tan e_{LT} = a e_{LT}$. Then the energy stored in the element due to this component will be equal to one-half the product of the final values, or $\frac{1}{2} f_{LT} \cdot b e_{LT} \cdot a$.

If all components increase slowly from zero to the final values f_L, f_T, f_{LT}, the total strain energy in this volume (ab) is given by

$$W = \frac{1}{2} \left[f_L \cdot e_L \cdot ab + f_T e_T ab + f_{LT} e_{LT} ab \right] \qquad (2)$$

and the energy per unit volume is

$$W = \frac{1}{2} \left[f_L e_L + f_T e_T + f_{LT} e_{LT} \right] \qquad (3)$$

Now in accordance with the generalized form of Hooke's Law, each component of stress is a linear combination of all the components of strain (just as in equations (1), each component of strain is a linear combination of all the components of stress). Such equations are of the following type:

$$\begin{aligned} f_L &= d_{11} e_L + d_{12} e_T + d_{13} e_{LT} \\ f_T &= d_{21} e_L + d_{22} e_T + d_{23} e_{LT} \\ f_{LT} &= d_{31} e_L + d_{32} e_T + d_{33} e_{LT} \end{aligned} \qquad (4)$$

Substitution of these equations into the equation for strain energy per unit volume gives:

$$W = \frac{1}{2}\left[d_{11}e_L^2 + d_{12}e_Le_T + d_{13}e_Le_{LT} + d_{21}e_Le_T + d_{22}e_T^2 + d_{23}e_Te_{LT} + d_{31}e_Le_{LT} + d_{32}e_Te_{LT} + d_{33}e_{LT}^2\right] \quad (5)$$

If the material is orthotropic (two axes of symmetry L and T), the strain enrgy function must be unchanged if the positive direction of any one of the axes is reversed. If, for example, the direction of the L axis is reversed, the strain energy function must be the same for the transformation of coordinates

$$L' = -L \quad \text{and} \quad T' = T \; ; \; e_{L'} = e_L \; , \; e_{T'} = e_T \; , \; e_{L'T'} = -e_{LT}$$

Then

$$W' = \frac{1}{2}\left[d_{11}e_L^2 + d_{12}e_Le_T - d_{13}e_Le_{LT} + d_{21}e_Le_T + d_{22}e_T^2 - d_{23}e_Le_{LT} - d_{31}e_Le_{LT} - d_{32}e_Te_{LT} + d_{33}e_{LT}^2\right] \quad (6)$$

Since W = W';

$$d_{13} = d_{23} = d_{31} = d_{32} = 0$$

and the final form of the strain energy function is given by:

$$W = \frac{1}{2}\left[d_{11}e_L^2 + 2A\,e_Le_T + d_{22}e_T^2 + d_{33}e_{LT}^2\right] \quad (7)$$

where

$$2A = d_{12} + d_{21}$$

Now the principal of potential energy (which is identical with strain energy in this case) states that the incremental increase in the strain energy produced by an incremental change in one of the strains is given by:

$$\frac{\partial W}{\partial e_L} = f_L \qquad \frac{\partial W}{\partial e_T} = f_T \qquad \frac{\partial W}{\partial e_{LT}} = f_{LT} \quad (8)$$

It follows from (7) and (8) that

$$f_L = d_{11} e_L + A e_T$$

$$f_T = A e_L + d_{22} e_T \qquad (9)$$

$$f_{LT} = d_{33} e_{LT}$$

Considering the similar set of equations for strain in terms of stresses gives (equations 1):

$$e_L = a_{11} f_L + a_{12} f_T$$

$$e_T = a_{12} f_L + a_{22} f_T$$

$$e_{LT} = a_{33} f_{LT}$$

Letting only one stress at a time be different from zero, gives, by inspection:

$$a_{11} = \frac{1}{E_L} \; ; \; a_{12} = -\frac{\nu_{LT}}{E_L} = a_{21} = -\frac{\nu_{TL}}{E_T} \; ; \; a_{22} = \frac{1}{E_T} \; ; \; a_{33} = \frac{1}{G_{LT}}$$

corresponding to the equations in IIIA, in the text.

Appendix B

Unit Cell Concepts

The Two Fiber "Unit Cell"

In the initial consideration of the problem, it was felt that a very highly or perfectly, oriented fiber structure would prove most amenable to theoretical treatment. The "Unit Cell" was pictured as two individual fibers bonded together, with the angle 2β between the fibers, and the angles $\alpha \pm \beta$ between the fibers and the direction of stress or force.

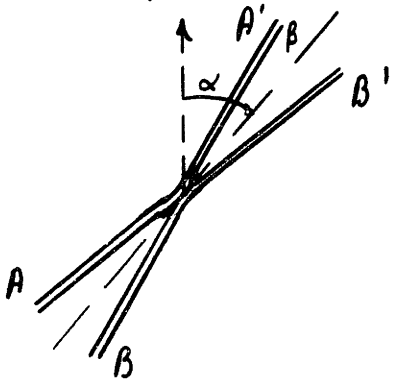

Such an arrangement is shown at left. It was subsequently recognized that such an arrangement does not measure fiber properties alone, but also properties of the bond as a function of α and β. Further, microscopic examination of Fabric A did not justify the use of this simplified fiber-bond arrangement, for the simplest building block of the fabric was vastly more complicated than just two fibers and one bond.

The experimental technique has been worked out for this test, and a short description follows. The procedure was originally developed by the author in 1951 to measure resin bond characteristics, and has been considerably revised and improved during this project. The jigs for testing two fiber assemblies are shown in Figure 14.1. The purpose of this arrangement was to allow the testing of fiber assemblies at seven angles of α, (0°, 15°, 30°, 45°, 60°, 75° and 90°) on the same mounting system. At the same

time, the points AA'BB" referred to in the previous sketch must be fixed and have some well-defined motion. The two adapters A and B were fitted in the jaws, and the complete test mount slipped onto the pins of the adapters. By restricting the jaws to vertical displacements only, the four fiber anchor points could only move vertically. By providing very fine wire pins in the Test Mounts D and E, the four fiber points were fixed and the angle β specified. Then simple changing of Jaw Mount location or test mount location on the specimen mounts provided the seven angles of test α at one fixed β . The angle β could be changed from 10^0 to 80^0 by the addition of other pins for the fiber mounts. The pins were of 0.016" piano wire and were initially placed 0.2" apart on each half of the specimen mount with $\beta = 14^0$. The fibers (9 denier viscose) were originally mounted parallel on the fiber mount shown as F in Figure 14.1. These fibers were then held close to the wax coated tip of the glass capillary tube of the microburet. (G). The capillary is drawn from standard glass tubing and calibrated. The usual deposition for 10-20 denier fibers was 25-50 micromilliliters ($25\text{-}50 \times 10^{-6}$ cc) of dilute resin emulsion or solution (for example Polyvinyl acetate of 15% solids content). This will usually deposit as an elliptical bond; by adjusting the amount of resin, either the fiber or the bond can be made to fail. After the fibers are bonded, the specimens are remounted on the specimen mounts, attaching the fibers at the pins with Neg-O-Lac (a permanent mounting medium for microscope slides). In test, the specimen mounts are slipped on the test mount C, and this fitted to the adapters A&B.

This experimental procedure was tried out and worked quite satisfactorily.

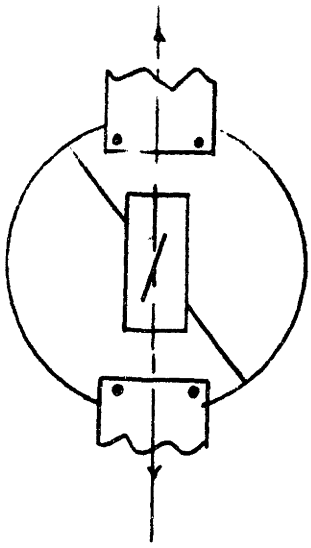

Testing one fiber as sketched at left gave a stress-strain curve in excellent agreement with standard tensile tests at two inch gauge. The dimensions of the various mounts are given in Figure 14.2

The Uniform Matrix of Bond Points

Since the structure of the fabric suggests a large number of intersecting fibers, arranged at various angles, and intersecting at finite points, the "unit cell" was hypothesized as a matrix of bonded points. A simplified diagram of this reasoning is shown in these sketches below:

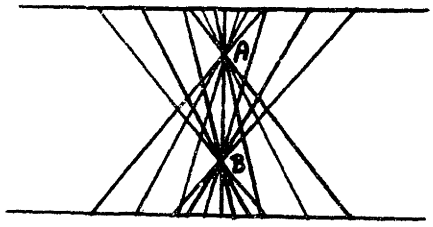

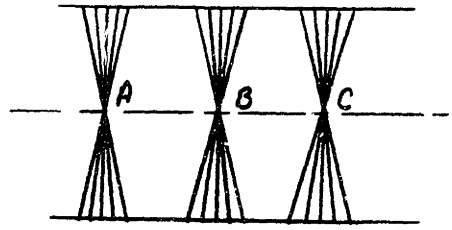

The fabric can be imagined as a series of matrix points, A & B, each containing the same number of fibers oriented at the same angles. This same pattern would repeat itself in both directions, giving a planar matrix of bond points, as suggested by A, B, and C. This type of arrangement appears promising from the standpoint of uniform displacement of matrix points, or of parallel boundary displacement. However, the analysis fails completely, if there are different numbers of fibers at the various matrix points, or if fibers end between matrix points. Thus the concept cannot

FIGURE 14.2

JIGS FOR TWO FIBER TESTS

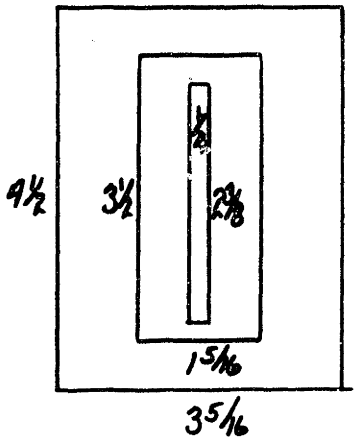

FIBER MOUNT - (1)

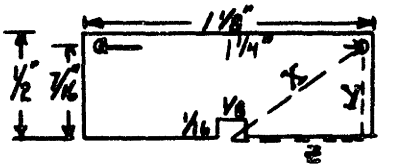

TEST MOUNTS - (20)

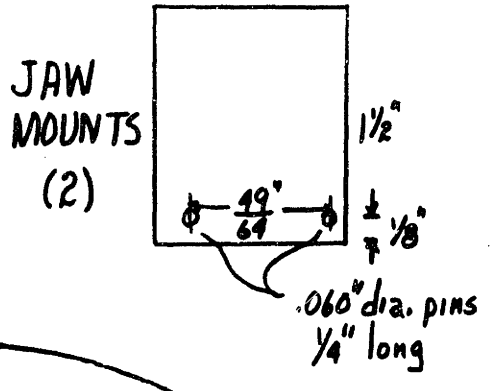

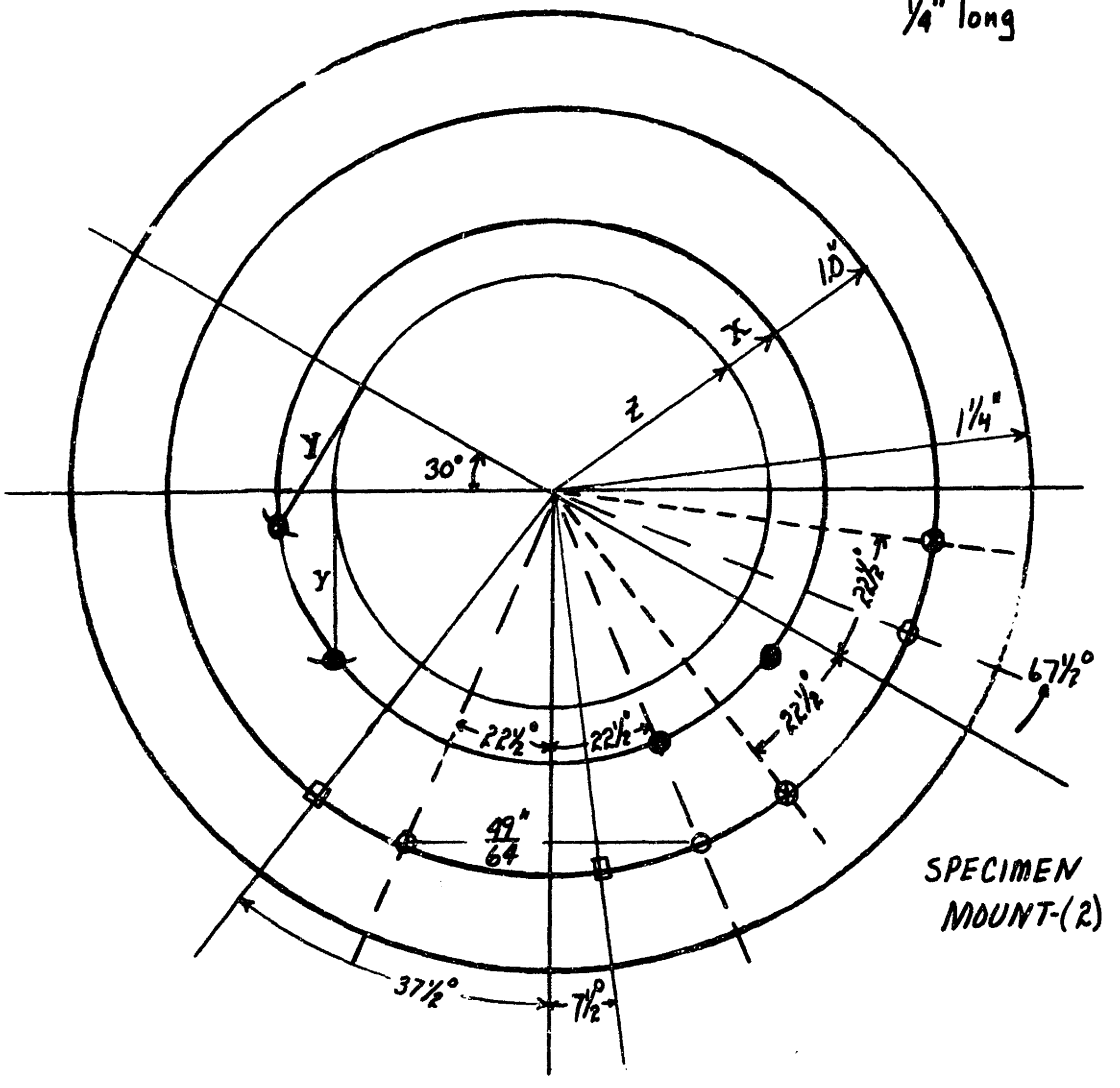

SPECIMEN
MOUNT-(2)

be adapted easily to account for non-uniformity and fiber ends. This approach was also discarded.

Appendix C.

Relationship between Number and Weight of Fibers in Unit Cell

Consider a non-woven fabric, with negligible binder by weight, to have an area density, D, in grams/sq. yd. Then the area density of one square inch = D/1296, and the weight of one unit cell of diameter A is

$$W = \frac{D}{1296} \cdot \frac{\pi}{4} A^2 \qquad (1)$$

For fibers of 1.5 denier (9000 meters weighs 1.5 grams), the length of fiber in one unit cell is:

$$\text{Fiber length in one unit cell} = \frac{D}{1296} \frac{\pi}{4} A^2 \cdot \frac{9000}{1.5} \cdot 39.4 \text{ inches} \qquad (2)$$

If the fibers are uniformly spaced, one from another (regradless of angle β) then the average length of each fiber can be found. If each fiber occupies a width t, and is A sinα long, all of the fiber lengths are given by the area of the circle, or $\frac{\pi}{4} A^2$. For the same number of fibers, A/t, their average length is given by the height of the rectangle whose area also equals $\frac{\pi}{4} A^2$. The area of this rectangle is $\bar{L} \cdot t \cdot \frac{A}{t} = \bar{L}A$ where $\bar{L}$ is the average fiber length. Thus equating the two areas, $\bar{L} = \pi/4$ A. Since the total length is given by equation 2, the number of straight, evenly spaced fibers will be

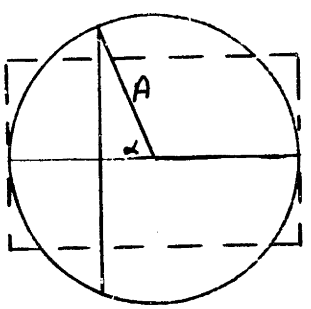

No. of fibers = $D \cdot A \cdot 183$

For fabric A, where D = 16 gms/sq. yd. and A = 0.0225".

No. of fibers in unit cell = 16x183x.0225

= 66 fibers.

The average no of fibers counted was 50. Considering the curved nature of the fibers, the amount of binder present (~2%) and the actual fiber denier*, the calculated number of fibers is closer to 50-55. The agreement is quite satisfactory.

For fabric B, D = 10.7 gm/sq. yd. and A = 0.0625. However, Fabric B contained about 7% binder by weight, and the average number of fibers is

No. of fibers in unit cell = 183 10.7(1-.07) .0625

= 113 fibers

The average number counted (in the recount of cells) was 68. However, in Fabric B much greater curvature of fibers was present. In addition, the moisture regain of the binder is not known. This, plus the change in fiber denier and the fiber bunching, places severe limitations on the accuracy of the calculated number of fibers. As discussed in the text, if fibers are bunched in proportion to their actual relative frequency as a function of β , the probability of errors in counting will be to change only the number of fibers counted. The counted $\overline{\phi(\beta)}$ will still be a good representation of the actual $\overline{\phi(\beta)}$. As this appears to be the case, by visual observation, then the grouped average of the 18 counts of unit cells is a good representation of the true $\overline{\phi(\beta)}$. Further, the same arguments concerning bunching imply that the estimated standard deviation of density, S_d, obtained from the counted fibers will be correct, or, at most, too small. The estimated standard deviation of stress S_σ will also be correct, or too small.

* The fiber denier of 1.5 is obtained at 50% RH. At 65% RH, the measured denier is approximately 1.57 due to the adsorption of moisture.

Appendix D

Boundary Conditions for the Analytical Solutions

In section VI, two sets of boundary conditions were noted for a standard tensile test. These were: 1) uniaxial tension where σ_y is real and $\sigma_x = \sigma_{yx} = 0$ and 2) a combination state where σ_y is real and $\sigma_x = e_{yx} = 0$. The true state of actual test specimens of finite length will lie somewhere between these two sets of boundary conditions, depending upon the type of jaw arrangement and the specimen length. The purpose here is to prove that the orthotropic and fiber web theory are consistent under the same boundary conditions; and to demonstrate how different boundary conditions can be used to better approximate the actual test conditons. The analysis will be carried out with the orthotropic equations of III.A., although the same results can be obtained from the fiber web theory by including shear strain in the transformation of fiber strain. These equations for strain in terms of stress were given by equations 3.5 as

$$e_y = a_{11} f_y + a_{12} f_x + a_{13} f_{yx}$$

$$e_x = a_{21} f_y + a_{22} f_x + a_{23} f_{yx}$$

$$e_{yx} = a_{31} f_y + a_{32} f_x + a_{33} f_{yx}$$

In the previous simplification, the stress fy was taken as real with fx = fyx = 0. Thus

$$e_y = a_{11} f_y$$

$$e_x = a_{21} f_y \qquad (f_x = f_{yx} = 0)$$

$$e_{yx} = a_{31} f_y$$

If, however, the boundary conditions $f_x = e_{yx} = 0$ are used, then results:

$$e_y = a_{11} f_y + a_{13} f_{yx}$$

$$e_x = a_{21} f_y + a_{23} f_{yx}$$

$$e_{yx} = a_{31} f_y + a_{33} f_{yx} = 0$$

Thus

$$f_{yx} = -\frac{a_{31}}{a_{33}} f_y$$

and

$$e_y = f_y \left[\frac{a_{11} a_{33} - (a_{13})^2}{a_{33}} \right]$$

In terms of the elastic moduli:

$$\frac{e_y}{f_y} = \frac{1}{E_y} = a_{11} \qquad (\sigma_x = \sigma_{yx} = 0) \qquad (1)$$

$$\frac{e_y}{f_y} = \frac{1}{E_y^*} = \left[a_{11} - \frac{(a_{13})^2}{a_{33}} \right] \qquad (\sigma_x = e_{yx} = 0) \qquad (2)$$

From the equations for a_{11}, a_{13} and a_{33} in section III.A. substitution into equation 2 above, and simplification, yields

$$\frac{1}{E_y} = \frac{\frac{\cos^4\theta}{G_{LT} E_L} + \frac{\sin^4\theta}{G_{LT} E_T} + \sin^2\theta \cos^2\theta \left[\frac{4}{E_L E_T} - \frac{4\nu_{LT}^2}{E_L^2} + \frac{2\nu_{LT}}{G_{LT} E_L} \right]}{\frac{1}{G_{LT}} + 4\left[\frac{1}{E_L} + \frac{1}{E_T} + \frac{2\nu_{LT}}{E_L} - \frac{1}{G_{LT}} \right] \sin^2\theta \cos^2\theta} \qquad (3)$$

Substitution of the values of the material constants expressed as functions of the fiber orientation distribution, namely:

$$E_L = \frac{E_f}{A_2}(A_2 A_3 - A_1^2) \qquad E_T = \frac{E_f}{A_3}(A_2 A_3 - A_1^2)$$

$$\nu_{LT} = \frac{A_1}{A_3} \qquad G_{LT} = A_1 E_f$$

gives, after simplification

$$\frac{E_f}{E_y^*} = \frac{A_2\cos^4\theta + A_3\sin^4\theta + 6A_1\sin^2\theta\cos^2\theta}{(A_2A_3 - A_1^2) + 4(A_1A_2 + A_1A_3 - A_2A_3 + 3A_1^2)\sin^2\theta\cos^2\theta} \qquad (4)$$

The inverse of this equation is the equation previously derived as equation 6.11.

In the same manner, with ν_{yx}^* defined as $-\frac{e_x}{e_y}$ for $\sigma_x = \sigma_{yx} = 0$, equations 3.5 reduce to

$$-\frac{e_x}{e_y} = \nu_{yx}^* = \frac{-a_{33}a_{21} + a_{13}a_{23}}{a_{33}a_{11} - (a_{13})^2} \qquad (5)$$

Thus the denominator of equation 5 is identical with the numerator of equation 4, and simplification of equation 5 gives

$$\nu_{yx}^* = \frac{A_1 + (A_2 + A_3 - 6A_1)\sin^2\theta\cos^2\theta}{A_2\cos^4\theta + A_3\sin^4\theta + 6A_1\sin^2\theta\cos^2\theta}$$

This is identical with equation 6.9 in the text.

Appendix E

Moments of the Product of Two Normally Distributed Variables

Following the notation of Haldane, the kth moment of x about the origin, μ_k', is

$$\mu_k' = E(x^k) = \sum_{x=0}^{x=\infty} x^k f(x)$$

where E is the expectation. Then the kth moment about the mean, (m), which is denoted μ_k, is

$$\mu_k = E\{(x-m)^k\} = \sum_{x=0}^{x=\infty} (x-m)^k f(x)$$

The first moment (k = 1) about the mean is

$$\mu_1 = E(x-m) = E(x) - m = m - m = 0$$

The second moment (k = 2) about the mean is

$$\mu_2 = E\{(x-m)^2\} = E(x^2 - 2xm + m^2)$$

$$= E(x^2) - 2m E(x) + m^2$$

$$= E(x^2) - m^2$$

$$= \mu_2' - m^2 = \mu_2' - (\mu_1')^2$$

Similarly

$$\mu_3 = \mu_3' - 3m\mu_2' + 2m^2$$

$$\mu_4 = \mu_4' - 4m\mu_3' + 6m^2\mu_2' - 3m^4$$

In order to avoid possible confusion, let us use the notation $\bar{X}^k$ instead of $\mu_k = \mu_k'$ for the variable x whose mean is zero. If this variable is normally distributed with mean of zero and standard devation S (denoted N [X: 0, S]) :

$\bar{X}^{2r+1}$ refer to the moments of odd order

$\bar{X}^{2r}$ refer to the moments of even order

Consider the case $N\left[X: 0, 1\right]$; the reduced normal variate. Since the distribution is symmetrical about zero, the moments of odd order about the mean are all zero. That is:

$$\bar{X}^{2r+1} = \frac{1}{2\pi}\int_{-\infty}^{\infty} x^{2r+1} e^{-\frac{x^2}{2}} dx = 0$$

For $\bar{X}^{2r}$, by substituting $x^2 = 2z$

$$\bar{X}^{2r} = \frac{1}{\sqrt{2\pi}}\int_{-\infty}^{\infty} x^{2r} e^{-x^2/2} dx = \frac{2^r}{\sqrt{\pi}}\int_{-\infty}^{\infty} z^{r-1/2} e^{-z} dz$$

$$= \frac{2^r}{\sqrt{\pi}}\Gamma(r+1/2)$$

where Γ (the Gamma Function) can be expressed in factorial form. Thus

$$\bar{X}^{2r} = (2r-1)(2r-3)(2r-5)\cdots\cdots 5\cdot 3\cdot 1 = \frac{(2r)!}{2^r r!}$$

Consider now the distribution of two <u>independent</u> reduced normal variates, x and y, or $N\left[X:0,1\right]$ and $N\left[Y: 0,1\right]$. When

$$r = 1 : \quad \bar{x}^2 = \bar{y}^2 = 1$$

$$r = 2 : \quad \bar{x}^4 = \bar{y}^4 = 3$$

Let $X = m_1(1 + k_1^{1/2}x)$ and $Y = m_2(1 + k_2^{1/2}y)$ where km^2 is variance or $\sigma_1^2 = k_1 m_1^2$ and $k^{1/2}$ is the coefficient of variation. Since the moments of odd orders for the variates x and y are all zero, we need only to consider even powers of x, y.

$$\therefore \overline{XY}^2 = E(X^2Y^2) = E(X^2)\,E(Y^2)$$
$$= m_1^2 m_2^2 (1 + k_1 \bar{x}^2)(1 + k_2 \bar{y}^2)$$
$$= m_1^2 m_2^2 (1 + k_1)(1 + k_2)$$

Thus is $m_1 m_2 = A$ (say, an area), the moments of XY about zero are

$$\mu_1' = m_1 m_2 = A$$
$$\mu_2' = m_1^2 m_2^2 (1 + k_1)(1 + k_2)$$
$$\mu_3' = A^3 (1 + 3k_1)(1 + 3k_2)$$
$$\mu_4' = A^4 (1 + 6k + 3k_1^2)(1 + 6k_2 + 3k_2^2)$$

Therefore

$$S^2 = \mu_2 = \mu_2' - (\mu_1')^2$$
$$= [(1 + k_1)(1 + k_2) - 1]\, m_1^2 m_2^2$$
$$= m_1^2 m_2^2 [k_1 + k_2 + k_1 k_2]$$

The equation for μ_2 recalling that $k_1 = C_1^2$, can be written

$$\frac{S_{12}^2}{m_1^2 m_2^2} = C_{12}^2 = C_1^2 + C_2^2 + C_1^2 C_2^2$$

or

$$S_{12}^2 = S_1^2 m_2^2 + S_2^2 m_1^2 + S_1^2 S_2^2$$

and denote this value for the independent case as $\left[S_{12}^2\right]_I$

If $N[X: m_x, S_x]$ and $N[Y: m_y, S_y]$ are correlated by ρ, Haldane gives the results

$$(m_{xy})_D = m_x m_y + \rho S_x S_y = [m_{xy}]_I + \rho S_x S_y$$

$$\left[S_{xy}^2\right]_D = S_x^2 m_y^2 + S_y^2 m_x^2 + 2\rho m_x m_y S_x S_y + (1+\rho^2) S_x^2 S_y^2$$

$$= \left[S_{xy}^2\right]_I + 2\rho m_x m_y S_x S_y + \rho^2 S_x^2 S_y^2$$

Thus, the standard deviation of the product of two dependent variables contains two additional terms whose magnitude depends on ρ. If we wish $\left[S_{xy}^2\right]_D$, that is, if the product XY is a constant, then

$$(1+\rho^2) S_x^2 S_y^2 + 2\rho(m_x m_y S_x S_y) + S_x^2 m_y^2 + m_x^2 S_y^2 \equiv 0$$

Solving for ρ

$$\rho = \frac{-m_x m_y \pm \sqrt{m_x^2 m_y^2 - (S_x^2 m_y^2 + S_y^2 m_x^2 + S_x^2 S_y^2)}}{S_x S_y}$$

Dividing by $m_x m_y$

$$\rho = \frac{-1 \pm \sqrt{1 - [C_x^2 + C_y^2 + C_x^2 C_y^2]}}{C_x C_y}$$

Since Cx and Cy are always positive, the value of the radical is always less than 1, and ρ will always be negative.

Appendix F

Unit Cell Rupture Strain

In Section VIII, an assumption was made concerning the strain of the unit cell when the first fiber ruptures. This very simplified method involved taking the unit cell rupture strain as the mean fiber rupture strain minus three standard deviations of the fiber rupture strain; or $(e_c)_{rup} = \bar{e}_m - 3S_{e_m}$. The pertinent question is whether the original assumptions on the behavior of the fibers within the unit cell justify a more exact approach to the problem of unit cell rupture strain. It is the author's contention that the basic assumptions so limit the exactness of the theory that a mathematical analysis of the rupture strain problem does not seem warranted. However, in the interest of completeness, the analytical steps can be outlined.

Given:

a. Distribution of fiber rupture strains, $f_m(e_m)$

b. Orientation distribution of fibers, $\phi(\beta)$

c. Constant unit cell strain, e_c, applied to all fibers.

Find:

Distribution function of e_c when first fiber breaks, as a function of e_m, $\phi(\beta)$ and the numbers of fibers, n.

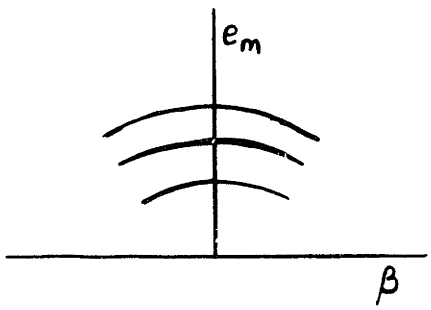

A plot of e_m vs. angle β gives lines of constant e_c, as shown at left. Consider for the moment only one fiber. The probability of its rupture

elongation being a certain value is given by $f_m(e_m)de_m$, as below. The probability that this same fiber lies at a particular angle β is given by $\phi(\beta)\,d\beta$. Then the probability of both occurring, if the events are independent, will be

$$P_b = \phi(\beta)\, f_m(e_m)\, d\beta\, de_m$$

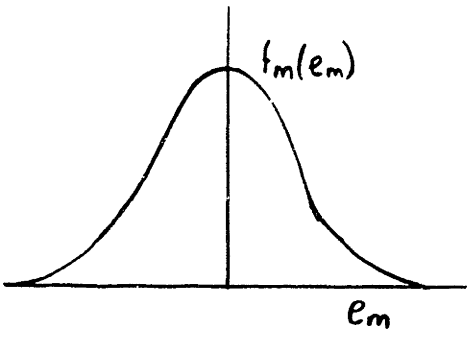

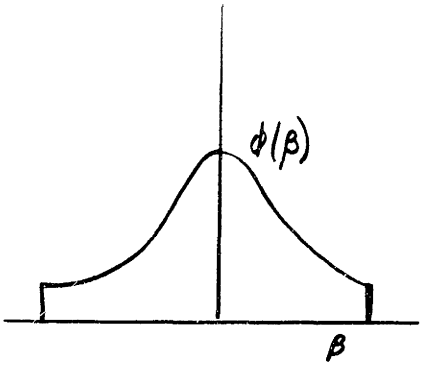

This represents a small area on the plot of e_m vs β, the area bounded by values of e_m, β, $e_m + de_m$ and $\beta + d\beta$. The variable e_m can be changed to e_c with the known relationship between them, $e_m = g(e_c, \beta)$ and thus

$$P_b = \phi(\beta) \cdot f_m\left[g(e_c,\beta)\right] \cdot \left[\frac{\partial g(e_c,\beta)}{\partial e_c}\right]_\beta d\beta\, de_c$$

The probability function of e_c at any β is given by the integration over β ;

$$f(e_c)de_c = \int_{-\pi/2}^{\pi/2} \phi(\beta)d\beta \left\{ f_m\left[g(e_c,\beta)\right] \cdot \left[\frac{\partial g(e_c,\beta)}{\partial e_c}\right]_\beta de_c \right\}$$

If this expression can be integrated, then the mean value for the one fiber can be found

$$\text{Mean} = \int_{-\infty}^{\infty} e_c \, f(e_c) \, de_c$$

For a number of fibers, n, the use of $f(e_c)$ in the analysis of Peirce will give the reduced <u>mean</u> <u>strain</u> for the unit cell when the first fiber fails; all others not failing.

This approach is independent of the forms of $\phi(\beta)$ and $f_m(e_m)$ It becomes useful only if the integration can be easily carried out. In view of the question of coupling (Sections VIII and IX), a solution by this method will be deferred for the present. There appears to be more value in pursuing the questions of basic fabric phenomena than in refinements of the analytical predictions at this time.

APPENDIX G

BIBLIOGRAPHY

1. Aroian, Leo A., "The Probability Function of the Product of Two Normally Distributed Variables", Annals of Math. Stat., 18, 1947, pp. 265-271

2. Cox, H. L. "The Elasticity and Strength of Paper and Other Fibrous Materials", British J. Of App. Physics, 3, 1952 pp. 72-79

3. Craig, C. C., "On the Frequency Function of xy", Annals of Math. Stat., 7 (1936) pp. 1-15

4. Den Hartog, J. P. Advanced Strength of Materials. McGraw-Hill, New York, 1952

Forest Products Laboratory Reports. Forest Products Laboratory, Madison, Wisconsin

5. 1328 and supplements, "Compression, Tension and Shear Tests on Yellow Poplar Plywood Panels of Sizes that do not Buckle with Tests made at various angles to the Face Grain"

6. 1503, Stress-Strain Relations in Wood and Plywood Considered as Orthotropic Materials.

7. 1803 and supplements, "Directional Properties of Glass-Fabric-Base Plastic Laminates Panels of Sizes that do not Buckle."

8. 1820 and supplement, "Mechanical Properties of Plastic Laminates"

9. 1853. "Tensile Properties of Glass-Fabric Laminates with Laminates Oriented in Any Way."

10. Haldane, J.B.S. "Moments of the Distributions of Powers and Products of Normal Variates." Biometrika, 32, 1942, pp. 226-241

11. Love, A.E.H. A Treatise on the Mathematical Theory of Elasticity, Dover Publications, New York, 1944

12. Modern Textiles, 39, April 1958, p. 35.

13. Peirce, F. T. "Tensile Tests for Cotton Yarns v. 'The Weakest Link', Theorems on the Strength of Long and Composite Specimens", J.T.I. 17, 1926 p. T355-T368

14. Platt, M. M. "Mechanics of Elastic Performance of Textile Materials" TRJ 22, 1952, pp. 695-728,

15. Timoshenko, S. Theory of Elasticity, McGraw-Hill Book Company, New York 1934.

FIGURE 3.2

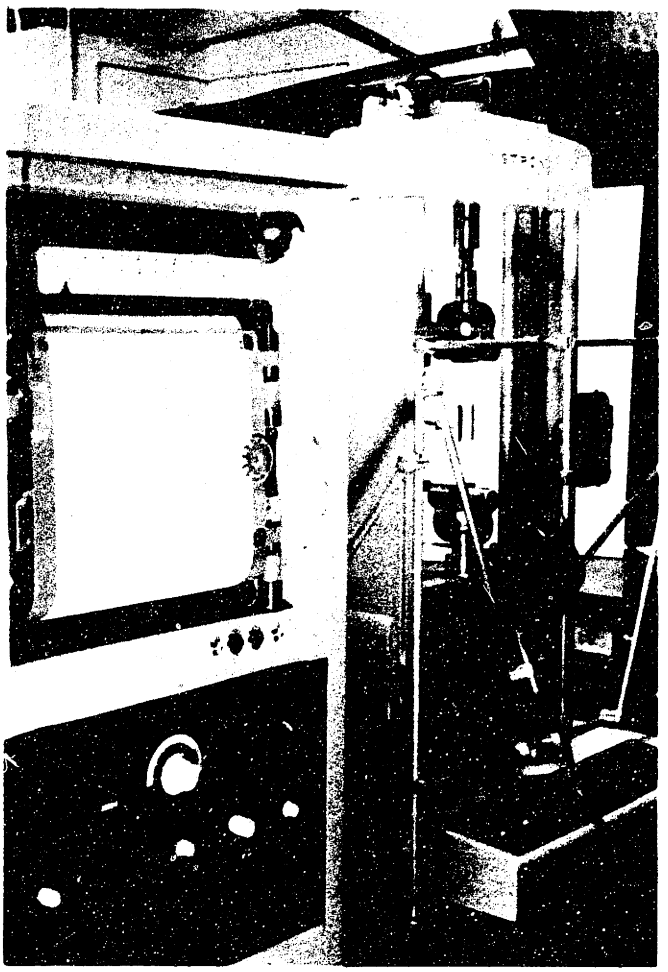

"INSTRON" TENSILE TESTER

FIGURE 3.5

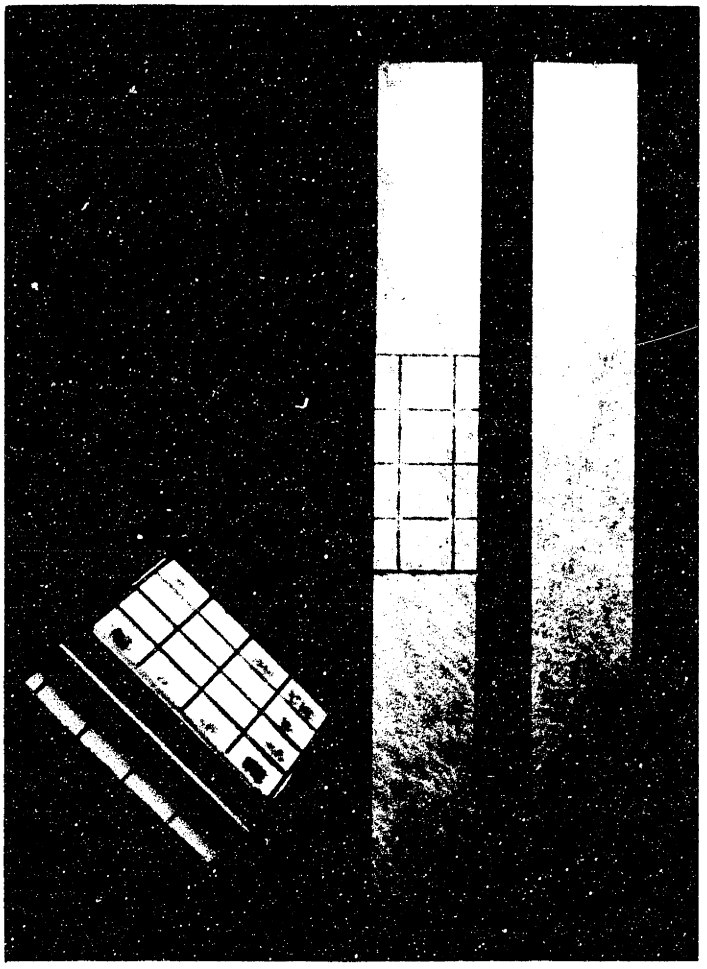

MARKING STAMP, GROUND-GLASS MAGNIFIER, AND

MARKED & UNMARKED FABRIC SPECIMENS

FIGURE 3.6

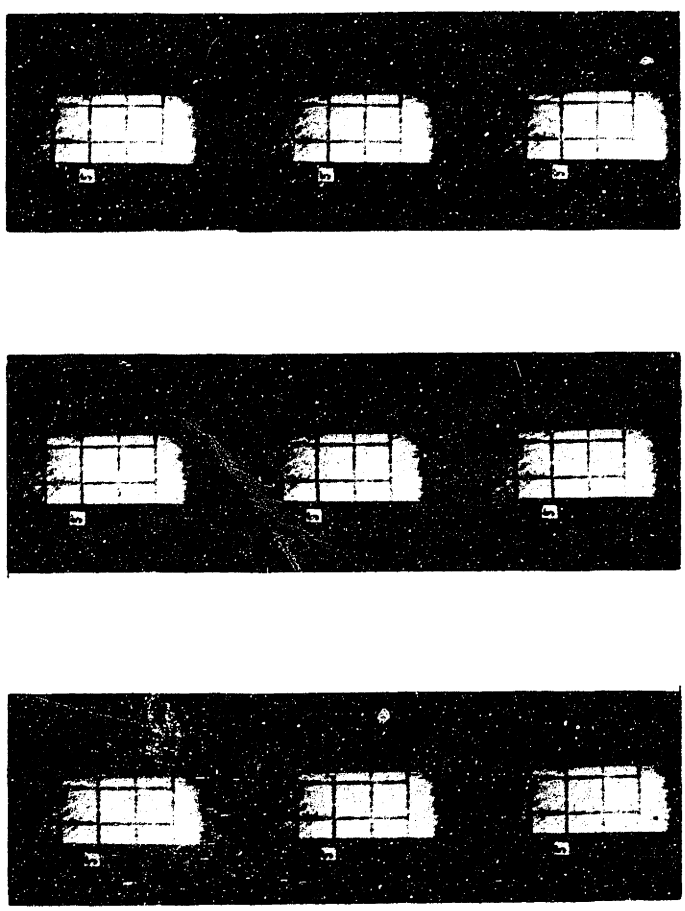

PHOTOGRAPHIC RECORD OF SUCCESSIVE STATES OF STRAIN

FIGURE 4.1

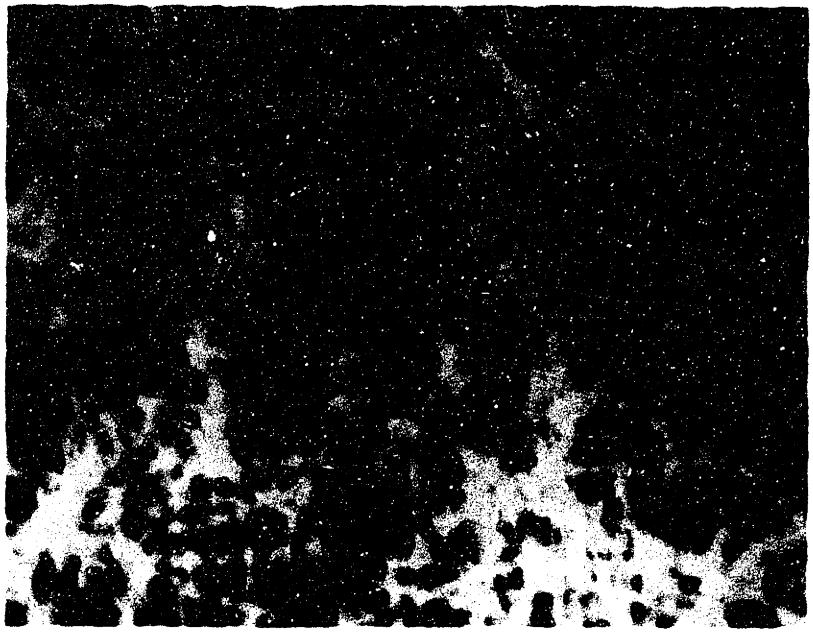

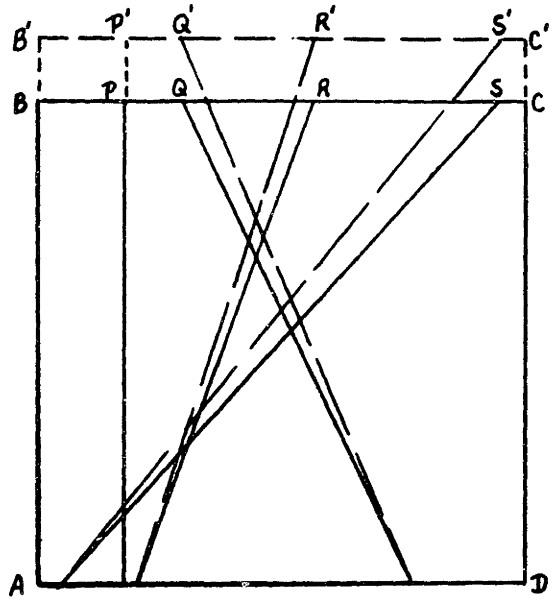

PHOTOMICROGRAPH AND SCHEMATIC OF UNIT CELL

FIGURE 4.2

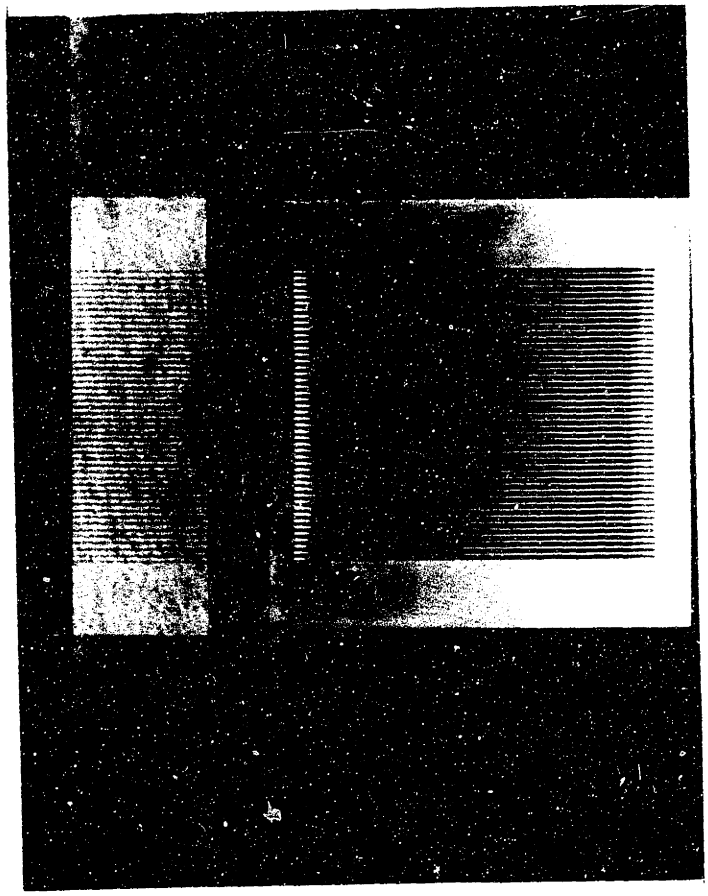

SPECIMEN AND MASK FOR EXPERIMENTS ON PARALLEL

BOUNDARY DISPLACEMENT

FIGURE 4.3

FABRIC A, PHOTOMICROGRAPHS OF UNIT CELL BEHAVIOR

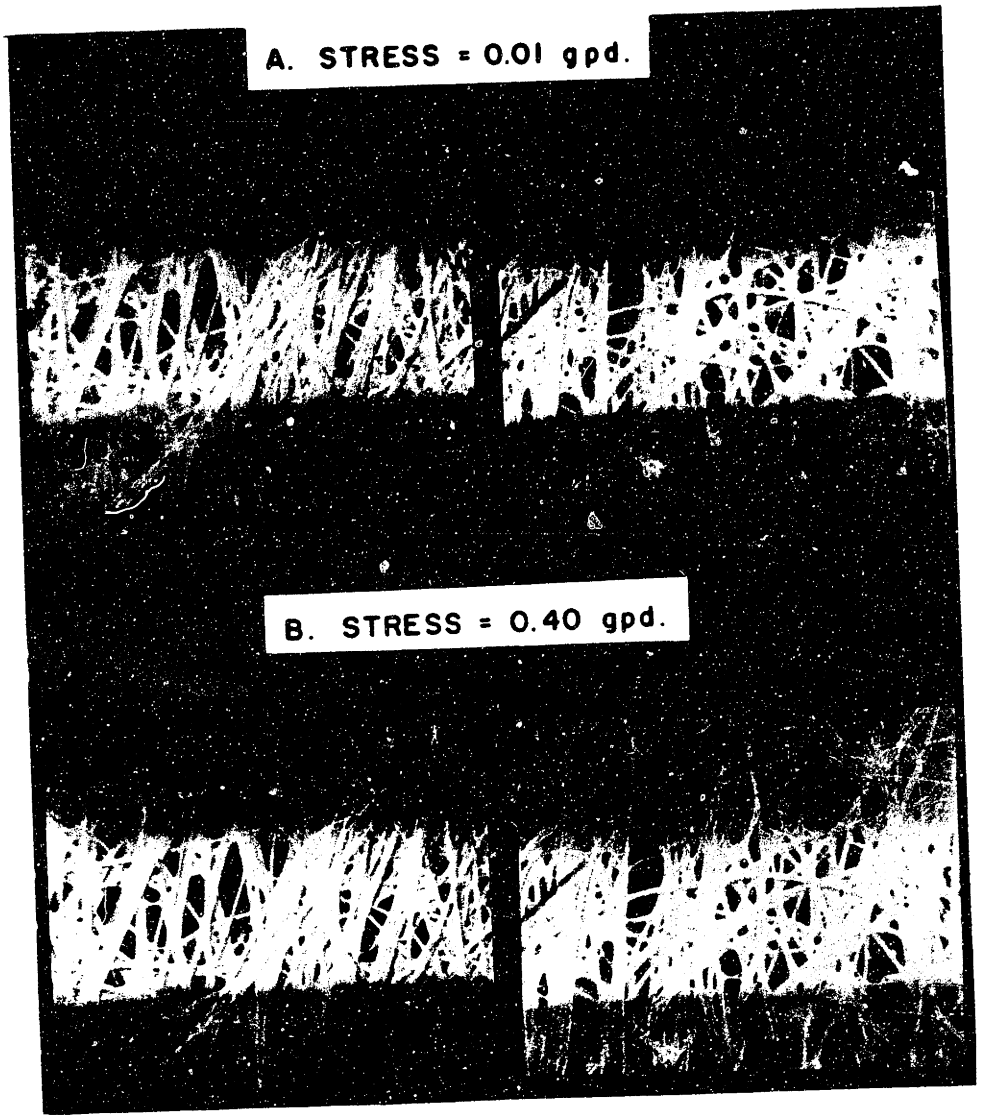

STRESS DIRECTION - VERTICAL

MAGNIFICATION: 40X (ONE INCH ON PHOTOGRAPH IS 0.04 INCHES ON FABRIC)

STRAIN AT 0.40 pgd IS APPROXIMATELY 3 %

FIGURE 5.1

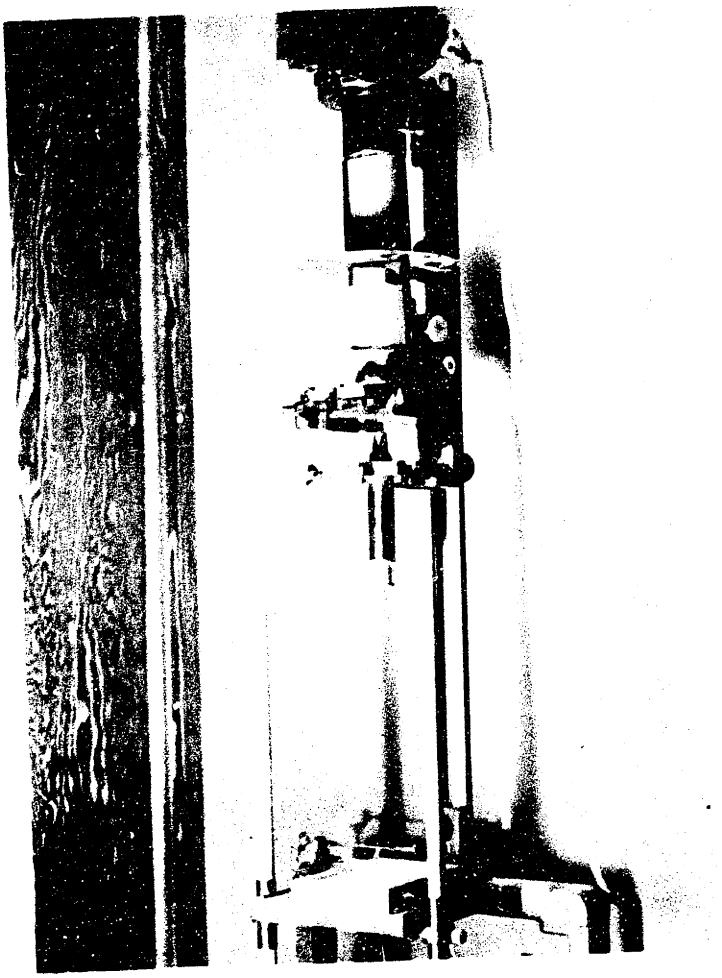

VERTICAL MICROSCOPE FOR FABRIC PHOTOMICROGRAPHS

FIGURE 5.2

SLIDE AND 20X ENLARGEMENT OF FABRIC A.

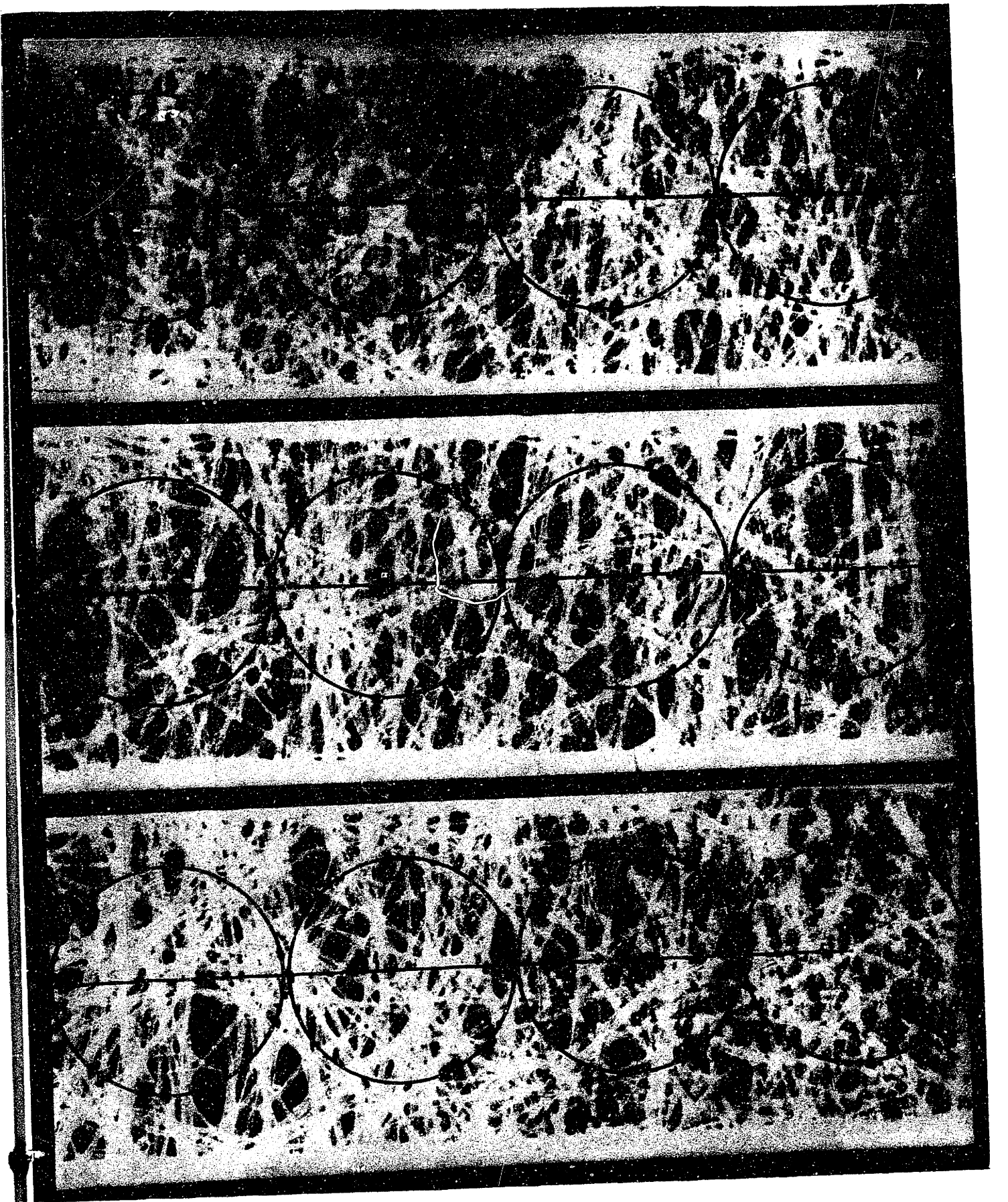

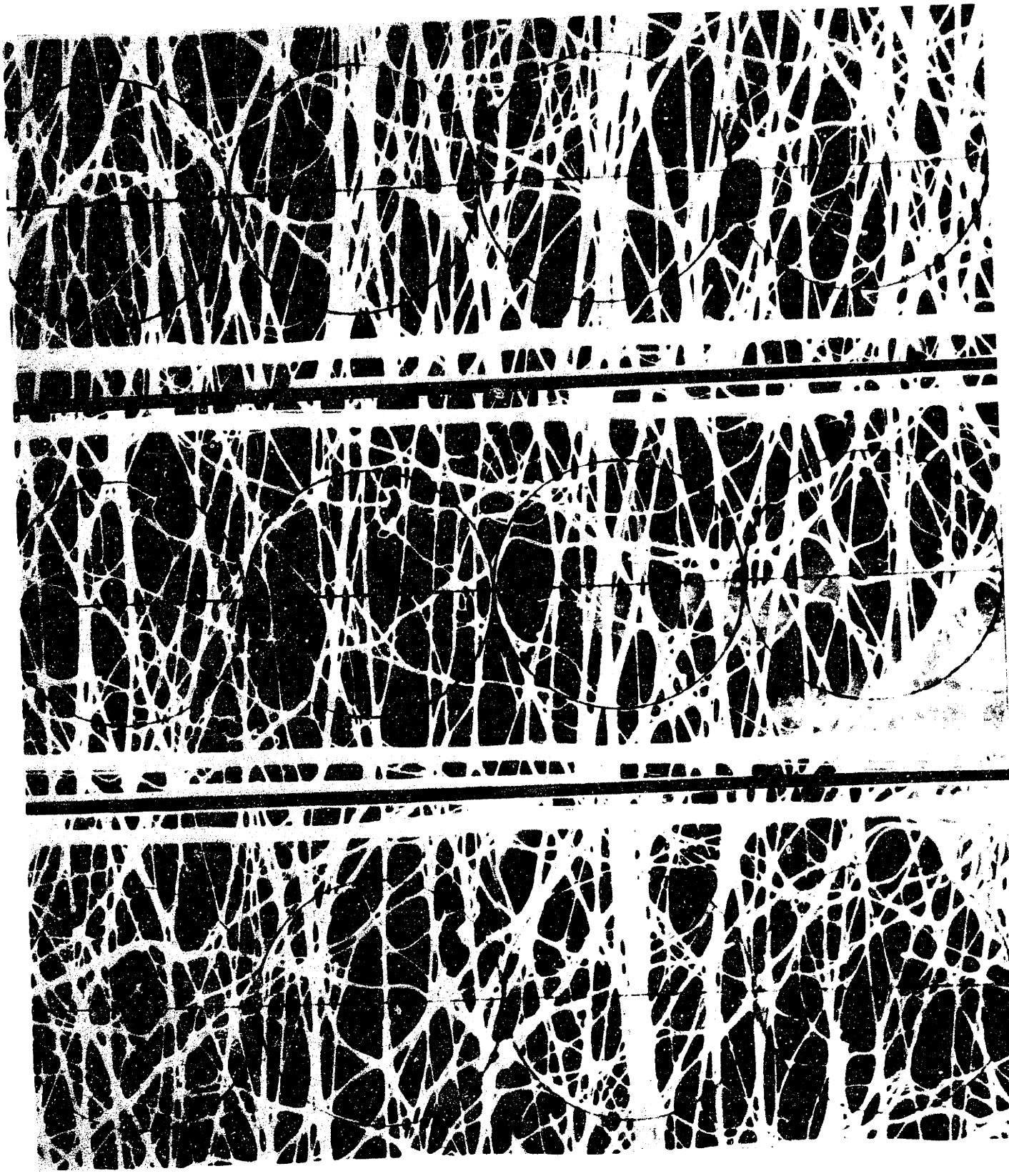

FIGURE 9.5

TWELVE ADJACENT UNIT CELLS, FABRIC B

FIGURE 14.1

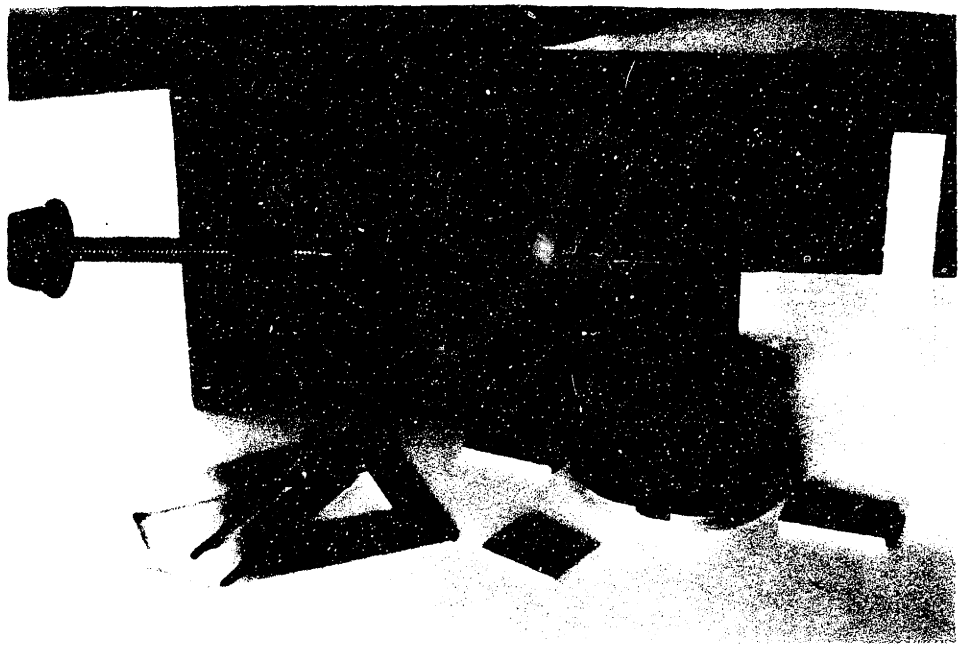

EQUIPMENT FOR SINGLE FIBER TESTS